TECHNISCHE UNIVERSITÄT MÜNCHEN

TUM Campus Straubing für Biotechnologie und Nachhaltigkeit

Electrochemical water oxidation to hydrogen peroxide at carbon-based anodes: Basic development and optimization of process parameters

Dhananjai Pangotra

Vollständiger Abdruck der von der promotionsführenden Einrichtung TUM Campus Straubing für Biotechnologie und Nachhaltigkeit der Technischen Universität München zur Erlangung des akademischen Grades eines

Doktors der Naturwissenschaften (Dr. rer. nat.)

genehmigten Dissertation.

Vorsitz: Prof. Dr. Rubén Dario Costa Riquelme

Prüfer der Dissertation: 1. Prof. Dr. Volker Sieber

                             2. Prof. Dr. Marc Ledendecker

Die Dissertation wurde am 03.04.2023 bei der Technischen Universität München eingereicht und von der promotionsführenden Einrichtung TUM Campus Straubing für Biotechnologie und Nachhaltigkeit am 12.08.2023 angenommen.

CONTENTS

ABSTRACT

This study examines a new method of producing hydrogen peroxide (H_2O_2) from water using carbon materials as anodes. Optimization of various parameters such as current density, electrolyte concentration, and pH was done to achieve high selectivity of water oxidation to H_2O_2. Sodium silicate (Na_2SiO_3) was found to significantly increase H_2O_2 production at high pH levels. A correlation between the activity of CO_3^{2-} ions and the increase in H_2O_2 production was observed in the study, leading to the proposal of a cyclic mechanism involving CO_3^{2-} ions for H_2O_2 production. The study also presents a process for producing H_2O_2 in continuous flow at high current densities, achieving the highest-ever reported H_2O_2 production rate. The use of bipolar plates as a low-cost and stable electrode for generating H_2O_2 was also investigated. Commercially available carbon electrode materials can selectively oxidize water to H_2O_2, which could have economically viable applications, as demonstrated in this study.

ACKNOWLEDGEMENTS

Furthermore, I am grateful for my colleagues at CBR who patiently listened to my talks in the PhD seminar. I extend my thanks to all the project partners from the CO2EXIDE project who provided their assistance during the project.

I also wish to express my gratitude to my friends in Straubing, Carlos, Barbara, Johanna, Rade, Vineel, Korby, Carlos (Spanish), who supported and encouraged me during my stay. Special mention goes to the Fantastic 4 and DFV, who were there to share coffee, lunch, drinks, and to talk about everything going on in our lives. I would also like to thank all my friends from Munich who have been a great support as well.

I would also like to thank Johanna for her love and patience with me, as well as for all the wonderful and beautiful moments we shared. Thanks to the whole Radomski family for their love and support. Finally, I am infinitely grateful for the constant support and love from my wonderful parents, my sister Mahima, and other family members, who have always been there for me, no matter where the future takes me.

1. INTRODUCTION

Fossil fuels have played a pivotal role in progressing society throughout the Industrial Revolution and still dominate the global energy market [1]. During development, humans have exploited natural resources, including fossil fuels [2]. The 20th century saw a rise in the dependence on fossil fuels due to technological advancements, urbanization, and transportation needs[3]. By 2040, the world's population is projected to reach 9.2 billion [4]. During the same period, global GDP is projected to double compared to the current situation [5]. High economic growth means rising living standards for people everywhere, as well as the expansion of the middle class in every country. Compared to 2015, population growth, GDP growth, and income growth will increase energy demand by about 25% in 2040 from 97 to 126 billion barrels, equivalent to North America and Latin America's current oil consumption [5].

To fulfill such demand, fossil fuels such as crude oil will remain at the top in terms of consumption [5][6][7]. With the increase in the expected demand, it will be challenging to meet the needs as fossil fuel reserves are depleting [7]. Considering the finite nature of these natural resources, it will result in higher prices, which will significantly impact the global economy. Besides their depletion, these fossil fuels also carry harmful environmental hazards [8]. In the past few decades, fossil fuel usage has contributed significantly to global climate change due to releasing carbon dioxide (CO_2) into the atmosphere [8]. Various estimates exist about how long fossil fuel reserves will last, but it is widely agreed that fossil fuels should not provide the majority of energy if we want to maintain the present level of CO_2 [9][10].

In December 2015, the Paris Agreement pledged to limit the average global temperature rise to below 1.5°C compared to pre-industrial levels [8][11]. In order to achieve that goal, greenhouse gas emissions must be drastically reduced. As long as fossil fuels like oil, coal, and natural gas are used as the primary feedstock for energy supply and the chemical industry, the targeted CO_2 emissions reduction cannot be met. A transition from fossil fuel-based energy resources to renewable ones is thus necessary. At the same time, renewable electricity generation is increasing, and the total share is projected to increase by 60% by 2026 compared to 2020 levels [12]. Future electricity generation
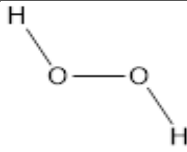
is expected to comprise a renewable share of 68% in 2030 and 86% percent in 2040 [13]. The enormous increase in the production of renewable energy and the corresponding decrease in production costs, with renewable energy now becoming cost-competitive with conventional electricity generation [14]. This cost-competitiveness has opened the door for new possibilities for using renewable electricity, one example being the "electrification" of the chemical industry [15]. This can be done by electrochemical conversion of abundant raw materials into valuable chemical products using renewable electricity, thus utilizing the electric energy to upgrade the chemicals [16]. This gives the advantage of using surplus electricity, which conventionally is stored in batteries [17].

With this backdrop, sustainable thinking and actions have been spreading to the chemical industry. New technologies and processes must meet the highest sustainability standards. A strategic goal will be to replace fossil-based production routes with new and innovative synthesis strategies within the next decade [18]. Electrochemical processes powered by renewable energy sources like windmills and photovoltaic system could provide an important chemical feed streams through "electrified" synthetic process [19]. One example is the production of hydrogen peroxide (H_2O_2), industrially produced via the fossil-based anthraquinone autooxidation (AO) process, which has several ecological drawbacks and can be substituted via the electrochemical process [20]. H_2O_2 can be synthesized electrochemically from renewable electricity via either reduction or oxidation of naturally abundant educts such as O_2 and H_2O. Therefore, an alternate "green" route for H_2O_2 synthesis is promising compared to the fossil-based AO process. This introduction discusses alternative methods to produce H_2O_2 based on literature and future research perspectives followed by a brief summary of current industrial processes.

1.1 Hydrogen peroxide

H_2O_2 is a colorless and odorless pale blue liquid, which is slightly more viscous than water in its pure form. It has a strong oxidizing capacity and considered to be a "green" oxidant as it releases only H_2O and O_2, as by-products [21]. As a green energy carrier, H_2O_2 is also capable of releasing 96 kJ mol^{-1} of energy when it decomposes into H_2O and O_2 [22]. A solution of 70 wt.% H_2O_2 has an energy density of 0.75 kWh L^{-1}, which is comparable to that of compressed H_2 gas at 350 bar [23]. Moreover, it has no severe toxicity and is noncorrosive [24]. At the same time, it is an unstable compound, which slowly decomposes in presence of light, heat as well as metal impurities such as iron, manganese, etc. Some of the properties of H_2O_2 are listed in **Table 1.1**. The H_2O_2 molecule shows an angled non-planar structure due to the repulsion of the hydrogen atom from the unpaired electrons of O atom.

Tab. 1.1 : Physical properties of H_2O_2.

Chemical Structure	
CAS number	7722-84-1
Chemical formula	H_2O_2
Molar mass	34.015 g mol^{-1}
Density	1.45 g cm^{-3}
Melting point	-0.43°C
Boiling point	150.2°C
Other names	Dihydrogen dioxide, hydrogen dioxide, hydrogen oxide, oxydol, peroxide

1.2 H_2O_2 – Application

H_2O_2 is a strong oxidizing agent with a broad range of applications. A major use of H_2O_2 is in the hydrogen peroxide to propylene oxide (HPPO) process, pulp and paper industry, and bleaching in textile industry [24][25][26]. Additionally, it is widely used in chemical syntheses, wastewater management, and disinfection [20]. H_2O_2 can effectively kill bacteria, fungi, viruses, and spores [27]. Other sectors where peroxide has emerged as an effective component are for the production of semiconductors (cleaning silicon wafers in the manufacture of printed circuit boards), agriculture (soil disinfectant), pharmaceutical and healthcare, as well as potential use as an energy source for H_2O_2 fuel cells [25][28]. In 1880, the first industrial plants producing H_2O_2 generated around 2000 tons per year, but both demand and production have since exploded [29]. The world's annual H_2O_2 production increased by a factor of four from 1990 to 2015 and is predicted to grow further. As of 2020, the market value of H_2O_2 was estimated at \$4 billion and is predicted to grow to \$5.2 billion by 2026 [30]. Due to its vast area of use, it is also considered as top 100 important chemicals in the world [31].

1.3   Industrial production

H_2O_2 was first discovered in 1818 by Louis-Jacques Thénard by reacting barium peroxide and hydrochloric acid (**Equation 1.1**) [32]. The first industrial production of H_2O_2 based on the reaction of BaO_2 and HNO_3 was implemented in 1873 [20]. This was followed by development of the electrosynthesis of H_2O_2 from O_2 using Hg–Au electrode in the year 1887, however, H_2O_2 concentration

produced was low [20][32].

$$BaO_2 + 2\,HCl \longrightarrow H_2O_2 + BaCl_2 \tag{1.1}$$

The anthraquinone auto-oxidation (AO) process described by H.J. Riedl and G. Pfleiderer in 1935, still dominates H_2O_2 production, with 95% of the world's annual production capacity [33]. This takes place on a relatively large scale with the capacity to produce tens of thousands of gallons per day [34]. The AO process involves remarkable risks associated with hydrogenation and oxidation reactions under high H_2O_2 pressure, and requires expensive Pd-based catalysts [34]. In the AO process, 2-alkylanthraquinone is hydrogenated to anthrahydroquinone on a Pd catalyst, which is further oxidized with O_2 in a separate chamber to re-produce alkylanthraquinone and an equimolar amount of H_2O_2 (**Figure 1.1a, b**) [24]. However, this process has a side reaction during the hydrogenation of the unsubstituted aromatic ring of alkylanthraquinone to 5,6,7,8-tetrahydroanthrahydroquinone, and thus requires additional steps of regeneration and separation of organic waste (**Figure 1.1 b,c**) [24]. The produced H_2O_2 is extracted from the organic solution using water, which is further purified and concentrated (up to 70 wt.%) and transported in large volumes [24]. Such a large volume of highly concentrated H_2O_2 is potentially explosive and causes storage and transport risks. Shipping H_2O_2 in lower concentrations presents the disadvantage of moving mainly water, thus negatively affecting carbon footprint and economic viability of the product. Aside from being costly, AO process requires a significant energy input (up to 17.6 kWh kg^{-1}) and cannot be implemented at the point of use [20][35]. Thus, a portable device for decentralized, on-demand H_2O_2 production, relying solely on water, air, and (renewable) electricity as inputs, offers a desirable local and "green" solution for H_2O_2 delivery where it is needed [36].

a)

2-ethylanthraquinone

anthrahydroquinone

b)

c)

2-ethylanthraquinone

5,6,7,8-tetrahydroanthrahydroquinone
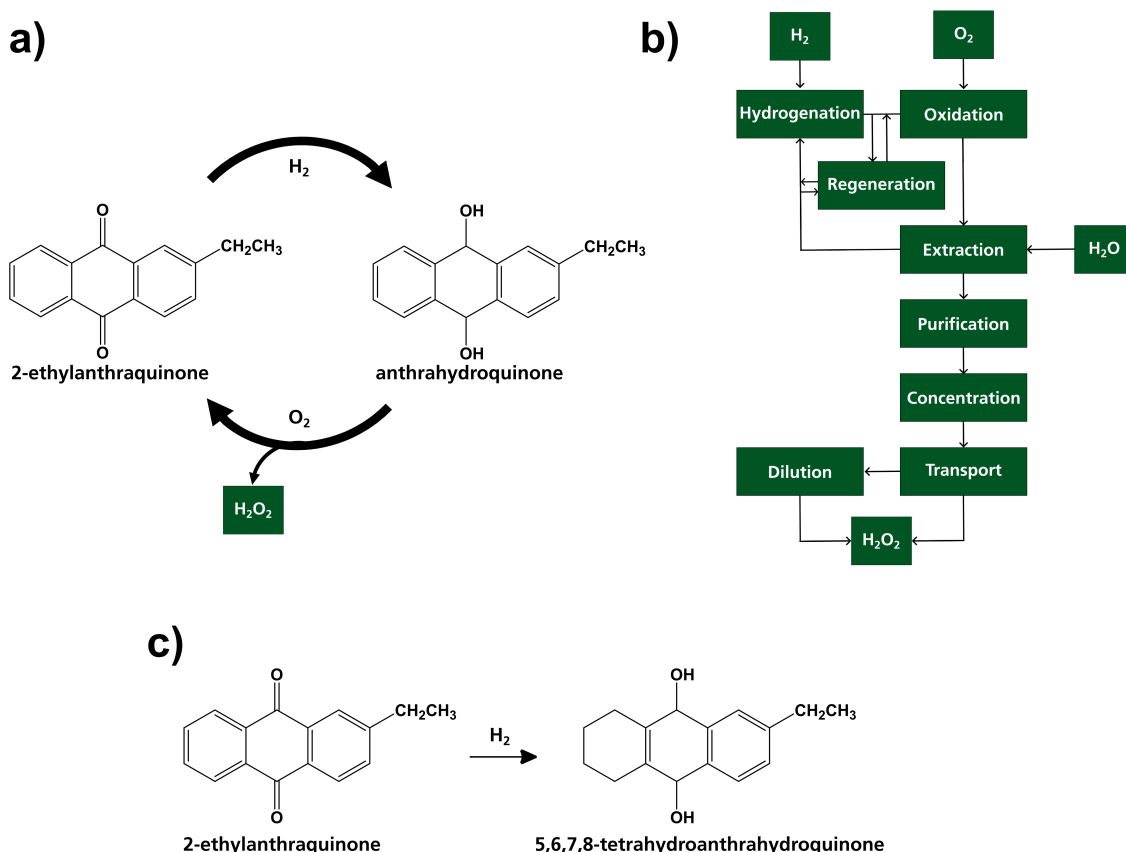
*Fig. 1.1 : **Anthraquinone autooxidation process. (a)** Reaction mechanism and **(b)** steps involved in the production of hydrogen peroxide via anthraquinone process. **(c)** Side reaction during the anthraquinone autooxidation process.*

H_2O_2 can also be prepared via the direct synthesis using H_2 and O_2 as described by H. Henkel and W. Weber in 1914 [32]. H_2 and O_2 are reacted in a pressurized vessel along with water using catalysts such as Pd, Pt, Ni, etc in a single step, without phase transfer or distillation process. However, this process has several disadvantages, mainly related to safety concerns due to the explosive mixture of H_2 and O_2 [20]. As a result, the mixture of H_2 and O_2 must be diluted with inert gases such as N_2 and CO_2 to operate below the explosive limit, which limits the productivity of the whole process [36]. In addition, this pathway forms water as a side product, and H_2O_2 decomposes during synthesis. As such, developing an alternate route, suitable for application in decentralized (small-scale and on-demand) production to produce H_2O_2 is highly relevant from a scientific and economic perspective [37].

1.4 Electrochemical pathway

An alternative way of producing H_2O_2 is via electrolysis for on-site and on-demand H_2O_2 production, avoiding risks related to storage and transport of highly concentrated H_2O_2 [38]. As electrochemical method is electricity-driven, it offers the potential for sustainable H_2O_2 production, provided that

only renewal electricity is utilized [16]. There are two approaches for the electrochemical synthesis of H_2O_2. One pathway is the partial reduction of O_2 as cathodic half-cell reaction, featuring either noble metal alloys such as Pd[39] and Pd-Au [40][41] or doped carbon [42] as electrocatalysts, shown in **Equation 1.2**. This reaction takes place with relatively high selectivity of up to 96% [40][43], with maximum productivity of up to 4330 mmol $gcat^{-1}$ h^{-1} has been reported for a Co−N−C catalyst [44]. The maximum H_2O_2 concentration achieved so far via the cathodic process is up to 20 wt.% H_2O_2 solution using a solid electrolyte setup [45][46]. Conductive polymers are commonly utilized as solid electrolytes in chemical processes to obtain pure products that are free of any salt impurities [45]. With this exception, the concentration of H_2O_2 produced through electrochemical methods is generally lower in comparison to the concentrations achievable through the currently employed AO process.

$$O_2 + 2\,H^+ + 2\,e^- \longrightarrow H_2O_2 \quad E^0 = 0.670V\,vs.\,SHE \tag{1.2}$$
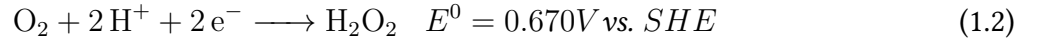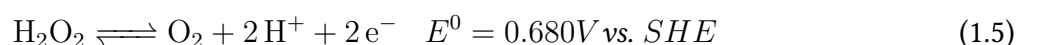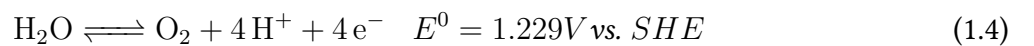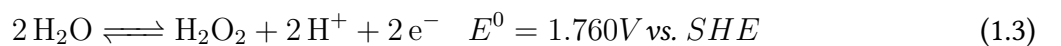
Another possible route to electrochemically produce H_2O_2 is through the $2e^-$ oxidation of water (water oxidation reaction, WOR, **Equation 1.3**). Compared to $2e^-$ ORR (**Equation 1.2**), $2e^-$ WOR does not rely on the gas-phase reactant and provides a new method for electrochemically producing H_2O_2 [47]. The competing $4e^-$ WOR to O_2 is thermodynamically favorable, however is an economically insignificant half-cell reaction and utilizes expensive and critical electrode materials such as iridium (**Equation 1.4**) [48]. Achieving selectivity is a key challenge in electrochemical H_2O_2 production. High potentials that convert H_2O to H_2O_2 can also produce O_2 or further oxidize/decompose H_2O_2 to O_2, thus reducing the efficiency (**Equation 1.3-1.5**). Consequently, an optimal electrocatalyst that exhibits high selectivity towards the production of H_2O_2 is essential.

The $2e^-$ WOR to H_2O_2 process is assumed to be a valuable supplement reaction at the anode since it can be coupled with the cathodic half-cell reaction to generate value-added products, which consequently enhances the overall efficiency of the whole production process. The cathodic half-cell reaction includes, the hydrogen evolution reaction (HER), cathodic production of H_2O_2 via oxygen reduction reaction (ORR), and CO_2 reduction reaction (CO_2RR), thus enabling productive utilization of both half-cell reactions.

$$2\,H_2O \rightleftharpoons H_2O_2 + 2\,H^+ + 2\,e^- \quad E^0 = 1.760V\,vs.\,SHE \tag{1.3}$$

$$H_2O \rightleftharpoons O_2 + 4\,H^+ + 4\,e^- \quad E^0 = 1.229V\,vs.\,SHE \tag{1.4}$$

$$H_2O_2 \rightleftharpoons O_2 + 2\,H^+ + 2\,e^- \quad E^0 = 0.680V\,vs.\,SHE \tag{1.5}$$

The anodic production of H_2O_2 has gained massive interest in the last years [20]. Using a carbon catalyst in sodium hydroxide (NaOH) electrolyte, 2e- WOR was first reported in 2004 for producing H_2O_2 [49]. This was followed by a series of studies performed using metal oxides as electrocatalysts [50][51][52][53][54][55][56][57][58][59]. One of the first studies on WOR using metal oxides was performed with MnO_x catalyst in a butylammonium sulfate (BAS)/base mixture (1.0 mol L^{-1}) with FE reaching up to 100% [50]. However, FE decreases as the pH increases due to the decomposition of H_2O_2, resulting in the generation of O_2. Additionally, applying potentials above 1.2 V *vs.* Ag/AgCl causes a decrease in the FE due to the O_2 evolution reaction competing at higher potentials and further oxidation of H_2O_2 [60][61].

Various electrode materials based on metal oxides, including $BiVO_4$, $CaSnO_3$, ZnO, WO_3, SnO_2, and TiO_2, which have been reported as active in the anodic synthesis of H_2O_2 [52][54][57][62]. Siahrostami *et al.*[62] presented a selectivity diagram regarding the properties of the catalysts that determine selectivity toward the one, two, and four-electron processes leading to OH radical, H_2O_2, and O_2 as products (**Figure 1.2**). Blue, green, and red highlighted colors indicate regions in which O_2, H_2O_2, or OH radical are expected to be the primary product, respectively, in terms of purely thermodynamic constraints. The selectivity diagram shows that IrO_2, RhO_2, and PtO_2 are thermodynamically located in the selectivity region for O_2 evolution, whereas WO_3, $BiVO_4$, and SnO_2 produce H_2O_2 and are well into the green region. On the other hand, TiO_2, which is known to form both OH radical and H_2O_2, is close to the border between those two species. MnO_2 is close to the edge of four electron oxidation (blue zone), where both O_2 and H_2O_2 may be produced. The selectivity diagram can be used to identify leads for new H_2O_2 production catalysts [55]. Based on the study, several promising candidate materials for catalysts selective towards H_2O_2 electrosynthesis have been identified, with $BiVO_4$ appearing to offer the best selectivity.
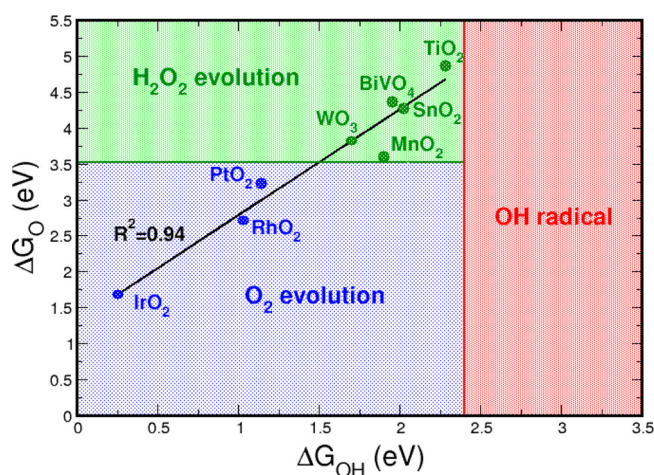

Fig. 1.2 : *Phase diagram of different metal oxides in terms of their binding energies with the reaction intermediates O^* vs. OH^*. Reprinted with permission from reference [62]. Copyright 2017 American Chemical Society.*

Likewise, Shi *et al.*[52] utilized density functional theory calculations to anticipate activity trends for water oxidation resulting in H_2O_2 production on four different metal oxides: WO_3, SnO_2, TiO_2, and $BiVO_4$. Their theoretical predictions were subsequently corroborated by experimental observations, where they determined that $BiVO_4$ exhibited the highest amount of H_2O_2 generation among these oxides, with a FE of approximately 98%.

Fuku *et al.*[51] investigated the effect of surface modification of a fluorine-doped tin oxide (FTO) substrate as an anode with various metal oxides ($BiVO_4$ and WO_3) for effective oxidative production and accumulation of H_2O_2. The metal oxides employed to generate H_2O_2 electrochemically enable high faradaic efficiencies (up to 80%), yet the achieved current densities (0.1 to 15 mA cm^{-2}) and concentrations of H_2O_2 are relatively low with respect to future industrial applications, where high current densities are desirable to scale up the electrochemical process. In order to produce the same quantity of H_2O_2, either a high current density or a larger electrode area is required. However, increasing the electrode area results in a significant increase in capital expenditure [30]. Therefore, it is essential to investigate electrode materials that can operate at current densities that are continuously relevant to industrial conditions (>100 mA cm^{-2}).

Another class of materials used for 2e$^-$ WOR is carbonaceous materials, which have been explored at current densities higher than 100 mA cm^{-2}. The anodic generation of H_2O_2 has been reported in 1 mol L^{-1} $HClO_4$ solutions at high current densities of 23 to 160 mA cm^{-2} using highly active boron-doped diamond (BDD) electrodes [63]. The concentration of H_2O_2 can range from 0.3 up to 1 mmol L^{-1}, with a concentration plateau at different maxima depending on the applied current density [64]. More recently, carbon-based materials, such as carbon fiber paper [21] and BDD [65], have shown exceptional performance for the anodic synthesis of H_2O_2, reaching a maximum production rate of 23.4 μmol min^{-1} cm^{-2}, which shows the potential of carbonaceous materials as electrodes to produce H_2O_2 [21]. A literature comparison of most recent studies on 2e- water oxidation to H_2O_2 is summarized in **Table 1.2**.

Tab. 1.2 : *A comparison of the reported work on 2e⁻ WOR to H₂O₂.*

Electrode	Electrolyte	pH	$[H_2O_2]_{max}$	Conditions*				Production rate	Peak FE	Ref.
			mmol L^{-1}	j/E	t	EA	VA	μmol min^{-1} cm^{-2}	%	
PTFE/CFP	1 M Na$_2$CO$_3$	12	3	100	420	0.36	25	23.4	66	[21]
BDD/Nb		11.9	-	39.8	10	1.13	8.5	3.9	31.7	[30]
BDD/Ti	2 M KHCO$_3$	8	~16	120	5	7.4	25	~8	28	[65]
			29	295				19.7	~22	
CaSnO$_3$/FTO			-	3.2V	10	-	30	~4.6	76	[54]
			~0.9	2.2V	720			-	-	
BiVO$_4$/FTO	1 M NaHCO$_3$	8.3		3.3V	-	1	20	5.7	70	[52]
WO$_3$/FTO			-	2.7V				0.57	48	
TiO$_2$/FTO			-	3.7V				1.01	19	
SnO$_2$/FTO			-	3.3V				1.53	50	

*j: Current density (mA cm^{-2}), E: Potential applied (V vs. RHE), t: Time (minutes), EA: Electrode area (cm^2), VA: Volume of anolyte (mL)

Additionally, the electrochemical oxidation of water to H₂O₂ is not only influenced by the choice of electrode, but also by other parameters, including electrolyte type, concentration, pH, etc. Izgorodin *et al.*[50] observed H₂O₂ accumulation in butylammonium sulfate (BAS) electrolyte, however, no H₂O₂ was detected when BAS was replaced by NaOH [66]. Moreover, the same group observed the best performance in terms of FE for a pH regime between 10.0 and 10.4 in BAS electrolyte. Likewise, Fuku *et al.*[51] investigated different electrolytes and observed that KHCO₃ is the most suitable electrolyte for producing H₂O₂, with maximum H₂O₂ concentration and FE of 30%. This could be explained because various percarbonate species, such as HCO$_4^-$ and C$_2$O$_6^{2-}$ can be generated by the oxidation of HCO$_3^-$ at high potentials. Such species quickly hydrolyze in aqueous solutions, decomposing into HCO$_3^-$ and H₂O₂ because of the instability of percarbonate, providing an additional synthetic route to H₂O₂ [51]. 2 mol L^{-1} KHCO₃ has been thus widely used for WOR to H₂O₂ as a standard electrolyte [51][65][67]. Fuku *et al.* also observed that H₂O₂ was generated in an aqueous phosphate buffer through the creation of peroxymonophosphate (HPO$_5^{2-}$), which then undergoes a conversion to H₂O₂.

1.5 Objectives of this work

Despite the studies that have been conducted on the electrochemical synthesis of H_2O_2 via anodic WOR, several important questions remain to be addressed before this technology can be industrially applied. The most suitable choice of anode material has yet to be identified. Various metal oxides and carbonaceous materials are attracting significant attention, however, it remains to be determined whether these materials can also perform the same at higher current densities. Additionally, it is unclear which specific electrolyte conditions are optimal for increasing H_2O_2 production. Lastly, while the electrochemical process for producing H_2O_2 is still being developed, it remains to be seen whether it will be able to compete with established industrial processes. Based on the unresolved questions discussed above, the following objectives have been established for the current doctoral thesis research.

1. Investigation of known electrocatalysts at high current densities to achieve high concentrations of H_2O_2

The primary objective of this thesis is to achieve high concentrations of H_2O_2 through $2e^-$ WOR at industrially relevant conditions and high production rates. Previous studies have investigated different metal oxides as active electrocatalysts for the $2e^-$ oxidation of water to H_2O_2 at current densities up to $15\,\mathrm{mA\,cm^{-2}}$. To study the performance of these metal catalysts at higher current densities, this present work aims at examining the performance of a series of metal oxides, such as $BiVO_4$, SnO_2, WO_3, MnO_x, and TiO_2, for the anodic oxidation of water to H_2O_2.

2. Development of a system with optimized electrolyte composition for maximal H_2O_2 productivity using commercially available carbon materials

To achieve high concentrations of H_2O_2, extensive optimization of electrolyte conditions, including pH, concentration, etc., has to be studied to understand the role of electrolytes for anodic H_2O_2. This objective aims to develop a system that can achieve maximal H_2O_2 productivity by finding the optimal composition of electrolyte that can be used with commercial carbon materials.

3. Utilization of the optimized conditions for continuous production of H_2O_2

The goal of this work is to use the conditions that have been previously optimized for the anodic production of H_2O_2 in a continuous flow process. In this research, the optimized conditions have to be adapted and used with the highly active BDD electrode to produce high concentrations of H_2O_2 in a scalable and continuous flow process.

4. Exploration of the possibility of using an inexpensive electrode material that is active towards H$_2$O$_2$ generation.

Despite their high activity towards H$_2$O$_2$ production, BDD electrodes typically consist of a thin coating on a metal substrate, such as niobium or tantalum, making them highly expensive. To make the production more cost-effective, alternative low-cost bipolar plates (BPP) have been explored as a means of increasing H$_2$O$_2$ production from water while keeping the cost low. The objective is to investigate the possibility of using an inexpensive electrode material that is active towards H$_2$O$_2$ generation.

2. MATERIALS AND METHODS

2.1 Materials

Tab. 2.1 : *List of chemicals used in this study. All chemicals in this study were used as received.*

Chemical/Enzyme/Reagent	Composition	Supplier	Product code
Potassium hydrogen carbonate	$KHCO_3$, 99.5%	Sigma Aldrich	60339
Potassium carbonate	K_2CO_3, ReagentPlus®, 99 %	Sigma Aldrich	209619
Titanium (IV) oxysulfate	$TiOSO_4$, $\geq 29\%$ Ti (as TiO_2) basis, technical	Sigma Aldrich	14023
Sodium metasilicate	Na_2O_3Si	Sigma Aldrich	307815
Potassium hydroxide	KOH, $\geq 99\%$, beads	Carl Roth	9356
Hexadecyltrimethylammonium bromide	CTAB, BioXtra, $\geq99\%$	Sigma Aldrich	H9151
Nitric acid	HNO_3, 65%	Merck	100456
Sodium orthovanadate	Na_3O_4V, 99.9%	Alfa Aesar	81104
n-heptane	$H_3C(CH_2)_5CH_3$, $\geq 99\%$	Carl Roth	8654
1-hexanol	$CH_3(CH_2)_5OH$, anhydrous, $\geq 99\%$	Sigma Aldrich	471402
Bismuth(III) nitrate pentahydrate	$Bi(NO_3)_3 \cdot xH_2O$, 99.999% (metals basis)	Sigma Aldrich	254150
Ethanol	EtOH $\geq99.8\%$ absolute	Carl Roth	9065
Tin chloride dihydrate	$SnCl_2 \cdot 2H_2O$, 99.99%	Sigma Aldrich	431508
Titanium isopropoxide	$Ti[OCH(CH_3)_2]_4$	Sigma Aldrich	377996
Ethylene glycol	$C_2H_6O_2$ anhydrous, 99.9%	Sigma Aldrich	324558
Citric acid	$HOC(COOH)(CH_2COOH)_2$, 99%	Sigma Aldrich	C0759
Manganese(II)nitrate tetrahydrate	$Mn(NO_3)_2 \cdot 4H_2O$	Sigma Aldrich	M4519
Sodium carbonate	Na_2CO_3 , $\geq99.5\%$, ACS, anhydrous	Carl Roth	A135
Hydrochloric acid	HCl	Carl Roth	6792
Sodium tungstate dihydrate	$Na_2WO_4 \cdot 2H_2O$, BioUltra, $\geq99.0\%$ (T)	Sigma Aldrich	72069
Potassium permanganate	$KMnO_4$,99.0-100.5%, NORMAPUR®	VWR	26910
Sulfuric acid	H_2SO_4, 96% Solution in Water	Fischer Scientific	133610026
Ruthenium oxide	RuO_2, 99.99% trace metals basis	Sigma Aldrich	238058
Nafion® 117 solution	5 wt%	Sigma Aldrich	70160
Horseradish peroxidase	HRP	Sigma Aldrich	P6782
2,2'-azino-bis(3-ethylbenzothiazoline-6-sulfonic acid)	ABTS	Sigma Aldrich	A1888

Tab. 2.2 : *List of consumables used in this study.*

Consumable	Supplier	Product code
Carbon cloth	Quintech	W1S1005
Carbon fiber paper	Quintech	TP-060
Gas diffusion layer	Quintech	H23C9
Glassy carbon rod	Metrohm	61247000
Carbon felt	Alfa Aesar	43200
DIACHEM®Boron doped diamond on Silicon	Condias	DIACHEM®BDD/Si
DIACHEM®Boron doped diamond on Tantalum	Condias	DIACHEM®BDD/Ta
Sigracell® Bipolar plates	SGL Carbon	TF6
Sigracell® Bipolar plates	SGL Carbon	PV15
Sigracell® Bipolar plates	SGL Carbon	FR10
Copper plate	Advent Research Materials Ltd.	CU130839
Ti/Ir Mesh	-	-
Nafion® 117 membrane	Ion Power	-
Fumasep cation exchange membrane	Fumatech	FLK-PK-130
Ag/AgCl reference electrode (3.5 mol L^{-1} KCl)	eDAQ	ET072-1
Microflow cell	Electrocell	MFC30009V3
H-cell	Gassner GmbH	-

Tab. 2.3 : List of devices used in this study.

Device	Supplier	Model
Conductometer	VWR	pHenomenal® CO 3100 H
pH meter	VWR	pH 3210
Spectrophotometer	Shimadzu	UV-1800
Strip reader	Macherey-Nagel	Quantofix Relax
Peristaltic pump	Watson-Marlow	-
Potentiostat	Autolab	PGSTAT128N
Scanning electron microscope	Carl Zeiss	DSM 940 A
Thermogravimetric analyser	Linseis	TG 1000
X-ray diffractometer	Rigaku	MiniFlex 600
Centrifuge	Beckmann Coulter GmbH	Avanti J-E
Heat plate and magnetic stirrer	Heidolph	505-30000-00-3
Muffel Oven	Nabertherm	-
Sonicator	VWR	USC-TH
Balance 1	Ohaus	-
Balance 2	Ohaus	Discovery
Milli Q Ultrapure system	Merck	Elix
Ice Machine	Ziegra	151148

Tab. 2.4 : List of softwares used in this study.

Software	Supplier	Purpose
Word	Microsoft	Text processing
Excel	Microsoft	Data plotting and analysis
Origin	OriginLab Corporation	Data plotting and analysis
ChemDraw	PerkinElmer	Chemical drawing tool
Nova	Metrohm Autolab	Data collection and control
Inkscape	Inkscape	Image editing software
ImageJ	National Institutes of Health	Image processing program
Endnote	Clarivate Analytics	Referencing
Rigaku PDXL	Rigaku	XRD analysis

Herein, the synthesis of the materials, catalyst immobilization, and detection method are described as a part of **Section 3.1**. The material and methods used in **Section 3.2** to **3.4** are described in respective chapters.

2.2 Synthesis of metal oxides

Different metal oxides have been reported to be active towards $2e^-$ WOR to H_2O_2. These metal oxides are $BiVO_4$, SnO_2, TiO_2, MnO_x, and WO_3. These metal oxides were synthesized and used as catalysts for WOR to produce H_2O_2. All oxides were synthesized and characterized prior to electrochemical investigation. The characterization and the results of electrochemical investigation of these materials are discussed in **Section 3.1**. The metal oxides were prepared by the following methods.

2.2.1 Hydrothermal synthesis of bismuth vanadate (BiVO$_4$)

$BiVO_4$ was prepared via the hydrothermal method by dissolving 0.74 g hexadecyltrimethylammonium bromide in 25 mL of acidic solution (HNO_3, 2 mol L^{-1}) of sodium orthovanadate [68]. The solution was stirred for 10 minutes, followed by adding 10 mL of n-heptane and 2 mL of 1-hexanol to obtain a yellow emulsion. The solution was then stirred for 1 hour before adding 1 mL of an acidic solution (2 mol L^{-1} HNO_3) of bismuth(III) nitrate pentahydrate dropwise to the vanadate solution. After stirring for 30 minutes, the suspension was transferred to a stainless-steel autoclave and heated at 433 K for 48 hours. The obtained product was centrifuged and washed several times with deionized water and ethanol and dried in air at 373 K.

2.2.2 Polymeric precursor method (PPM) for tin oxide (SnO$_2$) and titanium oxide (TiO$_2$)

SnO_2 and TiO_2 were prepared using the polymeric precursor method [69][70]. Metallic citrate was obtained by adding 0.01 mol of tin chloride dihydrate for SnO_2 or titanium isopropoxide for TiO_2 in 100 mL aqueous citric acid solution, keeping a molar ratio of 1: 6 (metal: citric acid) at 333 K. The system was kept under constant stirring until its complete dissolution. Afterward, the temperature was increased to 353 K, and a known quantity of ethylene glycol corresponding to a mass ratio of 60: 40 (ethylene glycol: citric acid) was added to this solution. At this temperature, a polyesterification reaction occurs, producing a polymeric resin.

The crystalline SnO_2 and TiO_2 powder were obtained after different calcination stages. In the first step, called the pre-calcination, the polymeric resin was heated at 623 K for 4 hours using a heat rate of 283 K min^{-1}. This was done to eliminate a large amount of organic material, such as citric acid and ethylene glycol, used in the synthesis. The second step involved heat treatment for obtaining a crystalline phase for SnO_2 and TiO_2. The resulting material was manually de-agglomerated in an agate mortar and further heat-treated in an oven at 1073 K for 2 hours at a heating rate of 278 K min^{-1}.

2.2.3   Coprecipitation of MnO_x

Manganese oxide was prepared via a hydroxycarbonate precursor that was generated by precipitating manganese(II) nitrate tetrahydrate with sodium carbonate. The precipitation was performed in an automated LABMAX® system that allows controlling of reaction parameters (temperature, dosing rate of reactants, stirring) which ensures reproducible synthesis. In a typical procedure, 0.2 mol L^{-1} Mn(NO$_3$)$_2$ and 1.6 mol L^{-1} Na$_2$CO$_3$ were dosed in the reactor filled up with 1.5 L deionized water. The precipitation was carried out at pH intervals between 5.2 and 7 and a temperature at 333 K. After the dosing, the resulting suspension was aged in the mother liquor at 333 K for 2 hours. During the aging period, the color of the precipitate turned light brown, signaling partial decomposition of hydroxycarbonate to an oxide. At the end of aging, the suspension was cooled down. The precipitate was filtered off, washed with distilled water, dried at 378 K overnight, and calcined in a muffle furnace at 593 K.

2.2.4   Hydrothermal synthesis of tungsten oxide (WO$_3$)

30 mL of a 3 mol L^{-1} hydrochloric acid solution was slowly added to 30 mL of a 0.125 mol L^{-1} aqueous sodium tungstate dihydrate solution using a funnel [71]. After stirring for one hour, the yellow precipitate of tungstic acid (H$_2$WO$_4$) was separated using a centrifuge (3000 rpm for 10 minutes). The solid obtained was then transferred to a 100 mL autoclave and 60 mL of distilled H$_2$O. The autoclave was closed and placed at 453 K for 16 hours in the oven. After 16 hours, the autoclave was cooled down, and the final product was separated using a centrifuge (3000 rpm, 60 min). The final precipitate was washed with 60 mL of distilled water, separated by centrifugation, and dried under vacuum.

2.3   Electrode Preparation (Metal Oxide Immobilization)

The metal oxide nanoparticles were first made into an ink by sonicating 5 mg of the catalyst (BiVO$_4$, SnO$_2$, WO$_3$, MnO$_x$, TiO$_2$, and RuO$_2$) with 200 μL of deionized water, 7.6 μL of Nafion® 117 solution and 192.6 μL of isopropyl alcohol, for 30 minutes, followed by the coating of the ink onto a 1 x 1 cm^2 carbon paper via drop-casting method on a heating plate at 333 K and stored overnight [72]. The back side of the electrode was covered with a scotch tape. The geometric area of the anode used was 1 cm^2, and the catalyst loading was 5 mg cm^{-2}.

2.4 Electrode Characterization

2.4.1 Scanning Electron Microscopy (SEM)

The morphology of the oxides and electrode materials were investigated using scanning electron microscopy (SEM) at 20 kV and 6 mm working distance. A double-sided scotch tape was used to attach the sample to the sample holder. The surface was qualitatively revealed in SEM images. The thickness of each carbon material was measured with ImageJ from at least 10 different areas of an SEM image.

2.4.2 X-Ray Diffraction (XRD)

X-ray diffraction (XRD) patterns were obtained using a Rigaku MiniFlex 600 diffractometer, with Cu Kα radiation with a wavelength λ of 0.154 nm and a silicon strip detector D/teX Ultra and were operated at 40 kV and 15 mA. The analysis was conducted in the 2θ range from 3° to 100° with a scanning rate of 0.1^o min-1. The measurements were analyzed using the Rigaku PDXL software, and the data were compared with the Crystallography Open Database (COD).

2.4.3 Thermogravimetric measurements

Thermogravimetric measurements were performed in a Linseis Thermogravimetric analyser, TG 1000. All measurements were recorded from 293 to 1173 K, using a heating rate of 278 K min^{-1} under air atmosphere.

2.5 Hydrogen Peroxide Quantification

The analytic quantification of H_2O_2 in an electrochemical system can be influenced by the type of electrolyte, pH, and other interfering species generated at the electrode. Therefore we used two methods to detect H_2O_2: detection strips and an enzymatic ABTS assay.

2.5.1 Detection Strips

H_2O_2 concentration was determined by Quantofix 100 detection strips which turns blue in the presence of H_2O_2 (**Figure 2.1**) [73]. Color intensity is measured photometrically by the Quantofix relax strip reader.
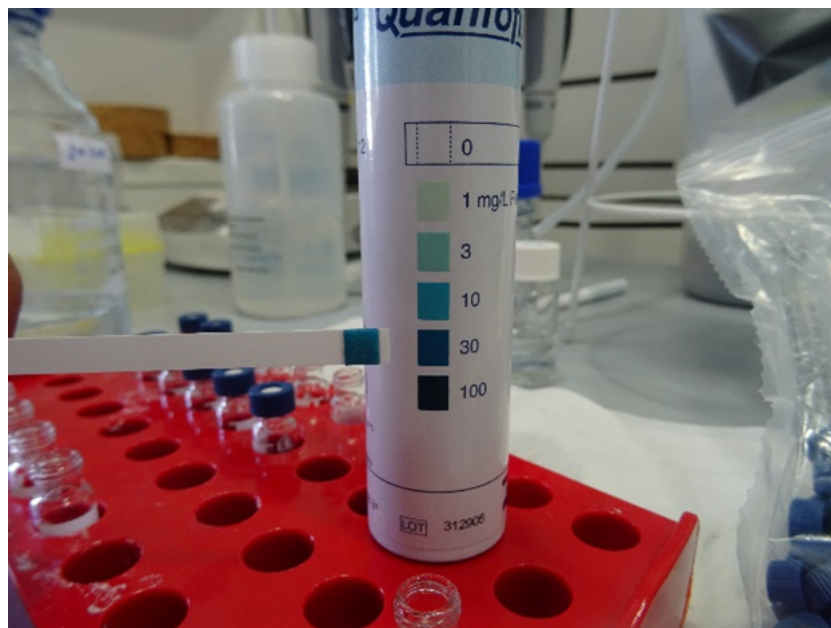
Fig. 2.1 : *Quantofix® detection strips for H_2O_2 quantification.*

2.5.2 ABTS Assay

An ABTS assay, where 2,2'-azino-bis(3-ethylbenzothiazoline-6-sulfonic acid) is used, provides more accurate H_2O_2 concentration estimates, especially for lower concentrations (as low as 1 μM). The one-electron oxidation of ABTS into $ABTS^+$ by H_2O_2 is catalyzed by horseradish peroxidase (HRP), as shown in **Equation 2.1**;

$$(2.1)$$
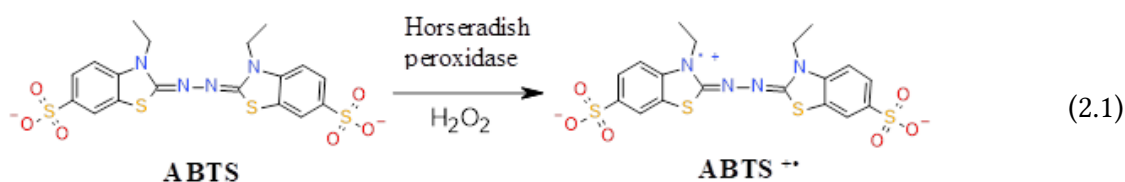
The reagents needed for the assay were first prepared fresh; 2 mmol L^{-1} ABTS (in 0.1 mol L^{-1} potassium phosphate buffer, KPi, pH 5.0) and 5 mg L^{-1} horseradish peroxidase (HRP). The ABTS assay was performed as follows: a 1 mL ABTS (colorless) solution was added to a standard cuvette, followed by the addition of 0.1 mL of the sample (typically H_2O_2; $KHCO_3$ for blank) and 0.1 mL of the HRP enzyme. This mixture was mixed well and then left undisturbed at 22 °C for 10 min. The absorbance of this (green) solution was measured at 405 nm using a UV-Vis spectrophotometer and the concentration was determined using the lambert beer equation (**Equation 2.2**). 0.5 mol L^{-1} $KHCO_3$ solution was used to make different concentrations of H_2O_2 in order to provide a calibration curve (**Figure 2.2**) [74][75]. The detection limit for this method is from 1 μmol L^{-1} to 1 mmol L^{-1}.

$$A = \epsilon Lc \qquad (2.2)$$

where A is the absorbance, ϵ is the molar extinction coefficient, L is the path length, and c is the concentration of the sample. The molar extinction coefficient (ϵ405nm) of oxidized ABTS is 36,800 L mol^{-1} cm^{-1} [76].
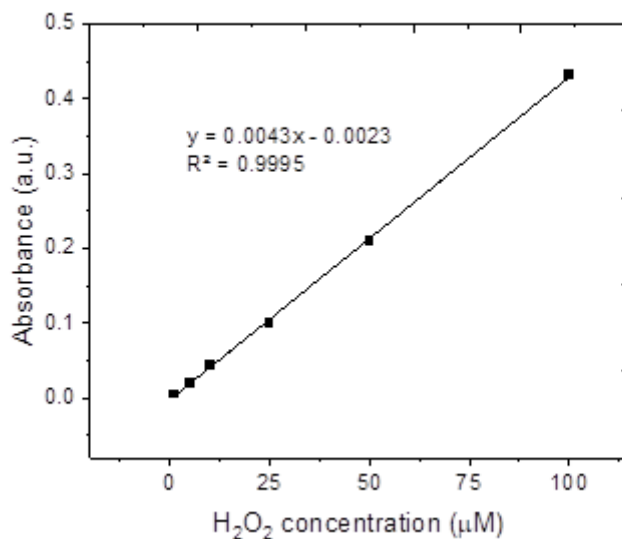

Fig. 2.2 : *Calibration curve to determine the H_2O_2 concentration using ABTS assay.*

2.5.3 TiOSO$_4$ colorimetry method

The TiOSO$_4$ method was used to quantify H_2O_2, as described in the literature [77][30][78]. The solution was prepared by mixing 0.1 mol L^{-1} TiOSO$_4$ in 2 mol L^{-1} H$_2$SO$_4$ before H_2O_2 detection. 25 μL of the H_2O_2 sample was mixed with 975 μL of a 0.1 mol L^{-1} TiOSO$_4$ solution in a standard cuvette. Upon the addition of H_2O_2, a color change from colorless to yellow occurs due to the formation of pertitanic acid (**Equation 2.3**). The absorbance of the solution was measured at 407 nm using a Shimadzu UV-1800 spectrophotometer. The molar extinction coefficient (ϵ407nm) is 6.89 x 10^2 L mol^{-1} cm^{-1} [79].

$$H_2O_2 + TiO_2{}^{2+} + H_2O \longrightarrow H_2TiO_4 + 2\,H^+ \tag{2.3}$$

2.6 Electrochemical experiments

Electrochemical characterizations including cyclic voltammetry (CV) and chronoamperometry (CA) were performed using an Autolab PGSTAT128N potentiostat/galvanostat with a 10 A booster controlled by the software NOVA 2.1 (Metrohm, Switzerland). For preliminary studies, a two-compartment H-cell divided by a Nafion®117 membrane was used. If not specified, a 2 mol L^{-1} sodium bicarbonate (KHCO$_3$, pH $\sim$8.4) was used as an electrolyte in both anodic and cathodic compartment. Each compartment of the H-cell was filled with 25 mL of electrolyte (**Figure 2.3**). The working electrode (metal

oxides on C-paper) with geometric area of 1 cm^2 was used. A 1.5 cm x 3 cm copper plate was chosen as a cathode and the reference electrode was a miniature Ag/AgCl Reference Electrode (eDAQ). The activities of synthesized BiVO$_4$, SnO$_2$, WO$_3$, MnO$_x$, TiO$_2$, and commercial RuO$_2$ catalysts were tested for the electrocatalytic oxidation of water to H$_2$O$_2$. Before each reaction, a CV was performed by sweeping the potential from OCP to + 2.0 V vs. Ag/AgCl at scan rate of 10 mV s^{-1}. H$_2$O$_2$ electrosynthesis was done potentiostatically by varying the potential from +1.2 V to +2.2 V vs. Ag/AgCl reference electrode for 10 minutes. A fresh electrolyte was used for each potential screening. The activity of the best material from the preliminary analysis was tested for long term. In order to compare it with the literature, the potentials are also reported against the reversible hydrogen electrode (RHE), calculated by the **Equation 2.4**.

$$\mathrm{E}_{(RHE)} = \mathrm{E}_{Ag/AgCl} + 0.059\,\mathrm{pH} + \mathrm{E^o}_{Ag/AgCl} \tag{2.4}$$

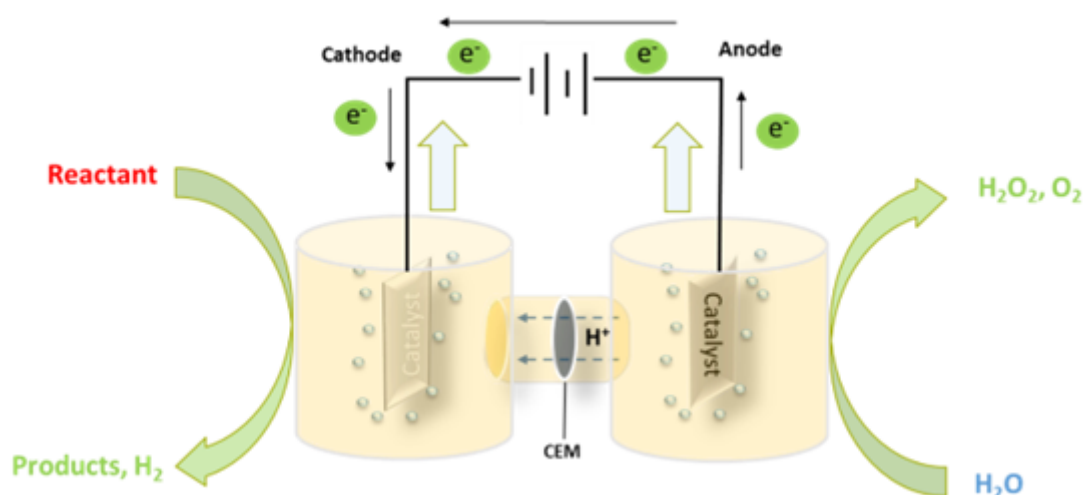where $\mathrm{E^o}_{Ag/AgCl}$ is equal to 0.1976 V

Fig. 2.3 : *Schematic diagram for the electrochemical H-cell used in this work.* *The reference electrode (RE) used is a mini-Ag/AgCl electrode. The counter electrode (CE) is a Cu-plate. The working electrode (WE) is metal oxide on a carbon substrate or pristine carbon paper.*

The activities of best materials from the preliminary analysis were tested with the flow cell. Carbon based materials were tested with a circular flow as shown in **Figure 2.4**. All the reactions were carried out at room temperature. Experiments underflow were performed using a microflow cell (Electrocell, Denmark). In this cell, 3 cm x 3.5 cm electrodes are separated by a Nafion®117 membrane. Carbonaceous electrodes were used as cathode and anode, respectively, with an electrode distance of 8 mm. 200 mL of electrolyte solution was circulated in each compartment with a 100 mL min^{-1} flow controlled by a flow pump from Watson-Marlow with a flow range from 5 mL min^{-1} to 120 mL min^{-1}.
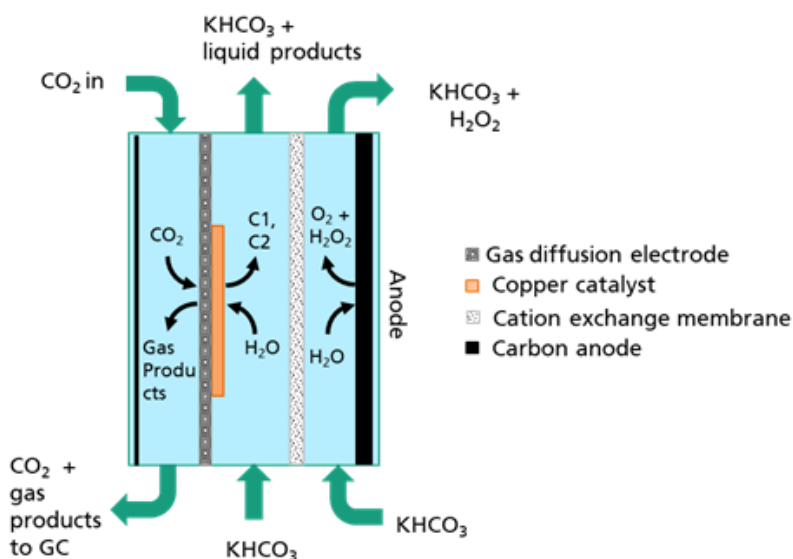
Fig. 2.4 : Schematic diagram for the electrochemical flow cell used in this work. *Flow cell with 10 cm^2 carbon electrodes (cathode and anode) at 8 mm electrode distance divided by a Nafion 117 membrane. The counter electrode (CE) is a Cu based electrode. The working electrode (WE) is a carbonaceous material.*

2.7 Calculations

The faradaic efficiency (FE) of the produced H_2O_2 was calculated by the following equation (**Equation 2.5**):

$$FE(\%) = \frac{H_2O_2 \text{ detected (in mol)} \times \text{ no. of electrons } \times \text{ Faraday constant (C mol}^{-1})}{\text{total charge passed (C)}} \times 100 \quad (2.5)$$
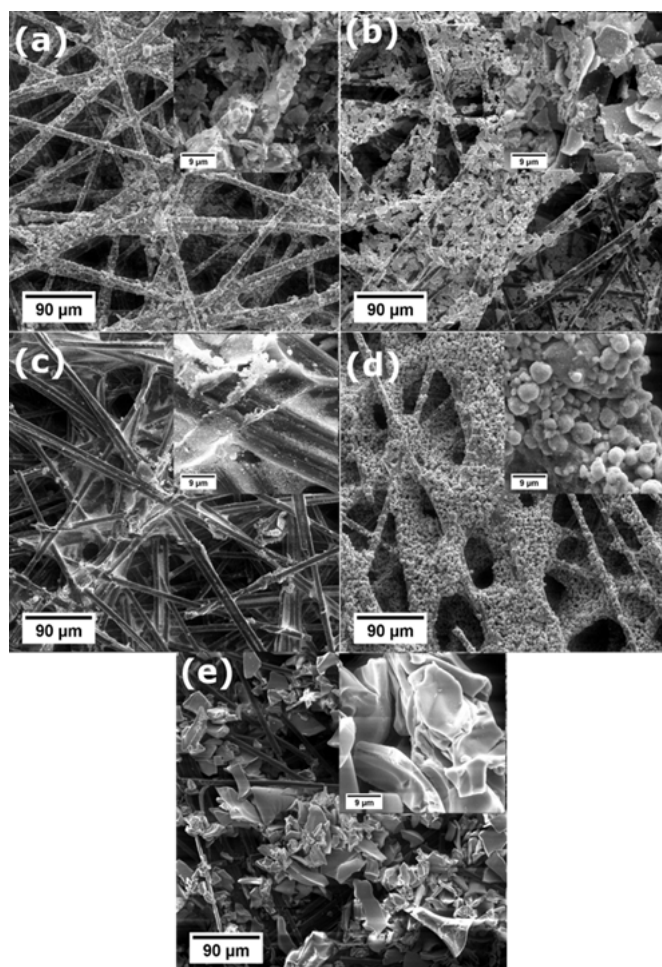
where the number of electrons is 2 for water oxidation to H_2O_2, and the Faraday constant is 96485 C mol^{-1}.

The production rate of the H_2O_2 produced is given by **Equation 2.6**:

$$\text{Production rate } (\mu\text{mol min}^{-1}\text{cm}^{-2}) = \frac{H_2O_2 \text{ detected (in } \mu\text{mol)}}{\text{time (min)} \times \text{ area of the electrode (cm}^2)} \quad (2.6)$$

3. RESULTS

3.1 $2e^-$ water oxidation to H_2O_2 using different metal oxides

In this chapter, material characterization of different synthesized metal oxides (Chapter 2) was performed, followed by the investigation of the electrochemical activity of these materials toward H_2O_2 production. Briefly, this chapter includes material characterization (XRD, SEM, and EDX), electrochemical characterization (linear sweep voltammetry (LSV), and chronoamperometry (CA)). This investigation aims to define the most effective catalyst for H_2O_2 production within the oxide material group of $BiVO_4$, SnO_2, WO_3, MnO_x, and TiO_2 immobilized on carbon paper. These synthesized materials were compared with commercial RuO_2 and blank carbon substrate. In the end, the long-term stability of the best material was investigated and reported in this chapter.

3.1.1 Material characterization

The structural morphology and the elemental analysis for the synthesized material were performed by SEM and EDX. The typical morphology of all the metal oxides is shown in Figure 1a-e. The morphological differences among all the metal oxide powders are clear from the SEM images (**Table 3.1** and **Figures 3.1a-e**).

Tab. 3.1 : SEM results for investigated metal oxides.

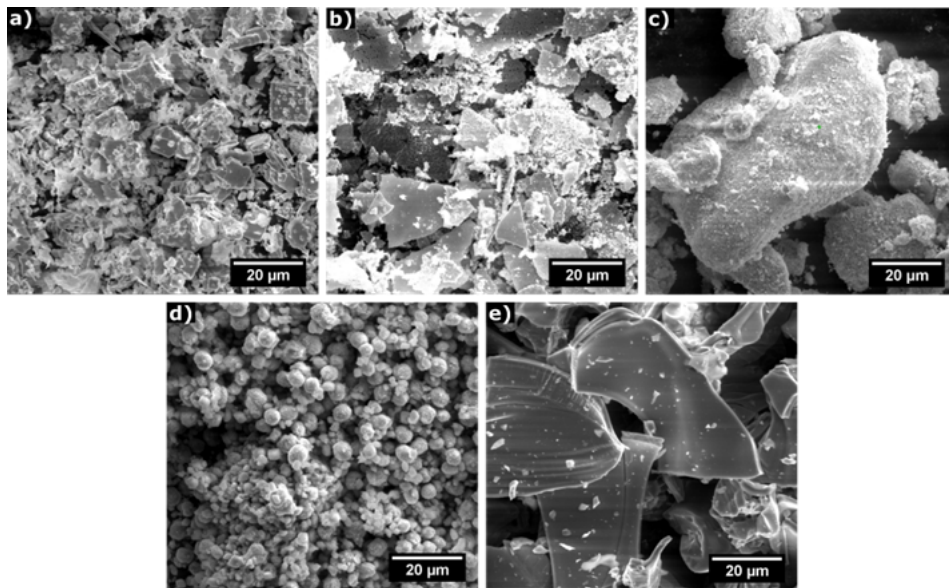| Metal oxide	SEM observation
$BiVO_4$	mixture of huge flat and defined particles, surrounded by smaller undefined particles
SnO_2	mixture of huger flat, defined particles (more sharp-edged than in BiVO4)
WO_3	uniform, porous-like surface of rounded
MnO_x	defined spherical
TiO_2	chiseled, sharp-edged, and flat

Fig. 3.1 : SEM images of (a) $BiVO_4$, (b) SnO_2, (c) WO_3, (d) MnO_x, and (e) TiO_2

The corresponding energy-dispersive X-ray spectroscopy (EDX) result is shown in **Figure 3.2**. The energy-dispersive X-ray spectroscopy revealed O, Bi, and V elements existed with an atomic ratio of C/O/V/Bi of 13:40:25:22 for $BiVO_4$. $BiVO_4$ had different atomic ratios of its constituent elements as observed in EDX analysis. One possible explanation is that the sample may have been synthesized under different conditions, such as temperature, pressure, and pH, which could affect the distribution of elements in the material. Another possibility is that there may be impurities or defects in the sample that could contribute to the observed variations in atomic ratios. Additionally, the EDX analysis may

have been performed on different regions of the sample, which could also result in differences in atomic ratios. Therefore, XRD analysis was also done, which has been discussed. In the case of SnO_2, the atomic ratio for C/O/Sn was 20:61:19, for WO_3 was 20:64:16 (C:O:W), for MnO_x was 2:37:61 (C:O:Mn), and for TiO_2 was 22:78 (O:Ti). The carbon content was presumably from the double-sided carbon tape used to immobilize the SEM sample stub.
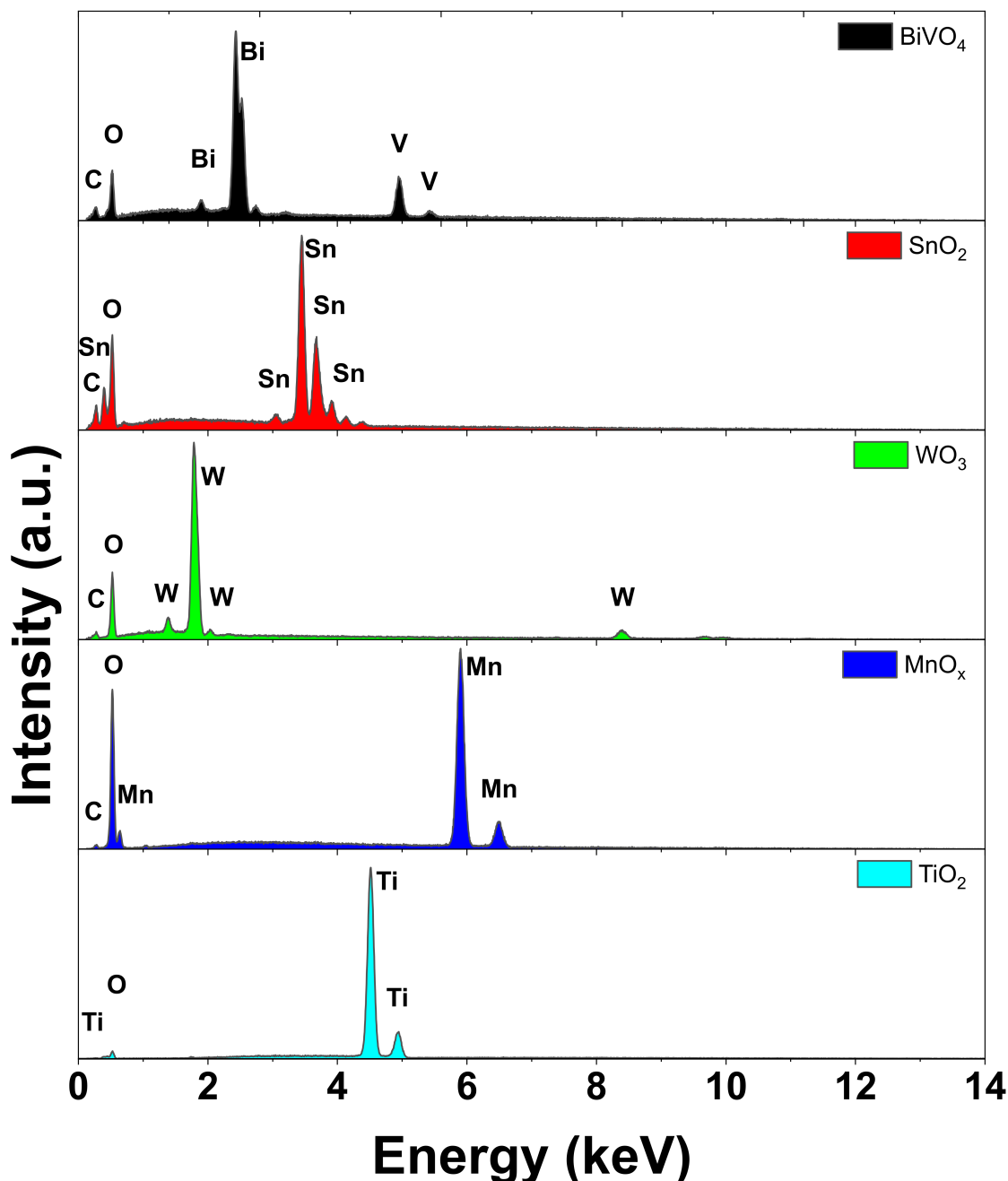

Fig. 3.2 : *EDX scan of different metal oxides used in this work*

The crystalline structure of the as-prepared $BiVO_4$, SnO_2, WO_3, MnO_x, and TiO_2, powders were evaluated by powder X-ray diffraction (XRD) patterns (**Figure 3.3**). XRD patterns of $BiVO_4$ powder prepared by hydrothermal synthesis revealed a polycrystalline nature (**Figure 3.3a**). The samples

exhibited the peaks characteristic of the $BiVO_4$ monoclinic phase (a = 5.193 Å, b = 5.0898 Å, c = 11.6972 Å) with space group *I112/b*. Some diffraction peaks, approximately at 32.26^o and 57.17^o, were ascribed to the $B_{11}VO_{19}$ cubic structure (a = b = c = 16.6434 Å) with space group *Fm-3m*. A third phase was also identified in the XRD patterns by the appearance of the diffraction peaks at 2θ = 10.96^o, 25.21^o, and 31.77^o ascribed to the BiV_8O_{16} tetragonal structure (a = b = 9.9331 Å, c = 2.9116 Å) with a space group *I4/m*.

XRD pattern of the SnO_2 powder (**Figure 3.3b**) indicated that all diffraction peaks could be perfectly indexed to a rutile SnO_2 tetragonal structure (a = b = 4.7357 Å, c = 3.1873 Å) with a space group P42/mnm. In case of WO_3, the XRD pattern revealed the orthorhombic WO_3 structure (a = 7.3590 Å, b = 12.5130 Å, c = 7.7040 Å) with a space group *Fmm2* (**Figure 3.3c**). XRD pattern of MnO_x powder (**Figure 3.3d**) prepared by the co-precipitation method can be perfectly indexed to a Hausmannite Mn_3O_4 tetragonal structure (a = b = 5.7691 Å, c = 9.4604 Å) with space group *I4_1/amd*. XRD pattern of TiO_2 powder prepared by PPM can be seen in as shown in **Figure 3.3e**. The obtained results show that the observed XRD peaks are perfectly indexed to a tetragonal rutile structure (a = b = 4.5933Å, c = 9.5139Å) with space group *P4_2/mnm*. Some diffraction peaks were also observed at 2θ approximately 25.33^o, 37.77^o, 48.10^o, 53.90^o, 54.88^o, 62.75^o and 75.01^o ascribed to the planes (101), (004), (200), (105), (211), (204) and (215), respectively, which can be indexed as tetragonal anatase TiO_2 crystalline secondary phase (a = b = 3.7852 Å, c = 9.5139 Å) with space group *I4_1/amd*.
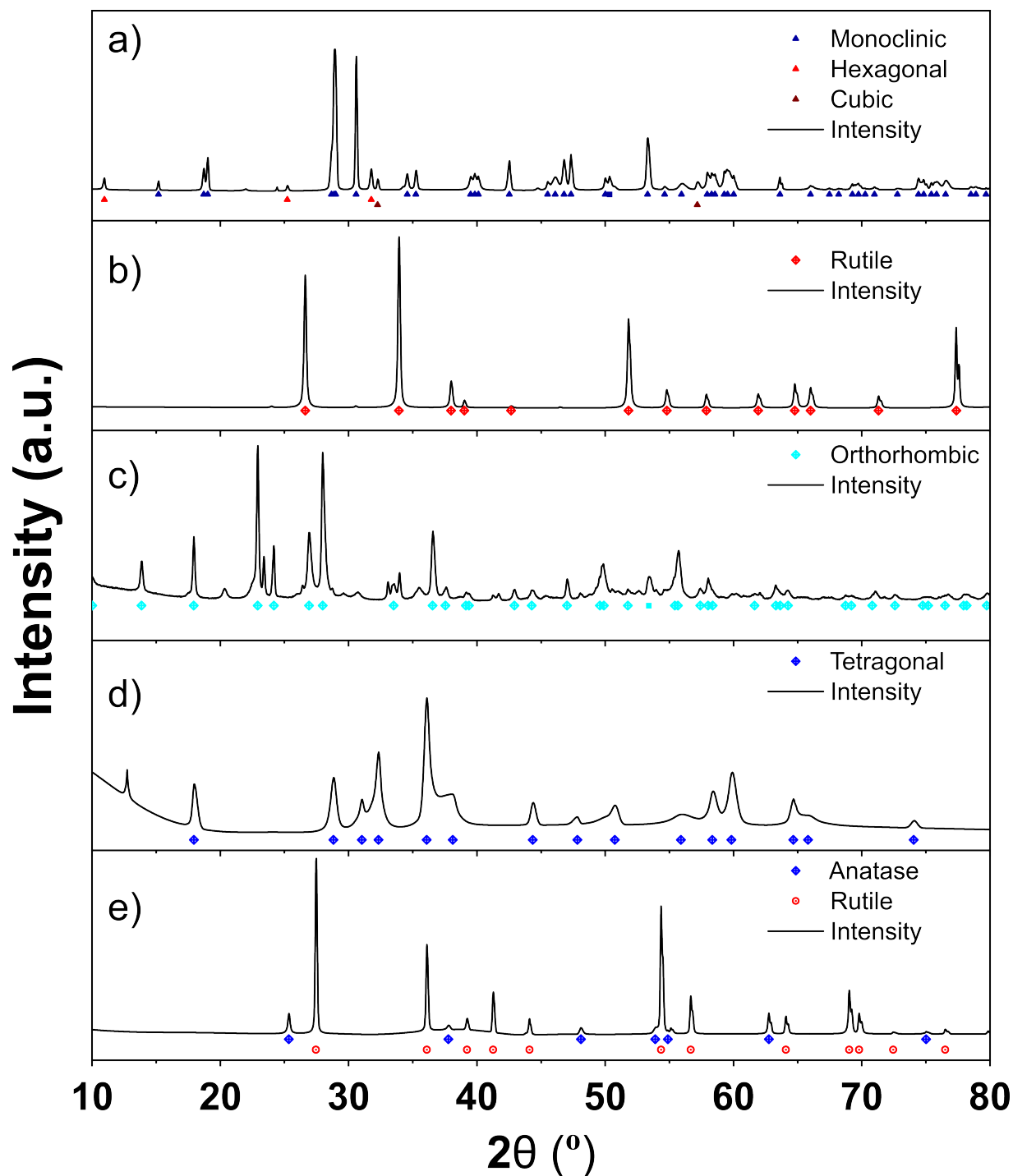
Fig. 3.3 : *XRD pattern for (a) BiVO$_4$, (b) SnO$_2$, (c) WO$_3$, (d) MnO$_x$, and (e) TiO$_2$*

Based on the characterization of these materials, all synthesized materials obtained the expected material properties. The material analysis was followed by the electrochemical characterization and investigation of the activity of these materials towards the 2e- oxidation of H_2O to H_2O_2.

3.1.2   Electrochemical measurements

Linear sweep voltammograms (LSV) for the all the metal oxides as well as for the carbon substrate were performed in 2 mol L^{-1} of KHCO$_3$ and are shown in **Figure 3.4**. RuO$_2$, which is known to be an

efficient O_2 evolution catalyst, had the lowest on-set potential ($\sim$0.95 V vs. Ag/AgCl), as compared to MnO_x ($\sim$1.05 V vs. Ag/AgCl), $BiVO_4$ ($\sim$1.16 V vs. Ag/AgCl), SnO_2 ($\sim$1.175 V vs. Ag/AgCl), WO_3 ($\sim$1.21 V vs. Ag/AgCl), and TiO_2 ($\sim$1.25 V vs. Ag/AgCl). The onset potential is described as the potential where the current density reached 1 mA cm^{-2}. The onset potential of blank carbon substrate was more positive ($\sim$1.45 V vs. Ag/AgCl) as compared to all metal oxides studied, indicating the effectiveness of the metal oxides to oxidize water. Increase in potential lead to increase in the current densities for all metal oxides, along with the increase in O_2 evolution seen visually.
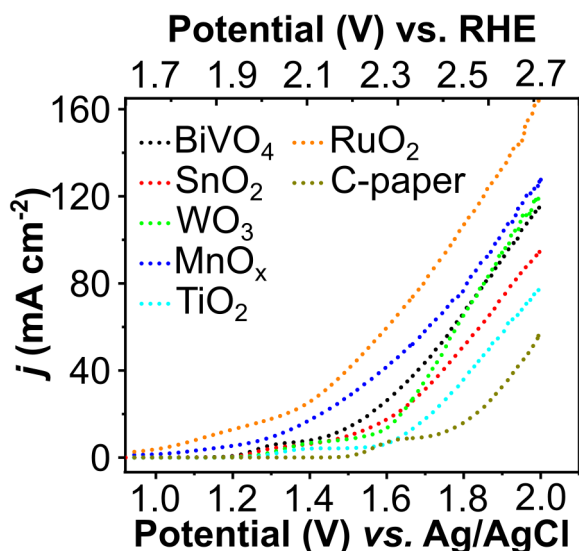

Fig. 3.4 : *Linear sweep voltammograms (LSV) during water oxidation using different metal oxides on carbon substrate in 2 mol L^{-1} KHCO$_3$ electrolyte at 10 mV s^{-1}*

To further optimize, potential screening was performed with the different metal oxides electrodes by varying the potentials from 1.2 V to 2.2 V vs. Ag/AgCl for the electrocatalytic water oxidation to H_2O_2 (**Figure 3.5a**). As expected, the H_2O_2 concentration increased with the increase in the potential for all metal oxides. $BiVO_4$ showed the best activity with the highest concentration of 546 μmol L^{-1} for H_2O_2 at 2.2 V vs. Ag/AgCl, whereas the H_2O_2 concentration was 451, 400, 342, 24, and 7 μmol L^{-1} for WO_3, SnO_2, TiO_2, MnO_x, and RuO_2 respectively, all within 10 min of electrolysis. The corresponding H_2O_2 concentration vs. current density revealed that with the increase in potential, the current density increased and so as the H_2O_2 concentration (**Figure 3.5b**). However, it should be noted that RuO_2 showed the highest current density at 311 mA cm^{-2}, though no H_2O_2 concentration was detected. RuO_2 is known to be a good OER catalyst, and this experimental result shows that regardless the current density in case of RuO_2 is higher, it is not selective towards H_2O_2 generation [80]. Except RuO_2, the corresponding production rates (**Figure 3.5c**) for other metal oxides increased with increase in the potential for all the materials investigated. The highest production rate per geometric area of electrode for $BiVO_4$, WO_3, SnO_2, TiO_2, MnO_x, and RuO_2 were 1.36, 1.12, 1.00, 0.8,

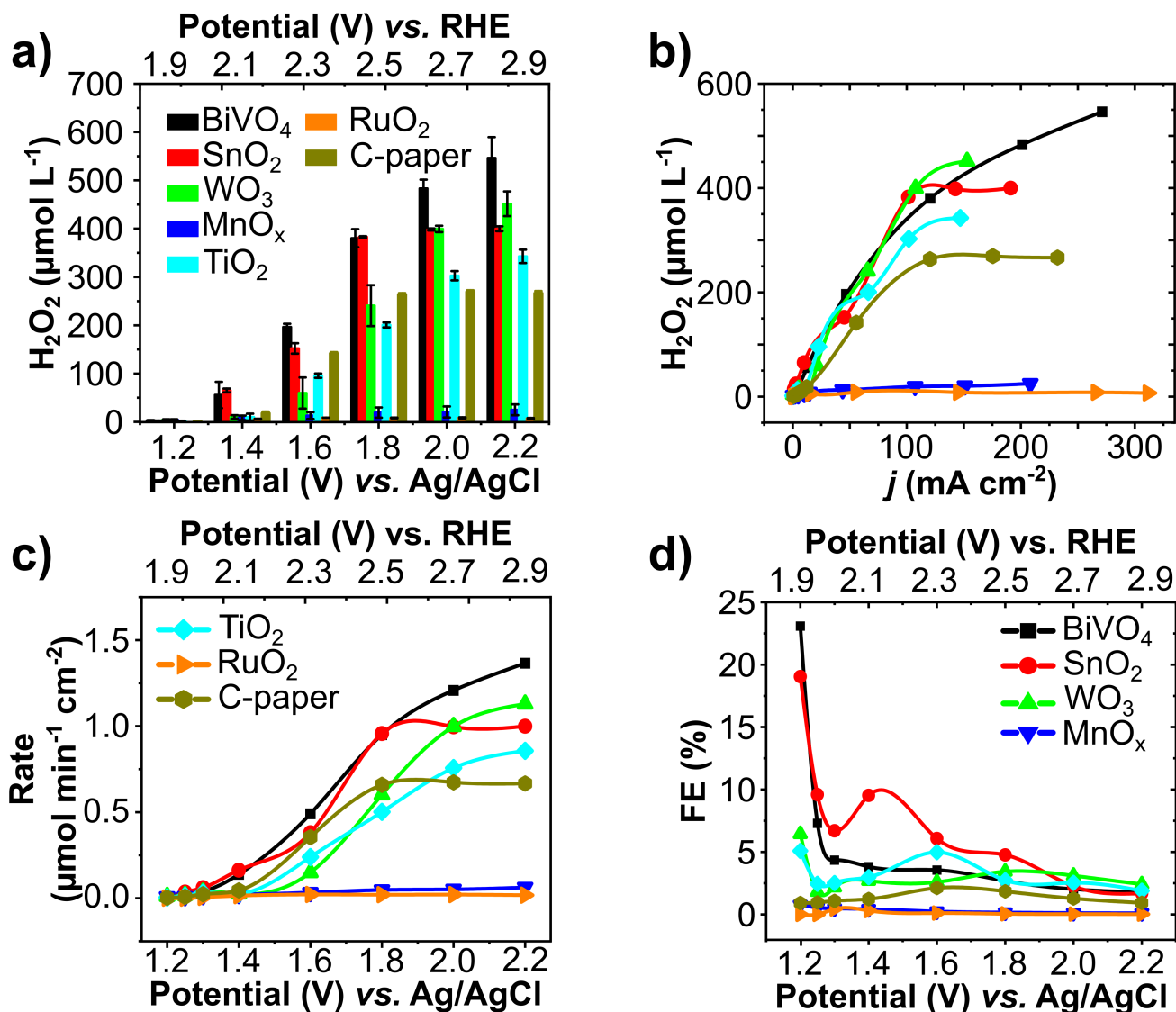0.82, 0.06, and 0.02 μmol min^{-1} cm^{-2} respectively.

Fig. 3.5 : *(a) H_2O_2 concentration vs. potential change and (b) current density for 10 minutes using the indicated metal oxide on carbon substrate using 2 mol L^{-1} $KHCO_3$ as an electrolyte (c) rate and (d) FE towards H_2O_2 production on different metal oxides in a two compartment H-cell.*

Although the current densities attained in this study are relatively higher than the one reported in the literature, the faradaic efficiencies (FE) are extremely lower as can be seen in **Figure 3.5d** and in Appendix A1, Table A1-4. For each metal oxide, the faradaic efficiency for H_2O_2 production decreased with increase in the potential. At 1.2 V vs. Ag/AgCl, for BiVO$_4$, the FE was $\sim$23%, which gradually decreased to 1.7% at 2.2 V vs. Ag/AgCl. Nevertheless, BiVO$_4$ turned out to be the best material amongst the investigated materials with maximum concentration of 546 μmol L^{-1} and FE of 23%. These results clearly demonstrate the predominance of H_2O_2 generation using the BiVO$_4$ electrode and its good activity compared to the metal oxides such as MnO$_x$ or RuO$_2$, as also reported in other study [52].

It should be noted that the high FE reported using metal oxides are as high as 81%, however, the corresponding current densities are as low as 15 mA cm^{-2} [51][52][53][54][57][59]. As soon as the current density is increased, it results in loss of FE and thus overall performance of the system, raising concerns on its industrial/commercial implementation. Further work was done to improve the catalyst immobilization on different substrate and has been reported in the Master Thesis of Thomas Stiller.

3.2   *Anodic production of hydrogen peroxide using commercial carbon materials*

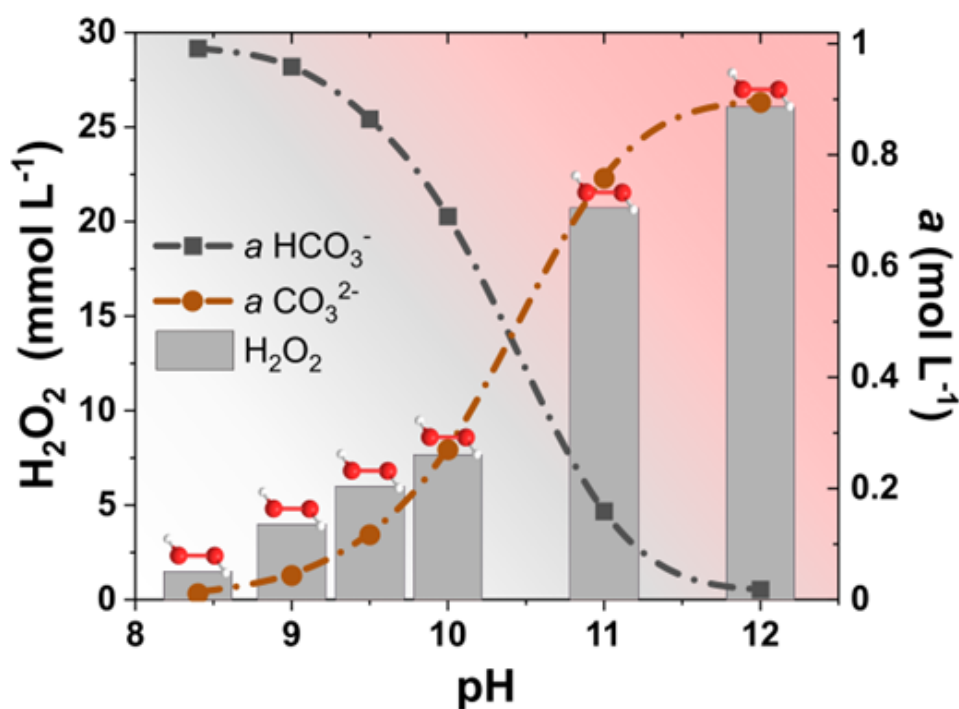Title: Anodic production of hydrogen peroxide using commercial carbon materials

Status: Published (2022)

Journal: Applied Catalysis B: Environmental

Publisher: Elsevier

Authors: Dhananjai Pangotra, Lénárd-István Csepei, Arne Roth, Carlos Ponce de León, Volker Sieber, Luciana Vieira

In this publication, optimization of the electrolyte conditions to achieve higher H_2O_2 concentrations was performed. Firstly, different inexpensive commercial carbon materials were screened for the activity towards the $2e^-$ water oxidation to H_2O_2 in a two-compartment H-cell. The most active material, the carbon fiber paper (CFP), was further used for the optimization of electrolyte conditions. These optimized operating conditions enabled the maximization of the activity, selectivity, efficiency, and stability of the electrochemical process, aiming high H_2O_2 concentration. A 10 cm^2 flow cell, offering more relevant operational conditions in the light of potential future applications and scale-up was used to study the impact of current density (j) and potential variation, pH control, electrolyte

concentration, and the presence of a chemical stabilizer. Calculation of ions' activities in bicarbonate electrolytes suggests a direct relationship between the CO_3^{2-} ions activity and an enhanced anodic H_2O_2 production. Through a direct interplay of CO_3^{2-} ions and Na_2SiO_3 as a chemical stabilizer, we have reached up to 33 mmol L^{-1} H_2O_2 in the anolyte at pH 12.6, the highest H_2O_2 ever achieved in such media. A cyclic mechanism based on the electrochemical formation of peroxodicarbonate is proposed. The experimental methodology and materials characterization are described in detail. These operating conditions can be readily used with any foremost catalyst to boost anodic H_2O_2 production.

Dhananjai Pangotra conceptualized and designed the experiment, performed all the lab work, did the data analysis, and wrote the first draft. Lénárd-István Csepei, Arne Roth, and Luciana Vieira supported the conceptualization. Lénárd—István Csepei did the calculation of the ionic activities of different carbonate species. Lénárd—István Csepei, Arne Roth, Carlos Ponce de León, Volker Sieber, and Luciana Vieira reviewed this work. Arne Roth, Volker Sieber, and Luciana Vieira supervised the research.

BACK   CLOSE WINDOW

Anodic production of hydrogen peroxide using commercial carbon materials

Dhananjai Pangotra [a,b], Lénárd-István Csepei [a], Arne Roth [a], Carlos Ponce de León [c], Volker Sieber [a,b], Luciana Vieira [a,*]

[a] *Fraunhofer Institute of Interfacial Engineering and Biotechnology IGB, Bio-, Electro-, and Chemocatalysis BioCat, Straubing Branch, Schulgasse 11a, 94315, Straubing, Germany*
[b] *Chair of Chemistry for Biogenic Resources, Campus Straubing for Biotechnology and Sustainability, Technical University of Munich, Schulgasse 16, 94315, Straubing, Germany*
[c] *Electrochemical Engineering Laboratory, Faculty of Engineering and Physical Sciences, University of Southampton, Highfield, Southampton SO17 1BJ, United Kingdom*

ARTICLE INFO

ABSTRACT

The electrochemical production of hydrogen peroxide (H_2O_2) from water is an appealing alternative to substitute the classic anthraquinone process. Herein, we show a process development to maximize the efficiency of the anodic production of H_2O_2. Carbon materials were used as anodes to optimize process parameters such as current density, electrolyte concentration, and the pH. We found that the electrolyte concentration, pH, and the presence of a chemical stabilizer have a substantial effect on the selectivity of water oxidation to H_2O_2. The addition of Na_2SiO_3 as a stabilizer increased the H_2O_2 production significantly at high pH regimes. A direct relationship between CO_3^{2-} ion activity and enhanced production of H_2O_2 was also observed. We report H_2O_2 concentrations in the anolyte up to 33 mmol L^{-1} at a current density of 100 mA cm^{-2} using commercial and low-cost carbon fiber paper.

1. Introduction

Hydrogen peroxide (H_2O_2) is a widely used industrial product. Because its decomposition generates oxygen (O_2) and water (H_2O) only, it is widely praised as a "green oxidant". It is used as an oxidizing agent in the chemical industry [1–3], in wastewater treatment [4,5], and as a propellant in the aerospace industry [6–8]. In refineries, H_2O_2 is applied for oxidative desulfurization of oil fractions to meet regulations referring to transportation fuels [9–13]. Changes in the limit of sulfur established by the International Maritime Organization (IMO) may lead to an exponential increase in H_2O_2 demand in this sector [14–16]. H_2O_2 also has a biocidal effect [17], thus it is used in low concentrations as a component of antiseptics [18] and hand sanitizers certified by the World Health Organization [19]. Recent research shows its promising results in the disinfection of personal protective equipment against the SARS-CoV-2 and COVID-19 virus [20–22]. While the healthcare industry's application was considered a relatively minor market, after the outbreak of COVID-19, the H_2O_2 demand in this branch increased dramatically [23].

Currently, H_2O_2 is produced via the anthraquinone (AO) process, an energy-demanding multistep method that requires large quantities of harmful organic solvents and fossil-based hydrogen [24,25]. Therefore, developing an alternate "green" route for H_2O_2 production is a subject of high scientific and economic interest [13]. The electrochemical synthesis of H_2O_2 from renewable electricity and naturally abundant educts O_2 and H_2O is a promising pathway compared to the current AO process [7]. There are two possible electrochemical routes for H_2O_2 production, i.e., via cathodic and anodic reactions. The cathodic route is based on the O_2 reduction in an aqueous medium (Eq. (1)) using catalysts based on carbon [26–29], noble metals (Au, Ag [7] and Pd [30]), noble metal alloys (e.g. Pt-Hg [31], Pd-Au [32]) or compounds like PtP$_2$ [33]. From the perspective of minimizing process costs, non-noble metal-based electrocatalysts such as Ni$_3$B are more attractive [34]. Many reactor designs, including pressurized-jet microfluidic flow-through reactor, have been developed to enhance O_2 solubility, maximizing reaction efficiency, and reducing energy consumption [35,36]. The anodic formation of H_2O_2 proceeds via two-electron oxidation of water (Eq. (2)) at the anode [7,37]. This anodic route is particularly promising because it can be combined with many cathodic reactions, including the cathodic production of H_2O_2 via oxygen reduction reaction (ORR), hydrogen
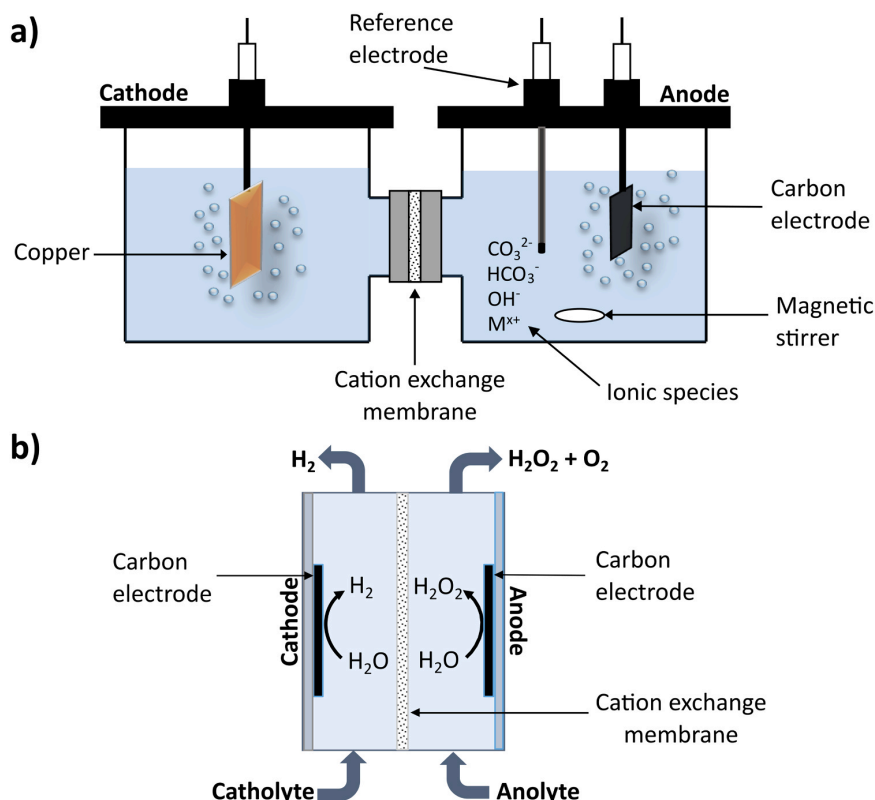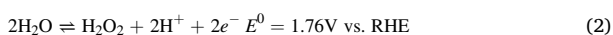
Fig. 1. Schematic representation of the utilized electrochemical cells. (a) H-cell equipped with a 1 cm^2 carbon anode and a 7.5 cm^2 cm copper plate cathode at 6 cm distance. (b) Flow cell with 10 cm^2 carbon electrodes (cathode and anode) at 8 mm electrode distance. 200 mL of the electrolyte solution in a reservoir was used in each flow cell compartment circulating at a rate of 100 mL min^{-1}. Both cells were separated by a Nafion 117 membrane.

evolution reaction (HER), and CO$_2$ reduction reaction (CO$_2$RR), thus enabling productive utilization of both half-cell reactions.

$$O_2 + 2H^+ + 2e^- \rightarrow H_2O_2 \; E^0 = 0.67V \text{ vs. RHE} \quad (1)$$

$$2H_2O \rightleftharpoons H_2O_2 + 2H^+ + 2e^- \; E^0 = 1.76V \text{ vs. RHE} \quad (2)$$

Recent research efforts regarding the anodic production of H$_2$O$_2$ have focused on catalyst materials and electrode development to enable high selectivity towards H$_2$O$_2$. Various metal oxides, including BiVO$_4$, CaSnO$_3$, ZnO, WO$_3$, SnO$_2$, and TiO$_2$, have been reported as active electrocatalysts for the anodic synthesis of H$_2$O$_2$ [37–42]. High faradaic efficiencies (up to 80%) have been reported for those systems, albeit only at low current densities (0.1–15 mA cm^{-2}) [37–42] with H$_2$O$_2$ production rate up to 5.7 μmol min^{-1} cm^{-2} [38]. Carbon-based materials coated with hydrophobic polymers (PTFE/CFP) have shown exceptional catalytic performance in terms of activity and electrode stability, with an excellent production rate of 23.4 μmol min^{-1} cm^{-2} in 1 mol L^{-1} Na$_2$CO$_3$ [43]. Boron-doped diamond (BDD) electrodes have also been reported as remarkable materials for water oxidation to H$_2$O$_2$, with outstanding production rates of 19.7 μmol min^{-1} cm^{-2} in 2 mol L^{-1} KHCO$_3$ [44]. Yet, the electrochemical oxidation of water to H$_2$O$_2$ depends not only on the choice of the electrode material but also on reaction parameters, particularly the current/potential applied, electrolyte concentration, pH, and H$_2$O$_2$ stabilizers [45,46].

The highest H$_2$O$_2$ concentration ever achieved by electrochemical methods was 20 wt% H$_2$O$_2$ solution via electrochemical O$_2$ reduction using a solid electrolyte setup [47]. With this exception, the concentration of H$_2$O$_2$ produced electrochemically is, in general, relatively low compared to that achievable by the current AO process. Nevertheless,

the relatively lower H$_2$O$_2$ concentrations achieved electrochemically are already promising for healthcare and environmental applications. Moreover, the electrochemical route would enable the decentralization of H$_2$O$_2$ production, requiring only an electrochemical device and electricity [45]. Decentralized electrocatalytic H$_2$O$_2$ production could be an enabling technology for local disinfectant production in the concept of future hospitals [48] as well as in remote places in the fight against COVID-19, SARS-CoV-2, MERS [49,50], Ebola [49,51], and Zika [49] viruses. Furthermore, an integrated solar-electricity-driven water treatment process would enable removing recalcitrant chemicals [52–54] and bacteria [54,55].

This study identifies and applies optimized electrolyte conditions for the anodic oxidation of water to H$_2$O$_2$. These optimized operating conditions enabled the maximization of the activity, selectivity, efficiency, and stability of the electrochemical process, aiming high H$_2$O$_2$ concentration. We have used unmodified commercial carbon materials as electrocatalysts due to their high surface area, relatively high conductivity, and chemical stability in alkaline electrolytes. These carbon materials are easy to use and have considerably low costs. Firstly, different carbon materials were screened for their catalytic activity in a two-compartment stationary H-cell. Carbon cloth, carbon fiber paper, carbon felt, glassy carbon, and carbon gas diffusion layer were used as electrode materials. Outperforming material was further investigated in a 10 cm^2 flow cell, offering more relevant operational conditions in the light of potential future applications and scale-up. The impact of current density (*j*) and potential variation, pH control, electrolyte concentration, and the presence of a chemical stabilizer has been analyzed and the most suitable reaction parameters for the anodic production of H$_2$O$_2$ in high concentrations have been identified. Additionally, the impact of HCO$_3^-$

and CO_3^{2-} ions' activity in the electrolyte on the electrochemical H_2O_2 production was examined, indicating clearly the importance of CO_3^{2-} ions for the anodic H_2O_2 production.

2. Material and methods

2.1. Characterization

The surface morphology of all the different carbon materials was examined by a scanning electron microscope (SEM Carl Zeiss DSM 940A Oberkochen, Germany) at 20 kV and 6 mm working distance. The electrode materials were placed onto a carbon tape on top of an alumina
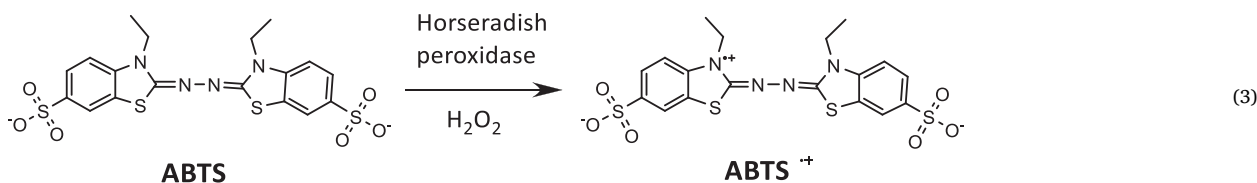

$$ \text{(3)} $$

plate sample holder. The thickness of each carbon material was measured with ImageJ from at least 10 different areas of an SEM image.

2.2. Electrochemical measurements

Electrochemical measurements were performed at room temperature and atmospheric pressure using an Autolab PGSTAT128N potentiostat/galvanostat coupled with a 10 A booster. Screening experiments were performed in a two-compartment H-Cell (Fig. 1a) with a three-electrode configuration separated by an ion-exchange membrane (Nafion 117, Ion Power, Germany). Carbon cloth (W1S1005), carbon fiber paper (TP-060), gas diffusion layer (Freudenberg, H23C9), all from Quintech, Germany, glassy carbon rod (Metrohm, 61247000) and carbon felt (Alfa Aesar, 43200) were used as electrodes without further treatment. Carbon samples with a geometric area of 1 cm^2 were used as anode, 7.5 cm^2 copper plate as cathode, and Ag/AgCl in 3.5 mol L^{-1} KCl (eDAQ) as a reference electrode. 25 mL of 2 mol L^{-1} potassium hydrogen carbonate (KHCO$_3$, Sigma Aldrich, 99.5%) was chosen as standard electrolyte [41] and was freshly prepared prior to each experiment. Linear sweep voltammetry (LSV) at 10 mV s^{-1} and chronopotentiometry at 50 mA cm^{-2} (related to the geometric area of the anode) were measured for each carbon material. The cell potential was recorded with a voltammeter. The pH of the electrolyte was regulated with the addition of potassium hydroxide (KOH, Carl Roth) salt or CO$_2$ bubbling. The electrolyte conductivity was measured with a conductometer (VWR pHenomenal® CO 3100 H) and the pH with a pH-meter (VWR pH 3210). Potassium carbonate (K$_2$CO$_3$, ≥99%, Carl Roth) and sodium metasilicate (Na$_2$SiO$_3$, Sigma Aldrich) were used as received.

After the material screening, the best performing electrode was evaluated by chronoamperometry with multiple potential steps. The concentration of H$_2$O$_2$ was measured at each step potential, in intervals of 0.2 V from +1.2 V to +2 V vs. Ag/AgCl, with 10 min at each step. The corresponding current densities were calculated using the geometric area of the electrode.

Flow cell experiments were carried out in a Microflow cell

(Electrocell, Denmark) (Fig. 1b) with 10 cm^2 (3 cm × 3.5 cm) electrodes separated by a Nafion 117 cation exchange membrane (CEM). 200 mL of the electrolyte solution was circulated in each compartment with a 100 mL min^{-1} flow controlled by a flow pump (Watson-Marlow) in a flow range varying from 2 to 120 mL min^{-1}.

2.3. H$_2$O$_2$ analysis

The analytic quantification of H$_2$O$_2$ in an electrochemical system can be influenced by the type of electrolyte, pH, and other interfering species generated at the electrode [56]. Therefore we used three methods to detect H$_2$O$_2$: an enzymatic assay, detection strips, and KMnO$_4$ titration.

The enzymatic assay is based on the one-electron oxidation of ABTS ABTS (2,2′-azino-bis(3-ethylbenzothiazoline-6-sulfonic acid), Sigma Aldrich) by H$_2$O$_2$ into the corresponding radical cation, ABTS$^{+•}$. This reaction is catalyzed by the enzyme horseradish peroxidase (HRP, Sigma Aldrich) [57,58] (Eq. (3)).

For this enzymatic method, 2 mmol L^{-1} ABTS (in 0.1 mol L^{-1} potassium phosphate buffer, KPi, pH 5.0) and 5.0 mg L^{-1} of horseradish peroxidase (HRP) were freshly prepared before use. A standard cuvette for the photometric investigation was prepared with 1 mL ABTS solution, 0.1 mL of the HRP enzyme, and 0.1 mL of the sample (H$_2$O$_2$ in 2 mol L^{-1} KHCO$_3$ solution). The solution was mixed well and kept for 10 min at room temperature. The progression of this enzymatic reaction is accompanied by a color change in the solution from colorless to green, depending on the concentration of H$_2$O$_2$. Thereafter, the absorbance of the solution was measured at 405 nm in a Shimadzu UV-1800 spectrophotometer. The molar extinction coefficient (ε_{405nm}) of oxidized ABTS is 36,800 M^{-1} cm^{-1}. The calibration curve is shown in Supporting Information, Fig. S1a.

For the detection with strips, the color intensity of the strip is measured with a strip reader (Quantofix Relax, Macherey-Nagel) [39, 44]. As for the titration with KMnO$_4$, a 100 mL electrolyte sample was acidified with 5 mL (1:5) sulfuric acid solution and titrated with 0.02 mol L^{-1} standardized KMnO$_4$ solution as reported in the literature [44,56,59].

All three detection techniques yield comparable results for the standard H$_2$O$_2$ solutions. A comparison for all three methods is shown in Supporting Information, Fig. S1b. In all the experiments herein shown, we determined the H$_2$O$_2$ concentration with the detection strip and confirmed it with the ABTS assay.

The faradaic efficiency (FE) of the produced H$_2$O$_2$ was calculated by the following equation (Eq. (4)):

$$ FE(\%) = \frac{H_2O_2 \ detected(mol) \times \text{no. of electrons} \ \times \ \text{Faraday constant (C mol}^{-1}\text{)}}{\text{total charge passed (C)}} \times 100 \tag{4} $$
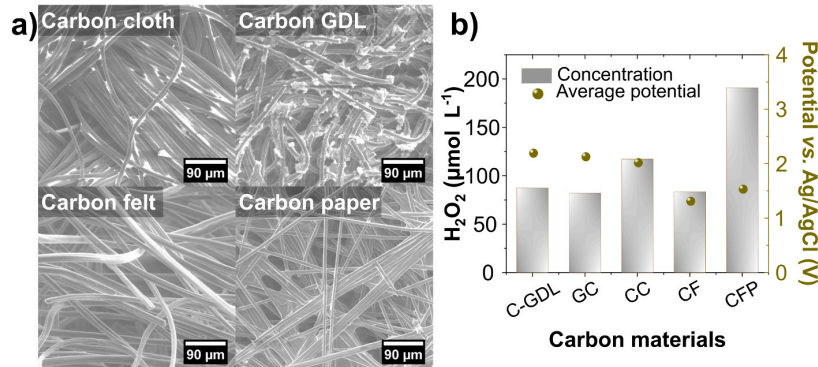
Fig. 2. Selection of carbon material for H_2O_2 synthesis. (a) SEM images of carbon cloth (CC), carbon gas diffusion layer (C-GDL), carbon felt (CF), and carbon fiber paper (CFP) used in this study. (b) H_2O_2 concentration in the anolyte and average electrode potential (vs. Ag/AgCl) during electrolysis using different carbon materials at 50 mA cm^{-2} for 10 min at room temperature.

Table 1

Performance of different carbon materials for H_2O_2 production. Anodic H_2O_2 production with different carbon materials as electrode after 10 min galvanostatic polarization at 50 mA cm^{-2}. The potential corresponds to the average electrode potential during electrolysis.

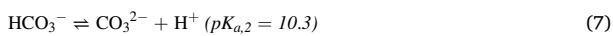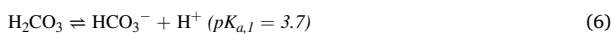| Carbon material	H_2O_2 concentration	Highest H_2O_2 production rate	Maximum H_2O_2 FE	Potential
	μmol L^{-1}	μmol min^{-1} cm^{-2}	%	V vs. Ag/AgCl
Carbon fiber paper (CFP)	190.9	0.48	3.1	1.5
Carbon cloth (CC)	117.2	0.29	1.9	2.0
Gas diffusion layer (C-GDL)	87.3	0.22	1.4	2.2
Carbon felt (CF)	83.5	0.21	1.3	1.3
Glassy carbon (GC)	82.0	0.21	1.3	2.1

where the number of electrons is 2 for water oxidation to H_2O_2, and the Faraday constant is 96485 C mol^{-1}.

The production rate of the H_2O_2 produced is given by Eq. (5):

$$Production\ rate(\mu mol\ min^{-1} cm^{-2}) = \frac{H_2O_2\ detected(\mu mol)}{time(min) \times area\ of\ the\ electrode(cm^2)} \quad (5)$$

2.4. Calculation of the ionic activities for HCO_3^- and CO_3^{2-}

To address the question of how the bicarbonate (HCO_3^-)/ carbonate (CO_3^{2-}) species affect the productivity of H_2O_2, a speciation analysis was carried out, taking into account the equilibrium of ions in the solution according to Eqs. (6) and (7). Depending on the pH of the solution, different carbonate species (H_2CO_3, HCO_3^-, and CO_3^{2-}) as well as H_2O_2 (as H_2O_2 and HOO^-) can be present in the solutions (Supporting Information, Fig. S2) [37,60,61].

$$H_2CO_3 \rightleftharpoons HCO_3^- + H^+ \ (pK_{a,1} = 3.7) \quad (6)$$

$$HCO_3^- \rightleftharpoons CO_3^{2-} + H^+ \ (pK_{a,2} = 10.3) \quad (7)$$

The molar fraction (α) of each species was calculated based on Eqs. (9) and (10). Since the experiments were carried out in highly

concentrated electrolytes which deviate from the ideal behavior of diluted electrolytes, the ion activities ($a_{HCO_3^-}$ and $a_{CO_3^{2-}}$) were calculated as shown in Eqs. (11) and (12) using the activity coefficient ($f_\pm$) shown in Eq. (13), where z_i is the charge of the ion, A is Debye-Hückel parameter (0.51 kg^{½} mol$^{-½}$, for water at 25 °C), and B is a temperature-dependent parameter. Based on the pH change and carbonate equilibria, we calculated the activity of HCO_3^- ($a(HCO_3^-)$) and CO_3^{2-} ($a(CO_3^{2-})$) ions dependent on the pH of the electrolyte during electrolysis for each concentration (c) of $KHCO_3$.

$$K_{a,i} = 10^{-pK_{a,i}} \quad (8)$$

$$\alpha_{HCO_3^-} = \frac{K_{a,1}.[H^+]}{[H^+]^2 + K_{a,1}.[H^+] + K_{a,1}.K_{a,2}} \quad (9)$$

$$\alpha_{CO_3^{2-}} = \frac{K_{a,1}.K_{a,2}}{[H^+]^2 + K_{a,1}.[H^+] + K_{a,1}*K_{a,2}} \quad (10)$$

$$a_{HCO_3^-} = \alpha_{HCO_3^-}.c_{KHCO_3}.f_\pm \quad (11)$$

$$a_{CO_3^{2-}} = \alpha_{CO_3^{2-}}.c_{KHCO_3}.f_\pm \quad (12)$$

$$logf_\pm = -\frac{A.Z_i^2 \bullet \sqrt{j}}{1 + B.a_i \bullet \sqrt{j}} \quad (13)$$

3. Result and discussion

3.1. Selection of carbon material

Commercial carbon materials were evaluated for the anodic synthesis of H_2O_2 in a two-compartment H-cell. The materials comprise carbon gas diffusion layer (C-GDL), glassy carbon (GC), carbon cloth (CC), carbon felt (CF), and carbon fiber paper (CFP). SEM images of each carbon electrode are depicted in Fig. 2a. All materials except GC were fibrous. CFP and CF were highly porous, whereas CC and C-GDL were more compact. The fibers' average thickness for C-GDL, CC, CF, and CFP was 11.0, 8.7, 15.5, and 7.9 μm, respectively.

The current densities of different materials upon anodic polarization were evaluated in a first screening step by LSV (Supporting Information, Fig. S3a). The lowest onset potential was observed for CF (1.16 V vs. Ag/AgCl) followed by CFP. Exceptionally high current densities of 399 and 177 mA cm^{-2} at 2 V vs. Ag/AgCl were obtained with CF and CFP electrodes, respectively, indicating high water oxidation affinity (to O_2 and/or H_2O_2) for these two materials.

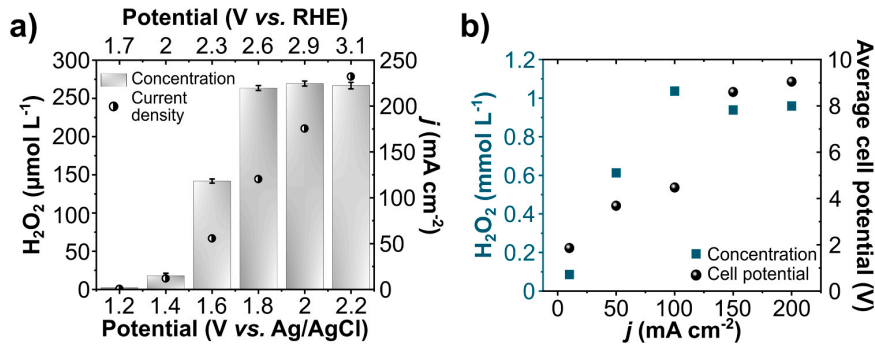In a second step, the H_2O_2 production was measured quantitatively after 10 min of galvanostatic polarization at 50 mA cm^{-2}, which

Fig. 3. Impact of operating potential and current density. (a) H_2O_2 concentration and current density at different applied potentials in 2 mol L^{-1} $KHCO_3$ in an H-Cell. (b) Final H_2O_2 concentration and average cell potential after 150 min of electrolysis at different applied current densities in a flow cell using 2 mol L^{-1} $KHCO_3$ at 100 mL min^{-1} flow rate.

provided a constant 30 C charge for each electrode material. Among the investigated carbon materials, CFP revealed the highest selectivity and FE towards H_2O_2, with a FE of 3.1% and a maximum production rate of 0.48 μmol min^{-1} cm^{-2}, followed by CC, C-GDL, CF, and GC as shown in Table 1 and Fig. 2b. Compared to the other carbon materials, CF and CFP showed the lowest electrode potential during the galvanostatic experiments, with 1.3 and 1.5 V vs. Ag/AgCl, respectively. The different electrochemical activity of the carbon materials toward WOR could be caused by the materials difference in electrode structure, the hydrophobicity of the surface, and due to the transport of the reaction products. The lowest activity of GC is likely due to its 2D structure. All carbon materials except GC are fibrous, with a 3D structure. Hence, the electrochemical active area of GC is considerably lower than the other carbon materials. CFP and CF are highly porous, whereas CC and C-GDL are more compact 3D structures, as shown in the SEM images of Fig. 2a. The product transport characteristics in the electrode materials are

determined by their porosity, permeability, and hydrophobicity [62]. CC and C-GDL materials are treated with PTFE. One side of CC and C-GDL consists of a microporous layer (MPL) made of carbon and a hydrophobic agent. Earlier reports have suggested an enhanced activity towards H_2O_2 production upon increasing the hydrophobicity [43]. However, we observed a lower electrochemical H_2O_2 production in CC and C-GDL (Table 1 and Fig. 2b). A summary of the technical specification of these carbon materials is shown in the Supporting Information, Table S2. Due to its low onset potential, higher H_2O_2 selectivity, production rate, and consequently the highest achieved H_2O_2 concentration, CFP was chosen for further investigations.

It should be noted that the H_2O_2 selectivity and production rate observed in these initial experiments on CFP are relatively low compared to values reported in the literature using PTFE/CFP in 1 mol L^{-1} Na_2CO_3 [43]. Nevertheless, these initial measurements have been conducted under operational conditions that had not been
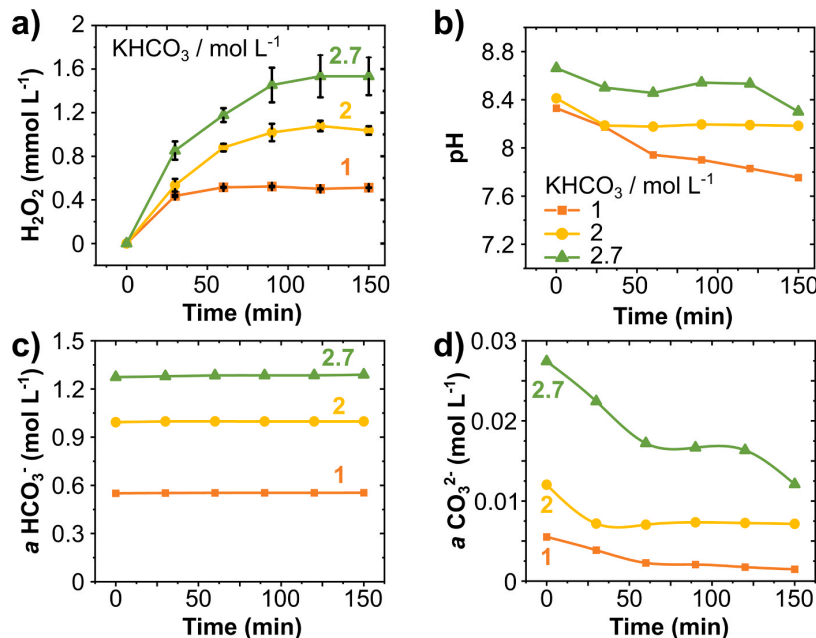

Fig. 4. Anodic H_2O_2 production in $KHCO_3$ electrolyte with different concentrations. (a) H_2O_2 production over time, (b) pH variation, (c) HCO_3^- activity, and (d) CO_3^{2-} activity in the anolyte circulated with 1, 2 and 2.7 mol L^{-1} $KHCO_3$ ■ ● ▲. Experiment conditions: flow cell at 100 mA cm^{-2} for 150 min and 200 mL anolyte circulated at 100 mL min^{-1}.
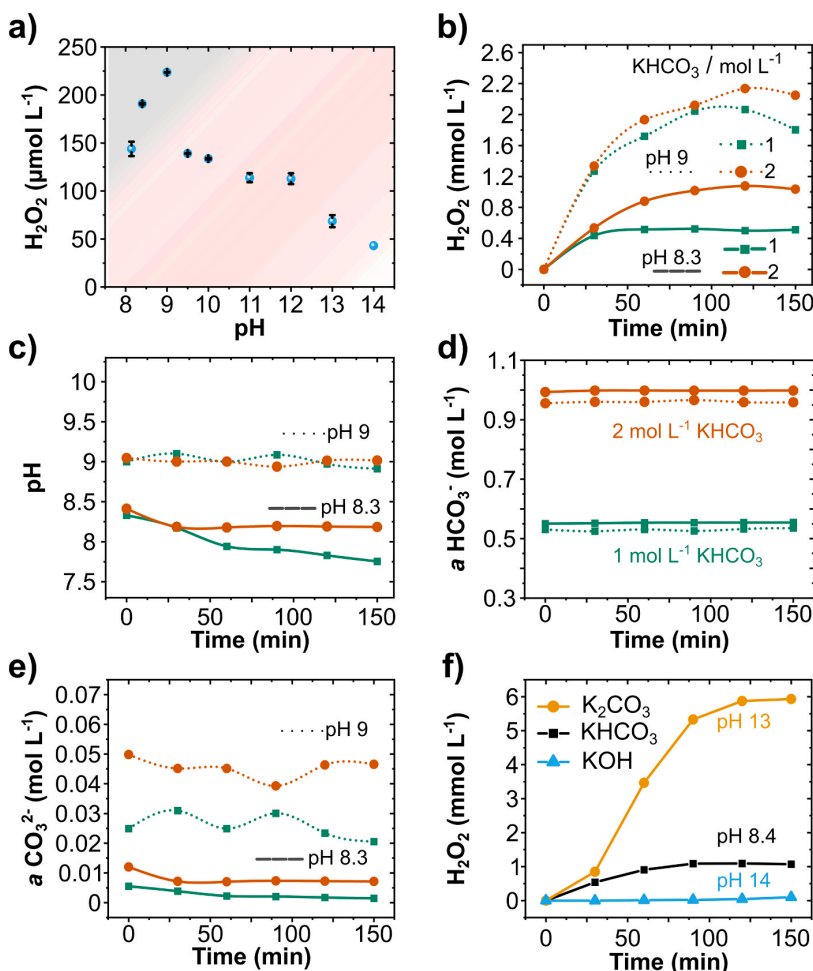
D. Pangotra et al.

Fig. 5. Study of the anodic H_2O_2 generation in 1 mol L^{-1} and 2 mol L^{-1} $KHCO_3$ electrolytes at different pH. (a) anodic H_2O_2 production with pH variation in 2 mol L^{-1} $KHCO_3$ at 50 mA cm^{-2} for 10 min in an H-cell. (b) H_2O_2 production, (c) pH change, and (d) $a(HCO_3^-)$ and (e) $a(CO_3^{2-})$ in the anolyte circulated with (■) 1 mol L^{-1} or (●) 2 mol L^{-1} $KHCO_3$. Solid lines correspond to non-regulated pH experiments. Dotted lines correspond to experiments with pH control at pH 9. (f) H_2O_2 production in ■ 2 mol L^{-1} $KHCO_3$, ● K_2CO_3, and ▲ KOH. 30 mmol L^{-1} of Na_2SiO_3 was added to 2 mol L^{-1} K_2CO_3 and to 2 mol L^{-1} KOH as a stabilizer to prevent decomposition of H_2O_2 at high pH. Experimental conditions for (b–e): flow cell at 100 mA cm^{-2} for 150 min with 200 mL electrolyte at 100 mL min^{-1}.
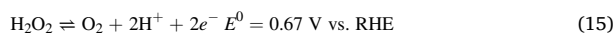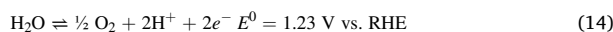
optimized. The following sessions will show how the optimization of reaction parameters is crucial to enhance the final anodic H_2O_2 production on CFP electrodes.

3.2. Effect of potential and current density

The anodic H_2O_2 production upon variation of potential and current density was evaluated on CFP electrodes. Potentiostatic experiments varying the potential positively stepwise from +1.2 V to +2.2 V vs. Ag/AgCl in an H-cell (Fig. 3a) showed the highest H_2O_2 concentration of 270 μmol L^{-1} at +2.0 V vs. Ag/AgCl with a current density (*j*) of ~175 mA cm^{-2}. The maximum production rate at this potential (+2.0 V) was 0.67 μmol min^{-1} cm^{-2} after 10 min (the potential screening data is shown in Supporting Information, Table S1 and Fig. S4a). At +1.8, +2.0, and +2.2 V vs. Ag/AgCl, the H_2O_2 formation rate stayed constant at 0.67 μmol min^{-1} cm^{-2}, despite the increase in current density from 120 to 232 mA cm^{-2} at the same potential range, indicating most of the current is consumed for O_2 evolution at more positive potentials. Further study at higher potentials led to an increase in the current density, though considerably lower H_2O_2 concentration, indicating a preference for water oxidation to O_2 (Supporting Information, Fig. S4b).

The setup was transferred to a flow cell, where galvanostatic experiments with the current density being raised stepwise from 10 to

200 mA cm^{-2} showed a maximum concentration of H_2O_2 (1.1 mmol L^{-1}) at 100 mA cm^{-2} (Fig. 3b). At 150 mA cm^{-2}, the H_2O_2 concentration had a peak at 120 min (1.2 mmol L^{-1}), decaying to 0.9 mmol L^{-1} after 150 min (H_2O_2 concentration versus time at different current densities is shown in Supporting Information, Fig. S4c). This decay in H_2O_2 concentration indicates the decomposition of the generated H_2O_2 on the electrode surface. The same behavior was observed at 200 mA cm^{-2}. Since the standard potential for H_2O_2 oxidation (0.67 V vs. RHE, Eq. (15)) is considerably lower than the standard potential for water oxidation to H_2O_2 (1.76 V vs. RHE, Eq. (2)), the electrogenerated H_2O_2 can decompose to O_2 in the vicinity of the electrified electrode surface. Moreover, H_2O_2 is chemically unstable and can self-decompose to O_2. An experiment of chemical stability for electrogenerated H_2O_2 showed a decay of 19% H_2O_2 during 2.5 h at an open circuit (Supporting Information, Fig. S5). Thus, a combined effect of self- and electro-decomposition of H_2O_2 can lead to a limitation of the H_2O_2 concentration to a level where formation and decomposition of H_2O_2 occur at the same rate [63]. Hence, at higher current densities (150 and 200 mA cm^{-2}), a combination of water oxidation to O_2 and H_2O_2 decomposition (Eqs. (14) and (15)) accounts for the lower H_2O_2 concentration.
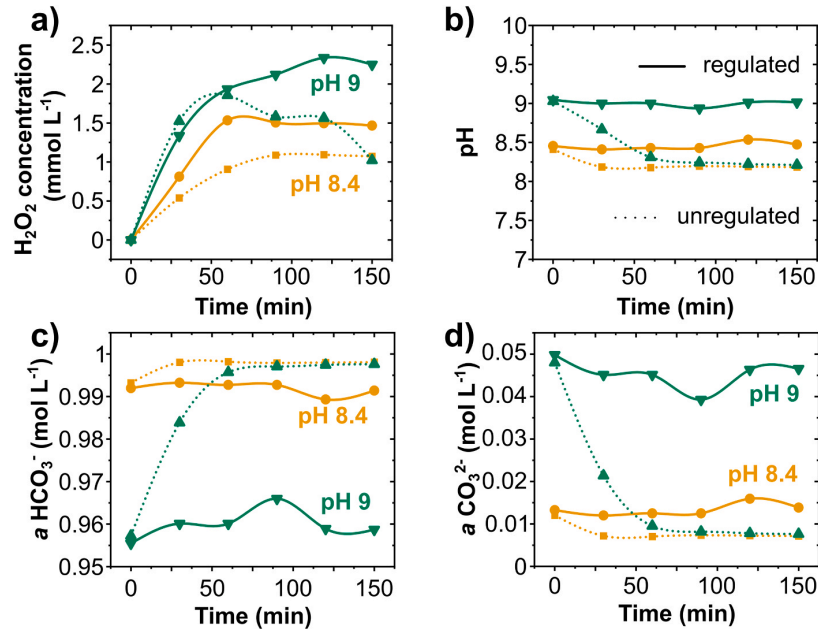
$$H_2O \rightleftharpoons \tfrac{1}{2} O_2 + 2H^+ + 2e^- \quad E^0 = 1.23 \text{ V vs. RHE} \tag{14}$$

$$H_2O_2 \rightleftharpoons O_2 + 2H^+ + 2e^- \quad E^0 = 0.67 \text{ V vs. RHE} \tag{15}$$

Fig. 6. Anodic H_2O_2 generation in 2 mol L^{-1} KHCO$_3$ electrolyte at different pH. (a) H_2O_2 concentration (b) pH change, (c) $a(HCO_3^-)$ and (d) $a(CO_3^{2-})$ in the anolyte in 2 mol L^{-1} KHCO$_3$ at (● , ■) pH 8.4, and (▼ , ▲) pH 9. Solid lines correspond to experiments with pH regulation during electrolysis. Dotted lines correspond to experiments without pH regulation. Experiment conditions: Flow cell at 100 mA cm^{-2} with 200 mL anolyte at a flow rate of 100 mL min^{-1}.
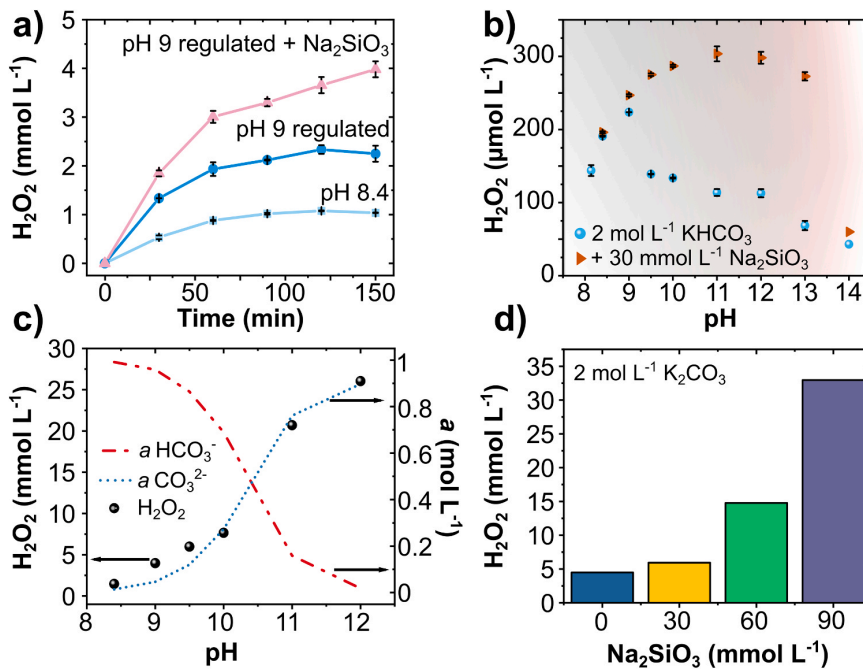

Fig. 7. Effect of Na$_2$SiO$_3$ stabilizer on H_2O_2 generation. (a) Anodic H_2O_2 concentration in 2 mol L^{-1} KHCO$_3$ electrolyte at (■) pH 8.4, (●) controlled pH 9, and (▲) at controlled pH 9 with 30 mmol L^{-1} of Na$_2$SiO$_3$ as a stabilizer after 150 min at 100 mA cm^{-2} in a flow cell. (b) Anodic H_2O_2 production with pH variation in 2 mol L^{-1} KHCO$_3$ with and without 30 mmol L^{-1} Na$_2$SiO$_3$ at 50 mA cm^{-2} for 10 min in an H-cell. (c) H_2O_2 concentration, a(HCO$_3^-$) and a(CO$_3^{2-}$) in the anolyte at different pH in 2 mol L^{-1} KHCO$_3$ after 150 min of electrolysis at 100 mA cm^{-2} in a flow cell. Up to pH 11, the stabilizer concentration used was 30 mmol L^{-1}. At pH 12, the stabilizer concentration was 90 mmol L^{-1}. (d) H_2O_2 production in 2 mol L^{-1} K$_2$CO$_3$ (pH 12.6) with different stabilizer concentrations after 150 min of electrolysis at 100 mA cm^{-2} in a flow cell.

Table 2

Summary of the electrolyte optimization for anodic H_2O_2 production on carbon fiber paper. Experimental conditions: 100 mA cm^{-2} for 150 min, carbon fiber paper anode, and 100 mL min^{-1} electrolyte flow rate. All experiments in this table were carried out with pH control during electrolysis.

Electrolyte	pH	Conductivity mS cm^{-1}	a (HCO_3^-) mol L^{-1}	a (CO_3^{2-}) mol L^{-1}	[Na_2SiO_3] mmol L^{-1}	[H_2O_2] mmol L^{-1}
2 mol L^{-1} $KHCO_3$	8.4	119.4	0.99	0.01	0	1.47
	9.0	123.5	0.96	0.05	0	2.25
	9.0	123.5	0.96	0.05	30	3.98
	9.5	139.2	0.86	0.12	30	5.98
	10.0	152.5	0.69	0.27	30	7.66
	11.0	166.3	0.16	0.76	30	20.70
	12.0	169.4	0.02	0.90	90	**26.04**
2 mol L^{-1} K_2CO_3	12.6	208.0	–	–	0	4.48
		211.0	–	–	30	5.93
		210.0	–	–	60	14.77
		210.0	–	–	90	**32.96**

At current densities higher than 100 mA cm^{-2}, a visual color change was observed in the electrolyte, which turned brown from colorless (Supporting Information, Fig. S6). The oxidation of the carbon surface caused erosion of the electrode, and graphitic carbon particles were exfoliated in the electrolyte [64]. SEM images of the carbon electrodes before and after 150 min of electrolysis at 200 mA cm^{-2} revealed a damaged electrode surface (Supporting Information, Fig. S6). The fiber thickness decreased from 7.9 μm to 3.5 μm, indicating electrode degradation.

The highest H_2O_2 concentration and the lowest cell potential were obtained at 100 mA cm^{-2}, thus this current density was applied for all following electrolyte optimization experiments. To examine electrode stability, cycles of 2.5 h at 100 mA cm^{-2} in 2 mol L^{-1} $KHCO_3$ were performed, in which the electrolyte was changed at every cycle of 2.5 h (Supporting Information, Fig. S7, and S8). Interestingly, upon changing the electrolyte, the H_2O_2 concentration quickly reached a similar concentration as the previous cycle (between 0.6 and 1 mmol L^{-1}), indicating that the maximum H_2O_2 concentration is limited by the electrochemical H_2O_2 decomposition. Moreover, the cell potential was rather constant throughout the cycles. Hence, the CFP electrodes are stable for 7 cycles at 100 mA cm^{-2} (17.5 h). After this time, carbon particles were observed in the anolyte reservoir, indicating oxidation and mechanical disintegration of the electrode.

3.3. Effect of electrolyte concentration

The anodic oxidation of water to H_2O_2 was evaluated in $KHCO_3$ electrolyte with concentrations of 1.0, 2.0, and 2.7 mol L^{-1}. The latter corresponds to a saturated $KHCO_3$ solution at room temperature, as the maximum solubility of $KHCO_3$ in water is 23 g/100 mL (2.3 mol L^{-1}) at 20 °C [65]. LSV of CFP electrodes in these three electrolytes showed
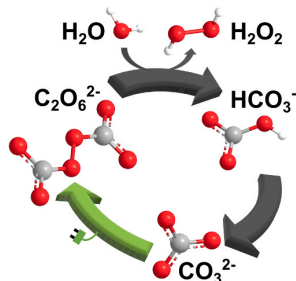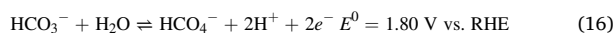

Fig. 8. Suggested mechanism for anodic H_2O_2 production in bicarbonate electrolytes. Bicarbonate ions (HCO_3^-) are deprotonated to carbonate (CO_3^{2-}) in alkaline electrolytes. CO_3^{2-} can be anodically oxidized to peroxodicarbonate ($C_2O_6^{2-}$) species. $C_2O_6^{2-}$ decomposes into HCO_3^- and hydrogen peroxide (H_2O_2), closing the cycle with a higher H_2O_2 concentration.

considerably higher current densities in more concentrated $KHCO_3$ solutions, indicating that HCO_3^- accelerates water oxidation (LSVs shown in Supporting Information, Fig. S9). Flow cell experiments at 100 mA cm^{-2} showed a three-fold increase in H_2O_2 production upon raising the bicarbonate concentration from 1.0 to 2.7 mol L^{-1} $KHCO_3$: from 0.5 to 1.5 mmol L^{-1} H_2O_2 after 150 min (Fig. 4a). The production rate rises from 0.29 to 0.56 μmol min^{-1} cm^{-2} after 30 min (peak of production rate, see Supporting Information, Fig. S10a, b). Hydrogen carbonate ions (HCO_3^-) have been described as a stabilizing agent and accounted for enhancing the water oxidation to H_2O_2 [32,37,41,44]. The described mechanism for enhancing H_2O_2 production in bicarbonate electrolytes involves the generation of peroxomonocarbonate (HCO_4^-) species at the anode through HCO_3^- oxidation (Eq. (16)). Subsequently, peroxocarbonate species decompose hydrolytically into H_2O_2 and bicarbonate ions, as given in Eq. (17) [37,43,46].

$$HCO_3^- + H_2O \rightleftharpoons HCO_4^- + 2H^+ + 2e^- \quad E^0 = 1.80 \text{ V vs. RHE} \quad (16)$$

$$HCO_4^- + H_2O \rightarrow H_2O_2 + HCO_3^- \quad (17)$$

The anodically produced H_2O_2 reaches a concentration plateau within 90 min of electrolysis (Fig. 4a). At more concentrated $KHCO_3$ electrolytes, the plateau rises to a higher H_2O_2 concentration range. These limiting values of the H_2O_2 concentration can be due to concurrent O_2 formation and electrodecomposition of H_2O_2 [44,66]. The higher rate of H_2O_2 generation increases the rate of H_2O_2 decomposition until a steady-state is reached. An experiment adding 0.9 mmol L^{-1} H_2O_2 as initial concentration led to a similar concentration plateau where no H_2O_2 was added (Supporting Information, Fig. S11), suggesting a dynamic steady-state with a limiting H_2O_2 concentration. Hence, the main challenge is to raise the plateau to the highest possible H_2O_2 concentration.

The pH of the $KHCO_3$ anolyte was constantly monitored and all electrolyte concentrations showed a pH decline during electrolysis (Fig. 4b). The initial pH in 1, 2, and 2.7 mol L^{-1} $KHCO_3$ are 8.3, 8.4, and 8.7, respectively. After 150 min, it decreased to 7.7, 8.1, and 8.3. This slight anolyte acidification is caused by the electro-oxidation of water (Eqs. (2) and (14)).

Based on pH variation during electrolysis, we calculated the variation of ionic activity for HCO_3^- (a(HCO_3^-)) and CO_3^{2-} (a(CO_3^{2-})) species in the electrolyte (Fig. 4c, d). The equilibrium between HCO_3^- and CO_3^{2-} ions is pH-dependent, and at a pH range from 8 to 9, the activity of HCO_3^- ions is higher than CO_3^{2-} (Supporting Information, Fig. S2). a(HCO_3^-) and a(CO_3^{2-}) increase accordingly with electrolyte concentration (Fig. 4c, d). In this pH range, a(CO_3^{2-}) is two orders of magnitude smaller than that of a(HCO_3^-) and decreases during electrolysis, whereas the activity of a(HCO_3^-) ions appears to be constant at each concentration (Fig. 4c, d). Varying the concentration of the electrolyte leads to a change in the pH, ionic activity for HCO_3^- and CO_3^{2-} ions in the electrolyte. Experiments with and without the addition of

Table 3
A comparison of the reported work on water oxidation to H_2O_2 with our present study.

Electrode	Cell type	Electrolyte	pH	$[H_2O_2]_{max}$	Conditions[a]					Production rate	Peak FE	Ref.
				$mmol\ L^{-1}$	j/E	t	EA	VA	S	$\mu mol\ min^{-1}\ cm^{-2}$	%	
PTFE/CFP	H-Cell	1 M Na_2CO_3	12	3	100	420	0.36	25	~30	23.4	66	[43]
BDD/Nb			11.9	–	39.8	10	1.13	8.5	–	3.93	31.7	[80]
BDD/Ti		2 M $KHCO_3$	8	~16	120	5	7.4	25	–	~8	28	[44]
BDD/Ti			8	29	295	5	7.4	25	–	19.7	~22	[44]
$CaSnO_3$/FTO	Undivided		8.3	–	3.2 V	10	–	30	–	~4.6	76	[39]
$CaSnO_3$/FTO			8.3	~0.9	2.2 V	720	–	30	–	–	–	[39]
$BiVO_4$/FTO		1 M $NaHCO_3$	8.3	–	3.1 V	–	1	20	–	5.7	70	[38]
CFP	Flow-Cell	2 M $KHCO_3$	8.4	1.47	100	150	10	200		0.5	1.7	This work
CFP			12	26	100	150	10	200	90	4	13.1	
CFP		2 M K_2CO_3	12.6	**33**	100	150	10	200	90	4.5	14.3	

[a] j: Current density (mA cm^{-2}), E: Potential applied (V vs. RHE), t: Time (min), EA: Electrode area (cm^2), VA: Volume of anolyte (mL), S: Stabilizer concentration (mmol L^{-1} Na_2SiO_3).

$KHCO_3$ during the electrolysis reveals that increasing the $KHCO_3$ concentration results in an increase of (i) H_2O_2 production, (ii) pH, (iii) conductivity, and (iv) activity of HCO_3^- and CO_3^{2-} ions (Supporting Information, Fig. S12a–e). It is possible that the higher anodic H_2O_2 production results from a combined effect of higher pH and ratio of the activity of HCO_3^- and CO_3^{2-} ions in the electrolyte. Thus, we have investigated these two parameters in more detail, discussed in the following sections.

3.4. Effect of pH

Experiments described in the previous section showed that a higher concentration of HCO_3^- ions boost H_2O_2 production. However, in the electrolyte, the distribution of the HCO_3^- and CO_3^{2-} ion is pH-dependent [37]. Upon carrying out long-term electrosynthesis, a significant pH shift was observed towards a more acidic electrolyte, which leads to a change of HCO_3^- / CO_3^{2-} ratio in the solution. Earlier studies reporting H_2O oxidation to H_2O_2 upon pH variation between 7 and 12.5 in 0.5 mol L^{-1} $KHCO_3$ showed lower H_2O_2 production at higher pH [37]. The authors attributed the lower H_2O_2 production in more alkaline electrolytes to the higher concentration of CO_3^{2-} ions.

In this work, we have investigated in detail the effect of pH variation on the anodic oxidation of water by adjusting the pH of a 2 mol L^{-1} $KHCO_3$ anolyte between 8 and 14. The pH was varied through CO_2 bubbling or KOH addition. LSVs in 2 mol L^{-1} $KHCO_3$ at pH 8.4, 9, 9.5, and 10 (Supporting Information, Fig. S13) revealed lower onset potential and higher current densities upon increasing the pH, indicating not only the increase in conductivity but also higher electrolyte reactivity in more alkaline medium.

Quantitative measurements in anolytes with pH from 8.14 to 14 were performed in an H-cell at a constant current of 50 mA cm^{-2} (Fig. 5a). The initial pH of a typical 2 mol L^{-1} $KHCO_3$ solution is 8.4. At this initial pH, 191 μmol L^{-1} H_2O_2 is formed anodically after 10 min. Decreasing the pH to 8.12 causes a decline in final H_2O_2 concentration to 144 μmol L^{-1}. Increasing the pH to 9 leads to a H_2O_2 concentration of 225 μmol L^{-1}. However, raising pH beyond 9 causes a decline in H_2O_2 production, caused by an increasing rate of decomposition of H_2O_2 in alkaline pH. Thus, at these conditions of electrolyte concentration and current density, the maximum H_2O_2 concentration was obtained at pH 9.

A set of flow cell experiments at 100 mA cm^{-2} was carried out in 1 mol L^{-1} and 2 mol L^{-1} $KHCO_3$, both at pH 8.3 and 9. Upon increasing the pH from 8.3 to 9, a fourfold increase in H_2O_2 production was achieved in 1 mol L^{-1} $KHCO_3$ (from 0.5 to 2 mmol L^{-1} H_2O_2) and a twofold in 2 mol L^{-1} $KHCO_3$ (from 1.1 to 2.4 mmol L^{-1} H_2O_2) (Fig. 5b). The pH was constantly monitored and regulated with KOH addition upon pH decrease (Fig. 5c). It is important to remark that the amount of KOH added is negligible compared to the $KHCO_3$ concentration; hence it does not impact the $a(HCO_3^-)$ or $a(CO_3^{2-})$. Furthermore, we observed that a slightly basic regime (at pH 9) enhances the electrochemical H_2O_2 production. Nevertheless, increasing the bicarbonate concentration from 1 to 2 mol L^{-1} $KHCO_3$ at pH 9 does not significantly improve the H_2O_2 final concentration. This suggests that it is not the HCO_3^- concentration but the pH regime or the CO_3^{2-} concentration being affected by the pH regime that enhances the H_2O_2 production.

Under basic conditions, HCO_3^- ions dissociate into proton (H$^+$) and carbonate ions (CO_3^{2-}) (Eq. (7)) [37,60]. Raising the pH from 8.3 to 8.4–9 in 1 and 2 mol L^{-1} $KHCO_3$ solutions showed that $a(HCO_3^-)$ is most affected by the electrolyte concentration, whereas $a(CO_3^{2-})$ varies accordingly with the pH change (Fig. 5d, e), due to the dissociation of bicarbonate in alkaline medium. In 1 mol L^{-1} $KHCO_3$, the average a(HCO_3^-) ions decreased by 5.5% upon increasing the pH (Fig. 5d), whereas the $a(CO_3^{2-})$ increased 10 times (Fig. 5e), however the absolute changes are the same. A similar behavior of lower $a(HCO_3^-)$ and higher $a(CO_3^{2-})$ is depicted for 2 mol L^{-1} $KHCO_3$ at pH 9. A correlation between the increase in $a(CO_3^{2-})$ and an enhanced H_2O_2 production was also observed, as higher H_2O_2 concentrations were obtained at higher pH.

CO_3^{2-} ions have been previously reported to be unsuitable for the selective oxidation of water to H_2O_2 compared to HCO_3^- ions [37,41]. On the other hand, Xia et al. [43] reported higher anodic H_2O_2 production in 1 mol L^{-1} Na_2CO_3 (pH 10.3) compared to 1 mol L^{-1} $NaHCO_3$ (pH 8.3), suggesting that CO_3^{2-} ion enhances the H_2O_2 production than the HCO_3^- ions. Considering the active role of CO_3^{2-} ions and the tendency of H_2O_2 to undergo base-catalyzed decomposition in alkaline media, we have changed the electrolyte from 2 mol L^{-1} $KHCO_3$ (pH 8.4) to 2 mol L^{-1} K_2CO_3 (pH 13). 30 mmol L^{-1} Na_2SiO_3 was added to the anolyte to inhibit the H_2O_2 decomposition at high pH [67]. Changing the electrolyte caused an increase in the anodic H_2O_2 production, namely from 1.1 mmol L^{-1} H_2O_2 in $KHCO_3$ to 5.9 mmol L^{-1} in the K_2CO_3 electrolyte (Fig. 5f). Keeping the pH high at around 14 and changing the electrolyte to 2 mol L^{-1} KOH + 30 mmol L^{-1} Na_2SiO_3 resulted in negligible production of H_2O_2. Thereby, the active role of carbonate ions, and not of the alkaline pH regime, in promoting water oxidation to H_2O_2 was confirmed.

During electrolysis, the pH of the 2 mol L^{-1} $KHCO_3$ electrolyte decreases due to the constant oxidation of OH$^-$ ions. In a typical experiment, the final pH of the anolyte is 8.2 after 150 min of anodic polarization, irrespective of the initial pH (9 or 8.4, Fig. 6). The final H_2O_2 concentration is also 1 mmol L^{-1} for both experiments. This pH decrease leads to a drop in both: $a(CO_3^{2-})$ and H_2O_2 production (Fig. 6). At pH 9, the peak production of H_2O_2 is achieved after 60 min (1.9 mmol L^{-1} H_2O_2), with a subsequent decline, presumably due to reduced $a(CO_3^{2-})$ (Fig. 6d). Active adjustment of the pH to achieve constant values at 8.4 and 9 throughout the electrolysis enhanced the H_2O_2 production considerably. For instance, pH regulation at 9 promoted an increase in H_2O_2 production after the 60 min peak, reaching 2.2 mmol L^{-1} H_2O_2 after 150 min. This correlation of higher pH, higher $a(CO_3^{2-})$, and higher H_2O_2 production endorses the hypothesis that

higher $a(CO_3^{2-})$ enhances the generation of H_2O_2 by either generating peroxocarbonate species or stabilizing the peroxide and avoiding its further anodic oxidation by forming a percarbonate adduct [68].

3.5. Effect of stabilizer

H_2O_2 is an unstable compound, decomposing to water and molecular oxygen, as shown in Eq. (18).

$$2H_2O_2 \rightarrow O_2 + 2H_2O \tag{18}$$

To slow down the H_2O_2 decomposition, organic stabilizers such as aryl alkyl ketones are used in practice [69]. These stabilizers are redox-active compounds, which can sacrificially oxidize if added to an electrolytic cell. To prevent the anodic degradation of such compounds during H_2O_2 production, we have chosen a non-redox active additive to stabilize H_2O_2, namely sodium metasilicate (Na_2SiO_3) [67]. Previous experiments using 4 mg mL^{-1} Na_2SiO_3 in 1 mol L^{-1} Na_2CO_3 showed high anodic production of H_2O_2, up to 3 mmol L^{-1} [43]. The working mechanism of Na_2SiO_3 as a H_2O_2 stabilizer is rather unclear. Literature reports for the stabilization mechanism include formation of complex between Na_2SiO_3 and H_2O_2 [70], formation of stable peroxide compounds, stopping the decomposition chain reactions by destruction of the free radicals, and formation of complexes with metal impurities [71]. Moreover, Na_2SiO_3 is also accounted for the stabilization of anodically produced peroxocarbonate species using BDD electrodes in Na_2CO_3 electrolytes [72]. However, the role of the metasilicate for H_2O oxidation to H_2O_2 has not been studied in depth.

We have investigated anolytes without and with Na_2SiO_3 and their effect on the anodic H_2O_2 generation. The addition of 30 mmol L^{-1} Na_2SiO_3 to the 2 mol L^{-1} $KHCO_3$ anolyte controlled at pH 9 caused a two-fold increase in H_2O_2 production: from 2.2 mmol L^{-1} to 4 mmol L^{-1} H_2O_2 (Fig. 7a). The maximum FE for H_2O_2 production increased from 1% to 4%, and the production rate increased fourfold (from 0.3 to 1.2 µmol min^{-1} cm^{-2}) (Supporting Information, Fig. S14a,b). Thus, the presence of Na_2SiO_3 in solution remarkably enhanced the formation and accumulation of H_2O_2 in the electrolyte.

The pH range of anolytes containing Na_2SiO_3 was varied from pH 8.4–14 in an H-cell at 50 mA cm^{-2}. This preliminary screening revealed higher production of H_2O_2 at elevated pH (> 9), with peak production of 300 µmol L^{-1} H_2O_2 at pH 11 (Fig. 7b). At pH above 11, the H_2O_2 production declined considerably, reaching 60 µmol L^{-1} at pH 14. Previous reports on anodic H_2O_2 production in different pHs show higher anodic H_2O_2 generation at pH below 11.4 [73]. In this study, the presence of Na_2SiO_3 inhibits H_2O_2 decomposition up to pH 11. At pH higher than 11, more stabilizer is required for increasing H_2O_2 concentrations (Supporting Information, Fig. S15a).

Experiments in the flow cell showed the same pattern: higher H_2O_2 concentrations were obtained in 2 mol L^{-1} $KHCO_3$ electrolytes containing Na_2SiO_3, even at higher pH (Fig. 7c). 26 mmol L^{-1} H_2O_2 was achieved at pH 12 in the presence of 90 mmol L^{-1} Na_2SiO_3, compared to 1.5 mmol L^{-1} at pH 8.4 without the stabilizer. These results suggest that higher pH enhances the electrochemical production of H_2O_2, provided that a chemical stabilizer hinders its subsequent decomposition.

Literature reports on anodic H_2O_2 production in different electrolytes and pH suggested that HCO_3^- ions promote H_2O_2 formation, whereas CO_3^{2-} ions aid to H_2O_2 decomposition [32]. K_2CO_3 electrolytes at pH 12.7 showed lower H_2O_2 production compared to other electrolytes with lower pH [74]. Regarding the pH variation, the Na_2SiO_3 stabilizer prevented H_2O_2 decomposition even in high alkaline conditions. Consequently, higher H_2O_2 concentrations were achieved at elevated pH. Calculations of $a(HCO_3^-)$ and $a(CO_3^{2-})$ in the electrolyte show a remarkable correspondence of higher H_2O_2 formation with higher $a(CO_3^{2-})$ upon pH variation (Fig. 7c).

To confirm the role of CO_3^{2-} ions on H_2O_2 production, K_2CO_3 electrolytes were utilized in the presence of Na_2SiO_3. K_2CO_3 electrolytes
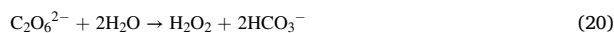
have been accounted for poor anodic production of H_2O_2 [74]. Nonetheless, we find considerably high H_2O_2 production upon increasing the Na_2SiO_3 concentration. An initial investigation in the H-Cell revealed higher stabilizer concentration results in high H_2O_2 production, particularly in high pH regimes (Supporting Information, Fig. S17). In the presence of 90 mol L^{-1} Na_2SiO_3, 33 mmol L^{-1} H_2O_2 was obtained after 150 min with a final FE of 14% (Fig. 7d), which is at least 20 times higher than the H_2O_2 concentration obtained in 2 mol L^{-1} $KHCO_3$ without the stabilizer. Thus, the influence of CO_3^{2-} ions is evident on the $2e^-$ oxidation of water to H_2O_2, as long as a chemical stabilizer is present to avoid peroxide decomposition.

3.6. Summary of work and proposed mechanism

Variation of $KHCO_3$ concentration in the anolyte revealed higher H_2O_2 production in more concentrated solutions. Literature reports proposed that the HCO_3^- ions oxidize to HCO_4^- during the anodic polarization (Eq. (16)). Subsequently, HCO_4^- decomposes to HCO_3^-, thereby releasing H_2O_2 (Eq. (17)) [37,43,46]. Therefore, HCO_3^- ions contribute to enhanced H_2O_2 formation.

However, increasing the $KHCO_3$ concentration results in a pH rise, which subsequently increases the activity of CO_3^{2-} ions due to the HCO_3^- / CO_3^{2-} equilibrium. Our results of pH screening in 2 mol L^{-1} $KHCO_3$ are in agreement with the literature, showing that highly alkaline electrolytes are unfavorable for anodic H_2O_2 production [37]. Nevertheless, the addition of Na_2SiO_3 to the anolyte stabilized the H_2O_2 production even in pH regimes higher than 12. Changing the anolyte to 2 mol L^{-1} K_2CO_3 in the presence of Na_2SiO_3 at pH 12 confirmed the influence of the CO_3^{2-} ions activity in boosting H_2O_2 formation. A summary of the electrolyte optimization is given in Table 2, which shows an enhance in the anodic H_2O_2 production by a factor of 20 upon optimizing the electrolyte conditions.

Literature reports on anodic processes in carbonate electrolytes have shown that CO_3^{2-} ions can be oxidized to peroxodicarbonate ($C_2O_6^{2-}$) (Eq. (19)) [46,68,75]. Various carbon-based materials, including boron-doped diamond, have been accounted for producing peroxodicarbonate ions in solution [75–78]. Due to the poor stability of peroxocarbonate ions in aqueous solutions, it hydrolyses to form H_2O_2 and HCO_3^- (Eq. (20)) [68,72,78]. HCO_3^- ions are deprotonated to CO_3^{2-} at high pH, which consequently can undergo oxidation to $C_2O_6^{2-}$ (Eq. (7) and Fig. 8). We suggest a promotion effect of CO_3^{2-} ions in alkaline medium resulting in higher production of H_2O_2, provided a suitable amount of stabilizer is present in the electrolyte. *In situ* studies to identify the anodic generation of $C_2O_6^{2-}$ ions would be required to validate the peroxocarbonate mechanism.

$$2CO_3^{2-} \rightarrow C_2O_6^{2-} + 2e^- \quad E^0 = 1.80 \text{ V vs. RHE} \tag{19}$$

$$C_2O_6^{2-} + 2H_2O \rightarrow H_2O_2 + 2HCO_3^- \tag{20}$$

The proposed crucial role of CO_3^{2-} ions in H_2O_2 formation is based on the activity profile of carbonate and bicarbonate ions and the H_2O_2 production at different pH values (Fig. 7c). At higher pH values, the chemical equilibrium of HCO_3^- / CO_3^{2-} shifts to carbonate. Simultaneously, the H_2O_2 production increases, as long as a stabilizer is present to avoid H_2O_2 decomposition. Moreover, carbonate ions can be oxidized to peroxodicarbonate and release H_2O_2 via hydrolysis. In parallel to our investigations, the group of Gill et al. [63] demonstrated the role of carbonate in promoting anodic H_2O_2 production: first, a rotating ring disc electrode showed that H_2O_2 was not readily detected in the ring, but only with a time delay. This indicates oxidation of the electrolyte species followed by hydrolysis, thereby promoting H_2O_2 production. *In situ* infrared spectroscopy (ATR-FTIR) studies by the same group confirmed the role of carbonate and the presence of HCO_4^- or $C_2O_6^{2-}$ peroxo-intermediates on the electrode surface at the potentials of H_2O_2 generation [63]. In contrast to our results presented here, Gill et al. reported higher H_2O_2 productivity in HCO_3^- than in CO_3^{2-} electrolyte.

This difference lays in the use of stabilizers in our experiments. Chemical stabilizers enabled a superior reaction performance in higher pH regimes and higher CO_3^{2-} activities. The high pH of CO_3^{2-} solutions will lead to H_2O_2 decomposition in the absence of a stabilizer and consequently, a lower productivity compared to HCO_3^- solutions. DFT calculations by Mavrikis et al. also indicated an important role of CO_3^{2-} ions in enhancing the H_2O_2 production in an electrolyte mixture of 1:1 $KHCO_3$ and K_2CO_3, thus supporting our hypothesis [79].

A comparison of our results with those reported in the literature is summarized in Table 3. In this study, a maximum H_2O_2 concentration of 33 mmol L^{-1} was obtained, which is, to the best of our knowledge, the highest reported concentration of anodically produced H_2O_2 using CFP. Although the faradaic efficiency of 14.3% is not high, it is the highest FE obtained at such current density using pristine CFP [43]. The FE and the production rates, usually defined as performance parameters, are comparatively low and require further improvement by using foremost active electrode materials. Nonetheless, it is important to point out that we have used a low-cost, readily available carbon material as a working electrode. Additionally, a comparatively more significant 10 cm^2 flow cell and higher electrolyte volume have been utilized in this study to demonstrate improvements in the H_2O_2 accumulation by optimizing the electrolyte composition and operating conditions.

4. Conclusion

The performance of low-cost commercial carbon materials as anodes for anodic H_2O_2 production was investigated through variation and optimization of a broad range of electrolyte composition and operating parameters. We showed that carbon fiber paper exhibited good selectivity toward water oxidation to H_2O_2 and used it for further in-depth examinations. This study highlights the importance of tuning reaction conditions such as potential, current density, electrolyte concentrations, pH values, and utilization of stabilizer to boost the electrochemical water oxidation to H_2O_2. Supported by the calculated activity of carbonate species in the electrolyte, the experimental data suggested a strong correlation between the $a(CO_3^{2-})$ and enhanced H_2O_2 generation in $KHCO_3$ anolytes. Keeping the activity of CO_3^{2-} ions high by regulating the pH regime to remain stable at 9 almost doubled the H_2O_2 production, reaching 2.2 mmol L^{-1}. Thus, CO_3^{2-} does not compete, but acts as a reaction mediator promoting H_2O_2 production. Adding Na_2SiO_3 to the electrolyte as a stabilizer remarkably boosted the anodic generation of H_2O_2 at higher pH regimes·H_2O_2 concentration up to 26 mmol L^{-1} was obtained in 2 mol L^{-1} $KHCO_3$ at pH 12. Finally, this study illustrated the importance of suitable electrolyte conditions for improving the electrochemical oxidation of water to H_2O_2. Optimized electrolyte conditions (90 mmol L^{-1} Na_2SiO_3 in 2 mol L^{-1} K_2CO_3) led to H_2O_2 concentrations up to 33 mmol L^{-1}, at least 20 fold higher than in 2 mol L^{-1} $KHCO_3$, which is used as a standard electrolyte. Future approaches will emphasize the optimized electrolyte condition with highly active electrode materials to enhance the anodic production of H_2O_2. This is subject to our ongoing work.

CRediT authorship contribution statement

Dhananjai Pangotra: Conceptualization, Investigation, Formal analysis, Validation, Writing – original. draft. **Lénárd-István Csepei:** Conceptualization, Writing – review & editing. **Arne Roth:** Conceptualization, Supervision, Writing – review & editing. **Carlos Ponce de León:** Writing – review & editing. **Volker Sieber:** Supervision, Writing – review & editing. **Luciana Vieira:** Conceptualization, Supervision, Writing – review & editing.

Declaration of Competing Interest

The authors declare that they have no known competing financial interests or personal relationships that could have appeared to influence the work reported in this paper.

Appendix A. Supporting information

Supplementary data associated with this article can be found in the online version at doi:10.1016/j.apcatb.2021.120848.

References

[1] C.P. Gordon, H. Engler, A.S. Tragl, M. Plodinec, T. Lunkenbein, A. Berkessel, J. H. Teles, A.-N. Parvulescu, C. Copéret, Efficient epoxidation over dinuclear sites in titanium silicalite-1, Nature 586 (2020) 708–713, https://doi.org/10.1038/s41586-020-2826-3.

[2] A. Pokutsa, A. Zaborovsky, P. Bloniarz, T. Pacześniak, D. Maksym, J. Muzart, Cyclohexane oxidation: relationships of the process efficiency with electrical conductance, electronic and cyclic voltammetry spectra of the reaction mixture, React. Kinet. Mech. Catal. 132 (2021) 123–137, https://doi.org/10.1007/s11144-020-01913-6.

[3] G. Lewandowski, M. Kujbida, A. Wróblewska, Epoxidation of 1,5,9-cyclododeca-triene with hydrogen peroxide under phase-transfer catalysis conditions: influence of selected parameters on the course of epoxidation, React. Kinet. Mech. Catal. 132 (2021) 983–1001, https://doi.org/10.1007/s11144-021-01960-7.

[4] D. Horová, J. Nováková, L. Pelíšková, J. Kohout, J. Šafář, K. Hrachovcová, V. Tokarová, Synthesis of MFI structured iron silicates and their catalytic performance in phenol removal by wet peroxide oxidation, React. Kinet. Mech. Catal. 130 (2020) 1077–1092, https://doi.org/10.1007/s11144-020-01804-w.

[5] İ. Kıpçak, E.Kurtaran Ersal, Catalytic wet peroxide oxidation of a real textile azo dye Cibacron Red P-4B over Al/Fe pillared bentonite catalysts: kinetic and thermodynamic studies, React. Kinet. Mech. Catal. 132 (2021) 1003–1023, https://doi.org/10.1007/s11144-021-01962-5.

[6] A.S. Gohardani, J. Stanojev, A. Demairé, K. Anflo, M. Persson, N. Wingborg, C. Nilsson, Green space propulsion: opportunities and prospects, Prog. Aerosp. Sci. 71 (2014) 128–149, https://doi.org/10.1016/j.paerosci.2014.08.001.

[7] S.C. Perry, D. Pangotra, L. Vieira, L.-I. Csepei, V. Sieber, L. Wang, C. Ponce de León, F.C. Walsh, Electrochemical synthesis of hydrogen peroxide from water and oxygen, Nat. Rev. Chem. 3 (2019) 442–458, https://doi.org/10.1038/s41570-019-0110-6.

[8] ISRO working on green fuels like hydrogen peroxide for rockets, The Economic Times Chennai, 2020. ⟨https://energy.economictimes.indiatimes.com/news/renewable/isro-working-on-green-fuels-like-hydrogen-peroxide-for-rockets/80045159⟩. (Accessed 2 January 2021).

[9] J.M. Ramos, J.A. Wang, S.O. Flores, L.F. Chen, N. Nava, J. Navarrete, J. M. Domínguez, J.A. Szpunar, Ultrasound-assisted synthesis and catalytic activity of mesostructured FeOx/SBA-15 and FeOx/Zr-SBA-15 catalysts for the oxidative desulfurization of model diesel, Catal. Today 349 (2020) 198–209, https://doi.org/10.1016/j.cattod.2018.04.059.

[10] F. Bibak, G. Moradi, Oxidative desulfurization of model oil and oil cuts with MoO3/SBA-15: experimental design and optimization by Box–Behnken method, React. Kinet. Mech. Catal. 131 (2020) 935–951, https://doi.org/10.1007/s11144-020-01852-2.

[11] T.A.G. Duarte, S.M.G. Pires, I.C.M.S. Santos, M.M.Q. Simões, M.G.P.M.S. Neves, A. M.V. Cavaleiro, J.A.S. Cavaleiro, A Mn(iii) polyoxotungstate in the oxidation of organosulfur compounds by H_2O_2 at room temperature: an environmentally safe catalytic approach, Catal. Sci. Technol. 6 (2016) 3271–3278, https://doi.org/10.1039/c5cy01564b.

[12] R. Ghubayra, C. Nuttall, S. Hodgkiss, M. Craven, E.F. Kozhevnikova, I. V. Kozhevnikov, Oxidative desulfurization of model diesel fuel catalyzed by carbon-supported heteropoly acids, Appl. Catal. B Environ. 253 (2019) 309–316, https://doi.org/10.1016/j.apcatb.2019.04.063.

[13] J.S.J. Hargreaves, Y.-M. Chung, W.-S. Ahn, T. Hisatomi, K. Domen, M.C. Kung, H. H. Kung, Minimizing energy demand and environmental impact for sustainable NH_3 and H_2O_2 production—a perspective on contributions from thermal, electro-, and photo-catalysis, Appl. Catal. A Gen. 594 (2020), 117419, https://doi.org/10.1016/j.apcata.2020.117419.

[14] J. Casey, IMO 2020 to impact European refineries, Hydrocarbon Engineering, 2020. ⟨https://www.hydrocarbonengineering.com/clean-fuels/20012020/imo-2 020-to-impact-european-refineries/⟩. (Accessed 28 December 2020).

[15] A. Halff, L. Younes, T. Boersma, The likely implications of the new IMO standards on the shipping industry, Energy Policy 126 (2019) 277–286, https://doi.org/10.1016/j.enpol.2018.11.033.

[16] T.P.V. Zis, K. Cullinane, The desulphurisation of shipping: past, present and the future under a global cap, Transp. Res. D Transp. Environ. 82 (2020), 102316, https://doi.org/10.1016/j.trd.2020.102316.

[17] E. Linley, S.P. Denyer, G. McDonnell, C. Simons, J.Y. Maillard, Use of hydrogen peroxide as a biocide: new consideration of its mechanisms of biocidal action, J. Antimicrob. Chemother. 67 (2012) 1589–1596, https://doi.org/10.1093/jac/dks129.

[18] J. Andrew Kielbania, Anti-microbial composition and method for making and using same, Bioneutral Laboratories Corporation, 2015.

[19] WHO-recommended handrub formulations, WHO Guidelines on Hand Hygiene in Health Care: First Global Patient Safety Challenge Clean Care Is Safer Care, WHO Press, 2009. ⟨https://www.ncbi.nlm.nih.gov/books/NBK144054/⟩. (Accessed 5 January 2021).

[20] J.C. Rubio-Romero, M.D.C. Pardo-Ferreira, J.A. Torrecilla-Garcia, S. Calero-Castro, Disposable masks: disinfection and sterilization for reuse, and non-certified manufacturing, in the face of shortages during the COVID-19 pandemic, Saf. Sci. 129 (2020), 104830, https://doi.org/10.1016/j.ssci.2020.104830.

[21] V. Saini, K. Sikri, S.D. Batra, P. Kalra, K. Gautam, Development of a highly effective low-cost vaporized hydrogen peroxide-based method for disinfection of personal protective equipment for their selective reuse during pandemics, Gut Pathog. 12 (2020) 29, https://doi.org/10.1186/s13099-020-00367-4.

[22] V.C.C. Cheng, S.C. Wong, G.S.W. Kwan, W.T. Hui, K.Y. Yuen, Disinfection of N95 respirators by ionized hydrogen peroxide during pandemic coronavirus disease 2019 (COVID-19) due to SARS-CoV-2, J. Hosp. Infect. 105 (2020) 358–359, https://doi.org/10.1016/j.jhin.2020.04.003.

[23] Hydrogen peroxide demand rises in battle against COVID-19, Hydrogen Peroxide: COVID-19, Research and Markets, 2020. ⟨https://www.researchandmarkets.com/issues/hydrogen-peroxide-demand-rises⟩. (Accessed 13 May 2021).

[24] G.P. Riedl H.-J, Production of Hydrogen Peroxide, 1939.

[25] S. Anantharaj, S. Pitchaimuthu, S. Noda, A review on recent developments in electrochemical hydrogen peroxide synthesis with a critical assessment of perspectives and strategies, Adv. Colloid Interface Sci. 287 (2021), 102331, https://doi.org/10.1016/j.cis.2020.102331.

[26] C.P. De Leon, D. Pletcher, Removal of formaldehyde from aqueous solutions via oxygen reduction using a reticulated vitreous carbon cathode cell, J. Appl. Electrochem. 25 (1995) 307–314, https://doi.org/10.1007/bf00249648.

[27] P.J.M. Cordeiro-Junior, M.S. Kronka, L.A. Goulart, N.C. Veríssimo, L.H. Mascaro, M.Cd Santos, R. Bertazzoli, M.Rd.V. Lanza, Catalysis of oxygen reduction reaction for H$_2$O$_2$ electrogeneration: the impact of different conductive carbon matrices and their physicochemical properties, J. Catal. 392 (2020) 56–68, https://doi.org/10.1016/j.jcat.2020.09.020.

[28] R.S. Rocha, R.B. Valim, L.C. Trevelin, J.R. Steter, J.F. Carneiro, J.C. Forti, R. Bertazzoli, M.R.V. Lanza, Electrocatalysis of hydrogen peroxide generation using oxygen-fed gas diffusion electrodes made of carbon black modified with quinone compounds, Electrocatalysis 11 (2020) 338–346, https://doi.org/10.1007/s12678-020-00591-1.

[29] J. Moreira, V. Bocalon Lima, L. Athie Goulart, M.R.V. Lanza, Electrosynthesis of hydrogen peroxide using modified gas diffusion electrodes (MGDE) for environmental applications: quinones and azo compounds employed as redox modifiers, Appl. Catal. B Environ. 248 (2019) 95–107, https://doi.org/10.1016/j.apcatb.2019.01.071.

[30] G.V. Fortunato, E. Pizzutilo, E.S.F. Cardoso, M.R.V. Lanza, I. Katsounaros, S. J. Freakley, K.J.J. Mayrhofer, G. Maia, M. Ledendecker, The oxygen reduction reaction on palladium with low metal loadings: the effects of chlorides on the stability and activity towards hydrogen peroxide, J. Catal. 389 (2020) 400–408, https://doi.org/10.1016/j.jcat.2020.06.019.

[31] A. Verdaguer-Casadevall, D. Deiana, M. Karamad, S. Siahrostami, P. Malacrida, T. W. Hansen, J. Rossmeisl, I. Chorkendorff, I.E. Stephens, Trends in the electrochemical synthesis of H$_2$O$_2$: enhancing activity and selectivity by electrocatalytic site engineering, Nano Lett. 14 (2014) 1603–1608, https://doi.org/10.1021/nl500037x.

[32] K. Fuku, Y. Miyase, Y. Miseki, T. Funaki, T. Gunji, K. Sayama, Photoelectrochemical hydrogen peroxide production from water on a WO$_3$ /BiVO$_4$ photoanode and from O$_2$ on an Au cathode without external bias, Chem. Asian J. 12 (2017) 1111–1119, https://doi.org/10.1002/asia.201700292.

[33] H. Li, P. Wen, D.S. Itanze, Z.D. Hood, S. Adhikari, C. Lu, X. Ma, C. Dun, L. Jiang, D. L. Carroll, Y. Qiu, S.M. Geyer, Scalable neutral H$_2$O$_2$ electrosynthesis by platinum diphosphide nanocrystals by regulating oxygen reduction reaction pathways, Nat. Commun. 11 (2020) 3928, https://doi.org/10.1038/s41467-020-17584-9.

[34] F. Ma, S. Wang, X. Liang, C. Wang, F. Tong, Z. Wang, P. Wang, Y. Liu, Y. Dai, Z. Zheng, B. Huang, Ni$_3$B as a highly efficient and selective catalyst for the electrosynthesis of hydrogen peroxide, Appl. Catal. B Environ. 279 (2020), 119371, https://doi.org/10.1016/j.apcatb.2020.119371.

[35] J.F. Pérez, J. Llanos, C. Sáez, C. López, P. Cañizares, M.A. Rodrigo, Towards the scale up of a pressurized-jet microfluidic flow-through reactor for cost-effective electro-generation of H$_2$O$_2$, J. Clean. Prod. 211 (2019) 1259–1267, https://doi.org/10.1016/j.jclepro.2018.11.225.

[36] J.F. Pérez, J. Llanos, C. Sáez, C. López, P. Cañizares, M.A. Rodrigo, On the design of a jet-aerated microfluidic flow-through reactor for wastewater treatment by electro-Fenton, Sep. Purif. Technol. 208 (2019) 123–129, https://doi.org/10.1016/j.seppur.2018.04.021.

[37] K. Fuku, K. Sayama, Efficient oxidative hydrogen peroxide production and accumulation in photoelectrochemical water splitting using a tungsten trioxide/bismuth vanadate photoanode, Chem. Commun. 52 (2016) 5406–5409, https://doi.org/10.1039/c6cc01605g.

[38] X. Shi, S. Siahrostami, G.L. Li, Y. Zhang, P. Chakthranont, F. Studt, T.F. Jaramillo, X. Zheng, J.K. Norskov, Understanding activity trends in electrochemical water oxidation to form hydrogen peroxide, Nat. Commun. 8 (2017) 701, https://doi.org/10.1038/s41467-017-00585-6.

[39] S.Y. Park, H. Abroshan, X. Shi, H.S. Jung, S. Siahrostami, X. Zheng, CaSnO$_3$: an electrocatalyst for two-electron water oxidation reaction to form H$_2$O$_2$, ACS Energy Lett. 4 (2018) 352–357, https://doi.org/10.1021/acsenergylett.8b02303.

[40] T. Kang, B. Li, Q. Hao, W. Gao, F. Bin, K.N. Hui, D. Fu, B. Dou, Efficient hydrogen peroxide (H$_2$O$_2$) synthesis by CaSnO$_3$ via two-electron water oxidation reaction, ACS Sustain. Chem. Eng. 8 (2020) 15005–15012, https://doi.org/10.1021/acssuschemeng.0c05449.

[41] K. Fuku, Y. Miyase, Y. Miseki, T. Gunji, K. Sayama, Enhanced oxidative hydrogen peroxide production on conducting glass anodes modified with metal oxides, ChemistrySelect 1 (2016) 5721–5726, https://doi.org/10.1002/slct.201601469.

[42] S.R. Kelly, X. Shi, S. Back, L. Vallez, S.Y. Park, S. Siahrostami, X. Zheng, J. K. Nørskov, ZnO as an active and selective catalyst for electrochemical water oxidation to hydrogen peroxide, ACS Catal. 9 (2019) 4593–4599, https://doi.org/10.1021/acscatal.8b04873.

[43] C. Xia, S. Back, S. Ringe, K. Jiang, F. Chen, X. Sun, S. Siahrostami, K. Chan, H. Wang, Confined local oxygen gas promotes electrochemical water oxidation to hydrogen peroxide, Nat. Catal. 3 (2020) 125–134, https://doi.org/10.1038/s41929-019-0402-8.

[44] S. Mavrikis, M. Göltz, S. Rosiwal, L. Wang, C. Ponce de León, Boron-Doped diamond electrocatalyst for enhanced anodic H$_2$O$_2$ production, ACS Appl. Energy Mater. 3 (2020) 3169–3173, https://doi.org/10.1021/acsaem.0c00093.

[45] X. Shi, S. Back, T.M. Gill, S. Siahrostami, X. Zheng, Electrochemical synthesis of H$_2$O$_2$ by two-electron water oxidation reaction, Chem 7 (2021) 38–63, https://doi.org/10.1016/j.chempr.2020.09.013.

[46] S. Mavrikis, S.C. Perry, P.K. Leung, L. Wang, C. Ponce de León, Recent advances in electrochemical water oxidation to produce hydrogen peroxide: a mechanistic perspective, ACS Sustain. Chem. Eng. 9 (2020) 76–91, https://doi.org/10.1021/acssuschemeng.0c07263.

[47] C. Xia, Y. Xia, P. Zhu, L. Fan, H. Wang, Direct electrosynthesis of pure aqueous H$_2$O$_2$ solutions up to 20% by weight using a solid electrolyte, Science 366 (2019) 226–231, https://doi.org/10.1126/science.aay1844.

[48] N. Gurieff, D. Green, I. Koskinen, M. Lipson, M. Baldry, A. Maddocks, C. Menictas, J. Noack, B. Moghtaderi, E. Doroodchi, Healthy power: reimagining hospitals as sustainable energy hubs, Sustainability 12 (2020) 8554, https://doi.org/10.3390/su12208554.

[49] A. Siddharta, S. Pfaender, N.J. Vielle, R. Dijkman, M. Friesland, B. Becker, J. Yang, M. Engelmann, D. Todt, M.P. Windisch, F.H. Brill, J. Steinmann, J. Steinmann, S. Becker, M.P. Alves, T. Pietschmann, M. Eickmann, V. Thiel, E. Steinmann, Virucidal activity of world health organization-recommended formulations against enveloped viruses, including Zika, Ebola, and emerging coronaviruses, J. Infect. Dis. 215 (2017) 902–906, https://doi.org/10.1093/infdis/jix046.

[50] G. Kampf, D. Todt, S. Pfaender, E. Steinmann, Persistence of coronaviruses on inanimate surfaces and their inactivation with biocidal agents, J. Hosp. Infect. 104 (2020) 246–251, https://doi.org/10.1016/j.jhin.2020.01.022.

[51] J.P. Wood, W. Richter, M. Sunderman, M.W. Calfee, S. Serre, L. Mickelsen, Evaluating the environmental persistence and inactivation of MS$_2$ bacteriophage and the presumed Ebola virus surrogate Phi6 using low concentration hydrogen peroxide vapor, Environ. Sci. Technol. 54 (2020) 3581–3590, https://doi.org/10.1021/acs.est.9b06034.

[52] I. Salmerón, K.V. Plakas, I. Sirés, I. Oller, M.I. Maldonado, A.J. Karabelas, S. Malato, Optimization of electrocatalytic H$_2$O$_2$ production at pilot plant scale for solar-assisted water treatment, Appl. Catal. B Environ. 242 (2019) 327–336, https://doi.org/10.1016/j.apcatb.2018.09.045.

[53] L. Li, Z. Hu, J.C. Yu, On-demand synthesis of H$_2$O$_2$ by water oxidation for sustainable resource production and organic pollutant degradation, Angew. Chem. Int. Ed. Engl. 59 (2020) 20538–20544, https://doi.org/10.1002/anie.202008031.

[54] Y. Jin, Y. Shi, Z. Chen, R. Chen, X. Chen, X. Zheng, Y. Liu, R. Ding, Enhancement of solar water disinfection using H$_2$O$_2$ generated in situ by electrochemical reduction, Appl. Catal. B Environ. 267 (2020), 118730, https://doi.org/10.1016/j.apcatb.2020.118730.

[55] G. Ferro, A. Fiorentino, M.C. Alferez, M.I. Polo-López, L. Rizzo, P. Fernández-Ibáñez, Urban wastewater disinfection for agricultural reuse: effect of solar driven AOPs in the inactivation of a multidrug resistant E. coli strain, Appl. Catal. B Environ. 178 (2015) 65–73, https://doi.org/10.1016/j.apcatb.2014.10.043.

[56] T.M. Gill, X. Zheng, Comparing methods for quantifying electrochemically accumulated H$_2$O$_2$, Chem. Mater. 32 (2020) 6285–6294, https://doi.org/10.1021/acs.chemmater.0c02010.

[57] S. Ranganathan, V. Sieber, Development of semi-continuous chemo-enzymatic terpene epoxidation: combination of anthraquinone autooxidation and the lipase-mediated epoxidation process, React. Chem. Eng. 2 (2017) 885–895, https://doi.org/10.1039/c7re00112f.

[58] E.N. Kadnikova, N.M. Kostić, Oxidation of ABTS by hydrogen peroxide catalyzed by horseradish peroxidase encapsulated into sol–gel glass, J. Mol. Catal. B Enzym. 18 (2002) 39–48, https://doi.org/10.1016/s1381-1177(02)00057-7.

[59] S. Hrn, dm. Mn, K. Ac, Status of hydrogen peroxide solution 10 V in commercialized samples, Pharm. Anal. Acta 8 (2017), https://doi.org/10.4172/2153-2435.1000567.

[60] O. Pedersen, T.D. Colmer, K. Sand-Jensen, Underwater photosynthesis of submerged plants - recent advances and methods, Front. Plant Sci. 4 (2013) 140, https://doi.org/10.3389/fpls.2013.00140.

[61] D.E. Richardson, H. Yao, K.M. Frank, D.A. Bennett, Equilibria, kinetics, and mechanism in the bicarbonate activation of hydrogen peroxide: oxidation of sulfides by peroxymonocarbonate, J. Am. Chem. Soc. 122 (2000) 1729–1739, https://doi.org/10.1021/ja9927467.

[62] A. El-kharouf, B.G. Pollet, Chapter 4 - gas diffusion media and their degradation, in: M.M. Mench, E.C. Kumbur, T.N. Veziroglu (Eds.), Polymer Electrolyte Fuel Cell Degradation, Academic Press, Boston, 2012, pp. 215–247, https://doi.org/10.1016/B978-0-12-386936-4.10004-1.

[63] T.M. Gill, L. Vallez, X. Zheng, The role of bicarbonate-based electrolytes in H_2O_2 production through two-electron water oxidation, ACS Energy Lett. 6 (2021) 2854–2862, https://doi.org/10.1021/acsenergylett.1c01264.

[64] Y. Yi, G. Weinberg, M. Prenzel, M. Greiner, S. Heumann, S. Becker, R. Schlögl, Electrochemical corrosion of a glassy carbon electrode, Catal. Today 295 (2017) 32–40, https://doi.org/10.1016/j.cattod.2017.07.013.

[65] H. Schultz, G. Bauer, E. Schachl, F. Hagedorn, P. Schmittinger, Potassium Compounds, Ullmann's Encyclopedia of Industrial Chemistry. ⟨https://doi.org/10.1002/14356007.a22_039⟩.

[66] P.A. Michaud, Electrochemical oxidation of water on synthetic boron-doped diamond thin film anodes, J. Appl. Electrochem. 33 (2003) 151–154, https://doi.org/10.1023/a:1024084924058.

[67] H. Lee, A.-H. Park, C. Oloman, Stability of hydrogen peroxide in sodium carbonate solutions, Tappi J. 83 (2000).

[68] J. Zhang, C.W. Oloman, Electro-oxidation of carbonate in aqueous solution on a platinum rotating ring disk electrode, J. Appl. Electrochem. 35 (2005) 945–953, https://doi.org/10.1007/s10800-005-7078-2.

[69] A.O. Terent'ev, Z.Y. Pastukhova, I.A. Yaremenko, L.G. Bruk, G.I. Nikishin, Promising hydrogen peroxide stabilizers for large-scale application: unprecedented effect of aryl alkyl ketones, Mendeleev Commun. 26 (2016) 329–331, https://doi.org/10.1016/j.mencom.2016.07.021.

[70] K. Hanna, Comment on "Inhibitory effect of dissolved silica on H_2O_2 decomposition by iron(III) and manganese(IV) oxides: implications for H_2O_2–based in situ chemical oxidation", Environ. Sci. Technol. 46 (2012) 3591–3592, https://doi.org/10.1021/es3002103.

[71] I. Charron, A. Couvert, A. Laplanche, C. Renner, L. Patria, B. Requieme, Treatment of odorous sulphur compounds by chemical scrubbing with hydrogen peroxide - stabilisation of the scrubbing solution, Environ. Sci. Technol. 40 (2006) 7881–7885, https://doi.org/10.1021/es060414d.

[72] E.J. Ruiz-Ruiz, Y. Meas, R. Ortega-Borges, J.L.Jurado Baizabal, Electrochemical production of peroxocarbonate at room temperature using conductive diamond anodes, Surf. Eng. Appl. Electrochem. 50 (2015) 478–484, https://doi.org/10.3103/S106837551406009X.

[73] F. Kuttassery, A. Sebastian, S. Mathew, H. Tachibana, H. Inoue, Promotive effect of bicarbonate ion on two-electron water oxidation to form H_2O_2 catalyzed by aluminum porphyrins, ChemSusChem 12 (2019) 1939–1948, https://doi.org/10.1002/cssc.201900560.

[74] W.D. Nicoll, A.F. Smith, Stability of dilute alkaline solutions of hydrogen peroxide, Ind. Eng. Chem. 47 (1955) 2548–2554, https://doi.org/10.1021/ie50552a051.

[75] S. Lips, S.R. Waldvogel, Use of boron-doped diamond electrodes in electro-organic synthesis, ChemElectroChem 6 (2019) 1649–1660, https://doi.org/10.1002/celc.201801620.

[76] P.Mvd Wiel, L.J.J. Janssen, J.G. Hoogland, Electrolysis of a carbonate-borate solution with a platinum anode—I. Current efficiency at perborate concentration of zero, Electrochim. Acta 16 (1971) 1217–1226, https://doi.org/10.1016/0013-4686(71)85110-1.

[77] C.P. Chardon, T. Matthée, R. Neuber, M. Fryda, C. Comninellis, Efficient electrochemical production of peroxodicarbonate applying DIACHEM®Diamond electrodes, ChemistrySelect 2 (2017) 1037–1040, https://doi.org/10.1002/slct.201601583.

[78] R.R.Rais Irkham, T.A. Ivandini, A. Fiorani, Y. Einaga, Electrogenerated chemiluminescence of luminol mediated by carbonate electrochemical oxidation at a boron-doped diamond, Anal. Chem. 93 (2021) 2336–2341, https://doi.org/10.1021/acs.analchem.0c04212.

[79] S. Mavrikis, M. Göltz, S.C. Perry, F. Bogdan, P.K. Leung, S. Rosiwal, L. Wang, C. Ponce de León, Effective hydrogen peroxide production from electrochemical water oxidation, ACS Energy Lett. 6 (2021) 2369–2377, https://doi.org/10.1021/acsenergylett.1c00904.

[80] K. Wenderich, B.A.M. Nieuweweme, G. Mul, B.T. Mei, Selective electrochemical oxidation of H_2O to H_2O_2 using boron-doped diamond: an experimental and techno-economic evaluation, ACS Sustain. Chem. Eng. 9 (2021) 7803–7812, https://doi.org/10.1021/acssuschemeng.1c01244.

3.2.1   Combination of cathodic and anodic production of H_2O_2

Herein, optimized conditions for anodic H_2O_2 production were applied for a combined cell producing H_2O_2 at the anode and the cathode. The oxygen reduction reaction has been reported to be highly selective for H_2O_2 production using carbon electrode [81]. Unmodified CFP was used as anode as well as cathode. The cathodic production of H_2O_2 from O_2 reduction was carried out using CFP on gas diffusion electrodes with a compressed air flow of 50 mL min^{-1}. The electrolysis was carried out galvanostatically in 2 mol L^{-1} KHCO$_3$ with 30 mmol L^{-1} of Na$_2$SiO$_3$ as a stabilizer at 100 mA cm^{-2} with an electrolyte flow of 100 mL min^{-1}. The pH was regulated to stay constant at 9. The concentration of H_2O_2 reached up to 54 mmol L^{-1} after 120 minutes with an initial FE of 56% at the cathodic compartment, whereas H_2O_2 concentration in the anolyte was 4 mmol L^{-1} after 150 minutes with an initial FE of 4%, reaching a total cell FE of 55% shown in **Figure 3.7**. It should be noted that the lower FE efficiency at the cathode was due to higher applied current density of 100 mA cm^{-2} as well as usage of compressed air. A chronopotentiometry measurement showed that at higher current density of 100 mA cm^{-2}, the electrode potential difference between the Argon (Ar) saturated electrolyte and the O_2 saturated electrolyte was lower as compared to the measurement at lower current density of 10 mA cm^{-2} (**Figure 3.6**).
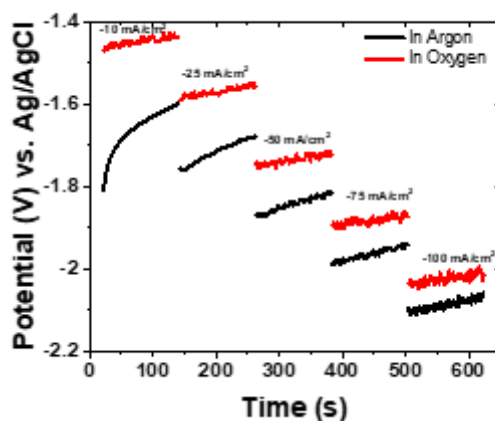
Fig. 3.6 : *Chronopotentiometric measurements (CP) of unmodified carbon paper at different current densities for 2 min each in 2 mol L^{-1} KHCO$_3$ solutions saturated with O_2 (red line) or Ar (black line).*
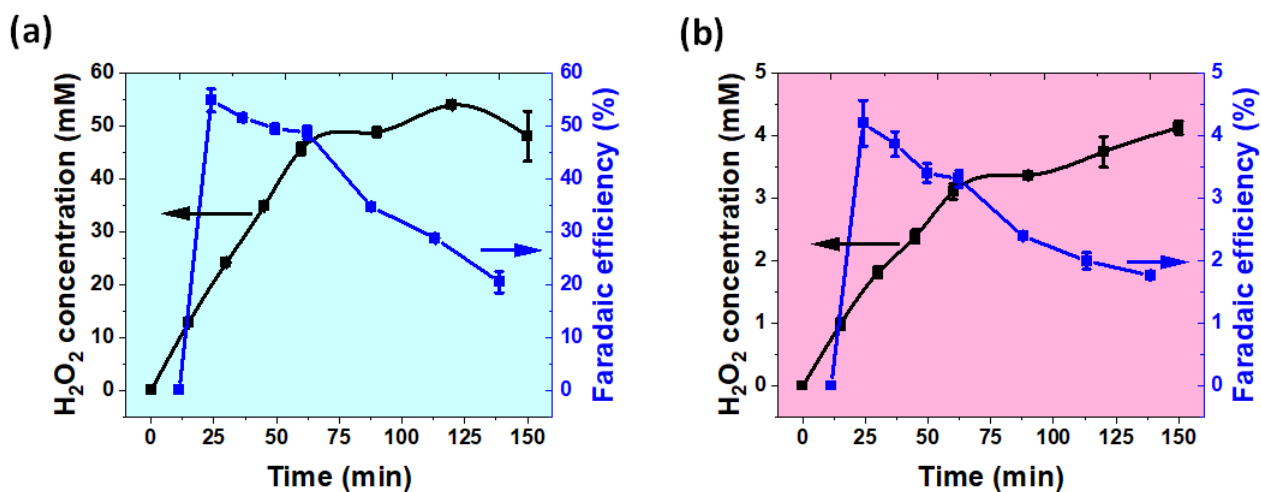
Fig. 3.7 : *A coupled experimental study combining anodic and cathodic synthesis of H_2O_2.* *Concentration (black line) and faradaic efficiency (blue line) for H_2O_2 production in the **(a)** cathodic and **(b)** anodic compartment during 150 minutes of electrolysis at 100 mA cm^{-2} using a flow cell with an electolyte flow rate of 100 mL min^{-1} in both comparments, and compressed air flow of 50 mL min^{-1} in cathodic chamber.*

Based on these experiments, further combined studies with improved electrode and electrocatalytic systems could pave the way towards achieving a 200% efficiency for H_2O_2 production.

3.3   Anodic generation of hydrogen peroxide in continuous flow

Title: Anodic generation of hydrogen peroxide in continuous flow

Status: Published (2022)

Journal: Green Chemistry

Publisher: Royal Society of Chemistry

DOI: doi.org/10.1039/D2GC02575B

Authors: Dhananjai Pangotra, Lénárd-István Csepei, Arne Roth, Volker Sieber, Luciana Vieira
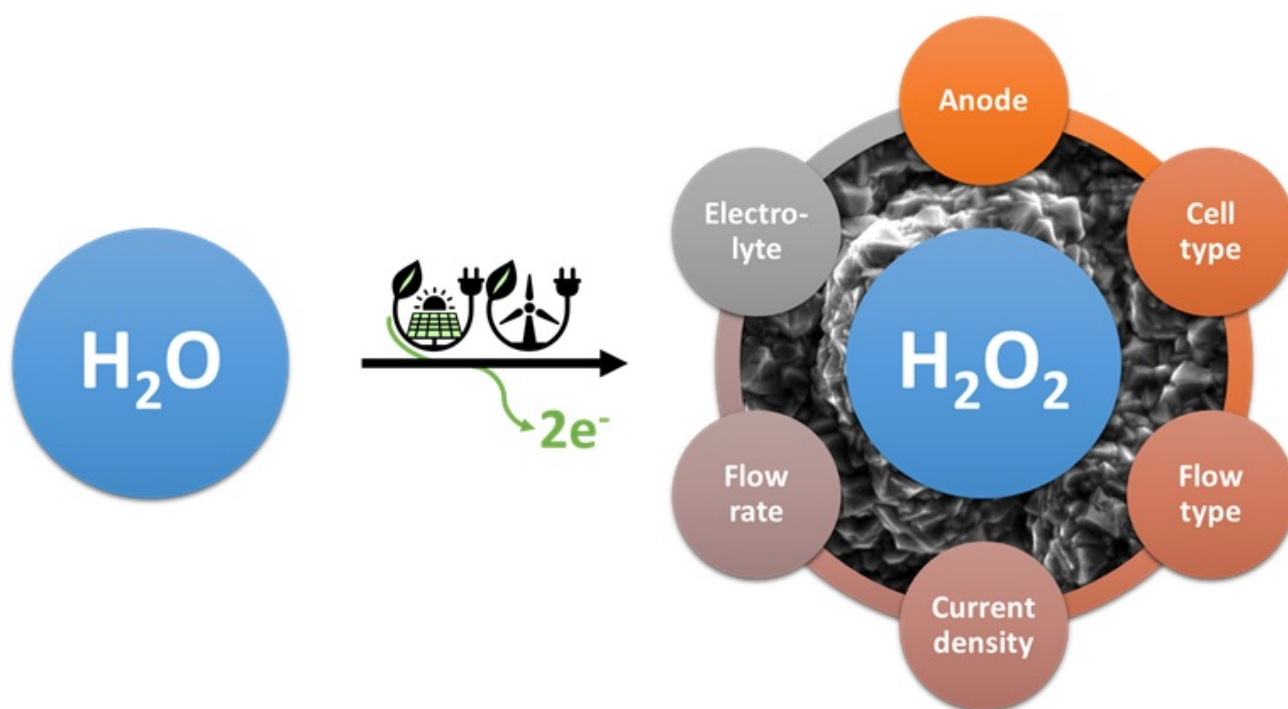
In this publication, the remarkable properties of a commercial BDD electrode for the anodic production of H_2O_2 in a scalable and continuous flow process was exploited. A continuous flow process in combination with an optimized carbonate-based electrolyte established in **Section 3.2** was used. Different flow setups (circular and single-pass) as well as the effect of flow rate were investigated and compared based on FE and production rate in continuous mode at current densities of up to 700 mA cm^{-2}. The experimental results shown in this article depict the crucial importance of the electrochemical process development beyond catalyst and electrolyte.

Dhananjai Pangotra conceptualized and designed the experiment, performed all the lab work, analyzed the data, and wrote the first draft. Lénárd-István Csepei, Arne Roth, and Luciana Vieira supported the conceptualization. Lénárd—István Csepei calculated the ionic activities of different carbonate species. Lénárd—István Csepei, Arne Roth, Volker Sieber, and Luciana Vieira reviewed this work. Arne Roth, Volker Sieber, and Luciana Vieira supervised the research.

Anodic generation of hydrogen peroxide in continuous flow

Green Chemistry

Cutting-edge research for a greener sustainable future

rsc.li/greenchem

ROYAL SOCIETY
OF CHEMISTRY
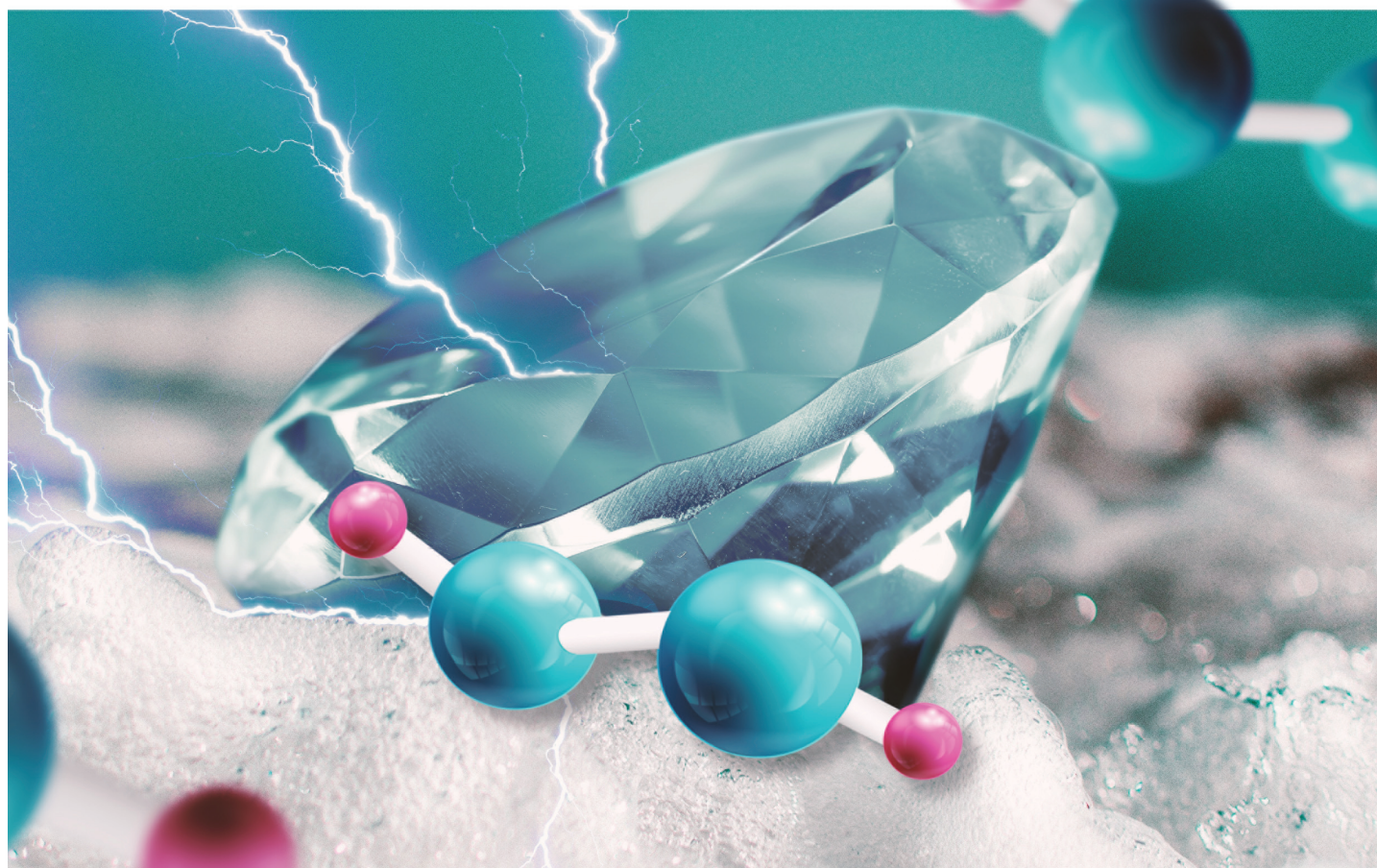
PAPER
Dhananjai Pangotra *et al.*
Anodic generation of hydrogen peroxide in continuous flow

Green Chemistry

Check for updates

Anodic generation of hydrogen peroxide in continuous flow†

Dhananjai Pangotra, [a,b] Lénárd-István Csepei,[a] Arne Roth,[a] Volker Sieber [a,b] and Luciana Vieira *[a]

The electrochemical production of hydrogen peroxide (H_2O_2) is an appealing green alternative to the classic anthraquinone process. Herein, we show the development of a process to produce H_2O_2 anodically in continuous flow at high current densities. The role of CO_3^{2-} ion activity in enhancing the anodic H_2O_2 generation using a commercial boron-doped diamond (BDD) electrode is investigated in detail. The process development comprising the optimization of electrolyte flow type and flow rates enabled electrochemical operation at current densities up to 700 mA cm^{-2}, with Faraday efficiencies up to 78%, and the highest-ever reported H_2O_2 production rate of 79 $\mu mol\ min^{-1}\ cm^{-2}$. Continuous flow experiments are essential for technical applications, which is one of the first upscaling steps. A continuous and stable H_2O_2 productivity with constant production rates for up to 28 hours was achieved. Our experiments unfold the importance of electrochemical process development and the interplay of the electrode, electrolyte, and operating cell parameters to achieve a highly efficient, scalable, stable, and continuous system for the $2e^-$ water oxidation to H_2O_2.

Introduction

Hydrogen peroxide (H_2O_2) is a widely used chemical with a market evaluated at \$4 billion in 2020, forecasted to grow to \$5.2 billion by 2026.[1] Its strong oxidizing capability enables a broad application in the chemical industry. Moreover, because it releases only water (H_2O) and oxygen (O_2) as a side-product, H_2O_2 is extensively used as a green oxidant. Industrial applications include drinking water[2,3] and wastewater treatment,[4,5] bleaching,[6] desulfurization of conventional energy carriers[7] and bio-based feedstocks,[8,9] sanitation,[10] organic synthesis,[11–13] and aerospace fuels.[14] New niche of applications in catalyst synthesis,[15] biofuel generation,[16] and desulfurization of biogas[17] are also expected to ramp up the demand for H_2O_2 in the future. Hence, in the context of these broad application spectra, H_2O_2 is among the 100 most essential chemicals globally.[18,19]

The industrial production of H_2O_2 is mainly through the anthraquinone autoxidation (AO) process. The AO-process is considerably energy-demanding (aggregate consumption up to 17.6 kW h kg^{-1} H_2O_2),[20] uses large amounts of organic solvents and involves remarkable risks associated with hydrogenation and oxidation reactions under high H_2/O_2 pressure.[21] Furthermore, it requires expensive palladium-based catalysts and complex, large-scale equipment.[22] The industrial AO process involves distillation of H_2O_2 to generate large volumes of concentrated solution (from 40 to 70 wt%),[23] which is required for its transportation and very specific applications. Nevertheless, the primary use of H_2O_2 in bleaching and disinfectant requires H_2O_2 concentrations from 3 to 8 wt%.[24,25] While transportation of H_2O_2 in high concentrations is risky, shipping in lower concentrations poses the disadvantage of moving mainly water, thus negatively affecting the carbon footprint and economic viability of the product. Therefore, a portable device for decentralized and on-demand H_2O_2 production only based on water, air, and (renewable) electric energy as input provides a desirable local and "green" solution for the supply of H_2O_2 where it is needed.

The electrochemical production of H_2O_2 is based on water, air, and renewable electric energy as primary feedstocks. Therefore, it is an elegant green solution for onsite and on-demand H_2O_2 production, also avoiding risks associated with large-scale storage and transportation of highly concentrated H_2O_2 solutions.[22] There are two electrochemical routes for H_2O_2 production: the cathodic oxygen reduction reaction (ORR, eqn (1)) and the anodic water oxidation reaction (WOR, eqn (2)). Both pathways involve a two-electron transfer reac-

[a] Fraunhofer Institute of Interfacial Engineering and Biotechnology IGB, Bio-, Electro-, and Chemocatalysis BioCat, Straubing Branch, Schulgasse 11a, 94315 Straubing, Germany. E-mail: luciana.vieira@igb.fraunhofer.de
[b] Chair of Chemistry for Biogenic Resources, Campus Straubing for Biotechnology and Sustainability, Technical University of Munich, Schulgasse 16, 94315 Straubing, Germany
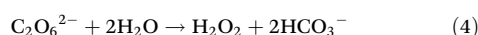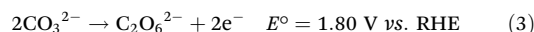†Electronic supplementary information (ESI) available. See DOI: https://doi.org/10.1039/d2gc02575b

Paper

tion.[22] The WOR pathway at the anode is particularly attractive because it can be coupled with cathodic reactions running on large scales, such as the CO_2 reduction reaction (CO_2RR) and the water electrolysis for hydrogen evolution reaction (HER).[26] Currently, both reactions are coupled with WOR to O_2, which besides being harmless, is an economically insignificant half-cell reaction and utilizes expensive and critical electrode materials such as iridium.[27,28] Combining anodic and cathodic processes that generate value-added products can enhance the overall cost efficiency of the whole production process.

$$O_2 + 2H^+ + 2e^- \rightarrow H_2O_2 \quad E° = 0.67 \text{ V } vs. \text{ RHE} \quad (1)$$

$$2H_2O \rightleftharpoons H_2O_2 + 2H^+ + 2e^- \quad E° = 1.76 \text{ V } vs. \text{ RHE} \quad (2)$$
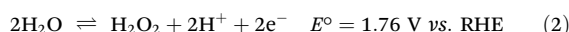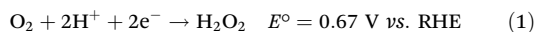
The electrochemical WOR to H_2O_2 has gained massive interest in the last years. A strong focus on catalyst development has been crucial for reaction improvement leading to a significant increase in efficiency, selectivity, and stability. Catalysts based on metal oxides such as $CaSnO_3$,[29–31] $BiVO_4$,[32] and ZnO,[33] as well as on metal porphyrin complexes of Ge[34] and Al[35] have been reported to be highly active catalysts for WOR. Another class of promising materials are boron-doped diamond (BDD) electrodes.[36–38] BDDs are robust electrodes with remarkably high overpotential for oxygen evolution reaction (OER). By suppressing O_2 evolution, high efficiency for H_2O_2 production is obtained on BDD.[39] Such materials have been used as anode for waste-water treatment for a long time.[40] Recent progress on the properties of BDD materials has significantly enhanced H_2O_2 production performance, leading to outstanding production rates of 74.6 µmol min^{-1} cm^{-2} H_2O_2 and peak faradaic efficiency (FE) of 87%.[38]

Nevertheless, all reports of WOR to H_2O_2 on BDD have so far been carried out in electrochemical H-cell setups.[37,38] In this context, the process transfer to electrochemical flow cells would be the first step toward technical applications, continuous production and scale-up.[41] Despite the remarkable benefits of electrochemical flow systems in terms of their operational conditions and scalability potential, only a few studies on WOR in flow cells have been reported up to date.[36,42]

Herein, we exploit the remarkable properties of a commercial BDD electrode for the anodic production of H_2O_2 in a scalable and continuous flow process. Our previous work reported a direct relationship between the ionic activity of CO_3^{2-} and enhanced anodic H_2O_2 production on commercial carbon fiber paper (CFP) anodes.[42] A cyclic mechanism of H_2O_2 production catalyzed by carbonate ions was proposed through the formation of peroxodicarbonate species ($C_2O_6^{2-}$) (eqn (3) and (4)).[42]

$$2CO_3^{2-} \rightarrow C_2O_6^{2-} + 2e^- \quad E° = 1.80 \text{ V } vs. \text{ RHE} \quad (3)$$

$$C_2O_6^{2-} + 2H_2O \rightarrow H_2O_2 + 2HCO_3^- \quad (4)$$

This mechanism was based on the correlation between the calculated activity of carbonate ions (CO_3^{2-}) in the electrolyte and the observed H_2O_2 formation rate, later confirmed by *in situ* infrared spectroscopy (ATR-FTIR) by Gill *et al.*[43]

In the present study, we extended the scope to show a continuous flow process using a commercial BDD electrode in combination with an optimized carbonate-based electrolyte system. We investigated and compared different flow setups (circular and single-pass) as well as the effect of flow rate on FE and production rate in continuous mode at current densities of up to 700 mA cm^{-2}. Our experimental results show the crucial importance of the electrochemical process development beyond catalyst and electrolyte.

Experimental section

Materials

Potassium hydrogen carbonate ($KHCO_3$, Sigma Aldrich, 99.5%), potassium carbonate (K_2CO_3, ReagentPlus®, 99%), titanium(IV) oxysulfate ($TiOSO_4$, ≥29% Ti (as TiO_2) basis, technical), and sodium metasilicate (Na_2SiO_3) were purchased from Sigma Aldrich. Potassium hydroxide (KOH, ≥85%) was obtained from Carl Roth. All materials and chemicals were used as received.

Electrochemical experiments

Electrochemical measurements were performed using an Autolab PGSTAT128N potentiostat/galvanostat equipped with a 10 A booster. A two-compartment H-cell divided by Nafion 117 (Ion Power, Germany) cation exchange membrane (CEM) was used for preliminary studies. The anode was a 5 cm^2 (geometric area) BDD electrode sputtered on a Si substrate and with boron doping between 2000 to 5000 ppm (DIACHEM®, Condias GmbH, Fig. S1, ESI†). The auxiliary cathode was an IrO_2/Ti mesh, and the reference electrode a Ag/AgCl system in 3.5 mol L^{-1} KCl (eDAQ). The gap between cathode and anode was 6 cm. Each compartment of the H-cell was filled with 25 mL of electrolyte. Linear sweep voltammetry (LSV) was recorded at a scan rate of 100 mV s^{-1}. Galvanostatic experiments were carried out at current densities ranging from 10 to 300 mA cm^{-2} using bicarbonate (HCO_3^-) and carbonate (CO_3^{2-}) electrolytes. Current densities were calculated based on the geometric area of the electrode. Chronopotentiometry measurements were performed under a constant stirring rate of 1000 rpm with a Teflon coated magnetic stirrer. An ice bath was used to avoid thermal decomposition of generated H_2O_2. The potentials are reported against the reversible hydrogen electrode (RHE), calculated by the eqn (5).

$$E_{(RHE)} = E_{Ag/AgCl} + 0.059 \, pH + E°_{Ag/AgCl} \quad E°_{Ag/AgCl} = 0.205 \text{ V} \quad (5)$$

Experiments under flow were performed using a microflow cell (Electrocell, Denmark) with a unique design from Siemens Energy for the CO2EXIDE project (Horizon 2020, grant agreement no. 768789). The cell was equipped with 10 cm^2 (3 × 3.5 cm) electrodes (cathode and anode) separated by a Nafion 117 membrane. A carbon electrode was used as a cathode, and DIACHEM® BDD/Ta (2000–5000 ppm B doping, Condias GmbH) was used as an anode, with an electrode distance of 8 mm. If not otherwise specified, the anolyte and catholyte

Green Chemistry

volume were 200 mL for each half-cell. The electrolyte flow was controlled by a flow pump (Watson-Marlow) in a flow range varying from 2 to 120 mL min^{-1}. The pH and conductivity of the electrolyte were monitored with a pH-meter (VWR pH 3210) and a conductometer (VWR pHenomenal® CO 3100 H), respectively. All flow experiments were carried out with 2 mol L^{-1} K$_2$CO$_3$. The electrolyte flow setup was varied as circular or single-pass. Circular flow experiments were performed at a constant flow rate of 100 mL min^{-1}, with Na$_2$SiO$_3$ as a stabilizer in the electrolyte and regulated at a pH of 12.6. The single-pass flow rate was varied between 5 and 100 mL min^{-1}. Moreover, in single-pass flow experiments, the electrolyte containing H$_2$O$_2$ was collected in a separate reservoir. Anolyte samples were collected periodically after having passed the cell and before collecting in the reservoir.

Quantitative product analysis

The quantification of the anodically generated H$_2$O$_2$ was performed using the TiOSO$_4$ method as described in the literature.[39,44,45] In short, 0.1 mol L^{-1} TiOSO$_4$ in 2 mol L^{-1} H$_2$SO$_4$ solution was prepared prior to the H$_2$O$_2$ detection. 25 μL of anolyte sample was mixed with 975 μL of 0.1 mol L^{-1} TiOSO$_4$ solution in a standard cuvette. In the presence of H$_2$O$_2$, a color change from colorless to yellow is observed due to the formation of pertitanic acid (eqn (6)). The absorbance of pertitanic acid was measured at 407 nm using a Shimadzu UV-1800 spectrophotometer. The molar extinction coefficient (ε_{407nm}) is 6.89×10^2 L mol^{-1} cm^{-1}.[46]

$$H_2O_2 + TiO^{2+} + H_2O \rightarrow H_2TiO_4 + 2H^+ \quad (6)$$
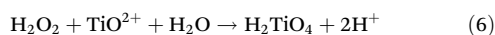
The faradaic efficiency (FE) was calculated with eqn (7):

$$FE(\%) = \frac{n_{H_2O_2} \times z \times F}{q} \times 100 \quad (7)$$

where $n_{H_2O_2}$ is the number of moles of H$_2$O$_2$ (in mol) produced, z is the electrons required for water oxidation to H$_2$O$_2$ ($z = 2$), F is the faradaic constant (96 485 C mol^{-1}), and q is the total charge passed (in Coulombs).

The H$_2$O$_2$ production rate is given by eqn (8):

$$\text{Production rate}(\mu mol\ min^{-1}\ cm^{-2})$$
$$= \frac{H_2O_2\ detected(\mu mol)}{time(min) \times area\ of\ the\ electrode(cm^2)}. \quad (8)$$

The energy consumption was calculated according to eqn (9).

$$EC(kW\ h\ kg^{-1}) = \frac{U \times z \times F}{M \times FE \times 3600} \times 100. \quad (9)$$

where U is the applied cell potential (in V), and M is the molar mass of H$_2$O$_2$ (in g mol^{-1}).

Calculation of ionic activities for HCO$_3^-$ and CO$_3^{2-}$

The ionic activity of the bicarbonate (a(HCO$_3^-$)) and carbonate (a(CO$_3^{2-}$)) ions were calculated as previous reported (eqn (S1)–(S6), ESI†).[42]

Results and discussion

With the objective of achieving unprecedented levels of performance for the anodic H$_2$O$_2$ generation under technically relevant and scalable operational conditions, this study is divided into two parts: (i) a preliminary evaluation of the electrolyte in an H-cell configuration and (ii) an electrochemical process optimization in a continuous flow reactor. In the first part, the effect of the electrolyte composition on WOR to H$_2$O$_2$ is qualitatively and quantitatively evaluated. In the second part, the process is transferred to a continuous flow reactor under optimized electrolyte conditions, where the effect of flow setup and flow rate is investigated and optimized towards higher anodic H$_2$O$_2$ productivity.

The electrolyte effect

Bicarbonate solutions have been widely used for WOR to H$_2$O$_2$.[37,43,47] The molar fraction of the bicarbonate (HCO$_3^-$)/carbonate (CO$_3^{2-}$) species in solution is dependent on the pH of the electrolyte (eqn (10) and (11)).

$$H_2CO_3 \rightleftharpoons HCO_3^- + H^+ \quad (pK_{a,1} = 3.7) \quad (10)$$

$$HCO_3^- \rightleftharpoons CO_3^{2-} + H^+ \quad (pK_{a,2} = 10.3) \quad (11)$$
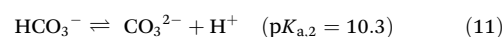
Basic pHs favor higher activity of carbonate ions, which promotes the WOR to H$_2$O$_2$ through the intermediate formation of peroxodicarbonate species (C$_2$O$_6^{2-}$, Scheme S1, ESI†).[42,43] Although the benefits of high pH are significant, it can be detrimental due to the low stability of H$_2$O$_2$ under alkaline conditions. Therefore, a chemical stabilizer was added to the anolyte to decelerate the alkaline decomposition of H$_2$O$_2$.[42]

WOR in 2 mol L^{-1} solutions of bicarbonate (KHCO$_3$, at pH 8.4) and carbonate (K$_2$CO$_3$, at pH 12.6) electrolytes were evaluated by linear sweep voltammetry (LSV) on BDD electrodes (Fig. 1a). The two electrolytes show a distinct current density profile. At +3.2 V vs. RHE, the current density is substantially higher for K$_2$CO$_3$ (155 mA cm^{-2}) compared to KHCO$_3$ (140 mA cm^{-2}). The onset potential, defined as the potential where the current density starts to increase exponentially, is also considerably lower for carbonate (+2.45 V vs. RHE) than for bicarbonate solutions (+2.66 V vs. RHE). Both aspects, higher current density and low onset potential, indicate a higher electrochemical activity for WOR in K$_2$CO$_3$ electrolytes compared to KHCO$_3$.

The effect of current density on H$_2$O$_2$ production for these two carbonate-based electrolytes (HCO$_3^-$ and CO$_3^{2-}$) was further evaluated by chronopotentiometry (CP) at pH 8.4 and pH 12.6 (Fig. 1b). Increasing the current density results in a higher H$_2$O$_2$ concentration for both electrolytes, yet carbonate-based electrolytes lead to higher overall H$_2$O$_2$ concentrations.[38,42,48] A maximum of 70 mmol L^{-1} of H$_2$O$_2$ was obtained in carbonate at 300 mA cm^{-2}, compared to only 16.4 mmol L^{-1} H$_2$O$_2$ in bicarbonate.

The FE at applied different current densities showed a peak of 57% in carbonate solutions at 100 mA cm^{-2}, whereas the
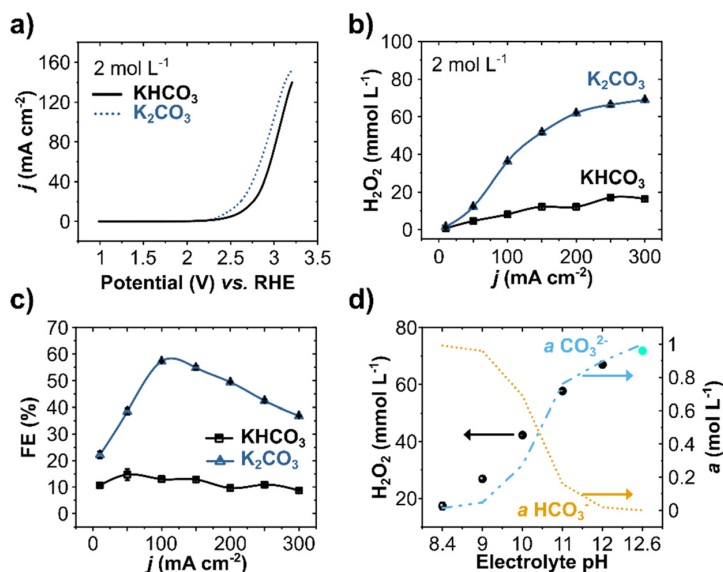
Paper

Fig. 1 WOR to H_2O_2 in 2 mol L^{-1} $KHCO_3$ and K_2CO_3 electrolytes. (a) Anodic LSV starting from +0.18 V *vs.* Ag/AgCl (calculated *vs.* RHE) with a scan rate of 100 mV s^{-1}. (b) H_2O_2 concentration and (c) FE at the indicated applied current densities for 10 minutes at each step. (d) Galvanostatic polarization at 300 mA cm^{-2} for 10 minutes in 2 mol L^{-1} $KHCO_3$ (at adjusted pH values from 8.4 to 12) and 2 mol L^{-1} K_2CO_3 (pH 12.6) and the corresponding calculated ionic activity for HCO_3^- and CO_3^{2-} ions. The experiments were performed using a 5 cm^2 BDD anode in a two-compartment H-cell cooled in an ice bath. The electrolyte was changed between the galvanostatic steps and kept under constant stirring of 1000 rpm.

FEs in bicarbonate electrolytes lay between 10 and 15% for all current densities (Fig. 1c). Higher FE for carbonate solutions (at least four times higher than in bicarbonate) confirms that higher pH regimes enhance the electrochemical production of H_2O_2 on BDD anodes, consistent with our previous studies with carbon anodes.[42] At current densities higher than 100 mA cm^{-2}, the FE decreases, reaching 36% at 300 mA cm^{-2}, where the highest H_2O_2 concentration was achieved. This lower FE, despite higher net H_2O_2 concentrations, indicates a combined effect of enhanced oxygen evolution and electrolytic H_2O_2 decomposition.[37] Notwithstanding, anodic H_2O_2 formation reached a partial current density (jH_2O_2) of 110 mA cm^{-2} and a production rate of 35 µmol min^{-1} cm^{-2} at 300 mA cm^{-2} (Fig. S3, ESI†).

As different carbonate species (H_2CO_3, HCO_3^-, and CO_3^{2-}) can be formed by varying the pH of the solution, the ionic activity for HCO_3^- ($a(HCO_3^-)$) and CO_3^{2-} ($a(CO_3^{2-})$) species in the electrolyte was calculated as a function of pH for the range of pH 8.4 to 12.6 (Fig. 1d). In the same pH range, the anodic H_2O_2 production at 300 mA cm^{-2} was evaluated experimentally. The pH of the 2 mol L^{-1} $KHCO_3$ was adjusted using KOH salt. The calculated activity profile for $a(HCO_3^-)$ and $a(CO_3^{2-})$ show a remarkable correlation with the experimentally measured anodic H_2O_2 production. Higher $a(CO_3^{2-})$ at higher pH values lead to significantly higher H_2O_2 concentrations. A considerable visual difference in the anode was also observed at higher pH values, as the O_2 evolution substantially decreased. Higher H_2O_2 production at higher pH is consistent with our proposed mechanism, which involves the oxidation of

carbonate ions to peroxodicarbonate species as intermediates.[42]

WOR in a continuous flow reactor

Envisioning the scale-up and technical application of anodic water oxidation to H_2O_2, a flow cell setup was used for further investigations. The electrochemical flow mode/setup (circular or single-pass), the electrolyte flow rate, and the long-term stability of the system were investigated and optimized.

Anodic H_2O_2 production in circular flow

Circular flow experiments allow the increase of product concentration in the electrolyte reservoir by recirculating it through the cell multiple times (Fig. 2a and Fig. S4, ESI†). Galvanostatic experiments on circular flow were carried out at current densities of 100, 200, and 300 mA cm^{-2} (Fig. 2b) with a constant flow rate of 100 mL min^{-1}. The highest H_2O_2 concentration was obtained at 200 mA cm^{-2} (58 mmol L^{-1}) after recirculating for 150 minutes. In all experiments, the FE reached its maximum peak at 15 minutes, and longer reaction times resulted in lower FE and formation rates (Fig. 2c and Fig. S5a, ESI†), indicating not only WOR to O_2 as also the electrochemical decomposition of H_2O_2. Such production rate decrease with time was also observed in H-cell experiments (Fig. S6, ESI†), and it is consistent with the literature.[37,42,49]

The specific electric energy consumption for the anodic H_2O_2 generation was calculated for the first reaction stage of high formation rate (first 15 minutes, Fig. 2d) and for the

Green Chemistry
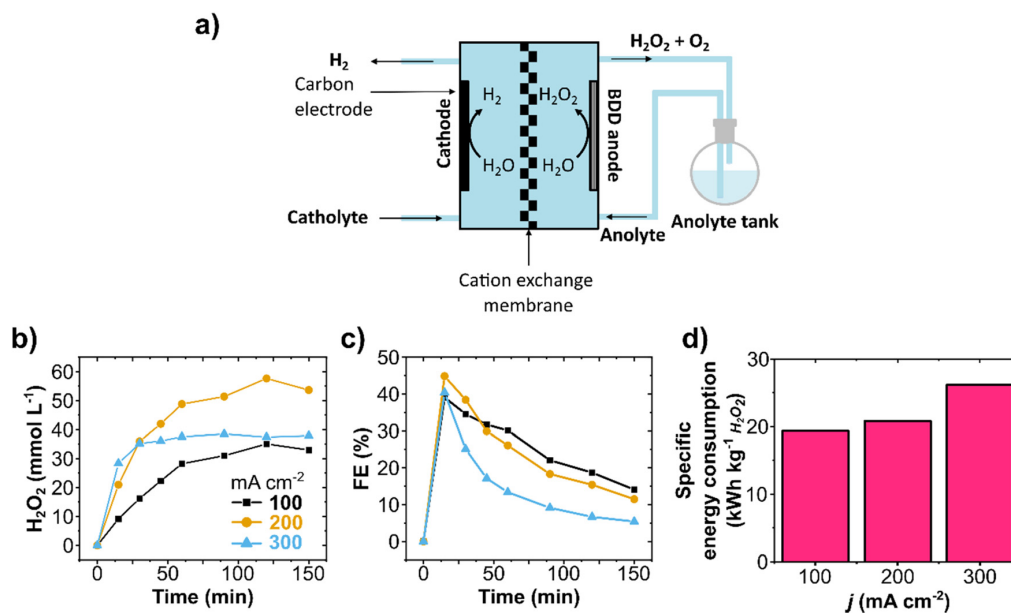
Fig. 2 Anodic H_2O_2 production in a circular flow reactor. (a) Schematic representation of the flow cell with circular flow. (b) H_2O_2 concentration and (c) FE obtained at different applied current densities. (d) Energy consumption to produce 1 kg of H_2O_2 based on the peak FE (at 15 min) at each applied current density. The flow cell was equipped with a carbon cathode and a BDD/Ta anode (both with a 10 cm^2 geometric area) separated by a Nafion 117 membrane. Each cell compartment contained a reservoir with 200 mL of 2 mol L^{-1} K_2CO_3 electrolyte circulating at 100 mL min^{-1} flow rate. 90 mmol L^{-1} Na_2SiO_3 was added to the anolyte as a chemical stabilizer to avoid H_2O_2 decomposition. The pH of the anolyte was kept constant at 12.6.

whole reaction time (150 minutes, Fig. S5c and Table S1, ESI†). The specific energy consumption of a product is one of the most basic approaches to determining the unit energy consumption.[50] The first reaction stage at 100 mA cm^{-2} had a specific energy consumption of 19.3 kW h kg^{-1}, which raised considerably to 26 kW h kg^{-1} at 300 mA cm^{-2}. After 150 minutes of reaction with recirculation (75 cycles), the specific energy consumption was as high as 196 kW h kg^{-1} at 300 mA cm^{-2} (Fig. S5c and Table S1, ESI†). At a flow rate of 100 mL min^{-1} and 200 mL anolyte volume, each recirculation cycle takes 2 minutes. The increase in energy consumption after 15 minutes is mainly due to the electrochemical H_2O_2 decomposition at the electrode surface, which can be particularly prominent at higher current densities (as observed at 300 mA cm^{-2}). It is important to notice that the aggregate energy consumption for classical anthraquinone process is in about 17.6 kW h kg^{-1} H_2O_2.[20] Hence, energy efficiency needs to be improved further for WOR-based H_2O_2 production. Therefore, a compromise in process parameters (current density, cell potential, cell design, membrane resistivity, *etc.*) should be found.

The effect of recirculating the electrolyte on the anodic generation and electrodecomposition of H_2O_2 was investigated stepwise by decreasing the electrolyte flow rate from 100 to 10 mL min^{-1} and limiting the recirculating steps to four (Fig. 3). Each cycle lasted for 20 minutes, thereafter the electrolyte was recirculated for a new pass cycle. An increase in H_2O_2

concentration was observed with each consecutive cycle at 100 and 300 mA cm^{-2}, albeit FE and production rate decreased. The H_2O_2 concentration in the anolyte reached 46 and 110 mmol L^{-1} after four cycles at 100 and 300 mA cm^{-2}, respectively (Fig. 3a). However, the FE decreased from 40% to 33% (1st to 4th cycle) at 100 mA cm^{-2} and from 45% (1st cycle) to 6% during the 4th cycle at 300 mA cm^{-2} (Fig. 3b). A drastic decrease in production rate (Fig. 3c) from 41 to 7 μmol min^{-1} cm^{-2} (70% decrease) at 300 mA cm^{-2} in comparison to only 12% decrease at 100 mA cm^{-2} was observed. The decrease in FE and formation rate with cycle is an effect of the decomposition of electrochemically produced H_2O_2 on the electrode surface after recirculation, particularly at high current densities, as also observed in continuous circular flow experiments. Additionally, the pH of the electrolyte also decreased with each cycle (Fig. 3d) due to the constant oxidation of OH^- ions to O_2. This pH decrease was more pronounced for higher current densities. Thus, the remarkable decline in production rate observed at 300 mA cm^2 can also be due to the drop in pH, as it plays a direct role in the $a(CO_3^{2-})$, consequently, in the peroxodicarbonate formation and H_2O_2.[42] A considerable drop in the electrolyte conductivity was observed at a high current density (Fig. S7a, ESI†). The cell potential remained, nevertheless, essentially constant during all four cycles (Fig. S7b, ESI†). Increasing the number of cycles increases the overall product concentration, however it has the drawback of decreasing the production rate, and consequently increasing

Paper
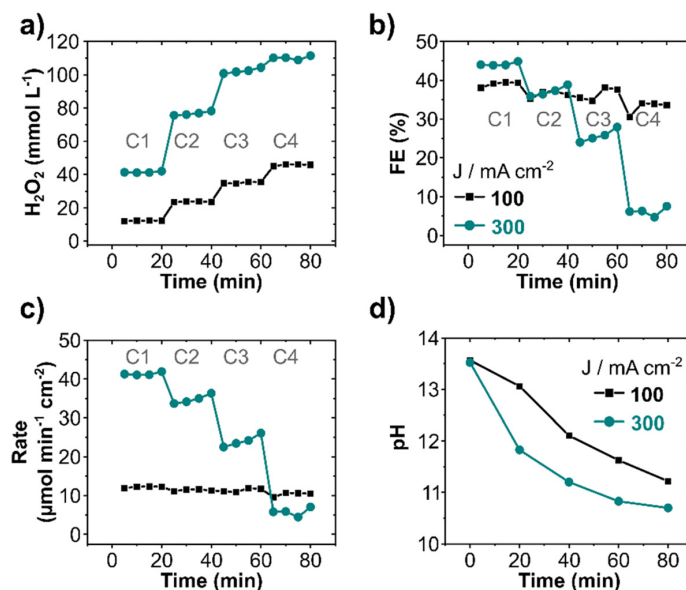
Fig. 3 H_2O_2 generation under electrolyte flow with multiple recirculation cycles. (a) Anodic H_2O_2 concentration, (b) FE, (c) production rate, and (d) pH change. The experiments were carried out in a flow cell equipped with 10 cm^2 BDD as anode and recirculated with 2 mol L^{-1} K$_2$CO$_3$ containing 90 mmol L^{-1} Na$_2$SiO$_3$ at 10 mL min^{-1} flow rate. The total volume of the electrolyte was 200 mL. Experiments were performed in 4 cycles of electrolyte flow (indicated as C1 to C4) of 20 minutes each.

the specific energy consumption for H_2O_2 production (Fig. S7c, ESI†).

Chemical stabilizers can slightly decrease the decomposition of H_2O_2 in the electrolyte. Sodium silicate (Na$_2$SiO$_3$) is a particularly attractive stabilizer because it is not redox-active, thus it does not affect the electrode reactions.[36,42] Circular flow experiments using anolyte with and without Na$_2$SiO$_3$ revealed that the silicate stabilizer considerably enhances H_2O_2 stability upon recirculation (Fig. S8, ESI†). Nevertheless, the challenge of anodic H_2O_2 decomposition can be tackled by regularly replacing the electrolyte in batches or optimizing the flow rate for maximum and continuous H_2O_2 productivity without recirculation (single-pass flow).

Single-pass flow

A single-pass flow mode was employed to minimize performance losses through electrochemical decomposition upon anolyte recirculation (Fig. 4a and Fig. S9, ESI†). In this setup, the anolyte containing the electrochemically generated H_2O_2 is not recirculated but optimized for maximum continuous production.

Electrolytic steps of 20 minutes at 10 mL min^{-1} electrolyte flow rate were carried out at current densities ranging from 100 to 700 mA cm^2. The concentration of anodically generated H_2O_2 was directly proportional to the current density (Fig. 4b). Starting at 12 mmol L^{-1} at 100 mA cm^{-2}, a maximum of 79 mmol L^{-1} H_2O_2 was obtained at 700 mA cm^{-2}. The H_2O_2 production rate was stable and constant during the 20 minutes step, and a maximum of 79 μmol min^{-1} cm^{-2} was obtained at

700 mA cm^2 (Fig. S10b and c, ESI†). To the best of our knowledge, this is the highest production rate for the anodic H_2O_2 generation so far reported. A detailed literature comparison of production rates is shown in Table S2, ESI†. The partial current density to produce H_2O_2 (jH$_2$O$_2$) reached 250 mA cm^{-2} (Fig. S10d, ESI†). It is important to remark that this single-pass setup allowed reaching considerably higher current densities, up to 700 mA cm^{-2}. In this regard, techno-economic studies show that the economic (cost-related) performance of anodic H_2O_2 generation can be enhanced by increasing the current density.[39,51]

A maximum FE of 50% was achieved at 300 mA cm^{-2} (Fig. 4b), which dropped to 35% at 700 mA cm^{-1}. This FE decreases upon increasing current density is likely due to an increase in O_2 evolution. Although the cell potential increased at higher current densities (from 4.7 V at 100 mA cm^{-2} to 9 V at 700 mA cm^{-2}, Fig. S11, ESI†), the total cell potential is still below the maximum recommended (11 V) to enable the technical feasibility of the setup in combination with HER.[39]

The specific energy consumption was around 20 kW h kg^{-1} for current densities up to 300 mA cm^{-2} (Fig. 4c). However, the energy consumption takes a steady steep at higher current densities, increasing to 40 kW h kg^{-1} at 700 mA cm^{-2}, as a considerable share of energy consumption is used for O_2 production.[42] Since the highest FE and relatively low specific energy consumption were obtained at 300 mA cm^{-2}, further optimizations with the single-pass flow were performed at this current density.

Paper
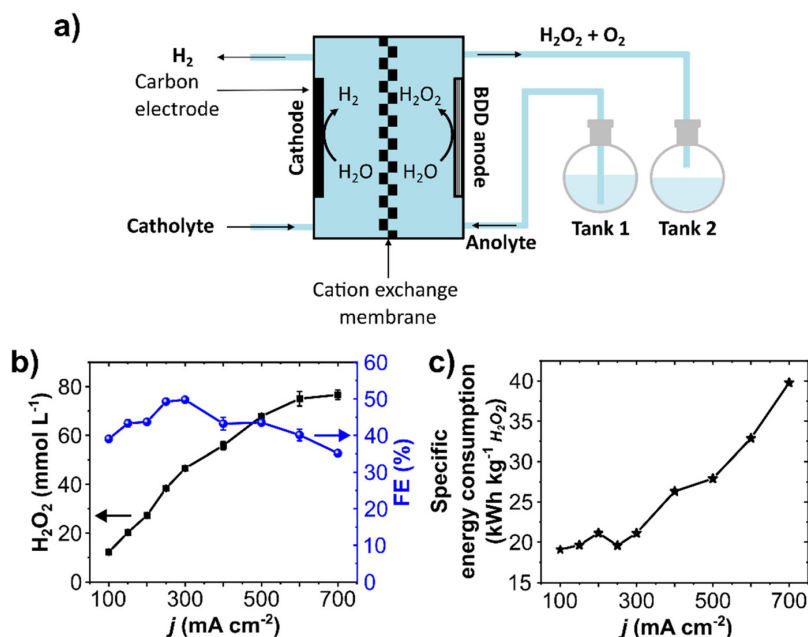
Fig. 4 Anodic H_2O_2 production in a single-pass mode flow reactor. (a) Schematic representation of the flow cell with a single-pass flow setup. (b) Average H_2O_2 concentration, FE, and (c) specific energy consumption at different current densities (20 minutes steps). 200 mL of 2 mol L^{-1} K_2CO_3 + 90 mmol L^{-1} Na_2SiO_3 was used as an anolyte at a 10 mL min^{-1} flow rate without recirculation. The flow cell was equipped with a BDD/Ta working electrode (10 cm^2 geometric area) and a carbon cathode.

Effect of stabilizers at single-pass flow

A chemical stabilizer is essential to avoid chemical and electrochemical decomposition of H_2O_2, particularly in a circular flow setup, as observed in our experiments with and without Na_2SiO_3, where higher H_2O_2 concentrations were obtained in the presence of the silicate (Fig. S8, ESI†).[42] However, in a single-pass flow mode, the electrochemical H_2O_2 decomposition can be minimized by optimizing the residence time of the electrolyte in contact with the electrode surface. Hence, a stabilizer may no longer be necessary.

To validate this hypothesis and to elucidate the effect of chemically stabilizing agents in a single-pass flow system, experiments at 300 mA cm^{-2} were carried out with and without a stabilizer. In a single-pass mode, a similar H_2O_2 concentration of 52 mmol L^{-1} was obtained, independently of the presence of Na_2SiO_3. However, when the electrochemically produced H_2O_2 was stored for 3 hours without any applied current, the H_2O_2 concentration decreased by 42% (from 52 to 29 mmol L^{-1}) in the absence of the stabilizer, compared to only 8% (53 to 49 mmol L^{-1}) in its presence (Fig. 5). Thus, the use of Na_2SiO_3 as a stabilizer in single-pass mode does not necessarily enhance the electrochemical H_2O_2 formation, it rather inhibits the chemical decomposition of H_2O_2 during storage and thereby increases its bench life. Hence, immediate use of H_2O_2 in on-site applications can abstain from chemical stabilizers, which could consequently influence the total process costs. In cases requiring intermediate storage of the
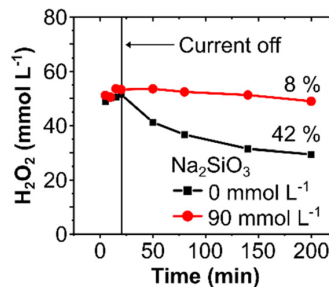
Fig. 5 Effect of stabilizer on the stability of electrochemically produced H_2O_2. Change in H_2O_2 concentration during electrolyte storage in the absence (■) and presence (●) of 90 mmol L^{-1} Na_2SiO_3 in 2 mol L^{-1} K_2CO_3. The H_2O_2 was anodically generated for 20 minutes at 300 mA cm^{-2}. Thereafter, electrolyte samples were taken at 30, 60, 120, and 180 minutes from the storage reservoir.

generated H_2O_2, however, stabilizers are recommended to avoid substantial chemical losses.

Effect of flow rate

The flow rate optimization maximizes the transient electrolyte time in the electrochemical cell and, consequently, the continuous anodic H_2O_2 production in single-pass flow. The experiments described to this point had a constant flow rate of 10 mL min^{-1}. Variation of the flow-rate in the range of 5 to

Paper

100 mL min^{-1} in single-pass flow at a constant current density of 300 mA cm^{-2} shows contrasting shapes for H$_2$O$_2$ concentrations and FE at different flow rates (Fig. 6a). Slower flow rates (5 mL min^{-1}) lead to higher H$_2$O$_2$ concentrations (75 mmol L^{-1}), however, to lower FE (40%). Speeding the flow rate decreases the residence time of a specific electrolyte volume in the vicinity of the electrode, thus minimizing relevant side-reactions, such as O$_2$ evolution and electrodecomposition of H$_2$O$_2$, and resulting in higher FE and production rate (Fig. 6b). Nevertheless, higher flow rates also decrease the H$_2$O$_2$ concentration and increase the required electrolyte volume per time, which can be costly. Therefore, a compromise between H$_2$O$_2$ concentration and FE must be considered depending on the application of anodic H$_2$O$_2$ production in continuous flow.

Moreover, the corresponding specific energy consumption decreased by around 50% (from 25 kW h kg^{-1} to 13 kW h kg^{-1}) upon increasing the flow rate from 5 to 100 mL min^{-1} (Fig. 6b). Considering the cost of renewable electricity of 3 cents($) per kW per h,[36,52] the specific electricity-related cost of anodic H$_2$O$_2$ generation ($ per kg H$_2$O$_2$) at 300 mA cm^{-2} is

estimated at $0.77 per kg at 5 mL min^{-1} and $0.4 per kg at 100 mL min^{-1} (Fig. S12, ESI†). Commercial H$_2$O$_2$ from the anthraquinone process is currently priced at $1.50 per kg without transportation costs.[36] Nonetheless, it should be noted that our figures for calculated specific energy consumption only include the electric energy required for electrochemical cell operation. Hence, the estimated electricity cost reported in this study is specific to this lab-scale electrochemical cell. Certainly, other operating costs (*e.g.*, material consumption, cell design, cathode material, membrane type, and downstream processing) could and will substantially contribute to the overall cost structure of H$_2$O$_2$ production *via* WOR. Yet, the cost of electricity to produce H$_2$O$_2$ at the anode can be further reduced by combining it with an optimized cathodic half-cell reaction such as HER, CO$_2$RR, or ORR to replace the current WOR to O$_2$.

Finally, a long-term stability study using the optimized single-pass flow setup was performed to produce H$_2$O$_2$ continuously. The stability of the electrochemical system is essential for its technical application, as it reduces the occurrence of component failures and the associated need to disassemble
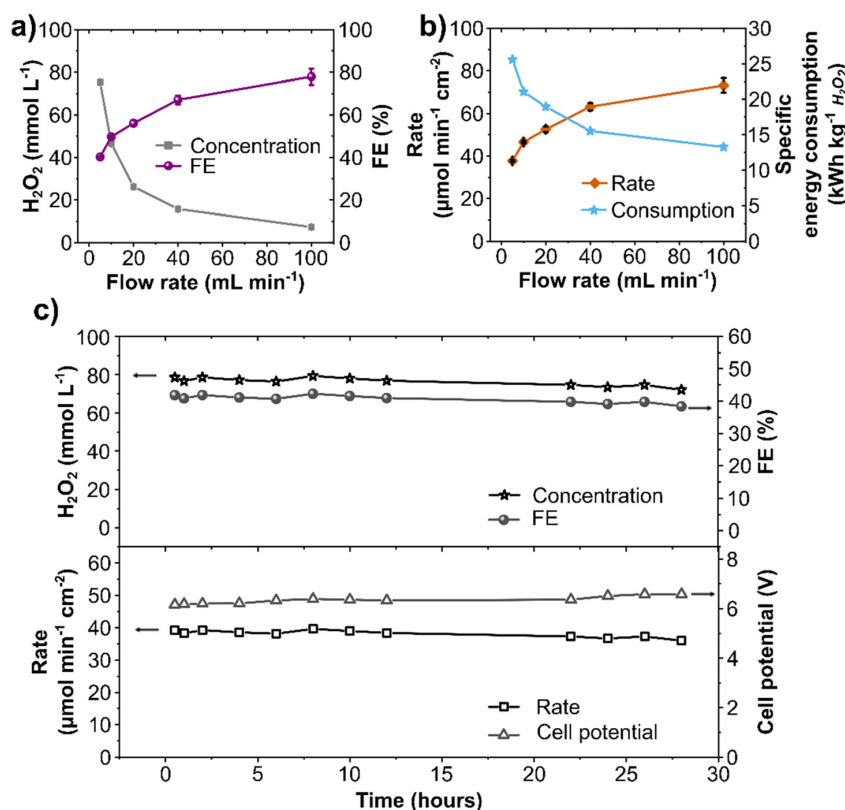
Fig. 6 Flow rate effect on the continuous anodic H$_2$O$_2$ generation. (a) Anodic H$_2$O$_2$ concentration and FE, (b) production rate and specific energy consumption to produce 1 kg H$_2$O$_2$ at different electrolyte flow rates. Experimental conditions: single-pass flow of 200 mL anolyte (2 mol L^{-1} K$_2$CO$_3$) at a constant current density of 300 mA cm^{-2}. The same electrolyte volume was used for each flow rate, resulting in different durations of the individual experiments. (c) Electrode stability test in a continuous flow setup: H$_2$O$_2$ concentration, FE, production rate, and cell potential at a 10 cm^2 BDD at a constant current density of 300 mA cm^{-2} with a single-pass flow mode of 2 mol L^{-1} K$_2$CO$_3$ electrolyte at a flow rate of 5 mL min^{-1}.

Green Chemistry

and reassemble the reactor.[53] Galvanostatic experiment at 300 mA cm^{-2} was performed in 2 mol L^{-1} K$_2$CO$_3$ at a 5 mL min^{-1} flow rate for 28 hours (Fig. 6c). Anolyte samples were taken directly from the electrochemical cell outlet, showing a continuous generation of H$_2$O$_2$ for 28 hours with a constant concentration of about 80 mmol L^{-1} and a constant FE of 40%. An average production rate of 40 μmol min^{-1} cm^{-2} was observed with a stable cell potential of 6.3 V throughout the experiment. This stability experiment highlights the effectiveness of an optimized electrochemical setup. Previous reports on electrode stability for WOR to H$_2$O$_2$ using carbonaceous electrodes are restricted to batch mode (H-cells) with low electrolyte volume and at current densities from 100 to 200 mA cm^{-2} with a maximum time of 10 hours.[31,36,38] Our last study using commercial carbon fiber paper electrodes reported stable operation for up to 17.5 hours at 100 mA cm^{-2}.[42] Herein, we expanded the potential of process development for WOR to H$_2$O$_2$ to reach considerably higher current densities and continuous stable production at a robust commercial BDD electrode. This is also the first comprehensive study of an electrochemical flow system for WOR to H$_2$O$_2$, which remains stable for 28 hours. Such investigations are essential for future technical electrochemical applications. Moreover, considering that BDD anodes are already used in several electrochemical industrial processes with a lifetime up to several months,[54] it can be expected that H$_2$O$_2$ generation through WOR at BDD anodes can also be operated with high stability and performance for a considerably longer time. Electrode and process stability is an important step forward in terms of scale-up and utilization.

Conclusions

This research work demonstrates that beyond the catalyst development, the process parameters (including electrolyte type, pH, flow type, and flow rate) can dramatically affect the efficiency of anodic H$_2$O$_2$ production and, consequently, the technical process implementation. The continuous flow process has been developed with commercially available and scalable BDD anodes. Hence, it highlights a robust, stable, and promising foundation for piloting. Future work includes the combination of the anodic H$_2$O$_2$ production with value-added cathodic reactions, with the objective of utilizing the invested redox equivalents most efficiently by exploiting both half-cells. Considering the still high capital expenses for BDD electrodes, other low-cost carbon-based materials are a promising area for further exploration in searching for efficient and scalable WOR to H$_2$O$_2$. In this context, such research should be performed with a clear perspective of future industrial applications, focusing on relevant and scalable process configurations, as well as resource efficiency, investment, operational cost, and operational stability.

The electrochemical H$_2$O$_2$ production is nonetheless not a replacement for the current industrial AO process. From the perspective of mobile electrochemical prototypes, this is rather

an expansion of the H$_2$O$_2$ market to accommodate decentralized solutions, especially in remote areas where transportation of H$_2$O$_2$ is difficult. As an additional benefit, the anodic H$_2$O$_2$ production could be combined with hydrogen production, thereby also diversifying and adding value to the hydrogen industry.

Author contributions

Dhananjai Pangotra: conceptualization, investigation, formal analysis, validation, writing – original draft. Lénárd-István Csepei: conceptualization, writing – review & editing. Arne Roth: conceptualization, supervision, writing – review & editing. Volker Sieber: supervision, writing – review & editing. Luciana Vieira: conceptualization, supervision, writing – review & editing.

Conflicts of interest

There are no conflicts to declare.

Acknowledgements

References

1 Global Hydrogen Peroxide Market Outlook, **https://www.expertmarketresearch.com/reports/hydrogen-peroxide-market**, (accessed 20 August 2021, 2021).

2 A. Rubio-Clemente, E. Chica and G. Peñuela, *Environ. Sci. Pollut. Res.*, 2019, **26**, 4462–4473.

3 Chlorine or Hydrogen Peroxide – Which is Better for Treating Water?, **https://www.uswatersystems.com/blog/chlorine-or-hydrogen-peroxide**, (accessed 17 May 2022, 2021).

4 D. Horová, J. Nováková, L. Pelíšková, J. Kohout, J. Šafář, K. Hrachovcová and V. Tokarová, *React. Kinet., Mech. Catal.*, 2020, **130**, 1077–1092.

5 A. D. Ortiz-Marin, E. R. Bandala, K. Ramírez, G. Moeller-Chávez, L. Pérez-Estrada, B. Ramírez-Pereda and L. E. Amabilis-Sosa, *React. Kinet., Mech. Catal.*, 2022, **135**, 639–654.

6 R. Hage and A. Lienke, *Angew. Chem., Int. Ed.*, 2005, **45**, 206–222.

View Article Online

Paper

Green Chemistry

7 N. de la Fuente, L. Chen, J. A. Wang, J. González and J. Navarrete, *React. Kinet., Mech. Catal.*, 2021, **132**, 1119–1135.

8 H. Shuangyang, Hi Tech Chemical Co Ltd, A kind of deodorization of crude sulfate turpentine and the production method of sulfate turpentine, CN106281041B, 2016.

9 Institute of Chemical Industry of Forest Products of CAF, Refining method for desulphurizing and deodorizing crude sulphate turpentine, CN101654597B, 2009.

10 J. C. Rubio-Romero, M. D. C. Pardo-Ferreira, J. A. Torrecilla-Garcia and S. Calero-Castro, *Saf. Sci.*, 2020, **129**, 104830.

11 G. Lewandowski, M. Kujbida and A. Wróblewska, *React. Kinet., Mech. Catal.*, 2021, **132**, 983–1001.

12 L. Pierri, A. Gemenetzi, A. Mavrogiorgou, J. Borges Regitano, Y. Deligiannakis and M. Louloudi, *Mol. Catal.*, 2020, **489**, 110946.

13 J. D. Tibbetts, W. B. Cunningham, M. Vezzoli, P. Plucinski and S. D. Bull, *Green Chem.*, 2021, **23**, 5449–5455.

14 A. S. Gohardani, J. Stanojev, A. Demairé, K. Anflo, M. Persson, N. Wingborg and C. Nilsson, *Prog. Aerosp. Sci.*, 2014, **71**, 128–149.

15 M. Hävecker, S. Wrabetz, J. Kröhnert, L.-I. Csepei, R. Naumann d'Alnoncourt, Y. V. Kolen'ko, F. Girgsdies, R. Schlögl and A. Trunschke, *J. Catal.*, 2012, **285**, 48–60.

16 S. T. Renu Singh, M. Srivastava and A. Shukla, *Agric. Eng. Int.: CIGR J.*, 2014, **16**, 173–181.

17 J. Krischan, A. Makaruk and M. Harasek, *J. Hazard. Mater.*, 2012, **215–216**, 49–56.

18 R. L. Myers, *The 100 Most Important Chemical Compounds: A Reference Guide*, Greenwood Press, 2007.

19 L. Pesterfield, *J. Chem. Educ.*, 2009, **86**, 1182.

20 A. T. Murray, S. Voskian, M. Schreier, T. A. Hatton and Y. Surendranath, *Joule*, 2019, **3**, 2942–2954.

21 J. M. Campos-Martin, G. Blanco-Brieva and J. L. Fierro, *Angew. Chem., Int. Ed.*, 2006, **45**, 6962–6984.

22 S. C. Perry, D. Pangotra, L. Vieira, L.-I. Csepei, V. Sieber, L. Wang, C. Ponce de León and F. C. Walsh, *Nat. Rev. Chem.*, 2019, **3**, 442–458.

23 J. García-Serna, T. Moreno, P. Biasi, M. J. Cocero, J.-P. Mikkola and T. O. Salmi, *Green Chem.*, 2014, **16**, 2320–2343.

24 X. Shi, S. Back, T. M. Gill, S. Siahrostami and X. Zheng, *Chem*, 2021, **7**, 38–63.

25 Evonik, Hydrogen Peroxide for Pulp and Paper Industry, https://active-oxygens.evonik.com/product/h2o2/downloads/applications-hydrogen-peroxide-for-the-pulp-and-paper-industry-en.pdf, (accessed 29 March 2022).

26 K. Wenderich, B. A. M. Nieuweweme, G. Mul and B. T. Mei, *ACS Sustainable Chem. Eng.*, 2021, **9**, 7803–7812.

27 C. Minke, M. Suermann, B. Bensmann and R. Hanke-Rauschenbach, *Int. J. Hydrogen Energy*, 2021, **46**, 23581–23590.

28 S. Kiemel, T. Smolinka, F. Lehner, J. Full, A. Sauer and R. Miehe, *Int. J. Energy Res.*, 2021, **45**, 9914–9935.

29 T. Kang, B. Li, Q. Hao, W. Gao, F. Bin, K. N. Hui, D. Fu and B. Dou, *ACS Sustainable Chem. Eng.*, 2020, **8**, 15005–15012.

30 S. Y. Park, H. Abroshan, X. Shi, H. S. Jung, S. Siahrostami and X. Zheng, *ACS Energy Lett.*, 2019, **4**, 352–357.

31 C. Zhang, R. Lu, C. Liu, L. Yuan, J. Wang, Y. Zhao and C. Yu, *Adv. Funct. Mater.*, 2021, **31**, 2100099.

32 X. Shi, S. Siahrostami, G. L. Li, Y. Zhang, P. Chakthranont, F. Studt, T. F. Jaramillo, X. Zheng and J. K. Norskov, *Nat. Commun.*, 2017, **8**, 701.

33 S. R. Kelly, X. Shi, S. Back, L. Vallez, S. Y. Park, S. Siahrostami, X. Zheng and J. K. Nørskov, *ACS Catal.*, 2019, **9**, 4593–4599.

34 T. Shiragami, H. Nakamura, J. Matsumoto, M. Yasuda, Y. Suzuri, H. Tachibana and H. Inoue, *J. Photochem. Photobiol., A*, 2015, **313**, 131–136.

35 F. Kuttassery, S. Mathew, S. Sagawa, S. N. Remello, A. Thomas, D. Yamamoto, S. Onuki, Y. Nabetani, H. Tachibana and H. Inoue, *ChemSusChem*, 2017, **10**, 1909–1915.

36 C. Xia, S. Back, S. Ringe, K. Jiang, F. Chen, X. Sun, S. Siahrostami, K. Chan and H. Wang, *Nat. Catal.*, 2020, **3**, 125–134.

37 S. Mavrikis, M. Göltz, S. Rosiwal, L. Wang and C. Ponce de León, *ACS Appl. Energy Mater.*, 2020, **3**, 3169–3173.

38 S. Mavrikis, M. Göltz, S. C. Perry, F. Bogdan, P. K. Leung, S. Rosiwal, L. Wang and C. Ponce de León, *ACS Energy Lett.*, 2021, **6**, 2369–2377.

39 K. Wenderich, B. A. M. Nieuweweme, G. Mul and B. T. Mei, *ACS Sustainable Chem. Eng.*, 2021, **9**, 7803–7812.

40 C. P. Chardon, T. Matthée, R. Neuber, M. Fryda and C. Comninellis, *ChemistrySelect*, 2017, **2**, 1037–1040.

41 S. Maljuric, W. Jud, C. O. Kappe and D. Cantillo, *J. Flow Chem.*, 2020, **10**, 181–190.

42 D. Pangotra, L.-I. Csepei, A. Roth, C. Ponce de León, V. Sieber and L. Vieira, *Appl. Catal., B*, 2022, **303**, 120848.

43 T. M. Gill, L. Vallez and X. Zheng, *ACS Energy Lett.*, 2021, **6**, 2854–2862.

44 B. J. Deadman, K. Hellgardt and K. K. Hii, *React. Chem. Eng.*, 2017, **2**, 462–466.

45 G. Eisenberg, *Ind. Eng. Chem., Anal. Ed.*, 1943, **15**, 327–328.

46 Z. Machala, B. Tarabova, K. Hensel, E. Spetlikova, L. Sikurova and P. Lukes, *Plasma Processes Polym.*, 2013, **10**, 649–659.

47 K. Fuku, Y. Miyase, Y. Miseki, T. Gunji and K. Sayama, *ChemistrySelect*, 2016, **1**, 5721–5726.

48 L. Fan, X. Bai, C. Xia, X. Zhang, X. Zhao, Y. Xia, Z.-Y. Wu, Y. Lu, Y. Liu and H. Wang, *Nat. Commun.*, 2022, **13**, 2668.

49 P. A. Michaud, M. Panizza, L. Ouattara, T. Diaco, G. Foti and C. Comninellis, *J. Appl. Electrochem.*, 2003, **33**, 151–154.

50 S. Palamutcu, in *Handbook of Life Cycle Assessment (LCA) of Textiles and Clothing*, ed. S. S. Muthu, Woodhead Publishing, 2015, pp. 31–61.

51 K. Wenderich, W. Kwak, A. Grimm, G. J. Kramer, G. Mul and B. Mei, *Sustainable Energy Fuels*, 2020, **4**, 3143–3156.

52 S. Chu, Y. Cui and N. Liu, *Nat. Mater.*, 2017, **16**, 16–22.

53 S. C. Perry, S. Mavrikis, L. Wang and C. Ponce de León, *Curr. Opin. Electrochem.*, 2021, **30**, 100792.

54 J. V. Macpherson, *Phys. Chem. Chem. Phys.*, 2015, **17**, 2935–2949.

3.4 Electrochemical Water Oxidation to Hydrogen Peroxide on Bipolar Plates

Title: Electrochemical Water Oxidation to Hydrogen Peroxide on Bipolar Plates

Status: Published (2023)

Journal: ACS Sustainable Chemistry & Engineering

Publisher: American Chemical Society

DOI: doi.org/10.1021/acssuschemeng.2c06314

Authors: Dhananjai Pangotra, Arne Roth, Volker Sieber, Luciana Vieira

Expanded graphite with polymer → Hot-pressed BPP → BPP used as anode
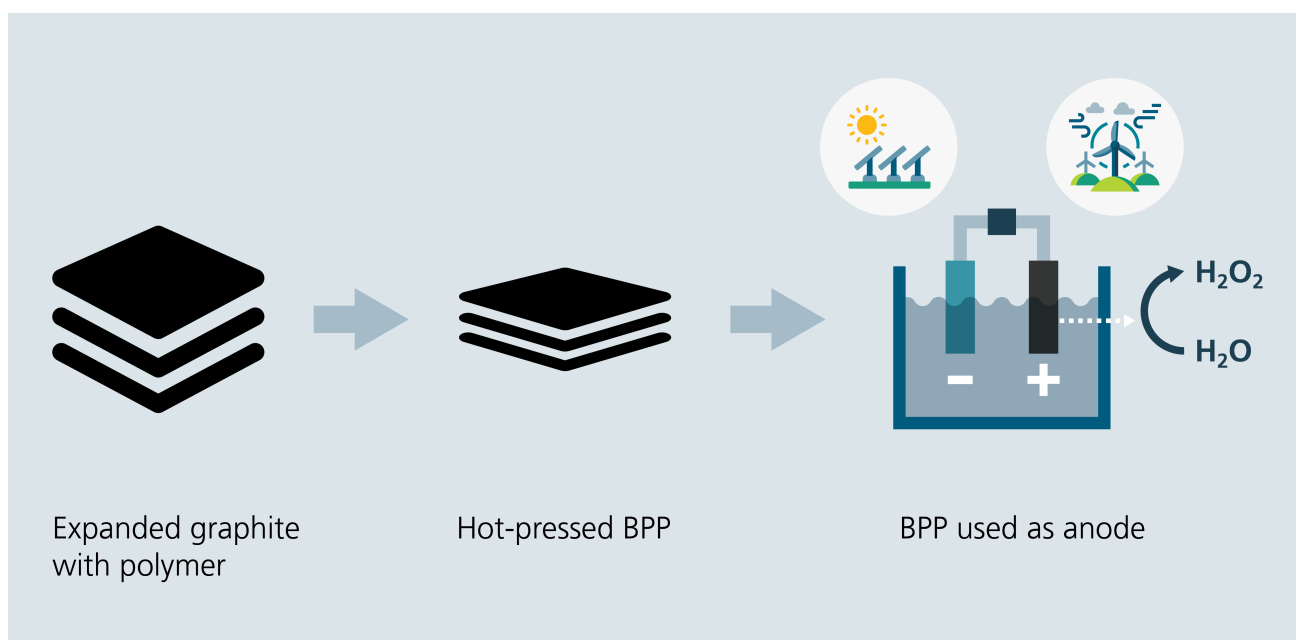
In this publication, the remarkable properties of a commercial BPP electrode for the anodic production of H_2O_2 in a scalable and continuous flow process was exploited. The experiments reveal that the fluoropolymer content in the BPP positively affects the H_2O_2 production. The results demonstrate that commercial carbon materials, such as BPP, can be used as a cost-effective and scalable alternative for anodic H_2O_2 production, enabling its potential use in various technical applications.

Dhananjai Pangotra conceptualized and designed the experiment, performed all the lab work, analyzed the data, and wrote the first draft. Arne Roth, and Luciana Vieira supported the conceptualization. Arne Roth, Volker Sieber, and Luciana Vieira reviewed this work. Arne Roth, Volker Sieber, and Luciana Vieira supervised the research.

Electrochemical Water Oxidation to Hydrogen Peroxide on Bipolar Plates

Electrochemical Water Oxidation to Hydrogen Peroxide on Bipolar Plates

Dhananjai Pangotra,* Arne Roth, Volker Sieber, and Luciana Vieira*

Read Online

ACCESS | 📊 Metrics & More | 📰 Article Recommendations | 🅢 Supporting Information

ABSTRACT: The electrochemical production of hydrogen peroxide (H_2O_2) via 2-electron ($2e^-$) water oxidation reaction (WOR) has gained colossal interest recently. Carbon materials are highly active for anodic H_2O_2 generation, particularly boron-doped diamond (BDD) electrodes. However, the cost of BDD is exceedingly high compared to basic carbon materials. Herein, we present a study of WOR on bipolar plates (BPP) as a low-cost alternative and stable electrode for generating H_2O_2 anodically. Three different commercial BPP with different polymer content were investigated, revealing an effect of the fluoropolymer content in the H_2O_2 generation. Our experiments show a stable production of H_2O_2 for up to 100 h at a current density of 200 mA cm^{-2}, with a constant faradaic efficiency of 40% obtained with a BPP sample with high content of fluoropolymer. This work demonstrates how commercial carbon electrode materials, that can be produced at large scale and low cost, can selectively oxidize water to H_2O_2. This combination of high performance with scalable and cheap production of the electrode material enables the economically viable technical application of anodic H_2O_2 production.

KEYWORDS: Expandable graphite, Electrocatalysis, Hydrogen peroxide, Anodic H_2O_2 production, Water oxidation

Expanded graphite with polymer → Hot-pressed BPP → BPP used as anode
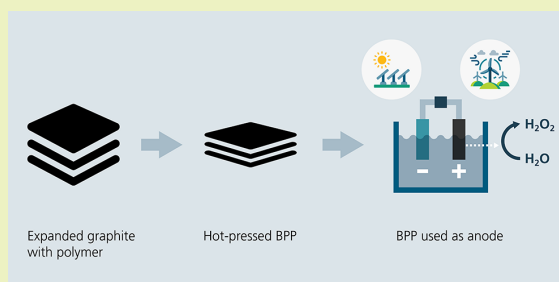
INTRODUCTION

Hydrogen peroxide (H_2O_2) is an important chemical product widely used in industry due to its strong oxidizing capability. It is applied for bleaching, disinfection, sanitation, chemical synthesis, and as aerospace fuel.[1−3] The anthraquinone auto-oxidation (AO) process accounts for by far the largest share of industrial H_2O_2 production. However, this industrial process requires hydrogenation steps with pressurized H_2 on Pd-based catalysts, followed by oxidation with O_2.[1] The remaining steps of the AO process include extraction of anthraquinone, distillation, and purification of H_2O_2, overall representing an energy-intensive process with considerably high operating costs.[4] Furthermore, the AO process is typically operated in large-scale centralized production plants, which inherently involves the need for transportation of the produced H_2O_2 to consumers, entailing the consumption of fossil fuels and the risks associated with the handling of a dangerous good such as H_2O_2. Considering the fact that 95% of the total global production volume of H_2O_2 (6 Mt/y) originates from the AO process,[5] these challenges and risks are substantial and clearly show that H_2O_2 production processes are urgently needed that use both renewable raw materials and renewable energy sources.

The electrochemical production of H_2O_2 provides a decentralized and on-demand alternative, which can easily be operated at the location where it is needed. Compared to the conventional AO process, the on-site electrochemical synthesis of H_2O_2 from renewable electric energy and the abundant raw materials oxygen (O_2) and water (H_2O) is appealing for many applications, particularly in remote places where transportation is difficult. Thus, it provides a green and sustainable solution for on-site and on-demand production. The most common electrochemical pathway to produce H_2O_2 is the cathodic $2e^-$ oxygen reduction reaction (ORR, eq 1), which has achieved significant progress in terms of production rate and faradaic efficiency (FE).[1,6,7] On the other hand, the anodic $2e^-$ water oxidation reaction (WOR, eq 2) has also gained considerable attention, as it can be coupled with various cathodic reactions, such as hydrogen generation from water or CO_2 reduction, and avoids sluggish and economically unattractive O_2 production.[8] Many metal oxide catalysts, such as $BiVO_4$, SnO_2, WO_3, $CaSnO_3$, ZnO, etc., have been reported to show high activity toward H_2O_2 generation via $2e^-$ WOR.[9−13] While most of the studies on oxide catalysts report high FE, the corresponding current densities are still far below 100 mA cm^{-2}, and the final

concentrations of H_2O_2 of up to 2 mmol L^{-1} are totally insufficient for industrial applications.[9−13] Low current densities imply large electrolyzers with large electrode areas, resulting in high capital expenditures.[14] Low H_2O_2 concentrations limit the potential for applications and require costly procedures to increase concentration (e.g., distillation). In addition to the electrode size and H_2O_2 concentration, high stability of the electrocatalyst, enabling continuous H_2O_2 generation for a longer period of time, represents a critical aspect for scale-up and technical application of the electrochemical process.

$$O_2 + 2H^+ + 2e^- \rightleftharpoons H_2O_2 \qquad E^0 = 0.68 \text{ V vs RHE} \tag{1}$$

$$2H_2O \rightleftharpoons H_2O_2 + 2H^+ + 2e^- \quad E^0 = 1.77 \text{ V vs RHE} \tag{2}$$
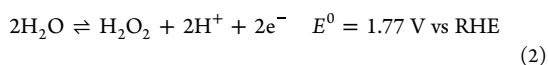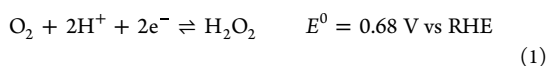
Boron-doped diamond (BDD) has been extensively used as electrode material to produce H_2O_2 via WOR at current densities of 100 mA cm^{-2} and higher.[15,16] BDD electrodes substantially outperform reported metal oxide materials with impressive production rates of 79 μmol min^{-1} cm^{-2} and FE of up to 87% and reaching H_2O_2 concentrations surpassing 100 mmol L^{-1} (0.3%).[17,18] Assuming further improvements of this technical approach, peroxide concentrations of about 1 mol L^{-1} (3%) are realistic, i.e., in the range of commercial 3% H_2O_2 solutions. This enables a wide field of applications in sanitation, disinfection, water treatment, bleaching, and cosmetic formulations. However, currently available BDD electrodes are costly to produce. They consist of a thin diamond layer on a metal substrate, typically niobium or tantalum, i.e., expensive materials.[16] Moreover, the coating process by chemical-vapor deposition (CVD) is complex and expensive. Such drawbacks hold back the technical implementation of BDD in the present scenario of electrosynthesis despite its splendid activity and robustness.[16] Hence, low-cost alternatives as all-carbon electrode materials are extremely attractive. In this context, carbonaceous materials such as commercial carbon fiber paper (CFP) have been recently reported as an electrode material for 2e$^-$ WOR. Such materials are cheap, their production is easily scalable, and they can be operated at current densities of up to 100 mA cm^{-2}.[19] However, pristine CFP has some performance-related shortcomings in terms of activity (maximum FE of 14%) and stability (oxidation of electrode surface) at high current densities.[19] Coating CFP and nickel oxide catalyst with PTFE considerably improves the activity, selectivity, and stability of the CFP electrode in anodic H_2O_2 production while operating at a current density up to 120 mA cm^{-2}.[20,21] An important factor for the improvement was the modification of the surface electronic properties of the electrocatalyst upon the addition of polymers, which in this case was fluoropolymer (PTFE).[21] Therefore, further expedition of such inexpensive carbonaceous materials with polymer modification is required to have a cost-effective system that is stable for hours at current densities beyond 100 mA cm^{-2}.

Inspired by the role of polymer modification in improving the water oxidation process, we have investigated different bipolar plates (BPP) as a low-cost anode alternative for the 2e$^-$ WOR to H_2O_2. BPPs are robust all-carbon electrodes used mainly as fuel cell components, accounting for 60−80% of total weight and 30−45% of stack cost.[22,23] The primary function of BPP in fuel cells includes the uniform distribution of reactants,

removing heat, conducting electric current from cell to cell, preventing leakage of gases and coolant, and providing structural support to the stacks.[24] BPPs manufactured from expanded graphite and polymers are particularly advantageous due to their ease of fabrication, high electrical conductivity, and excellent electrochemical and chemical stability.[25,26] Graphite polymer composite plates are typically prepared by mixing a polymer (such as a fluoropolymer or a thermoset resin) with expanded graphite in a kneader at high temperature, and compressing the mixture at a specific temperature and pressure.[23,27]

In our study presented here, the performance of BPP is compared to other carbon-based materials, such as BDD and CFP, which have been reported earlier as suitable electrode material in H_2O_2 generation through WOR. We have used commercial BPP samples made of expandable graphite and composed of different polymer types and loadings in its carbon structure. They differ in their electrical conductivity, mechanical strength, and chemical stability. The effect of BPP composition on the anodic generation of H_2O_2 is discussed in detail. We have studied its catalytic activity and long-term stability under technical relevant and scalable flow conditions, aiming for future application of BPP as components in low-cost mobile electrochemical devices for H_2O_2 generation.

RESULTS AND DISCUSSION

Three commercial BPP samples from Sigracell, namely FP6, FP15, and TR10 were analyzed for their catalytic activity toward WOR to H_2O_2. FP6 and FP15 are BPPs with fluoropolymer with a polymer content of 6 and 15 wt %, respectively, whereas TR10 contains 10 wt % of a thermoset resin.[28] The composition details of the BPP used as well as scanning electron microscopic (SEM) images are shown in the Supporting Information, Table S1 and Figure S1a. SEM images revealed only minor microcracks on the surface of all BPP samples, indicating sufficient binding of the graphitic material.[26] Energy-dispersive X-ray spectroscopy (EDX) mapping revealed the fluoride content as 2.2 wt % in FP6 and 6.7 wt % in FP15 (Supporting Information, Figure S1b), evenly distributed throughout the electrode surface (Supporting Information, Figure S2).

Linear sweep voltammetry (LSV) of the three BPP electrodes in 2 mol L^{-1} K_2CO_3 (Figure 1a) showed higher current densities for the thermoset resin TR10 compared to the fluoropolymers-based FP6 and FP15. This current density profile is consistent with the electrical resistivity of the BPP sample, as TR10 has the lowest electric resistivity compared to FP6 and FP15 (Figure 1a, and Supporting Information, Table S1). However, it is important to note that this current density is not specific to a determined WOR and can be a sum of O_2 and H_2O_2 generation. Thus, chemical analysis is always required, and all following experiments have H_2O_2 quantified by a reliable $TiOSO_4$ photometric method (Supporting Information, Figures S5−S7).

Galvanostatic experiments at different current densities of up to 300 mA cm^{-2} show FP15 as the most active material for anodic H_2O_2 generation, followed by FP6 and TR10 (Figure 1b). The H_2O_2 concentration with FP15 electrodes reached a maximum H_2O_2 concentration of 60 mmol L^{-1} at 300 mA cm^{-2} with a production rate of 30 μmol min^{-1} cm^{-2} (Figure 1b,d). The maximum FE of 38% was obtained at 200 mA cm^{-2} (Figure 1c). Higher current densities decreased FE, indicating
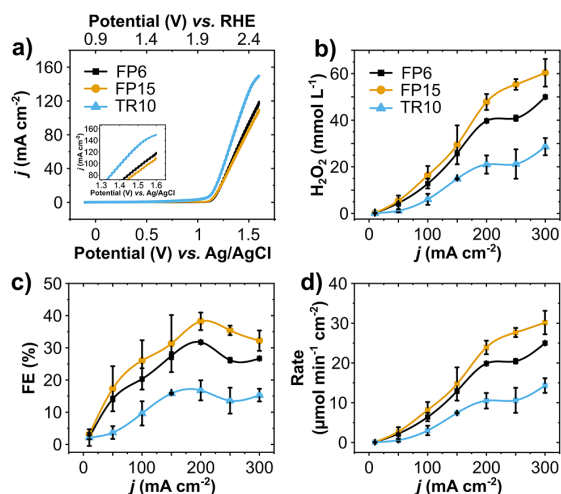
Figure 1. Electrochemical profile of BPP for WOR. (a) LSV of BPP samples in 2 mol L^{-1} K$_2$CO$_3$ at 100 mV s^{-1} scan rate. (b) H$_2$O$_2$ concentration, (c) FE and, (d) production rate in 10 min galvanostatic experiments at different applied current densities (10–300 mA cm^{-2}). All experiments were performed in a two-compartment H-cell cooled with an ice bath. The 2 mol L^{-1} K$_2$CO$_3$ electrolyte was kept under constant stirring of 1000 rpm. BPP anodes had a geometric area of 5 cm^2. H$_2$O$_2$ was quantified by the TiOSO$_4$ photometric method.

higher O$_2$ generation.[19] This different trend in galvanostatic polarization from LSV suggests that although the current density in TR10 is high, most of it is used for WOR to O$_2$, which is also confirmed by the low FE for H$_2$O$_2$ in the same material.

FP15 has a higher fluoropolymer content than FP6, whereas TR10 has no fluorine in its composition (Supporting Information, Figures S1, S2). The amount of fluoropolymer in a carbon electrode remarkably affects the WOR to H$_2$O$_2$. Xia et al.[20] have shown an enhanced activity toward WOR to H$_2$O$_2$ when coating different substrates (CFP, glassy carbon, nickel) with polytetrafluoroethylene (PTFE). The presence of a hydrophobic PTFE polymer can help to confine in situ generated O$_2$, thereby deviating from the 4e$^-$ WOR to O$_2$ pathway and increasing selectivity for H$_2$O$_2$. The intermediate species in the water oxidation mechanism, such as *O, *OH, and *OOH, interact with the electrode material, and the binding energy of these species on the electrode has a strong

influence on the reaction pathway and hence on the selectivity for the formation of either O$_2$ or H$_2$O$_2$.[11] Theoretical and experimental results by Xia showed that the presence of PTFE in the electrode surface weakens the binding of *OH intermediate species to active sites, hence increasing H$_2$O$_2$ generation.[20]

Venugopal et al. studied the impact of PTFE loading coated on nickel oxide catalysts on the WOR.[21] Because fluorine atoms are highly electronegative, it draws electrons away from the oxygen atoms in the adsorbed OH* intermediate. Consequently, the binding energy of the OH* intermediate decreases, which hinders the formation of adsorbed O* intermediates for 4e$^-$ oxidation to O$_2$ and favors the 2e$^-$ H$_2$O$_2$ pathway.

The anodic activity of FP15-BPP toward H$_2$O$_2$ at different current densities was compared to BDD (reportedly to be most active) and the low-cost alternative CFP (Figure 2). All of these materials were active toward WOR to H$_2$O$_2$, with an activity trend as CFP < BPP < BDD. The H$_2$O$_2$ concentration increased steadily upon increasing the current density for BPP and BDD. CFP reached a saturation limit at 200 mA cm^{-2}, which could be due a combination of water oxidation to O$_2$ and decomposition of the generated H$_2$O$_2$ at higher current densities, which accounts for the lower H$_2$O$_2$ concentration.[19] CFP was the least active of the tested electrode materials, with a H$_2$O$_2$ concentration of 6 mmol L^{-1} at 300 mA cm^{-2}, i.e., ten times lower than concentrations obtained with BPP-FP15. Although the H$_2$O$_2$ concentration and production rate in general increase upon raising the current density, the FE shows a specific maximum for the different electrode materials and decreases upon further increase of current density.[11] BPP showed a maximum FE of 38% at 200 mA cm^{-2}, whereas BDD peaked at 100 mA cm^{-2} with 58% FE. CFP showed FE in the range of 5–10% for the whole screened current density. The highest H$_2$O$_2$ concentration was 70 mmol L^{-1}, obtained with BDD electrodes after 10 min at 300 mA cm^{-2}, with a production rate of 35 μmol min^{-1} cm^{-2}.[18] At this current density of 300 mA cm^{-2}, the H$_2$O$_2$ concentrations obtained with BPP electrodes were quite similar (at 60 mmol L^{-1}).

In order to test the electrode materials in a setup of relevance for later scale-up and technical application, a flow cell system was used. Industrially relevant electrochemical processes are typically operated in flow cells, and therefore technically viable electrodes should be suitable for application in continuous processes, with stable performance in terms of activity and selectivity over long periods of time. CFP and PTFE/CFP electrodes have been reported to be stable for 2.5
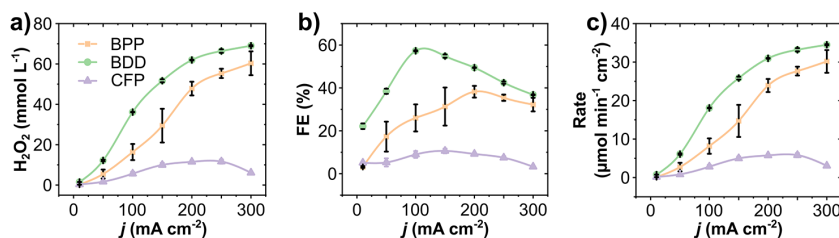
Figure 2. Comparison of carbon-based BPP, BDD, and CFP for H$_2$O$_2$ electrosynthesis through water oxidation. (a) H$_2$O$_2$ concentration, (b) FE, and (c) production rate at different applied current densities (10–300 mA cm^{-2}) and with duration of 10 min for each current density step in 2 mol L^{-1} K$_2$CO$_3$. All experiments were performed in a two-compartment H-cell cooled in an ice bath with constant stirring of 1000 rpm and using BPP, BDD,[18] and CFP as anode with a geometric area of 5 cm^2.
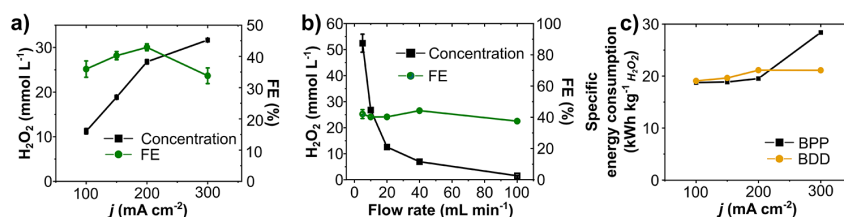
Figure 3. Current density and flow rate effect on the anodic H_2O_2 generation. (a) Anodic H_2O_2 concentration and FE at different current densities using a flow rate of 10 mL min^{-1}. (b) Anodic H_2O_2 concentration and FE at different electrolyte flow rates at a current density of 200 mA cm^{-2}. (c) Specific energy consumption to produce 1 kg of H_2O_2 at different current densities, comparing BPP and BDD systems (BDD data from our recent work[18]). Experimental conditions: single-pass flow of 200 mL anolyte (2 mol L^{-1} K_2CO_3). The same electrolyte volume was used for each current density and flow rate, resulting in different durations of the individual experiments for the flow-rate study.

h of operation in continuous flow, producing H_2O_2 at current densities of up to 120 mA cm^{-2}.[19,20] In a previous study, we compared multipass and single-pass flow setups using BDD electrodes, successfully showing constant production of 80 mmol L^{-1} H_2O_2 at current density of 300 mA cm^{-2} for 28 h.[18] In the multipass system, product concentration could be increased by recirculating the electrolyte through the cell several times (Supporting Information, Figure S4a). In a single-pass system, the process is optimized for maximum continuous production upon passing the electrolyte through the cell one single time (Supporting Information, Figure S4b).

In this study, the multi- and single-pass systems were compared using BPP as an anode. The multipass flow leads to an increase in concentration, however, challenges such as electrochemical H_2O_2 decomposition, electrode stability, and inability to operate at high current densities persist (Supporting Information, Figure S8). One possibility for the instability of the electrode using multipass flow is the oxidation and consequent exfoliation of the electrode, resulting from a combined effect of oxidative current and the presence of H_2O_2.[19,29] In contrast, single-pass flow enabled operation at high current densities with impressive production rates for BPP electrodes (Figure 3a and Supporting Information, Figures S10, S11).

The specific electric energy consumption for the anodic H_2O_2 generation using BPP was calculated and compared based on our previous work on BDD electrodes at a current density from 100 to 300 mA cm^{-2} at 10 mL min^{-1} (Figure 3c, and Supporting Information, Tables S4, S5).[18] The specific energy consumption was around 20 kWh kg^{-1} for current densities up to 200 mA cm^{-2} for both electrode materials, however, at 300 mA cm^{-2}, the specific energy consumption on BPP raised near to 30 kWh kg^{-1}, while remaining stable at around 20 kWh kg^{-1} for BDD (Figure 3c). This indicates that BPP performs competitively to BDD at current densities of up to 200 mA cm^{-2}, but BDD facilitates more efficient H_2O_2 synthesis at higher current densities.

However, this compares to a strong advantage of BPP in terms of material cost: Considering the cost of BPP, BDD, and CFP electrodes, BPP is by far the cheapest among these materials and could decrease the overall capital expenditure of the electrolysis cell (Supporting Information, Table S6). Thus, bipolar plates can be an economically attractive alternative to costly BDD electrodes for application in water oxidation to H_2O_2, with substantially cheaper production of the electrode material and only moderately lower performance. Given the current price difference of about 2 orders of magnitude between BDD and BPP (Supporting Information, Table S6),

CAPEX-related advantages of BPP are likely to remain even when assuming substantial cost reductions in BDD production, as simplistically estimated in the Supporting Information. However, a detailed techno-economic assessment considering the different relevant variables affecting investment-related and operating costs is required for a comprehensive comparison of the economic potentials and limitations of BPP and BDD-based systems.

Optimization of flow rate and current density in single-pass flow using BPP in a 10 cm^2 flow cell led to maximum FE of up to 44% and H_2O_2 concentrations of up to 50 mmol L^{-1} at a flow rate of 5 mL min^{-1} at 200 mA cm^{-2} under tested conditions (Figure 3b, and Supporting Information, Figures S10, S11). These flow parameters were therefore used for evaluating the long-term stability of the BPP electrode.

In those long-term experiments, the stability of the BPP electrode was evaluated for 100 h under continuous single-pass flow (Figure 4). Anolyte samples were taken directly from the cell outlet, and a constant generation of 50 mmol L^{-1} over the entire test period validated the suitability of BPP as stable electrode material for the anodic generation of H_2O_2. The cell potential was also stable at about 5.5 V, with a constant production rate of 25 μmol min^{-1} cm^{-2} and FE of 40%. After 100 h of operation, SEM images showed no changes in
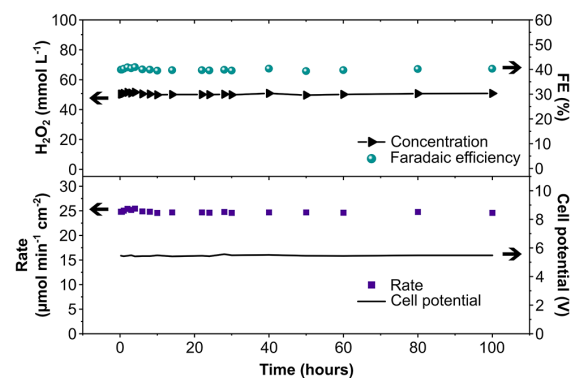
Figure 4. Long-term stability of BPP at continuous single-pass flow. H_2O_2 concentration, FE, production rate, and cell potential in a flow cell experiment with a single-pass flow rate of 5 mL min^{-1} for 100 h at a constant current density of 200 mA cm^{-2}, using a 10 cm^2 BPP-FP15 as an anode in 2 mol L^{-1} K_2CO_3 electrolyte. One L of 2 mol L^{-1} K_2CO_3 was used as a catholyte and was recirculated throughout the experiment. A total charge of 721646 C was supplied during 100 h of electrolysis.

morphology or structural damage to the electrode (Supporting Information, Figure S12). The EDX analysis also showed no significant difference in the elemental composition of the BPP electrode before and after operation (Supporting Information, Table S8). Stability is crucial for the industrial application of electrochemical systems, reducing the chances of component failures and the need for disassembling the reactor.[30] The presented results clearly show that BPP is stable in long-term operation, without any loss of performance over 100 h, enabling synthesis at technically relevant current densities and with substantial FE compared to other carbonaceous electrodes.

CONCLUSION

In summary, we presented for the first time the application of commercial BPP electrodes for the $2e^-$ WOR to H_2O_2. BPP, an inexpensive material widely used in fuel cell research and application, is a promising active electrode material for anodic H_2O_2 generation. An outstanding electrode stability over 100 h for continuous H_2O_2 generation under relevant operational conditions (high current density, flow cell setup) shows the potential of BPP as a low-cost electrode for water oxidation to H_2O_2. In comparison to other electrode materials, the performance of BPP electrodes were found slightly inferior compared to BDD. However, the much lower costs of BPP compared to BDD is likely to overcompensate for this disadvantage. This issue requires careful trade-off analysis for each specific application case. Generally, the performance of BPP in anodic H_2O_2 reduction is substantially superior to any other low-cost material.[19] The hydrophobic fluorinated polymer in BPPs enhances the formation of H_2O_2 by confining oxygen on the electrode surface. Improvement in the BPP polymer content, cell design, and electrochemical parameters can still enhance the BPP activity to achieve a similar performance as BDD. Furthermore, a deeper understanding of the role of hydrophobic polymers on the electrode to promote H_2O_2 production is necessary, and the present work is intended to trigger comprehensive research activities in this direction.

ASSOCIATED CONTENT

Supporting Information

The Supporting Information is available free of charge at https://pubs.acs.org/doi/10.1021/acssuschemeng.2c06314.

> Material and methods used in this study; a brief discussion regarding the electrochemical setups and detection methods used; a comparison table of this work with other works (PDF)

AUTHOR INFORMATION

Corresponding Authors

Dhananjai Pangotra − *Fraunhofer Institute of Interfacial Engineering and Biotechnology IGB, Bio-, Electro-, and Chemocatalysis BioCat, Straubing Branch, 94315 Straubing, Germany; Chair of Chemistry for Biogenic Resources, Campus Straubing for Biotechnology and Sustainability, Technical University of Munich, 94315 Straubing, Germany;* orcid.org/0000-0003-2974-6917; Email: dhananjai.pangotra@igb.fraunhofer.de

Luciana Vieira − *Fraunhofer Institute of Interfacial Engineering and Biotechnology IGB, Bio-, Electro-, and Chemocatalysis BioCat, Straubing Branch, 94315 Straubing,*

Germany; orcid.org/0000-0003-1466-6447; Email: luciana.vieira@igb.fraunhofer.de

Authors

Arne Roth − *Fraunhofer Institute of Interfacial Engineering and Biotechnology IGB, Bio-, Electro-, and Chemocatalysis BioCat, Straubing Branch, 94315 Straubing, Germany*

Volker Sieber − *Fraunhofer Institute of Interfacial Engineering and Biotechnology IGB, Bio-, Electro-, and Chemocatalysis BioCat, Straubing Branch, 94315 Straubing, Germany; Chair of Chemistry for Biogenic Resources, Campus Straubing for Biotechnology and Sustainability, Technical University of Munich, 94315 Straubing, Germany;* orcid.org/0000-0001-5458-9330

Complete contact information is available at:
https://pubs.acs.org/10.1021/acssuschemeng.2c06314

Author Contributions

Conceptualization: D.P., A.R., and L.V. Investigation, Formal analysis, Validation: D.P. Supervision: A.R., V.S., and L.V. Writing−original draft: D.P. Writing−review and editing: A.R., V.S., and L.V.

Notes

The authors declare no competing financial interest.

REFERENCES

(1) Perry, S. C.; Pangotra, D.; Vieira, L.; Csepei, L.-I.; Sieber, V.; Wang, L.; Ponce de León, C.; Walsh, F. C. Electrochemical synthesis of hydrogen peroxide from water and oxygen. *Nature Reviews. Chemistry* **2019**, *3* (7), 442−458.

(2) Gohardani, A. S.; Stanojev, J.; Demairé, A.; Anflo, K.; Persson, M.; Wingborg, N.; Nilsson, C. Green space propulsion: Opportunities and prospects. *Progress in Aerospace Sciences* **2014**, *71*, 128−149.

(3) Saini, V.; Sikri, K.; Batra, S. D.; Kalra, P.; Gautam, K. Development of a highly effective low-cost vaporized hydrogen peroxide-based method for disinfection of personal protective equipment for their selective reuse during pandemics. *Gut Pathogens* **2020**, *12* (1), 29.

(4) Murray, A. T.; Voskian, S.; Schreier, M.; Hatton, T. A.; Surendranath, Y. Electrosynthesis of Hydrogen Peroxide by Phase-Transfer Catalysis. *Joule* **2019**, *3* (12), 2942−2954.

(5) Campos-Martin, J. M.; Blanco-Brieva, G.; Fierro, J. L. Hydrogen peroxide synthesis: an outlook beyond the anthraquinone process. *Angew. Chem., Int. Ed. Engl.* **2006**, *45* (42), 6962−84.

(6) Chen, Z.; Chen, S.; Siahrostami, S.; Chakthranont, P.; Hahn, C.; Nordlund, D.; Dimosthenis, S.; Nørskov, J. K.; Bao, Z.; Jaramillo, T. F. Development of a reactor with carbon catalysts for modular-scale, low-cost electrochemical generation of H_2O_2. *React. Chem. Eng.* **2017**, *2*, 239−245.

(7) Xia, C.; Xia, Y.; Zhu, P.; Fan, L.; Wang, H. Direct electrosynthesis of pure aqueous H_2O_2 solutions up to 20% by weight using a solid electrolyte. *Science* **2019**, *366* (6462), 226−231.

(8) Miyase, Y.; Iguchi, S.; Miseki, Y.; Gunji, T.; Sayama, K. Electrochemical H_2O_2 Production and Accumulation from H_2O by

Composite Effect of Al_2O_3 and $BiVO_4$. *J. Electrochem. Soc.* **2019**, *166* (13), H644−H649.

(9) Fuku, K.; Miyase, Y.; Miseki, Y.; Gunji, T.; Sayama, K. Enhanced Oxidative Hydrogen Peroxide Production on Conducting Glass Anodes Modified with Metal Oxides. *ChemistrySelect* **2016**, *1* (18), 5721−5726.

(10) Fuku, K.; Sayama, K. Efficient oxidative hydrogen peroxide production and accumulation in photoelectrochemical water splitting using a tungsten trioxide/bismuth vanadate photoanode. *Chem. Commun. (Camb)* **2016**, *52* (31), 5406−9.

(11) Shi, X.; Siahrostami, S.; Li, G. L.; Zhang, Y.; Chakthranont, P.; Studt, F.; Jaramillo, T. F.; Zheng, X.; Norskov, J. K. Understanding activity trends in electrochemical water oxidation to form hydrogen peroxide. *Nat. Commun.* **2017**, *8* (1), 701.

(12) Park, S. Y.; Abroshan, H.; Shi, X.; Jung, H. S.; Siahrostami, S.; Zheng, X. $CaSnO_3$: An Electrocatalyst for Two-Electron Water Oxidation Reaction to Form H_2O_2. *ACS Energy Letters* **2019**, *4* (1), 352−357.

(13) Kelly, S. R.; Shi, X.; Back, S.; Vallez, L.; Park, S. Y.; Siahrostami, S.; Zheng, X.; Nørskov, J. K. ZnO As an Active and Selective Catalyst for Electrochemical Water Oxidation to Hydrogen Peroxide. *ACS Catal.* **2019**, *9*, 4593−4599.

(14) Leow, W. R.; Lum, Y.; Ozden, A.; Wang, Y.; Nam, D.-H.; Chen, B.; Wicks, J.; Zhuang, T.-T.; Li, F.; Sinton, D.; Sargent, E. H. Chloride-mediated selective electrosynthesis of ethylene and propylene oxides at high current density. *Science* **2020**, *368* (6496), 1228−1233.

(15) Mavrikis, S.; Göltz, M.; Rosiwal, S.; Wang, L.; Ponce de León, C. Boron-Doped Diamond Electrocatalyst for Enhanced Anodic H_2O_2 Production. *ACS Applied Energy Materials* **2020**, *3* (4), 3169−3173.

(16) Wenderich, K.; Nieuweweme, B. A. M.; Mul, G.; Mei, B. T. Selective Electrochemical Oxidation of H_2O to H_2O_2 Using Boron-Doped Diamond: An Experimental and Techno-Economic Evaluation. *ACS Sustainable Chem. Eng.* **2021**, *9* (23), 7803−7812.

(17) Mavrikis, S.; Göltz, M.; Perry, S. C.; Bogdan, F.; Leung, P. K.; Rosiwal, S.; Wang, L.; Ponce de León, C. Effective Hydrogen Peroxide Production from Electrochemical Water Oxidation. *ACS Energy Letters* **2021**, *6*, 2369−2377.

(18) Pangotra, D.; Csepei, L.-I.; Roth, A.; Sieber, V.; Vieira, L. Anodic generation of hydrogen peroxide in continuous flow. *Green Chem.* **2022**, *24* (20), 7931−7940.

(19) Pangotra, D.; Csepei, L.-I.; Roth, A.; Ponce de León, C.; Sieber, V.; Vieira, L. Anodic production of hydrogen peroxide using commercial carbon materials. *Applied Catalysis B: Environmental* **2022**, *303*, No. 120848.

(20) Xia, C.; Back, S.; Ringe, S.; Jiang, K.; Chen, F.; Sun, X.; Siahrostami, S.; Chan, K.; Wang, H. Confined local oxygen gas promotes electrochemical water oxidation to hydrogen peroxide. *Nature Catalysis* **2020**, *3* (2), 125−134.

(21) Venugopal, A.; Egberts, L. H. T.; Meeprasert, J.; Pidko, E. A.; Dam, B.; Burdyny, T.; Sinha, V.; Smith, W. A. Polymer Modification of Surface Electronic Properties of Electrocatalysts. *ACS Energy Letters* **2022**, *7*, 1586−1593.

(22) Hermann, A.; Chaudhuri, T.; Spagnol, P. Bipolar plates for PEM fuel cells: A review. *Int. J. Hydrogen Energy* **2005**, *30* (12), 1297−1302.

(23) Yao, K.; Adams, D.; Hao, A.; Zheng, J. P.; Liang, Z.; Nguyen, N. Highly Conductive and Strong Graphite-Phenolic Resin Composite for Bipolar Plate Applications. *Energy Fuels* **2017**, *31* (12), 14320−14331.

(24) Besmann, T. M.; Klett, J. W.; Henry, J. J.; Lara-Curzio, E. Carbon/Carbon Composite Bipolar Plate for Proton Exchange Membrane Fuel Cells. *J. Electrochem. Soc.* **2000**, *147* (11), 4083.

(25) Hamilton, P. J.; Pollet, B. G. Polymer Electrolyte Membrane Fuel Cell (PEMFC) Flow Field Plate: Design, Materials and Characterisation. *Fuel Cells* **2010**, *10* (4), 489−509.

(26) Kim, S.; Yoon, Y.; Narejo, G. M.; Jung, M.; Kim, K. J.; Kim, Y.-J. Flexible graphite bipolar plates for vanadium redox flow batteries. *International Journal of Energy Research* **2021**, *45* (7), 11098−11108.

(27) Arai, T.; Tominaga, Y.; Asai, S.; Sumita, M. A study on correlation between physical properties and interfacial characteristics in highly loaded graphite−polymer composites. *J. Polym. Sci., Part B: Polym. Phys.* **2005**, *43* (18), 2568−2577.

(28) Minke, C.; Hickmann, T.; dos Santos, A. R.; Kunz, U.; Turek, T. Cost and performance prospects for composite bipolar plates in fuel cells and redox flow batteries. *J. Power Sources* **2016**, *305*, 182−190.

(29) Peng, Y.; Liu, H. Effects of Oxidation by Hydrogen Peroxide on the Structures of Multiwalled Carbon Nanotubes. *Ind. Eng. Chem. Res.* **2006**, *45* (19), 6483−6488.

(30) Perry, S. C.; Mavrikis, S.; Wang, L.; Ponce de León, C. Future perspectives for the advancement of electrochemical hydrogen peroxide production. *Current Opinion. Electrochemistry* **2021**, *30*, No. 100792.

4. DISCUSSION & OUTLOOK

The electrochemical production of H_2O_2 from water and O_2 has caught significant attention to substitute the classic AO process. The technology is envisioned as a sustainable alternative to the conventional energy-demanding AO process for H_2O_2 production [20]. The electrochemical technology is aimed to produce H_2O_2 at the point of use instead of transporting it in concentrated form, with the objective to electrify and decentralize the production of H_2O_2. While considerable R&D has been devoted to the cathodic O_2 reduction to H_2O_2, comparably little attention has been dedicated to the anodic H_2O_2 production via water oxidation reaction (WOR). In addition, the most recent literature on WOR to H_2O_2 focuses on catalyst development in lab-scale H-cells, i.e., in batch [52][53][54][57][58][65][82]. For industrial implementation, a continuous, robust, and scalable electrochemical flow cell system for anodic H_2O_2 production is required. Recent work done as part of the doctoral thesis work substantially contributes to the progress in this field for continuous H_2O_2 production from water. The discussion is divided into four parts, as discussed below.

4.1   Use of metal oxides as electrocatalysts at high current densities – The starting point

Various metal oxides, including $BiVO_4$, $CaSnO_3$, ZnO, WO_3, SnO_2, and TiO_2, have been reported as active electrocatalysts for the anodic synthesis of H_2O_2. These metal oxides have been reported to show good selectivity, mostly on a fluorine doped tin oxide (FTO) substrate, however only operating at low current densities. The major advantage of using FTO substrate is its low cost, its suitability for a wide area of applications, and its high chemical stability. However, FTO is not suitable for operation at high current densities [51]. Therefore, in this work, the substrate was changed from FTO to carbon paper due to its high surface area, relatively high conductivity, and chemical stability in alkaline electrolytes. The activity of the reported metal oxides, including $BiVO_4$, SnO_2, WO_3, MnO_x, and TiO_2, were investigated for anodic H_2O_2 synthesis at high current densities. At a low current density, $BiVO_4$ had the highest FE ($\sim$23%) at 0.1 mA cm^{-2} with a production rate of 0.00816 μmol min^{-1} cm^{-2} (**Section 3.1, Figure 3.5c, d**). As soon as the current was increased, FE dropped to 1.7%, but at the same time, the production rate reached up to 1.36 μmol min^{-1} cm^{-2} at a current density of

270 mA cm^{-2} (**Section 3.1, Figure 3.5b-d**), during same time. Thus, higher current density leads to an increase in the H$_2$O$_2$ production rate/concentration, however, at the expense of FE. With the extra overpotential for driving larger currents, the water oxidation reaction favors O$_2$ evolution, leading to significant decreases in H$_2$O$_2$ selectivity [83] Metal oxides are difficult to use together with operation at high current densities. With the current state of the art and based on this work, using metal oxides as electrocatalysts is far from industrial implementation. Further work needs to be done to immobilize the catalysts on different substrates by using different binders and applying heat treatments, to be used at high current densities. Nevertheless, this approach appears to be ineffective [84]. Therefore, this work was shifted to using carbon-based materials as electrodes rather than using metal oxides that are expensive and unsustainable [54].

4.2 Commercial carbon materials as electrodes for H$_2$O$_2$ synthesis – A step back

In this part of work, a process development to maximize the efficiency and the concentration of H$_2$O$_2$ for 2e$^-$ WOR was conducted using different commercial carbon materials. Along with the screening of various carbon materials, different process parameters, such as current density, electrolyte concentration, and the pH were optimized. Since H$_2$O$_2$ is known to be unstable which decomposes into water and molecular oxygen, sodium metasilicate (Na$_2$SiO$_3$) was added to the electrolyte as H$_2$O$_2$ stabilizer.

The carbon materials used in this study are divided into two types:
1. <u>2D carbon material</u>: Glassy carbon (GC)
2. <u>3D carbon materials</u>: Carbon fiber paper (CFP), Carbon cloth (CC), Carbon gas diffusion layer (C-GDL), Carbon felt (CF)

The 3D electrode materials are further divided into the following two categories:
1. <u>Woven type</u>: Carbon cloth (CC)
2. <u>Non-woven type</u>: carbon fiber paper (CFP), carbon gas diffusion layer (C-GDL) and carbon felt (CF)

All carbon materials except GC are fibrous. CFP and CF are highly porous, whereas CC and C-GDL are more compact 3D structures, as shown in the SEM images (**Figure 2a**) in **Section 3.2**.

All commercial carbon materials were used as received. One side of CC and C-GDL consist of a microporous layer (MPL) made of carbon and a hydrophobic layer, which is often beneficial for

immobilizing catalysts for electrochemical reaction with gases (e.g., O_2 or CO_2 reduction). The MPL typically is made of carbon black mixed with a hydrophobic polymer such as polytetrafluoroethylene (PTFE), which prevents flooding into the porous gas diffusion electrode. Earlier reports from Xia *et al.* have suggested an enhanced activity towards H_2O_2 production with increasing the hydrophobicity of carbon materials [21].

Therefore, CC and C-GDL were also tested, which have a hydrophobic layer. Nevertheless, the experiments with CC and C-GDL showed lower electrochemical activity towards WOR than CFP upon applying a constant charge of 30 Coulombs (C) at 50 mA current (**Table 1** and **Figure 2b**, **Section 3.2**). The carbon materials activity toward WOR to H_2O_2 (based on the H_2O_2 production rates) follows the order: CFP > CC > C-GDL > CF > GC. The differences in electrochemical activity could emerge from the structural and morphological differences amongst the studied materials. CFP and CF are highly porous, whereas CC and C-GDL are more compact 3D structures, as shown in the SEM images of **Figure 2a** in **Section 3.2**. Other factors include the difference in thickness, electronic resistivity, the presence of a microporous hydrophobic layer (MPL), and the porosity. The product transport characteristics in the electrode materials are determined by their porosity, permeability, and hydrophobicity [85].

The reason for this difference in reactivity could be the following:
(i) The different carbon materials were employed with the same geometric area (1 cm^2), but they have different thicknesses and 3D structures.
(ii) Glassy carbon is a 2D electrode, and the electrochemically active area is therefore considerably smaller than other porous 3D carbon materials, resulting in lower H_2O_2 production.
(iii) The surface of the carbon felt (CF) is highly porous. Thus, a higher current density was observed during LSV measurements, indicating high O_2/H_2O_2 production.
affinity. However, due to high porosity of the CF, the electrogenerated H_2O_2 may be readily oxidized to O_2 in the pores of the carbon felt, resulting in lower H_2O_2 concentration. (iv) The hydrophobicity of carbon cloth (CC) and carbon gas diffusion layer (C-GDL) could also be the reason for their lower activity compared to the carbon fiber paper (CFP). In fact, this difference should increase the production rate, as reported in **Section 3.4** and other studies [21][86].

In this work, we attested that the selectivity of water oxidation to H_2O_2 is greatly influenced by the applied currents, concentration of electrolyte, pH of the electrolyte as well as stabilizer. A direct relationship between CO_3^{2-} ion activity and enhanced production of H_2O_2 was observed, where higher CO_3^{2-} concentration lead to higher H_2O_2 concentration. Based on calculations of the ionic

species activity in the electrolyte and its correlation with the observed experimental results, a cyclic mechanism involving CO_3^{2-} species was proposed (**Section 3.2**). The proposed catalytic cycle involves the formation of peroxodicarbonate as unstable intermediate, rapidly decomposing to H_2O_2 and CO_3^{2-}. This mechanism was later confirmed by in situ infrared spectroscopy (ATR-FTIR) by Gill *et al.*[67] They used electrochemical and spectroscopic techniques to investigate the role of bicarbonate electrolyte species (HCO_3^- and CO_3^{2-}) in the WOR to H_2O_2. Experiments on a rotating ring disc electrode showed that H_2O_2 was not readily detected in the disc but formed only with a time delay. This observation suggests oxidation of the electrolyte followed by hydrolysis, thereby promoting H_2O_2 production. In situ infrared spectroscopy (ATR-FTIR) confirmed the carbonate (HCO_3^- and/or CO_3^{2-}) role and the presence of HCO_4^- or $C_2O_6^{2-}$ peroxo intermediates. However, Gill *et al.*[67] reported higher H_2O_2 productivity in CO_3^{2-} electrolyte, but rather in HCO_3^-, similar to the results reported by Fuku *et al.*[51]. The difference is in using Na_2SiO_3 as a stabilizer, stabilizing H_2O_2 in high pH electrolytes, such as K_2CO_3. Without the stabilizer and the higher pH of the CO_3^{2-} solution will lead to H_2O_2 decomposition. Therefore, higher H_2O_2 concentration was observed in CO_3^{2-} electrolyte, compared to HCO_3^- in the presence of stabilizer as shown in this work (**Figure 7b** in **Section 3.2**).

Mavrikis *et al.* have proposed a similar mechanism for H_2O_2 production using BDD electrodes in $K_2CO_3/KHCO_3$ solutions [82]. The H_2O_2 concentration increased from 28.5 to 37.7 mmol L^{-1}, upon switching the electrolyte concentration from 1 to 4 mol L^{-1} K_2CO_3 at a current density of 100 mA cm^{-2}. Furthermore, DFT calculations revealed that CO_3^{2-} ion positively enhances the H_2O_2 production by forming $C_2O_6^{2-}$ as an intermediate, as proposed in this PhD work.

Regarding the use of chemical stabilizer, Na_2SiO_3 has been proven to be one of the most effective compounds to stabilize H_2O_2, and it is used widely in industrial applications [87]. Nevertheless, the working mechanism of Na_2SiO_3 as a H_2O_2 stabilizer is rather unclear. Literature reports for the stabilization mechanism include forming a complex between Na_2SiO_3 and H_2O_2 [88], forming stable peroxide compounds, stopping the decomposition chain reactions by the destruction of the free radicals, and formation of complexes with metal impurities that could catalyze H_2O_2 decomposition [87].

Typically, organic stabilizers such as aryl alkyl ketones are added to slow down the H_2O_2 decomposition in commercial H_2O_2 solutions. Such stabilizers enhance the lifetime of H_2O_2. However, these stabilizers are redox-active compounds, which oxidize/reduce more easily than H_2O_2, thus preventing H_2O_2 decomposition. At the same time, when added to the electrolyte, such stabilizers would

also be oxidized/reduced in the electrochemical environment. Thus, to prevent the contamination of the H_2O_2 solution with organic degradation products, Na_2SiO_3 was chosen as a non-redox active additive to stabilize H_2O_2.

Although the present study on CFP (**Section 3.2**) has facilitated the enhancement of H_2O_2 productivity 20-fold by using optimized electrolyte composition, the performance parameter, such as the FE and production rate obtained in this part of work using CFP are comparatively lower than those reported in the literature (**Table 3** in **Section 3.2**). One strategy to enhance these performance parameters is to use the optimized electrolyte composition in combination with a state-of-the-art active catalyst such as BDD electrode. Therefore, BDD has been investigated along with the optimized electrolyte conditions and discussed in **Section 4.3**.

4.3   Boron doped diamond in combination with the optimized electrolyte

Optimum electrolyte conditions (2 mol L^{-1} K_2CO_3 with 12 g L^{-1} Na_2SiO_3) led to a 20-fold increase in H_2O_2 production over 2 mol L^{-1} $KHCO_3$ when using CFP as an anode (**Section 3.2** and **4.2**). However, the overall performance of the electrolyte was hampered by the poor selectivity of CFP electrode (maximum FE for anodic production of H_2O_2 of 14%). Recent improvements in the properties of BDD and other carbon materials have enhanced the performance of H_2O_2 production, resulting in a production rate of 74.6 μmol min^{-1} cm^{-2} and FE of 87% [21][65][82]. However, all these WOR studies on carbon-based materials have been conducted in electrochemical H-cells, i.e. batch systems, which are not industrially relevant. The transfer to electrochemical flow cells is necessary as the first step towards functional applications, continuous production, and scale-up, which has been done in this study. Additionally, a direct relationship between the ionic activity of CO_3^{2-} and enhanced anodic H_2O_2 production was established on a commercial CFP anode, as discussed in **Section 3.2**. Thus, BDD was used to extend the scope to show a continuous flow process in combination with an optimized carbonate-based electrolyte system.

In this work, a detailed investigation into the performances of different flow setups (circular and single-pass, (**Figure 2a** and **4a** in **Section 3.3**)) at high current densities (up to 700 mA cm^{-2}) was carried out and compared. The idea of this work lies in the new electrochemical process development, which greatly facilitates the scale-up for the anodic production of H_2O_2.

Firstly, the effect of activity for HCO_3^- ($a(HCO_3^-)$) and CO_3^{2-} ($a(CO_3^{2-})$) species in the electrolyte showed a remarkable correlation with the anodic H_2O_2 production using BDD as an anode.

Higher $a(CO_3^{2-})$ in electrolyte lead to comparatively higher H_2O_2 concentration as observed using a CFP electrode (**Section 3.2**). Secondly, a comparison of two flow setups (circular and single−pass) revealed that the single-pass flow mode was more efficient in terms of the overall performance. In the circular flow mode, the concentration increases with time, however, the FE and the production rate decreases. FE and production rate decrease due to the decay of already generated H_2O_2 on the electrode surface, even in the presence of a chemical stabilizer. This electrochemical H_2O_2 decomposition is higher at higher current densities, resulting in a rapid decrease in FE and production rate, as observed in the experiments (**Figure 2** in **Section 3.3**).

In single−pass flow, however, the performance loss is minimized since the electrolyte does not recirculate with already generated H_2O_2. Single-pass flow facilitated anodic H_2O_2 generation at high current densities, with the highest-ever reported H_2O_2 production rate of 79 μmol min^{-1} cm^{-2} at 700 mA cm^{-2} (**Figure 4** in **Section 3.3**). An additional investigation with and without the stabilizer (Na_2SiO_3) was carried out in a single-pass flow at 300 mA cm^{-2}. Both experiments led to similar H_2O_2 concentration after electrolysis, however, H_2O_2 decomposed faster in the absence of the stabilizer when kept for 3 hours without applying any current (**Figure 5** in **Section 3.3**). The chemical stabilizer does not necessarily enhance the electrochemical H_2O_2 formation, it rather inhibits the chemical decomposition of H_2O_2 during storage and thereby increases its bench life. Thus, chemical stabilizers can be abstained if H_2O_2 is used immediately after single-pass production, reducing the total process cost.

One important aspect to emphasize during the continuous production of H_2O_2 is the flow rate of the electrolyte passing through the electrochemical cell. Flow rate investigation in single-pass revealed high FE and production rate at high flow rates, however, lower H_2O_2 concentration. A faster flow rate reduces the residence time of an electrolyte volume near the electrode, thus minimizing relevant side-reactions such as oxygen evolution and H_2O_2 electrodecomposition, which leads to higher efficiency and production rate. It is, therefore, necessary to consider a compromise between H_2O_2 concentration and FE based on the application of continuous flow anodic H_2O_2 production.

Specifically, this work adds to the pertinent research field an innovative, practical, and straightforward solution that can be readily applied in academia and industry. In this work, a complete process development at high current densities (up to 700 mA cm^{-2}) and the so far highest anodic H_2O_2 concentration of 110 mmol L^{-1}, maximum FE of 78%, and H_2O_2 production rate of 79 μmol min^{-1} cm^{-2}. The continuous production of 80 mmol L^{-1} H_2O_2 for up to 28 hours is described for the first time, showcasing the robustness of the BDD electrode which can further be utilized for piloting.

4.4   Bipolar plate − Thinking of the future

The performance of BDD electrodes surpasses the reported metal oxides and commercial carbon-based materials with impressive production rates, as discussed in **Sections 3.1-3.3**. However, BDD's current market price and its preparation complexity hold back its implementation in the present scenario, despite its splendid activity and robustness [30]. Wenderich *et al.*[30][55] performed a techno-economic analysis on the electrochemical oxidation of H_2O to H_2O_2 using a BDD anode in combination with cathodic H_2 production, intending to decrease the Levelized Cost of Hydrogen (LCH) produced at the cathode. A sensitivity analysis yielded in two critical aspects for lowering the LCH: reducing the cost of the anode and increasing the current density. For a cost-effective system, further exploration of inexpensive carbonaceous materials is required in combination with a current density greater than 100 mA cm^{-2} as suggested by the sensitivity analysis, which is stable for hours.

Various carbonaceous materials, including commercial carbon fiber paper (CFP), have been investigated to scale up to larger electrode areas and operate at high current densities. However, there were some performance-related shortcomings, including activity (CFP) and long-term stability (PTFE/CFP) [21]. PTFE coatings were applied to CFP and NiOx (PTFE/CFP and PTFE/NiOx systems) to enhance the activity, selectivity, and stability of 2e$^-$ WOR to produce H_2O_2 [21][86]. The electrochemical investigation led to an increase in the FE and production rate with modified electrodes. This improvement could be attributed to the modification of surface electronic properties of the electrocatalyst by adding polymers, which in this case was fluoropolymer (PTFE) [21][86].

By looking at polymer modification as a critical factor in improving the water oxidation process, we have explored different bipolar plates (BPP) as a low-cost anode alternative for 2e$^-$ WOR to H_2O_2. The BPP with the highest fluoro polymer content had the highest activity. This can be related to the electronegativity of the fluorine in the polymer, which reduces the binding energy of OH radical on the electrode surface and enhances the H_2O_2 production pathway. Fluorine atoms are highly electronegative, which draw electrons away from the oxygen atoms in the adsorbed OH* intermediate. This lowers the binding energy of the OH* intermediate, making it hard to form the adsorbed O* intermediate for 4e$^-$ oxidation to O_2 and, thus, easy to form H_2O_2 via 2e$^-$ oxidation. Hence, we observe high catalytic activity on H_2O_2 formation, with the BPP sample having the most fluoropolymer content. The BPP was active and stable for up to 100 hours, continuously producing H_2O_2. A summary of the comparison between the findings of this work and those previously reported in the literature is shown in Table 4.1. More work should be devoted to further enhance the H_2O_2 productivity of this material by modifying the electrode using higher fluorine content. A detailed study is necessary to

understand the role of hydrophobic polymers on the electrode to enhance H_2O_2 production.

***Tab. 4.1** : A comparison of the reported work on $2e^-$ WOR to H_2O_2 with this work.*

Electrode	Electrolyte	pH	$[H_2O_2]_{max}$	Production rate	Peak FE	Ref.
			mmol L^{-1}	μmol min^{-1} cm^{-2}	%	
PTFE/CFP	1 M Na$_2$CO$_3$	12	3	23.4	66	[21]
BDD/Nb		11.9	-	3.9	31.7	[30]
BDD/Ti	2 M KHCO$_3$	8	~16	~8	28	[65]
			29	19.7	~22	
CaSnO$_3$/FTO			-	~4.6	76	[54]
			~0.9	-	-	
BiVO$_4$/FTO	1 M NaHCO$_3$	8.3		5.7	70	[52]
WO$_3$/FTO				0.57	48	
TiO$_2$/FTO			-	1.01	19	
SnO$_2$/FTO				1.53	50	
CFP	2 M K$_2$CO$_3$	12.6	33	4.5	14.3	This work
BDD/Ta			80	79	78	
BPP-FP15			50	25	44	

4.5   Future perspective

Aside from eliminating hazardous solvents and reactants used in conventional chemical processes, electrochemical processes allow for decentralized, small-scale, and on-demand manufacturing using simple, non-hazardous feed streams, such as water, air, and (renewable) electricity, as in the case of electrochemical synthesis of H_2O_2. Due to the vast range of applications of H_2O_2, decentralized production has enormous potential in technical fields such as bleaching, sanitation, water treatment, etc. Nonetheless, a decentral process requires a continuous and stable production rate, which was the focus of this work. A clear vision of future industrial applications is needed when conducting such research, focusing on resource efficiency, investment, operational costs, and operational stability. From the point of view of mobile electrochemical prototypes, electrochemical H_2O_2 production is more a matter of expanding the H_2O_2 market to host decentralized solutions, especially in remote areas where transportation of H_2O_2 is difficult. In addition, anodic production of H_2O_2 could be combined for example with hydrogen production, thus diversifying and adding value to the hydrogen industry.

5. REFERENCES

[1] David I. Stern and Astrid Kander. The role of energy in the industrial revolution and modern economic growth. *The Energy Journal*, 33(3):125–152, 2012.

[2] Ernie Jowsey. Economic aspects of natural resource exploitation. *International Journal of Sustainable Development & World Ecology*, 16(5):303–307, 2009.

[3] Vaclav Smil. Energy in the twentieth century: Resources, conversions, costs, uses, and consequences. *Annual Review of Energy and the Environment*, 25(1):21–51, 2000.

[4] Demographics and Human Development. https://www.dni.gov/index.php/gt2040-home/gt2040-structural-forces/demographics-and-human-development (accessed 08.09.2022).

[5] 2017 Outlook for Energy: A View to 2040. 2017.

[6] Statista Daily demand for crude oil worldwide from 2006 to 2020, with a forecast until 2026*. https://www.statista.com/statistics/271823/daily-global-crude-oil-demand-since-2006/ (accessed 10 January 2023).

[7] Kuo, G. When Fossil Fuels Run Out, What Then? (accessed 10 January 2023).

[8] Harro van Asselt. Governing fossil fuel production in the age of climate disruption: Towards an international law of 'leaving it in the ground'. *Earth System Governance*, 9:100118, 2021.

[9] George A. Olah, G. K. Surya Prakash, and Alain Goeppert. Anthropogenic chemical carbon cycle for a sustainable future. *Journal of the American Chemical Society*, 133(33):12881–12898, 2011.

[10] Nicola Armaroli and Vincenzo Balzani. The future of energy supply: Challenges and opportunities. *Angewandte Chemie International Edition*, 46(1-2):52–66, 2007.

[11] Change, U. N. F.-C. o. C., International Solar Alliance Mobilizing USD 1 Trillion for Solar Energy by 2030. Paris, 2015.

[12] IEA Renewable electricity growth is accelerating faster than ever worldwide, supporting the emergence of the new global energy economy. https://www.iea.org/news/renewable-electricity-growth-is-accelerating-faster-than-ever-worldwide-supporting-the-emergence-of-the-new-global-energy-economy (accessed 09.09.2022).

[13] Agora Energiewende. www.agora-energiewende.de (accessed 8 January 2023).

[14] Alireza Salmachi, Tara Hosseini, Raheel Ahmed Shaikh, Alex Dinovitser, and Derek Abbott. Techno-economic assessment of hydrogen pipe storage in decommissioned wellbores sourced from surplus renewable electricity. *International Journal of Hydrogen Energy*, 47(56):23710–23720, 2022.

[15] Kevin M. Van Geem and Bert M. Weckhuysen. Toward an e-chemistree: Materials for electrification of the chemical industry. *MRS Bulletin*, 46(12):1187–1196, 2021.

[16] Yang Song, Udishnu Sanyal, Dhananjai Pangotra, Jamie D. Holladay, Donald M. Camaioni, Oliver Y. Gutiérrez, and Johannes A. Lercher. Hydrogenation of benzaldehyde via electrocatalysis and thermal catalysis on carbon-supported metals. *Journal of Catalysis*, 359:68–75, 2018.

[17] Stephen Comello and Stefan Reichelstein. The emergence of cost effective battery storage. *Nature Communications*, 10(1):2038, 2019.

[18] Gabriella Fiorentino, Maddalena Ripa, and Sergio Ulgiati. Chemicals from biomass: technological versus environmental feasibility. a review. *Biofuels, Bioproducts and Biorefining*, 11(1):195–214, 2017.

[19] Soliu O. Ganiyu, Carlos A. Martínez-Huitle, and Manuel A. Rodrigo. Renewable energies driven electrochemical wastewater/soil decontamination technologies: A critical review of fundamental concepts and applications. *Applied Catalysis B: Environmental*, 270:118857, 2020.

[20] Samuel C. Perry, Dhananjai Pangotra, Luciana Vieira, Lénárd-István Csepei, Volker Sieber, Ling Wang, Carlos Ponce de León, and Frank C. Walsh. Electrochemical synthesis of hydrogen peroxide from water and oxygen. *Nature Reviews Chemistry*, 3(7):442–458, 2019.

[21] Chuan Xia, Seoin Back, Stefan Ringe, Kun Jiang, Fanhong Chen, Xiaoming Sun, Samira Siahrostami, Karen Chan, and Haotian Wang. Confined local oxygen gas promotes electrochemical water oxidation to hydrogen peroxide. *Nature Catalysis*, 3(2):125–134, 2020.

[22] Xiao Yan, Wen-Wu Shi, and Xin-zhong Wang. Carbon based electrocatalysts for selective hydrogen peroxide conversion. *New Carbon Materials*, 37(1):223–236, 2022.

[23] Shu Hu. Membrane-less photoelectrochemical devices for H_2O_2 production: efficiency limit and operational constraint. *Sustainable Energy & Fuels*, 3(1):101–114, 2019.

[24] J. M. Campos-Martin, G. Blanco-Brieva, and J. L. Fierro. Hydrogen peroxide synthesis: an outlook beyond the anthraquinone process. *Angew Chem Int Ed Engl*, 45(42):6962–84, 2006.

[25] R. Ciriminna, L. Albanese, F. Meneguzzo, and M. Pagliaro. Hydrogen peroxide: A key chemical for today's sustainable development. *ChemSusChem*, 9(24):3374–3381, 2016.

[26] Martin Ragnar, Gunnar Henriksson, Mikael E. Lindström, Martin Wimby, Jürgen Blechschmidt, and Sabine Heinemann. *Pulp*, pages 1–92.

[27] Ezra Linley, Stephen P. Denyer, Gerald McDonnell, Claire Simons, and Jean-Yves Maillard. Use of hydrogen peroxide as a biocide: new consideration of its mechanisms of biocidal action. *Journal of Antimicrobial Chemotherapy*, 67(7):1589–1596, 2012.

[28] Pratima Bajpai. *Pulp and Paper Industry*. Elsevier, 2015.

[29] Gustaaf Goor, Jürgen Glenneberg, Sylvia Jacobi, Jal Dadabhoy, and Elize Candido. *Hydrogen Peroxide*, pages 1–40.

[30] Kasper Wenderich, Birgit A. M. Nieuweweme, Guido Mul, and Bastian T. Mei. Selective electrochemical oxidation of H_2O to H_2O_2 using boron-doped diamond: An experimental and techno-economic evaluation. *ACS Sustainable Chemistry & Engineering*, 9(23):7803–7812, 2021.

[31] Richard L. Myers. *The 100 Most Important Chemical Compounds: A Reference Guide*. Greenwood Press, 2007.

[32] Sumanth Ranganathan and Volker Sieber. Recent advances in the direct synthesis of hydrogen peroxide using chemical catalysis—a review. *Catalysts*, 8(9):379, 2018.

[33] G. Pfleiderer Riedl H.-J. Production of hydrogen peroxide. 1939.

[34] S. Anantharaj, S. Pitchaimuthu, and S. Noda. A review on recent developments in electrochemical hydrogen peroxide synthesis with a critical assessment of perspectives and strategies. *Advances in Colloid and Interface Science*, 287:102331, 2021.

[35] Alexander T. Murray, Sahag Voskian, Marcel Schreier, T. Alan Hatton, and Yogesh Surendranath. Electrosynthesis of hydrogen peroxide by phase-transfer catalysis. *Joule*, 3(12):2942–2954, 2019.

[36] Jingkun An, Yujie Feng, Qian Zhao, Xin Wang, Jia Liu, and Nan Li. Electrosynthesis of H_2O_2 through a two-electron oxygen reduction reaction by carbon based catalysts: From mechanism, catalyst design to electrode fabrication. *Environmental Science and Ecotechnology*, 11:100170, 2022.

[37] Justin S. J. Hargreaves, Young-Min Chung, Wha-Seung Ahn, Takashi Hisatomi, Kazunari Domen, Mayfair C. Kung, and Harold H. Kung. Minimizing energy demand and environmental

impact for sustainable nh3 and H_2O_2 production—a perspective on contributions from thermal, electro-, and photo-catalysis. *Applied Catalysis A: General*, 594:117419, 2020.

[38] Yongyu Pang, Huan Xie, Yuan Sun, Maria-Magdalena Titirici, and Guo-Liang Chai. Electrochemical oxygen reduction for H_2O_2 production: catalysts, ph effects and mechanisms. *Journal of Materials Chemistry A*, 8(47):24996–25016, 2020.

[39] Guilherme V. Fortunato, Enrico Pizzutilo, Eduardo S. F. Cardoso, Marcos R. V. Lanza, Ioannis Katsounaros, Simon J. Freakley, Karl J. J. Mayrhofer, Gilberto Maia, and Marc Ledendecker. The oxygen reduction reaction on palladium with low metal loadings: The effects of chlorides on the stability and activity towards hydrogen peroxide. *Journal of Catalysis*, 389:400–408, 2020.

[40] Samira Siahrostami, Arnau Verdaguer-Casadevall, Mohammadreza Karamad, Davide Deiana, Paolo Malacrida, Björn Wickman, María Escudero-Escribano, Elisa A. Paoli, Rasmus Frydendal, Thomas W. Hansen, Ib Chorkendorff, Ifan E. L. Stephens, and Jan Rossmeisl. Enabling direct H_2O_2 production through rational electrocatalyst design. *Nature Materials*, 12(12):1137–1143, 2013.

[41] Thomas Richards, Jonathan H. Harrhy, Richard J. Lewis, Alexander G. R. Howe, Grzegorz M. Suldecki, Andrea Folli, David J. Morgan, Thomas E. Davies, E. Joel Loveridge, David A. Crole, Jennifer K. Edwards, Paul Gaskin, Christopher J. Kiely, Qian He, Damien M. Murphy, Jean-Yves Maillard, Simon J. Freakley, and Graham J. Hutchings. A residue-free approach to water disinfection using catalytic in situ generation of reactive oxygen species. *Nature Catalysis*, 4(7):575–585, 2021.

[42] Jisung Park, Yuta Nabae, Teruaki Hayakawa, and Masa-aki Kakimoto. Highly selective two-electron oxygen reduction catalyzed by mesoporous nitrogen-doped carbon. *ACS Catalysis*, 4(10):3749–3754, 2014.

[43] Euiyeon Jung, Heejong Shin, Wytse Hooch Antink, Yung-Eun Sung, and Taeghwan Hyeon. Recent advances in electrochemical oxygen reduction to H_2O_2: Catalyst and cell design. *ACS Energy Letters*, 5(6):1881–1892, 2020.

[44] Yanyan Sun, Luca Silvioli, Nastaran Ranjbar Sahraie, Wen Ju, Jingkun Li, Andrea Zitolo, Shuang Li, Alexander Bagger, Logi Arnarson, Xingli Wang, Tim Moeller, Denis Bernsmeier, Jan Rossmeisl, Frédéric Jaouen, and Peter Strasser. Activity–selectivity trends in the electrochemical production of hydrogen peroxide over single-site metal–nitrogen–carbon catalysts. *Journal of the American Chemical Society*, 141(31):12372–12381, 2019.

[45] C. Xia, Y. Xia, P. Zhu, L. Fan, and H. Wang. Direct electrosynthesis of pure aqueous H_2O_2 solutions up to 20% by weight using a solid electrolyte. *Science*, 366(6462):226–231, 2019.

[46] Hui Li, Peng Wen, Dominique S. Itanze, Zachary D. Hood, Shiba Adhikari, Chang Lu, Xiao Ma, Chaochao Dun, Lin Jiang, David L. Carroll, Yejun Qiu, and Scott M. Geyer. Scalable neutral H_2O_2 electrosynthesis by platinum diphosphide nanocrystals by regulating oxygen reduction reaction pathways. *Nature Communications*, 11(1):3928, 2020.

[47] Xinjian Shi, Seoin Back, Thomas Mark Gill, Samira Siahrostami, and Xiaolin Zheng. Electrochemical synthesis of H_2O_2 by two-electron water oxidation reaction. *Chem*, 7(1):38–63, 2021.

[48] Chaojie Song and Jiujun Zhang. *Electrocatalytic Oxygen Reduction Reaction*, pages 89–134. Springer, London, 2008.

[49] Yuji Ando and Tadayoshi Tanaka. Proposal for a new system for simultaneous production of hydrogen and hydrogen peroxide by water electrolysis. *International Journal of Hydrogen Energy*, 29(13):1349–1354, 2004.

[50] Alex Izgorodin, Ekaterina Izgorodina, and Douglas R. MacFarlane. Low overpotential water oxidation to hydrogen peroxide on a MnOx catalyst. *Energy & Environmental Science*, 5(11):9496–9501, 2012.

[51] Kojiro Fuku, Yuta Miyase, Yugo Miseki, Takahiro Gunji, and Kazuhiro Sayama. Enhanced oxidative hydrogen peroxide production on conducting glass anodes modified with metal oxides. *ChemistrySelect*, 1(18):5721–5726, 2016.

[52] X. Shi, S. Siahrostami, G. L. Li, Y. Zhang, P. Chakthranont, F. Studt, T. F. Jaramillo, X. Zheng, and J. K. Norskov. Understanding activity trends in electrochemical water oxidation to form hydrogen peroxide. *Nat Commun*, 8(1):701, 2017.

[53] Ting Kang, Bei Li, Qinglan Hao, Weijie Gao, Feng Bin, Kwun Nam Hui, Dong Fu, and Baojuan Dou. Efficient hydrogen peroxide (H_2O_2) synthesis by $CaSnO_3$ via two-electron water oxidation reaction. *ACS Sustainable Chemistry & Engineering*, 8(39):15005–15012, 2020.

[54] So Yeon Park, Hadi Abroshan, Xinjian Shi, Hyun Suk Jung, Samira Siahrostami, and Xiaolin Zheng. $CaSnO_3$: An electrocatalyst for two-electron water oxidation reaction to form H_2O_2. *ACS Energy Letters*, 4(1):352–357, 2019.

[55] K. Fuku, Y. Miyase, Y. Miseki, T. Funaki, T. Gunji, and K. Sayama. Photoelectrochemical hydrogen peroxide production from water on a WO$_3$ /BiVO$_4$ photoanode and from O$_2$ on an au cathode without external bias. *Chem Asian J*, 12(10):1111–1119, 2017.

[56] Yuta Miyase, Shoji Iguchi, Yugo Miseki, Takahiro Gunji, and Kazuhiro Sayama. Electrochemical H$_2$O$_2$ production and accumulation from h2o by composite effect of Al$_2$O$_3$ and BiVO$_4$. *Journal of The Electrochemical Society*, 166(13):H644–H649, 2019.

[57] Sara R. Kelly, Xinjian Shi, Seoin Back, Lauren Vallez, So Yeon Park, Samira Siahrostami, Xiaolin Zheng, and Jens K. Nørskov. Zno as an active and selective catalyst for electrochemical water oxidation to hydrogen peroxide. *ACS Catalysis*, 9(5):4593–4599, 2019.

[58] Chaoqi Zhang, Ruihu Lu, Chao Liu, Ling Yuan, Jing Wang, Yan Zhao, and Chengzhong Yu. High yield electrosynthesis of hydrogen peroxide from water using electrospun casno 3 @carbon fiber membrane catalysts with abundant oxygen vacancy. *Advanced Functional Materials*, 31(26):2100099, 2021.

[59] K. Fuku and K. Sayama. Efficient oxidative hydrogen peroxide production and accumulation in photoelectrochemical water splitting using a tungsten trioxide/bismuth vanadate photoanode. *Chem Commun (Camb)*, 52(31):5406–9, 2016.

[60] Ciaran McDonnell-Worth and Douglas R. MacFarlane. Ion effects in water oxidation to hydrogen peroxide. *RSC Advances*, 4(58):30551–30557, 2014.

[61] Shunichi Fukuzumi, Yong-Min Lee, and Wonwoo Nam. Solar-driven production of hydrogen peroxide from water and dioxygen. *Chemistry – A European Journal*, 24(20):5016–5031, 2018.

[62] S. Siahrostami, G. L. Li, V. Viswanathan, and J. K. Norskov. One- or two-electron water oxidation, hydroxyl radical, or H$_2$O$_2$ evolution. *J Phys Chem Lett*, 8(6):1157–1160, 2017.

[63] P-A. Michaud, M. Panizza, L. Ouattara, T. Diaco, G. Foti, and Ch. Comninellis. Electrochemical oxidation of water on synthetic boron-doped diamond thin film anodes. *Journal of Applied Electrochemistry*, 33(2):151–154, 2003.

[64] P.-A. Michaud M. A. Rodrigo B. Marselli, J. Garcia-Gomez and Ch. Comninellis. Electrogeneration of hydroxyl radicals on boron-doped diamond electrodes. *J. Electrochem. Soc.*, 150(3):D79–D83, 2003.

[65] Sotirios Mavrikis, Maximilian Göltz, Stefan Rosiwal, Ling Wang, and Carlos Ponce de León. Boron-doped diamond electrocatalyst for enhanced anodic H_2O_2 production. *ACS Applied Energy Materials*, 3(4):3169–3173, 2020.

[66] Jiali Liu, Yousheng Zou, Bingjun Jin, Kan Zhang, and Jong Hyeok Park. Hydrogen peroxide production from solar water oxidation. *ACS Energy Letters*, 4(12):3018–3027, 2019.

[67] Thomas Mark Gill, Lauren Vallez, and Xiaolin Zheng. The role of bicarbonate-based electrolytes in H_2O_2 production through two-electron water oxidation. *ACS Energy Letters*, 6(8):2854–2862, 2021.

[68] Yu Jianqiang and Kudo Akihiko. Hydrothermal synthesis of nanofibrous bismuth vanadate. *Chemistry Letters*, 34(6):850–851, 2005.

[69] Vagner R. de Mendonça, Osmando F. Lopes, Raul P. Fregonesi, Tania R. Giraldi, and Caue Ribeiro. TiO_2-SnO_2 heterostructures applied to dye photodegradation: The relationship between variables of synthesis and photocatalytic performance. *Applied Surface Science*, 298:182–191, 2014.

[70] L. H. Oliveira, A. P. de Moura, F. A. La Porta, I. C. Nogueira, E. C. Aguiar, T. Sequinel, I. L. V. Rosa, E. Longo, and J. A. Varela. Influence of Cu-doping on the structural and optical properties of $CaTiO_3$ powders. *Materials Research Bulletin*, 81:1–9, 2016.

[71] Haidong Zheng, Jian Zhen Ou, Michael S. Strano, Richard B. Kaner, Arnan Mitchell, and Kourosh Kalantar-zadeh. Nanostructured tungsten oxide – properties, synthesis, and applications. *Advanced Functional Materials*, 21(12):2175–2196, 2011.

[72] Matt S. Naughton, Geun Ho Gu, Akash A. Moradia, and Paul J. A. Kenis. Tailoring electrode hydrophobicity to improve anode performance in alkaline media. *Journal of Power Sources*, 242:581–588, 2013.

[73] Thomas Mark Gill and Xiaolin Zheng. Comparing methods for quantifying electrochemically accumulated H_2O_2. *Chemistry of Materials*, 32(15):6285–6294, 2020.

[74] Ekaterina N. Kadnikova and Nenad M. Kostić. Oxidation of abts by hydrogen peroxide catalyzed by horseradish peroxidase encapsulated into sol–gel glass.: Effects of glass matrix on reactivity. *Journal of Molecular Catalysis B: Enzymatic*, 18(1):39–48, 2002.

[75] Sumanth Ranganathan and Volker Sieber. Development of semi-continuous chemo-enzymatic terpene epoxidation: combination of anthraquinone autooxidation and the lipase-mediated epoxidation process. *Reaction Chemistry & Engineering*, 2(6):885–895, 2017.

[76] B. A. Otieno, C. E. Krause, and J. F. Rusling. *Chapter Seven - Bioconjugation of Antibodies and Enzyme Labels onto Magnetic Beads*, volume 571, pages 135–150. Academic Press, 2016.

[77] Benjamin J. Deadman, Klaus Hellgardt, and King Kuok Hii. A colorimetric method for rapid and selective quantification of peroxodisulfate, peroxomonosulfate and hydrogen peroxide. *Reaction Chemistry & Engineering*, 2(4):462–466, 2017.

[78] George Eisenberg. Colorimetric determination of hydrogen peroxide. *Industrial & Engineering Chemistry Analytical Edition*, 15(5):327–328, 1943.

[79] Zdenko Machala, Barbora Tarabova, Karol Hensel, Eva Spetlikova, Libusa Sikurova, and Petr Lukes. Formation of ros and rns in water electro-sprayed through transient spark discharge in air and their bactericidal effects. *Plasma Processes and Polymers*, 10(7):649–659, 2013.

[80] Zhong Ma, Yu Zhang, Shizhong Liu, Wenqian Xu, Lijun Wu, Yu-Chi Hsieh, Ping Liu, Yimei Zhu, Kotaro Sasaki, Julie N. Renner, Katherine E. Ayers, Radoslav R. Adzic, and Jia X. Wang. Reaction mechanism for oxygen evolution on RuO_2, IrO_2, and $RuO_2@IrO_2$ core-shell nanocatalysts. *Journal of Electroanalytical Chemistry*, 819:296–305, 2018.

[81] V. L. Kornienko, G. A. Kolyagin, G. V. Kornienko, V. A. Parfenov, and I. V. Ponomarenko. Electrosynthesis of H_2O_2 from O_2 in a gas-diffusion electrode based on mesostructured carbon cmk-3. *Russian Journal of Electrochemistry*, 54(3):258–264, 2018.

[82] Sotirios Mavrikis, Maximilian Göltz, Samuel C. Perry, Felix Bogdan, Pui Ki Leung, Stefan Rosiwal, Ling Wang, and Carlos Ponce de León. Effective hydrogen peroxide production from electrochemical water oxidation. *ACS Energy Letters*, pages 2369–2377, 2021.

[83] Lei Fan, Xiaowan Bai, Chuan Xia, Xiao Zhang, Xunhua Zhao, Yang Xia, Zhen-Yu Wu, Yingying Lu, Yuanyue Liu, and Haotian Wang. CO_2/carbonate-mediated electrochemical water oxidation to hydrogen peroxide. *Nature Communications*, 13(1):2668, 2022.

[84] Thomas Stiller. *Oxide Materials for the Electrocatalytic Oxidation of Water to Hydrogen Peroxide*. Thesis, 2020.

[85] Ahmad El-kharouf and Bruno G. Pollet. *Chapter 4 - Gas Diffusion Media and their Degradation*, pages 215–247. Academic Press, Boston, 2012.

[86] Anirudh Venugopal, Laurentius H. T. Egberts, Jittima Meeprasert, Evgeny A. Pidko, Bernard Dam, Thomas Burdyny, Vivek Sinha, and Wilson A. Smith. Polymer modification of surface electronic properties of electrocatalysts. *ACS Energy Letters*, pages 1586–1593, 2022.

[87] Isabelle Charron, Annabelle Couvert, Alain Laplanche, Christophe Renner, Lucie Patria, and Benoît Requieme. Treatment of odorous sulphur compounds by chemical scrubbing with hydrogen peroxide - stabilisation of the scrubbing solution. *Environmental Science & Technology*, 40(24):7881–7885, 2006.

[88] K. Hanna. Comment on "Inhibitory effect of dissolved silica on H_2O_2 decomposition by Iron(III) and Manganese(IV) oxides: Implications for H_2O_2−based in situ chemical oxidation". *Environmental Science & Technology*, 46(6):3591–3592, 2012.

APPENDIX

A 2e⁻ water oxidation to H₂O₂ using different metal oxides

Table A.1 *Current densities obtained by varying the potentials (vs. Ag/AgCl) using different metal oxide electrodes.*

Current density (mA cm^{-2})							
Potential (V)	BiVO$_4$	SnO$_2$	WO$_3$	MnO$_2$	TiO$_2$	RuO$_2$	C-paper
1.2	0.03	5.82	2.72	0.25	5.80	2.77	-
1.4	19.67	6.10	5.80	12.66	6.10	14.72	11.04
1.6	54.11	44.96	35.18	40.10	34.99	66.74	47.65
1.8	146.91	116.62	93.69	113.13	85.75	161.64	97.81
2.0	233.43	151.25	127.25	149.44	125.96	307.95	153.67
2.2	337.20	183.69	168.06	199.81	155.54	321.10	203.27

Table A.2 *Concentration of H₂O₂ obtained by varying the potentials (vs. Ag/AgCl) using different metal oxide electrodes.*

Concentration (μmol L^{-1})							
Potential (V)	BiVO$_4$	SnO$_2$	WO$_3$	MnO$_2$	TiO$_2$	RuO$_2$	C-paper
1.2	0.00	0.00	0.00	0.00	0.00	0.00	0.00
1.4	82.97	61.18	13.90	3.67	17.12	6.46	14.74
1.6	189.38	141.31	92.12	6.17	91.17	8.74	139.14
1.8	361.69	381.05	283.07	8.67	195.57	7.46	260.45
2.0	465.15	400.54	392.71	9.14	312.24	7.03	266.17
2.2	503.10	394.64	425.93	13.79	328.79	6.03	262.48

Table A.3 *Production rates of H₂O₂ obtained by varying the potentials (vs. Ag/AgCl) using different metal oxide electrodes.*

Rate (µmol min^{-1} cm^{-2})							
Potential (V)	BiVO$_4$	SnO$_2$	WO$_3$	MnO$_2$	TiO$_2$	RuO$_2$	C-paper
1.2	0.00	0.00	0.00	0.00	0.00	0.00	0.00
1.4	0.21	0.15	0.03	0.01	0.04	0.02	0.04
1.6	0.47	0.35	0.23	0.02	0.23	0.02	0.35
1.8	0.90	0.95	0.71	0.02	0.49	0.02	0.65
2.0	1.16	1.00	0.98	0.02	0.78	0.02	0.67
2.2	1.26	0.99	1.06	0.03	0.82	0.02	0.66

Table A.4 *Faradaic efficiency for H_2O_2 obtained by varying the potentials (vs. Ag/AgCl) using different metal oxide electrodes.*

FE (%)							
Potential (V)	$BiVO_4$	SnO_2	WO_3	MnO_2	TiO_2	RuO_2	C-paper
1.2	0.00	0.00	0.00	0.00	0.00	0.00	0.00
1.4	3.61	7.70	1.91	0.23	2.13	0.34	1.10
1.6	2.84	2.68	2.20	0.12	2.18	0.10	2.39
1.8	1.97	2.62	2.45	0.06	1.86	0.04	2.16
2.0	1.64	2.11	2.49	0.05	2.00	0.02	1.43
2.2	1.23	1.71	2.01	0.06	1.70	0.02	1.01

B   *Supplementary Information for Anodic production of hydrogen peroxide using commercial carbon materials*

Supplementary Information for

Anodic production of hydrogen peroxide using commercial carbon materials

Dhananjai Pangotra [a,b], Lénárd-István Csepei [a], Arne Roth [a], Carlos Ponce de León [c], Volker Sieber [a,b], Luciana Vieira *,[a]

[a] Fraunhofer Institute of Interfacial Engineering and Biotechnology IGB, Bio-, Electro-, and Chemocatalysis BioCat, Straubing Branch, Schulgasse 11a, 94315, Straubing, Germany

[b] Chair of Chemistry for Biogenic Resources, Campus Straubing for Biotechnology and Sustainability, Technical University of Munich, Schulgasse 16, 94315, Straubing, Germany

[c] Electrochemical Engineering Laboratory, Faculty of Engineering and Physical Sciences, University of Southampton, Highfield, Southampton, SO17 1BJ, United Kingdom

* Corresponding author.

Email address: luciana.vieira@igb.fraunhofer.de (L. Vieira).

List of figures

List of tables

Supporting information

a)

b)

Fig. S1. Different methods to detect H₂O₂. **(a)** Calibration curve for H_2O_2 detection using ABTS assay and detected with UV-vis photometer at 405 nm in different electrolytes. **(b)** Comparison of three different methods (ABTS assay, detection strips, and $KMnO_4$ titration) by preparing three known concentrations of H_2O_2 [1, 2].
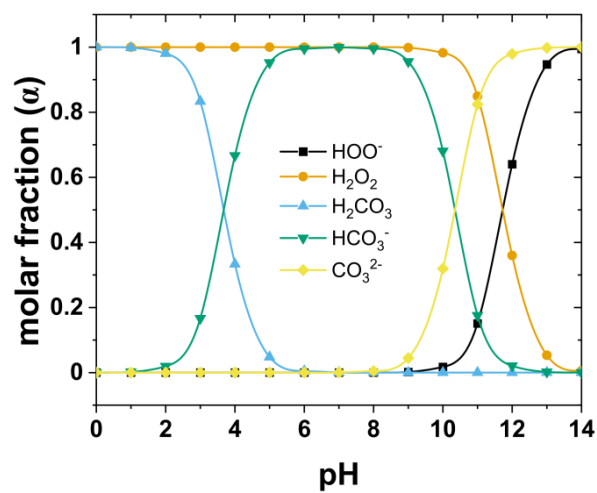
Fig. S2. pH dependence on different ionic species. Ionic species as a function of pH in the carbonate-bicarbonate-H_2O_2 containing solution [3, 4].
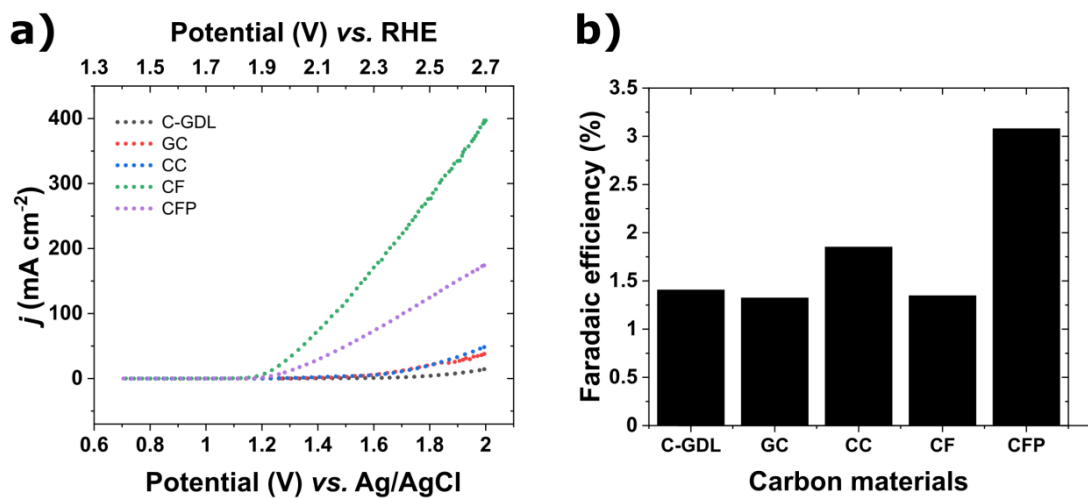
Fig. S3. Study on different carbon materials for H₂O₂ synthesis. (a) LSV curves obtained using different carbon materials in 2 mol L^{-1} KHCO₃ electrolyte at a scan rate of 10 mV s^{-1}. **(b)** FE towards H₂O₂ production for different carbon materials during electrolysis at 50 mA cm^{-2} for 10 minutes at room temperature.

Table S1 Summary of the potential screening performed using CFP

Potential	Concentration	Highest production rate	Maximum H_2O_2 FE	Average Cell potential	Average current density
V vs. Ag/AgCl	*$\mu mol\ L^{-1}$*	*$\mu mol\ min^{-1}\ cm^{-2}$*	*%*	*V*	*$mA\ cm^{-2}$*
1.2	1.1	0.00	0.9	2.3	0.97
1.4	18.0	0.05	1.2	2.9	12.12
1.6	141.9	0.35	2.1	3.6	45.65
1.8	263.6	0.66	1.8	5.4	120.44
2.0	269.4	0.67	1.3	6.2	175.51
2.2	266.7	0.67	0.9	7.2	232.19

Table S2 Specifications of carbon materials used in this study. All data is provided by the materials supplier.

Carbon material	Supplier	Sample	Structure	Thickness μm	Electrical resistivity $m\Omega cm^2$	Porosity %	PTFE treated	MPL Layer
Carbon fiber paper (CFP)	Quintech	TP-060	3D	190	80 mΩcm	78	No	No
Carbon cloth (CC)	Quintech	W1S1005	3D	410	<13	-	Yes	Yes
Gas diffusion layer (C-GDL)	Quintech	H23C9	3D	250	8	-	Yes	Yes
Carbon felt (CF)	Alfa Aesar	43200	3D	6350	-	-	No	No
Glassy carbon (GC)	Metrohm	61247000	2D	2 mm*	-	0	No	No

Diameter of the rod
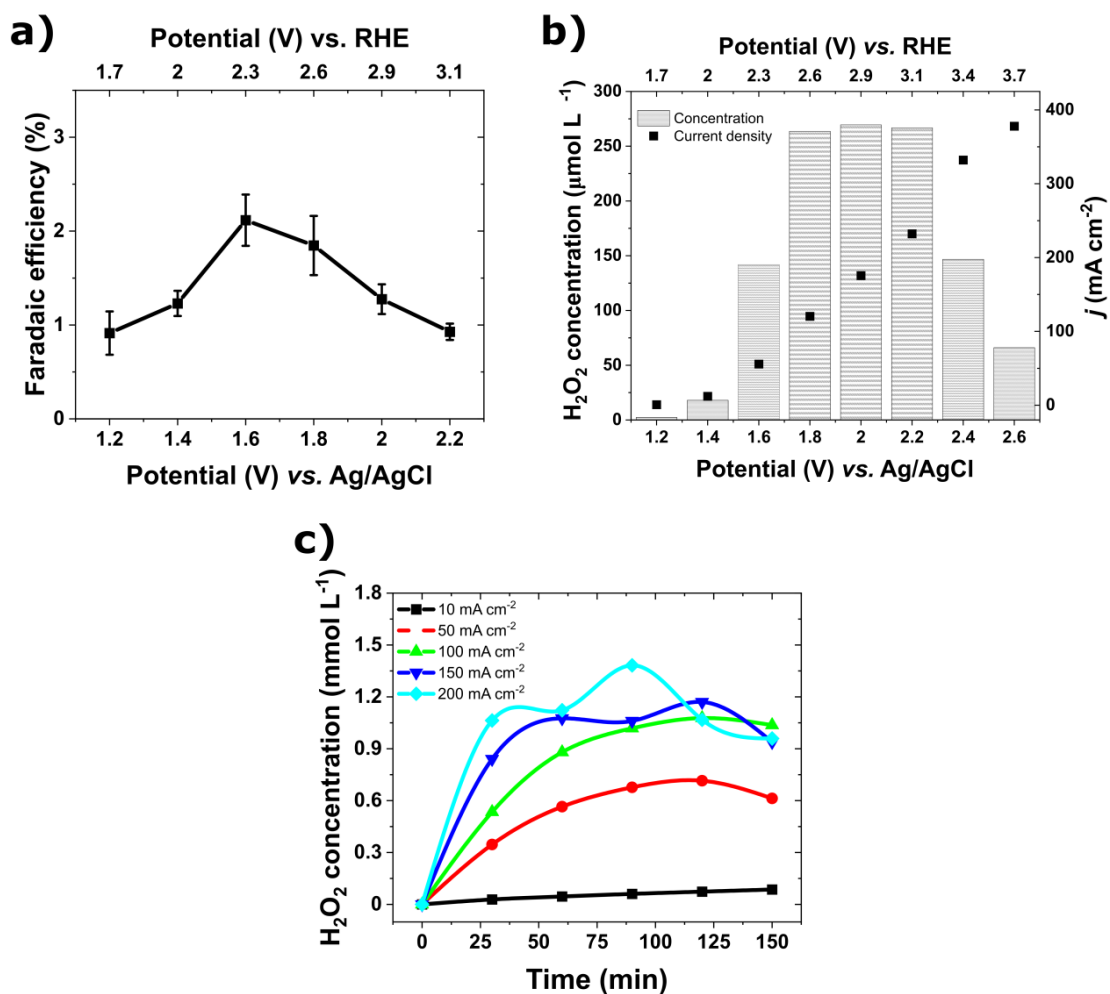
Fig. S4. Impact of operating potential/current density. (a) FE *vs.* potential for H_2O_2 production in 2 mol L^{-1} $KHCO_3$ using a two compartment H-Cell. **(b)** H_2O_2 concentration and current density at different applied potentials in 2 mol L^{-1} $KHCO_3$ in an H-Cell. **(c)** H_2O_2 concentration during electrolysis in 2 mol L^{-1} $KHCO_3$ using a flow cell with a flow rate of 100 mL min^{-1} at different current densities (*j*): (■) 10 mA cm^{-2}, (●) 50 mA cm^{-2}, (▲) 100 mA cm^{-2}, (▼) 150 mA cm^{-2}, and (◆) 200 mA cm^{-2}.
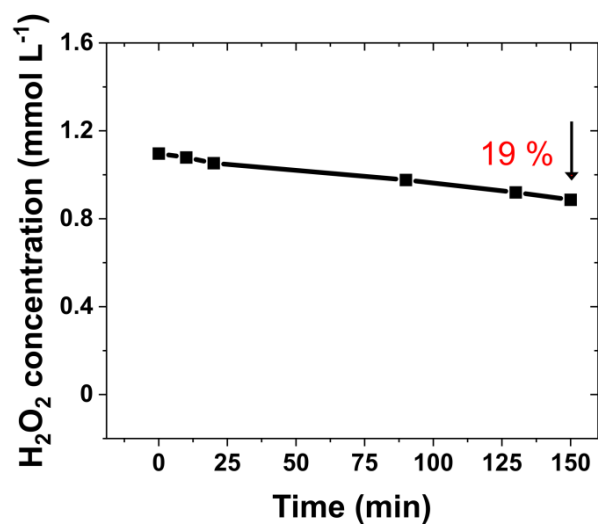
Fig. S5. Stability of electrogenerated H₂O₂. H_2O_2 concentration *vs.* time without the influence of current. 1.1 mmol L^{-1} H_2O_2 was produced electrochemically on a CFP anode at 100 mA cm^{-2} for 2.5 hours in 2 mol L^{-1} KHCO$_3$ without a stabilizer. The H_2O_2 concentration decreased 19 % (from 1.1 mmol L^{-1} to 0.89 mmol L^{-1}) after 2.5 hours at an open circuit.
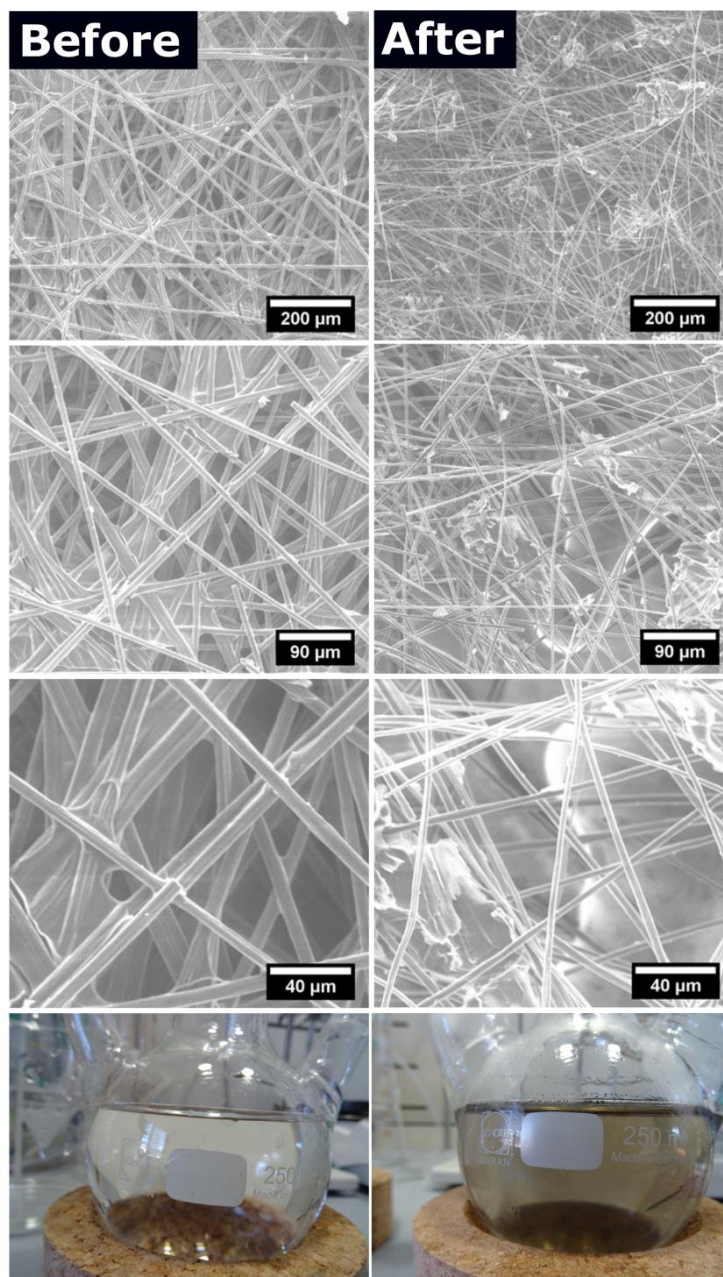
Fig. S6. SEM and electrolyte images for the C-electrode used. Before and after images of CFP used for electrolysis at 200 mA cm^{-2} using 2 mol L^{-1} KHCO$_3$ as an electrolyte for 150 minutes.
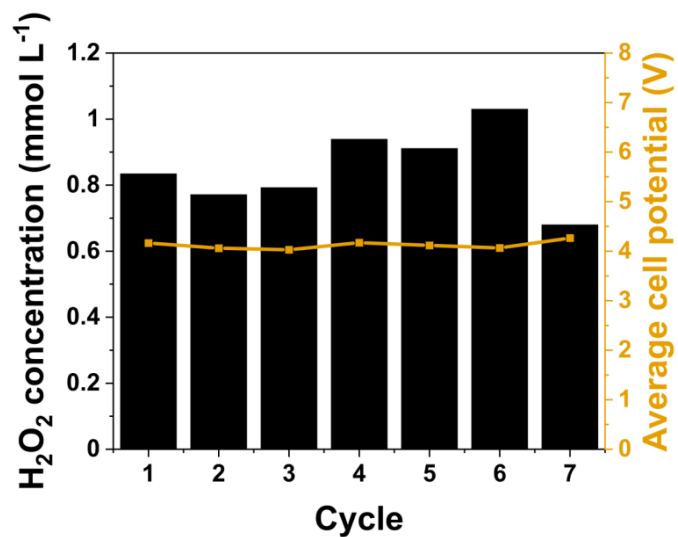
Fig. S7. Long-term stability of CFP electrode. Peak H_2O_2 concentration during seven successive cycles. Each successive cycle was performed at 100 mA cm^{-2} for 2.5 hours in 2 mol L^{-1} KHCO$_3$ using a flow cell with an electrolyte flow rate of 100 mL min^{-1}, without changing the CFP electrode. After each cycle, the electrolyte was replaced with a fresh solution.
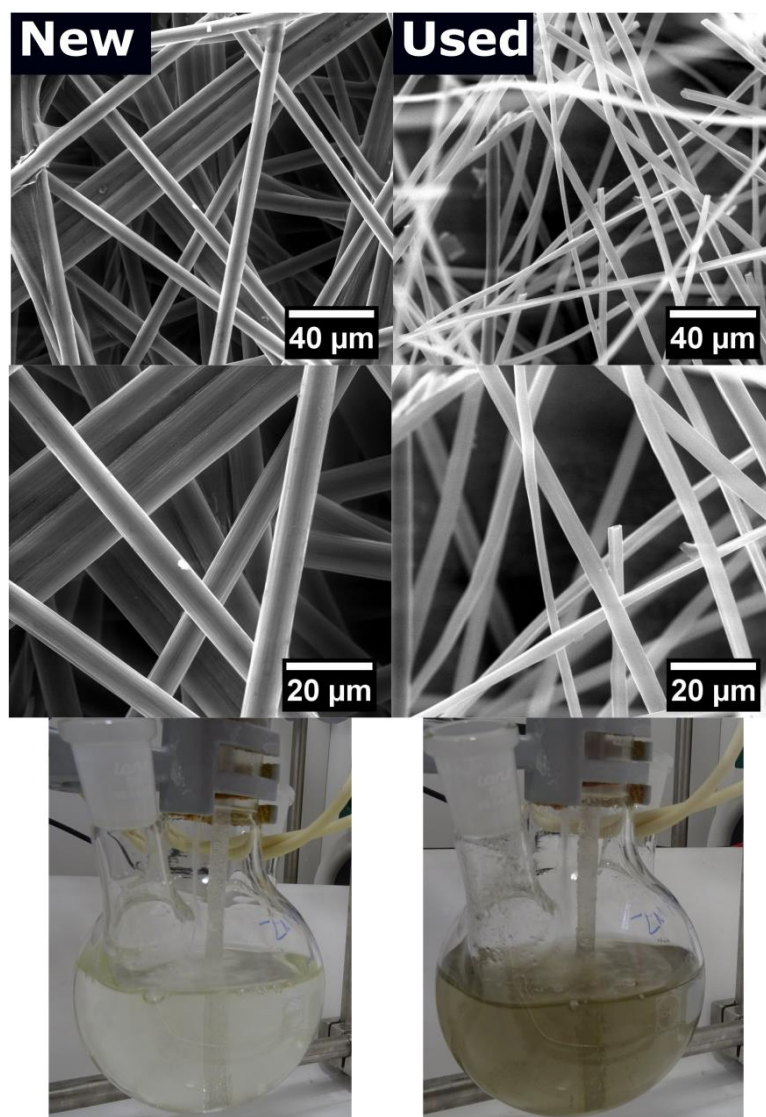
Fig. S8. SEM and electrolyte images for the C-electrode used for 17.5 hours. Before and after images of CFP used for electrolysis at 100 mA cm^{-2} using 2 mol L^{-1} KHCO$_3$ as an electrolyte for 17.5 hours.
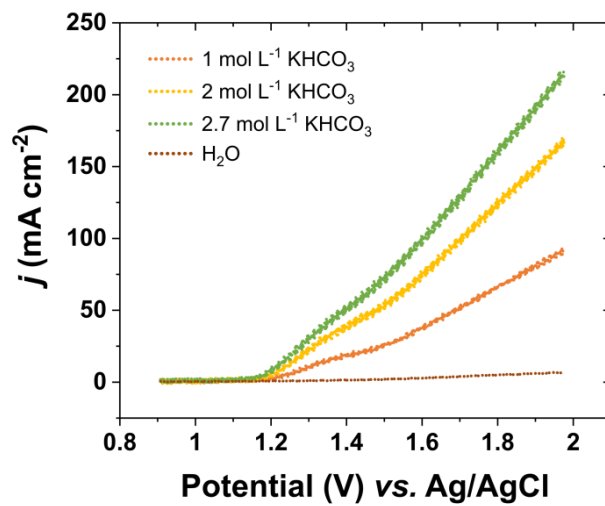
Fig. S9. Study on different concentrations of KHCO₃ electrolyte. LSV curves obtained using carbon fiber paper in different concentration of $KHCO_3$ electrolyte at a scan rate of 100 mV s^{-1}.
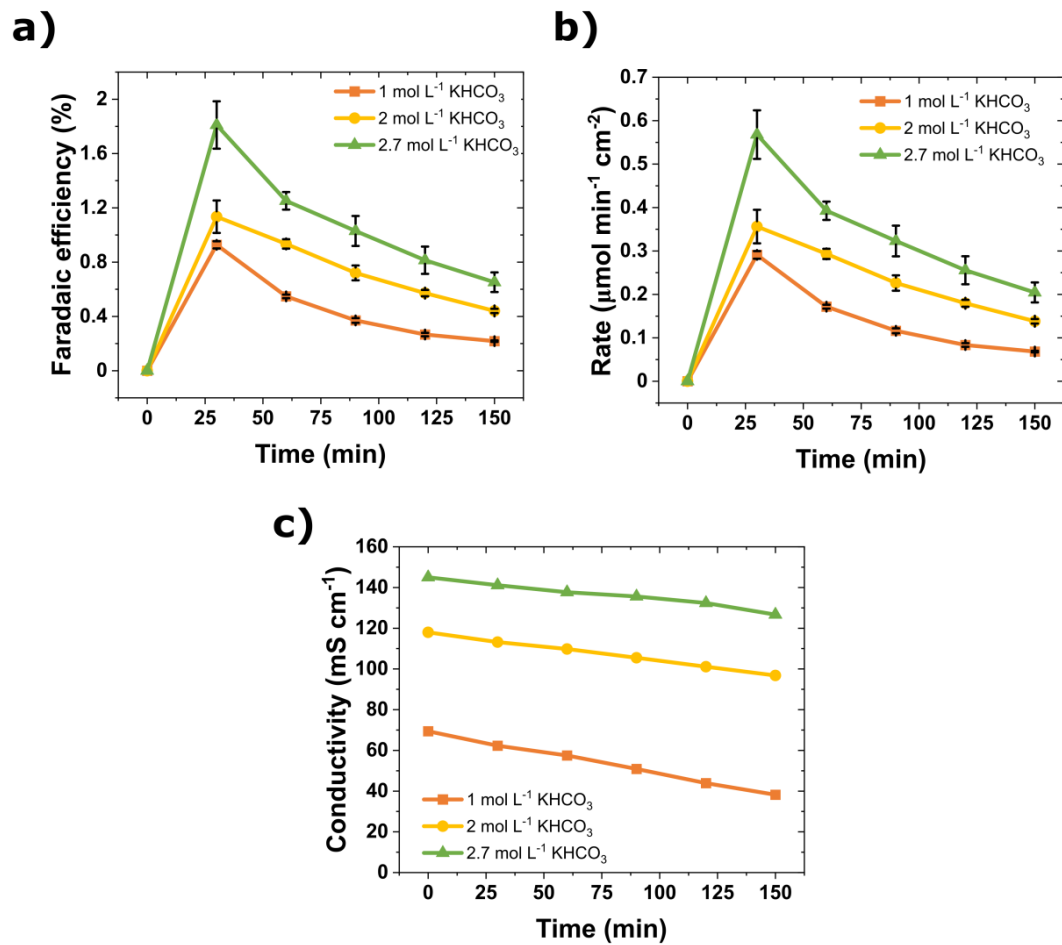
Fig. S10. Study of key parameters in the anodic generation of H₂O₂ at different concentrations of KHCO₃ electrolyte. (a) FE, **(b)** production rate of H_2O_2, and **(c)** change in conductivity in the anolyte circulated with KHCO₃: (■) 1 mol L^{-1}, (●) 2 mol L^{-1}, and (▲) 2.7 mol L^{-1}. Experiment conditions: flow cell at 100 mA cm^{-2} for 150 min and 200 mL anolyte circulated at 100 mL min^{-1}.
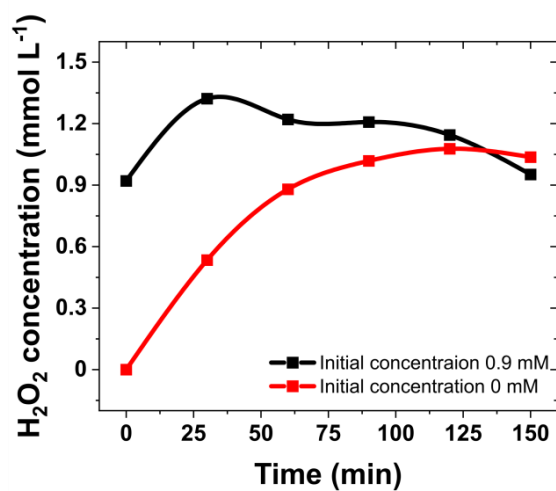
Fig. S11. Comparison for electrolysis with different initial concentration of H_2O_2. H_2O_2 concentration in the anolyte using 2 mol L^{-1} $KHCO_3$ with an initial H_2O_2 concentration of (■) 0.9 mmol L^{-1}, and (●) 0 mmol L^{-1}. Experiment conditions: flow cell at 100 mA cm^{-2} for 150 min and 200 mL anolyte circulated at 100 mL min^{-1}.
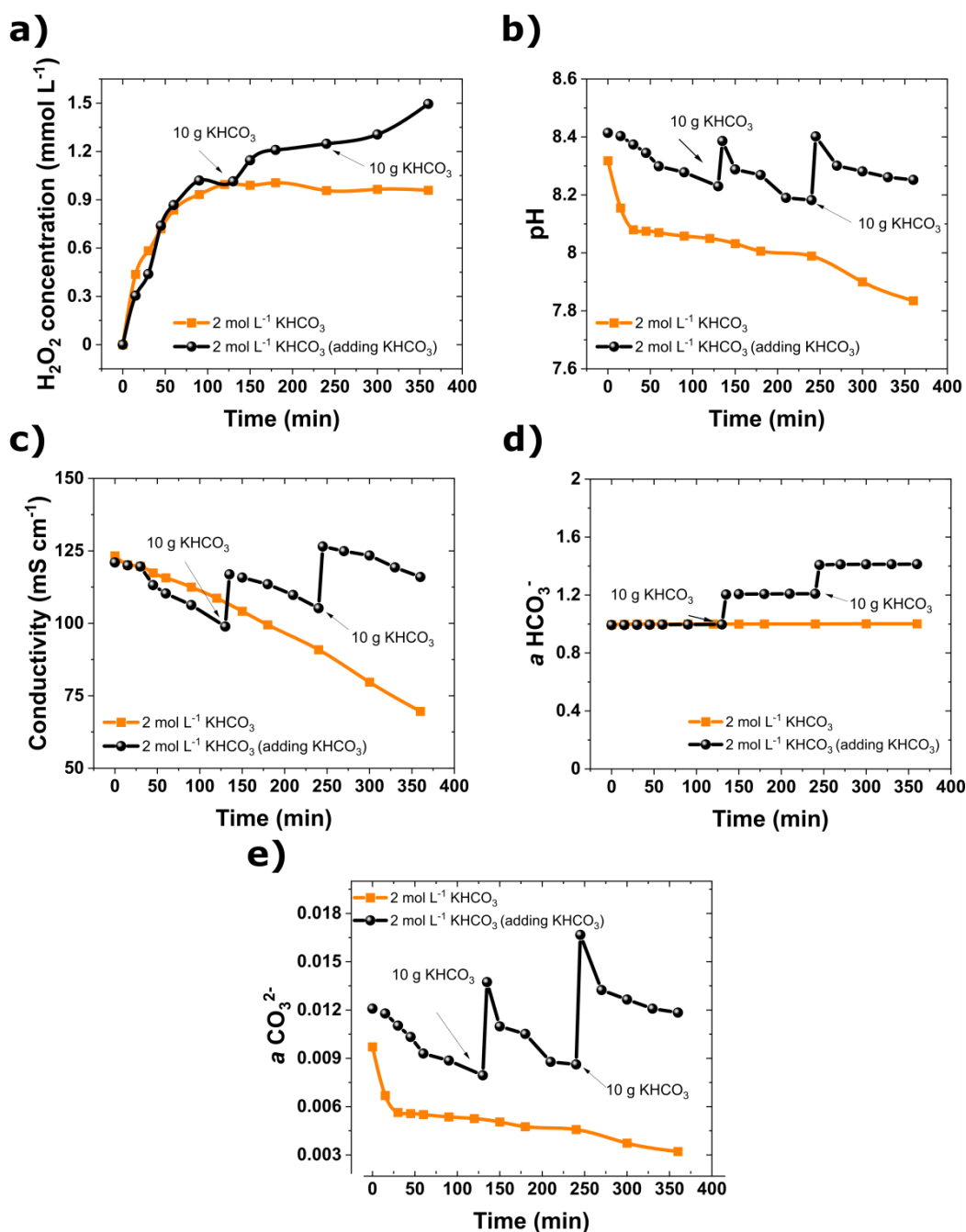
Fig. S12. A comparison of different parameters with and without adding KHCO₃. (a) H_2O_2 concentration, **(b)** pH change, **(c)** conductivity, **(d)** HCO_3^- activity and **(e)** CO_3^{2-} activity in the anolyte during 360 min of electrolysis at 100 mA cm⁻² in 200 mL 2 mol L⁻¹ KHCO₃ (black curves) and addition of the KHCO₃ salt to the 2 mol L⁻¹ KHCO₃ electrolyte (orange curve) using a flow cell with a flow rate of 100 mL min⁻¹.

To avoid a decrease in ion activity and pH, 10 g of $KHCO_3$ was added to the 2 mol L^{-1} $KHCO_3$ electrolyte after 130 and 240 minutes of electrolysis to reach an electrolyte concentration of 2.5 and 3.0 mol L^{-1} $KHCO_3$, respectively (**Fig. S12a**). A step increase in the pH and conductivity of the electrolyte was observed each time that $KHCO_3$ was added to the solution (**Fig. S12b, c**). The conductivity increased from 99 to 117 mS cm^{-1} in the first addition and from 105 to 126 mS cm^{-1} in the second (**Fig. S12c**). The activity of HCO_3^- and CO_3^{2-} ions in the electrolyte during the electrolysis was calculated based on the pH change (**Fig. S12d, e**). The activity of both HCO_3^- and CO_3^{2-} ions increased due to the rise in electrolyte concentration. The HCO_3^- activity increased from 0.99 to 1.2 and thereafter from 1.2 to 1.4 after the second addition, whereas the CO_3^{2-} ions activity increased from 0.008 to 0.014 and 0.009 to 0.016. The activity of CO_3^{2-} ions (in 2 mol L^{-1} $KHCO_3$ solution at pH 8.4) is two orders of magnitude smaller than that of HCO_3^- (Supporting Information, **Fig. S2**) and decreases during electrolysis, whereas the activity of HCO_3^- ions appears to be constant at each addition. A comparison of the electrolysis with and without the addition of $KHCO_3$ reveals that increasing the $KHCO_3$ concentration results in an increase of H_2O_2 production, pH and conductivity of the electrolyte, as well as an increase in activity of HCO_3^- and CO_3^{2-} ions (**Fig. S12a-e**).
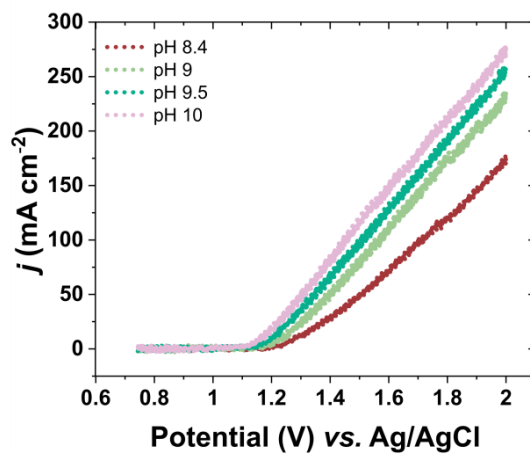
Fig. S13. Study on the impact of pH on H₂O₂ generation. LSV curves obtained using carbon fiber paper in different pH of 2 mol L^{-1} KHCO$_3$ electrolyte at a scan rate of 100 mV s^{-1}. The pH was adjusted by adding KOH.
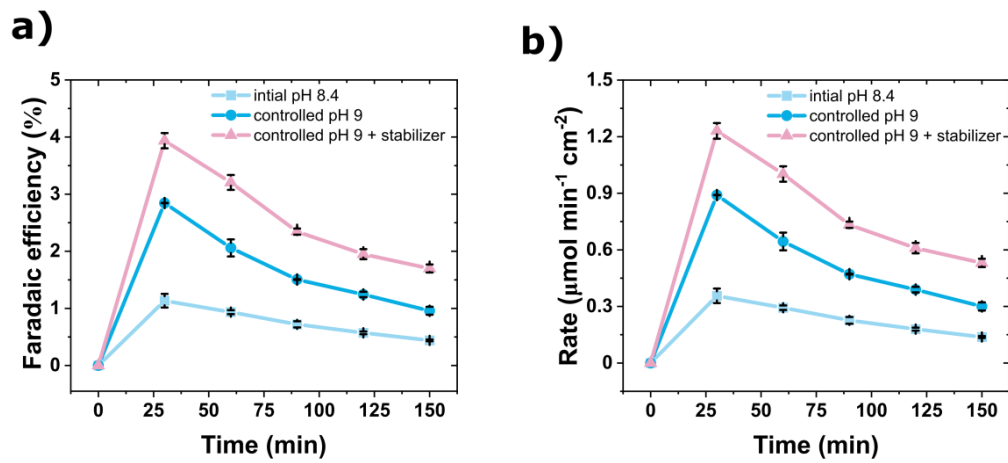
Fig. S14. Study on the impact of Na$_2$SiO$_3$ stabilizer on H$_2$O$_2$ generation. (a) Faradaic efficiency and **(b)** production rate of H$_2$O$_2$ during 150 minutes of electrolysis at 100 mA cm^{-2} using a flow cell with a flow rate of 100 mL min^{-1} in 2 mol L^{-1} KHCO$_3$ at (■)pH 8.4, (●) controlled pH 9, and (▲) at controlled pH 9 with 30 mmol L^{-1} of Na$_2$SiO$_3$ as a stabilizer. Experiment conditions: Flow cell at 100 mA cm^{-2} with 200 mL anolyte at a flow rate of 100 mL min^{-1}.

20
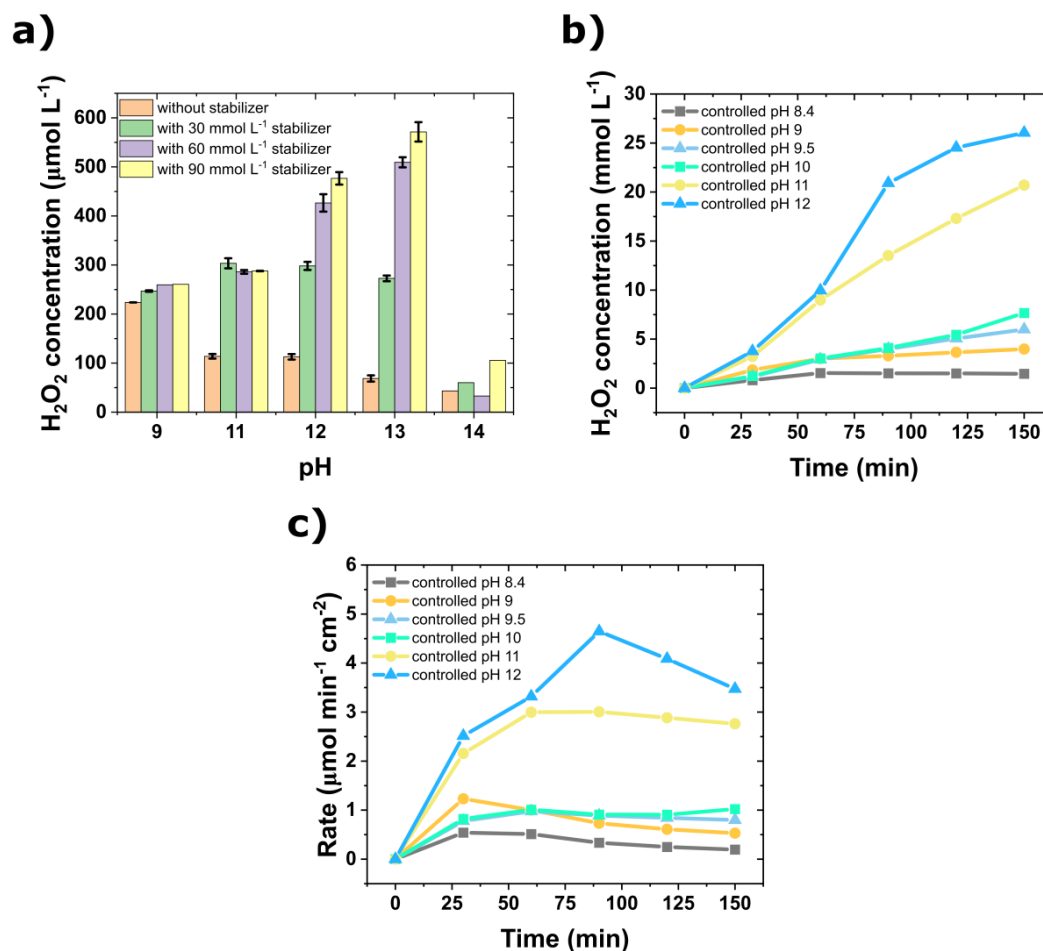
Fig. S15. Optimization of stabilizer concentration in the anodic generation of H₂O₂ in 2 mol L⁻¹ KHCO₃ electrolytes at different pH levels. (a) Anodic H₂O₂ production with pH variation in 2 mol L⁻¹ KHCO₃ at 50 mA cm⁻² for 10 minutes in an H-cell with different amounts of stabilizer. Different concentrations of Na₂SiO₃ stabilizer (0, 30, 60, and 90 mmol L⁻¹) were used at pH values of 9, 11, 12, 13, and 14. **(b)** Faradaic efficiency and **(c)** production rate of H₂O₂ during 150 minutes of electrolysis at 100 mA cm⁻² in a flow cell in different controlled pH of 2 mol L⁻¹ KHCO₃. Upto pH 11, the stabilizer concentration used was 30 mmol L⁻¹. At pH 12, the stabilizer concentration was 90 mmol L⁻¹.
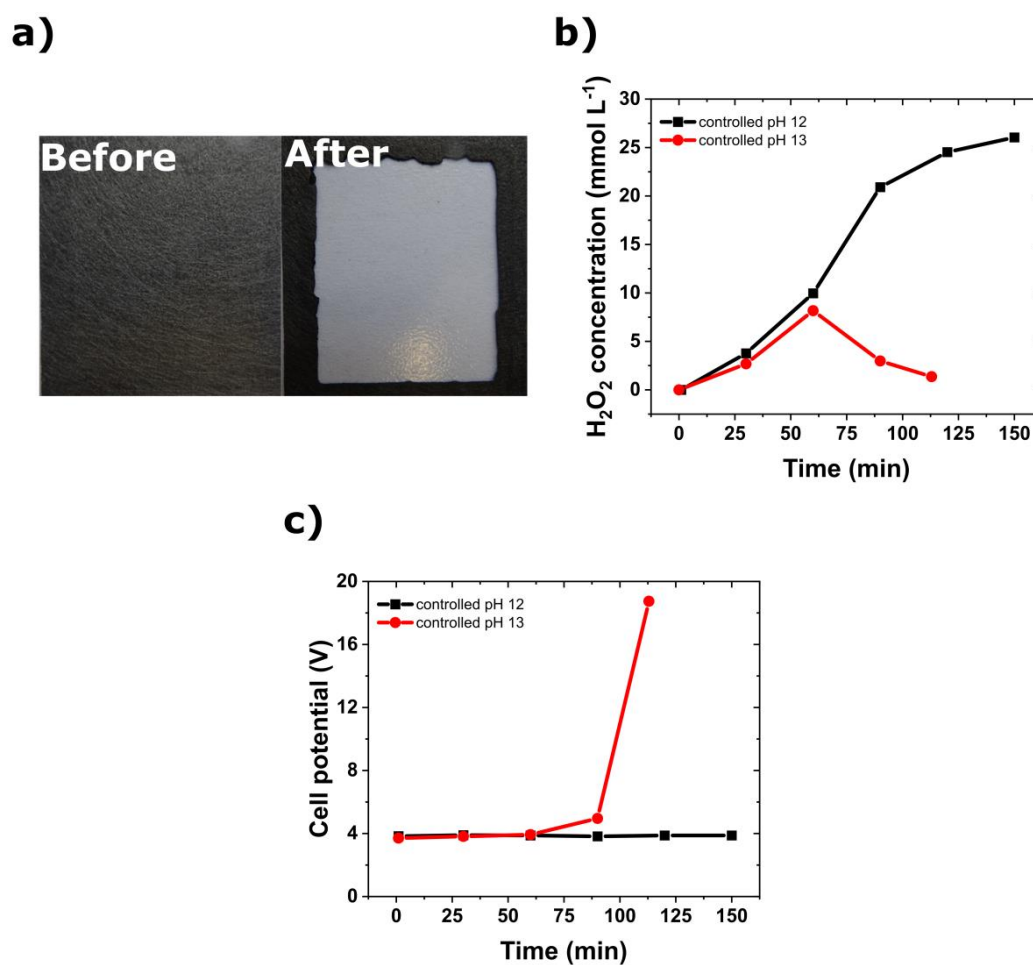
Fig. S16. Anodic production of H$_2$O$_2$ in 2 mol L^{-1} KHCO$_3$ electrolyte at pH 13. (a) Before and after pictures of the CFP electrode after 120 minute electrolysis at 100 mA cm^{-2} in a flow cell in 2 mol L^{-1} KHCO$_3$ at pH 13. Comparison of **(b)** H$_2$O$_2$ concentration and **(c)** cell potential at 100 mA cm^{-2} using a flow cell with a flow rate of 100 mL min^{-1} in 2 mol L^{-1} KHCO$_3$ controlled at (■) pH 12 and (●) pH 13 in presence of 90 mmol L^{-1} Na$_2$SiO$_3$.
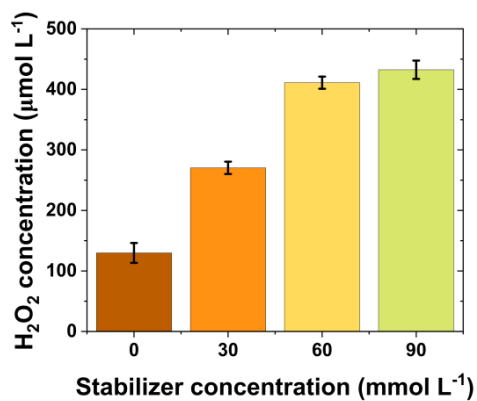
Fig. S17. H₂O₂ concentration as a function of Na₂SiO₃ concentration in 2 mol L⁻¹ K₂CO₃ electrolyte. Anodic H₂O₂ production in 2 mol L⁻¹ K₂CO₃ containing 0, 30, 60, and 90 mmol L⁻¹ Na₂SiO₃ at 50 mA cm⁻² for 10 minutes in an H-cell. The initial pH of the electrolyte contaning 0, 30, 60, and 90 mmol L⁻¹ Na₂SiO₃ was 12.6, 12.9, 13.1, and 13.3 respectively.

References

[1] S. Ranganathan, V. Sieber, Development of semi-continuous chemo-enzymatic terpene epoxidation: combination of anthraquinone autooxidation and the lipase-mediated epoxidation process, React. Chem. Eng., 2 (2017) 885-895. https://doi.org/10.1039/c7re00112f.

[2] T.M. Gill, X. Zheng, Comparing Methods for Quantifying Electrochemically Accumulated H_2O_2, Chem. Mater., 32 (2020) 6285-6294. https://doi.org/10.1021/acs.chemmater.0c02010.

[3] D.E. Richardson, H. Yao, K.M. Frank, D.A. Bennett, Equilibria, Kinetics, and Mechanism in the Bicarbonate Activation of Hydrogen Peroxide: Oxidation of Sulfides by Peroxymonocarbonate, J. Am. Chem. Soc., 122 (2000) 1729-1739. https://doi.org/10.1021/ja9927467.

[4] K. Fuku, K. Sayama, Efficient oxidative hydrogen peroxide production and accumulation in photoelectrochemical water splitting using a tungsten trioxide/bismuth vanadate photoanode, Chem. Commun., 52 (2016) 5406-5409. https://doi.org/10.1039/c6cc01605g.

C   Supplementary Information for Anodic generation of hydrogen peroxide in continuous flow

Supplementary Information for

Anodic generation of hydrogen peroxide in continuous flow

Dhananjai Pangotra [a,b], Lénárd-István Csepei [a], Arne Roth [a], Volker Sieber [a,b], Luciana Vieira *[,a]

[a] Fraunhofer Institute of Interfacial Engineering and Biotechnology IGB, Bio-, Electro-, and Chemocatalysis BioCat, Straubing Branch, Schulgasse 11a, 94315, Straubing, Germany

[b] Chair of Chemistry for Biogenic Resources, Campus Straubing for Biotechnology and Sustainability, Technical University of Munich, Schulgasse 16, 94315, Straubing, Germany

List of figures

List of tables

List of schemes

Figure S1 SEM images of used BDD electrode. SEM images of used BDD in this study at different magnification.

The molar fractions for each species were calculated using **Eqs. S2** and **S3**. The experiments were done in highly concentrated electrolytes, which differ from the ideal behavior of diluted electrolytes. As a result, the ion activities ($a_{HCO_3^-}$ and $a_{CO_3^{2-}}$) were calculated as shown in **Eqs. S4** and **S5** using the activity coefficient ($f_\pm$) shown in **Eq. S6**, where z_i is the charge of the ion, A is the Debye-Hückel parameter (0.51 kg$^{1/2}$ mol$^{-1/2}$, for water at 25 °C), and B is a temperature-dependent parameter. In response to pH changes and carbonate equilibrium, we calculated the activity of HCO$_3^-$ (a(HCO$_3^-$)) and CO$_3^{2-}$ (a(CO$_3^{2-}$)) ions during electrolysis for each concentration (c) of KHCO$_3$.

$$K_{a,i} = 10^{-pK_{a,i}} \tag{S1}$$

$$\alpha_{HCO_3^-} = \frac{K_{a,1}.[H^+]}{[H^+]^2 + K_{a,1}.[H^+] + K_{a,1}.K_{a,2}} \tag{S2}$$

$$\alpha_{CO_3^{2-}} = \frac{K_{a,1}.K_{a,2}}{[H^+]^2 + K_{a,1}.[H^+] + K_{a,1}*K_{a,2}} \tag{S3}$$

$$a_{HCO_3^-} = \alpha_{HCO_3^-}.c_{KHCO_3}.f_\pm \tag{S4}$$

$$a_{CO_3^{2-}} = \alpha_{CO_3^{2-}}.c_{KHCO_3}.f_\pm \tag{S5}$$

$$\log f_\pm = -\frac{A.z_i^2.\sqrt{j}}{1+B.a_i.\sqrt{j}} \tag{S6}$$
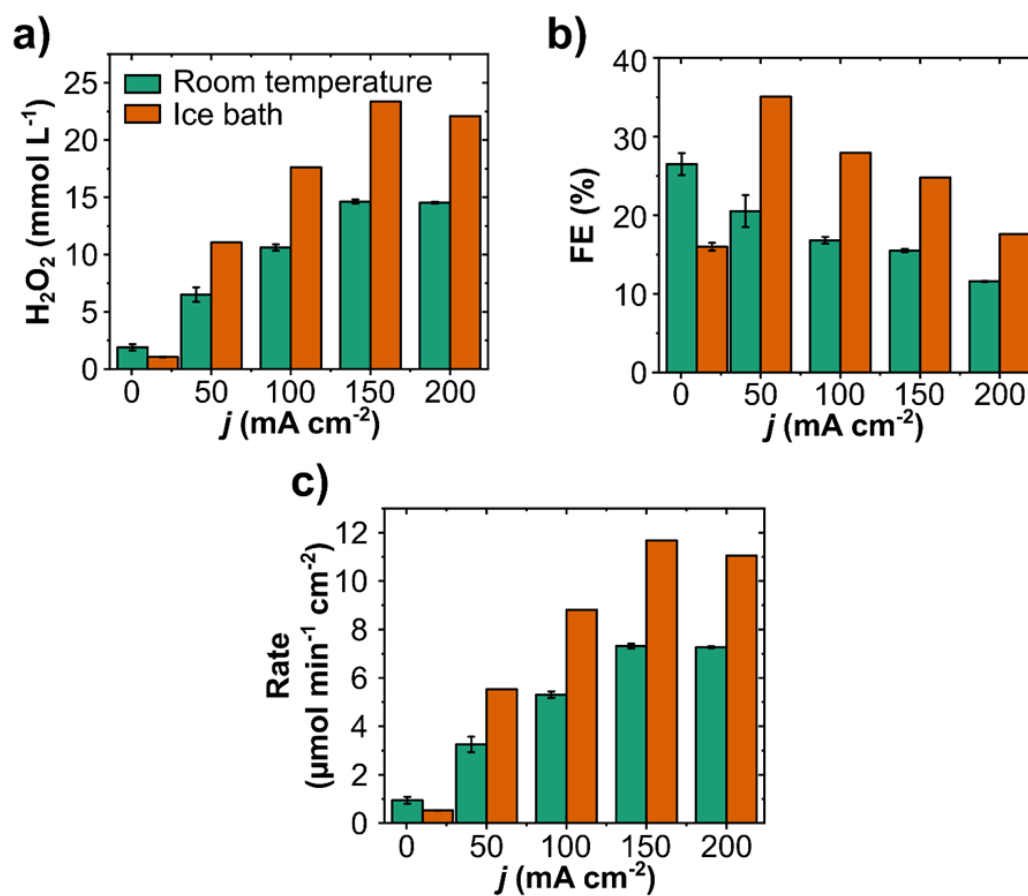
Figure S2 Comparison of electrolyte conditions using BDD as anode. Anodic H_2O_2 **(a)** concentration **(b)** FE, and **(c)** production rate for H_2O_2 production against applied current density during 10 minutes in 25 mL 2 mol L^{-1} $KHCO_3$ (pH 9) at room temperature and in ice bath using 5 cm^2 BDD as an anode in a two compartment H-cell.

6
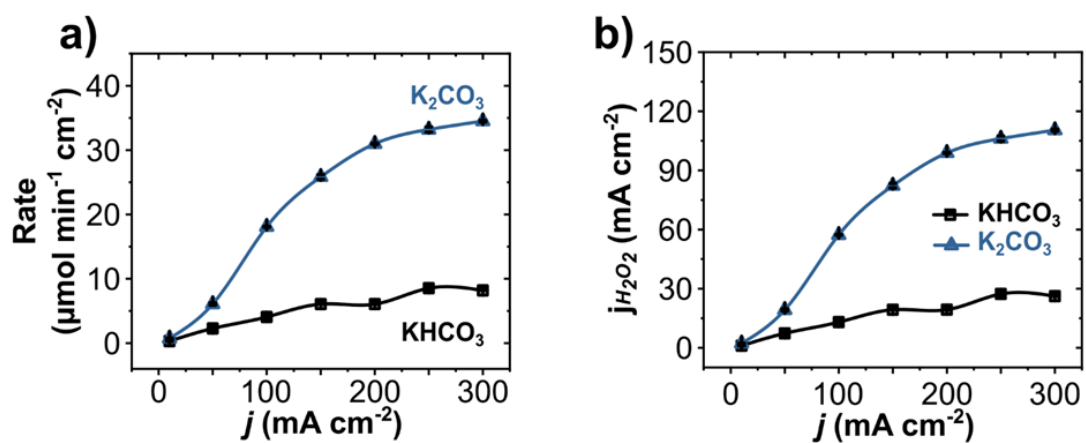
Figure S3 Comparison of electrolyte conditions using BDD as anode. Anodic H_2O_2 **(a)** production rate and **(b)** partial current density for H_2O_2 production against applied current density during 10 minutes in (■) 2 mol L^{-1} $KHCO_3$ at pH 8.4, and (▲) 2 mol L^{-1} K_2CO_3 at pH 12.6 on 5 cm^2 BDD as an anode.

7
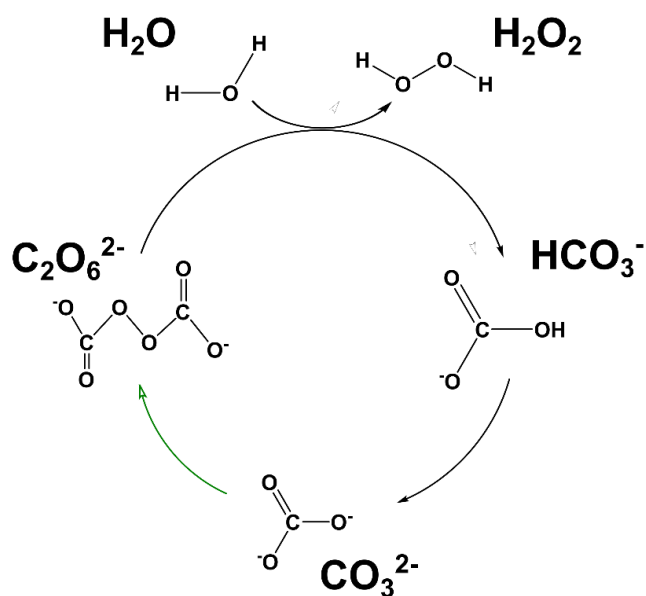
Scheme S1 Scheme for anodic H₂O₂ production in carbonate electrolyte. Carbonate (CO_3^{2-}) can be anodically oxidized to peroxodicarbonate ($C_2O_6^{2-}$) species. $C_2O_6^{2-}$ undergoes hydrolysis to form bicarbonate (HCO_3^-) and hydrogen peroxide (H_2O_2). In alkaline electrolytes, HCO_3^- ions are deprotonated to CO_3^{2-}, which closes the cycle with a higher concentration of H_2O_2.[1]
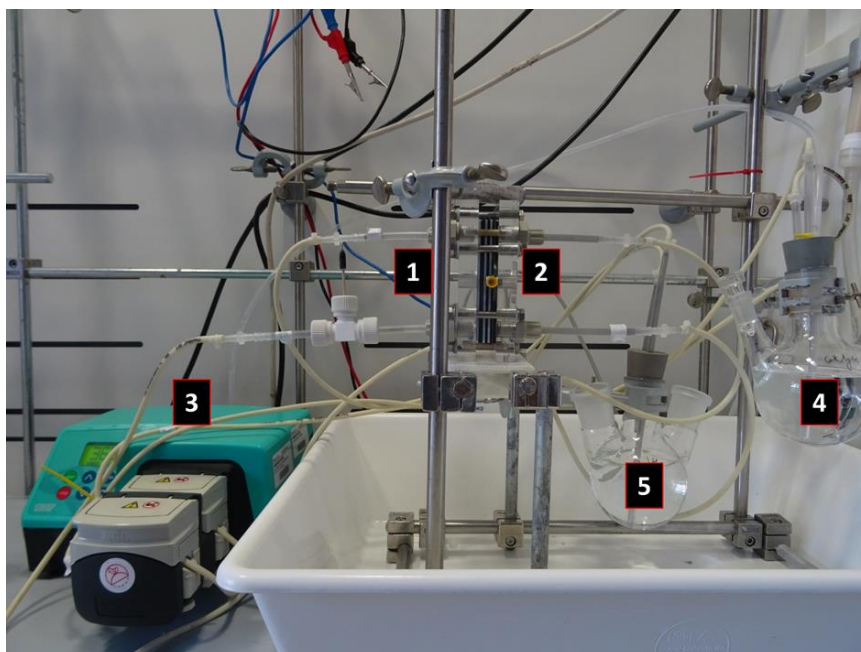
Figure S4 Experimental setup for circular flow. (1) Cathodic compartment, **(2)** anodic compartment, **(3)** flow pump, **(4)** catholyte tank, and **(5)** anolyte tank. The anolyte collected in **(5)** is recirculated to the anodic half-cell and the product is collected in the same reservoir.
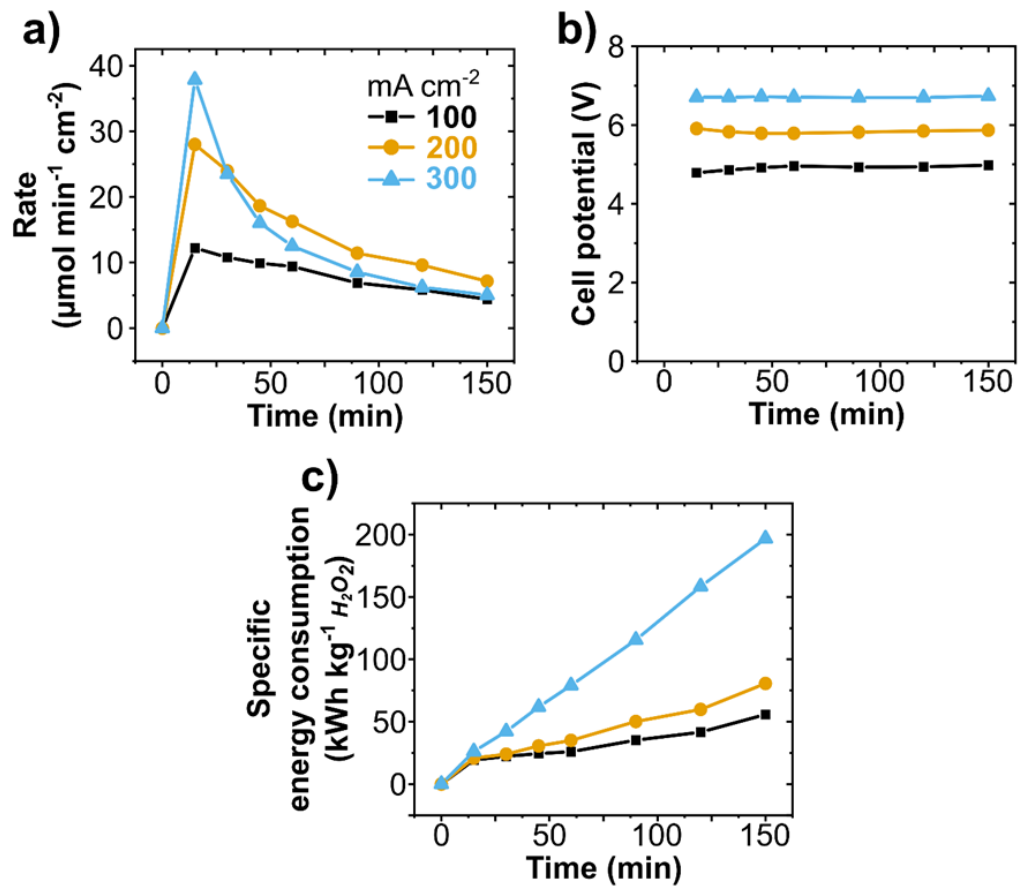
Figure S5 Anodic H₂O₂ production in a circular flow reactor. Anodic H₂O₂ **(a)** production rate, **(b)** cell potential, and **(c)** specific energy consumption to produce 1 kg of H₂O₂ at different current densities using a circular flow system.

Table S1 Anodic H₂O₂ production in a circular flow reactor. Faradaic efficiency and corresponding specific energy consumption to produce 1 kg of H_2O_2 over time at different current densities using a circular flow system.

Time	Faradaic efficiency (%)			Specific energy consumption (kWh^{-1} kg^{-1})		
(min)	*100 mA cm^{-2}*	*200 mA cm^{-2}*	*300 mA cm^{-2}*	*100 mA cm^{-2}*	*200 mA cm^{-2}*	*300 mA cm^{-2}*
15	39.09	44.86	40.41	0.58	0.62	0.79
30	34.55	38.42	25.08	0.67	0.72	1.27
45	31.72	29.91	17.13	0.73	0.92	1.86
60	30.13	26.09	13.37	0.78	1.05	2.37
90	22.07	18.31	9.14	1.06	1.50	3.47
120	18.70	15.41	6.67	1.25	1.80	4.75
150	14.08	11.48	5.40	1.67	2.42	5.90
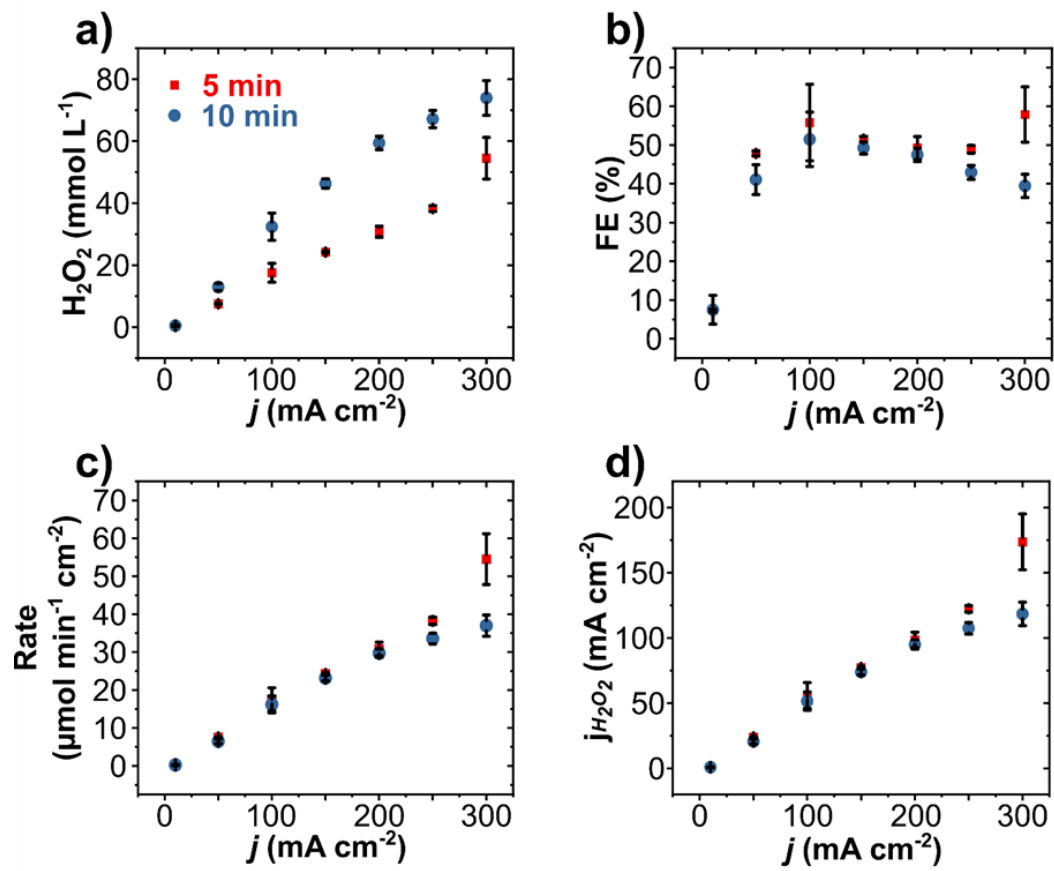
Figure S6 Comparison of the sampling time during electrolysis in H-Cell. (a) Anodic H_2O_2 concentration, **(b)** FE, **(c)** production rate, and **(d)** partial current density at different applied current densities for 5 or 10 minutes. The electrolyte was 2 mol L^{-1} K_2CO_3 at pH 12.6 and the anode a 5 cm^2 BDD.
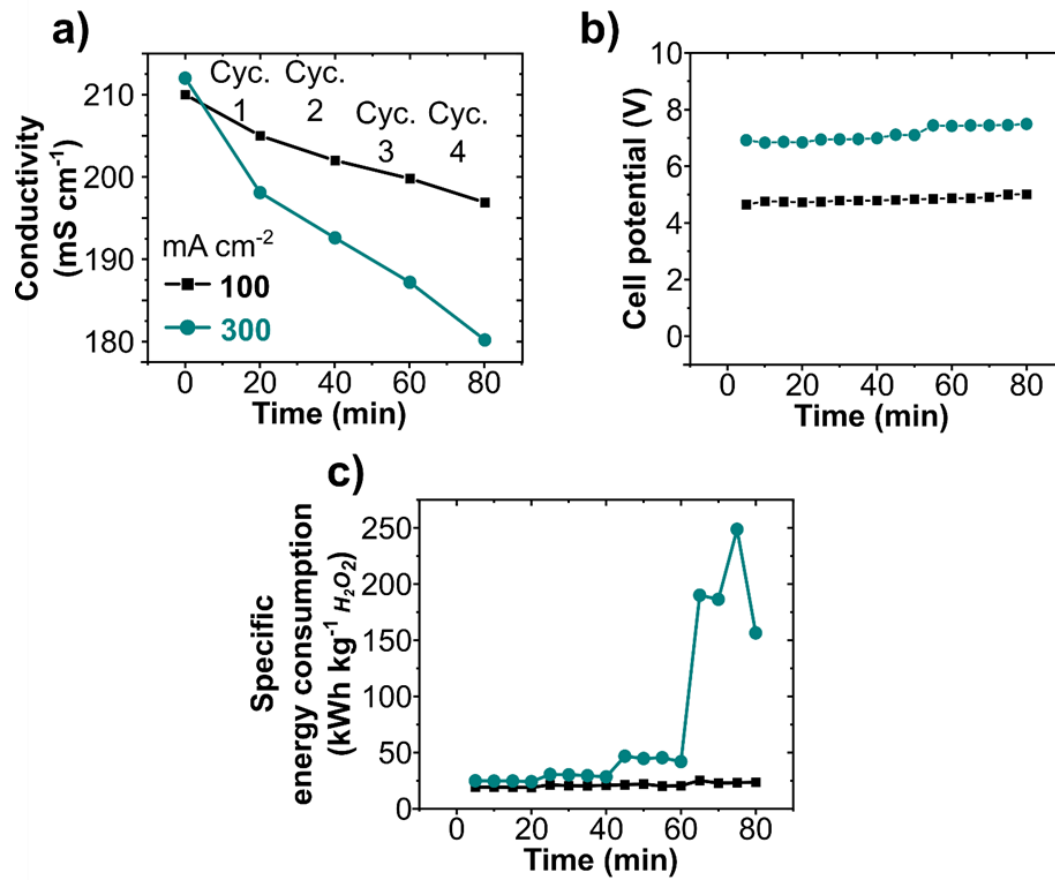
Figure S7 H₂O₂ generation with multiple electrolyte flow cycles. Change in **(a)** conductivity of the electrolyte, **(b)** cell potential, and **(c)** energy consumption against time at a current density of 100 and 300 mA cm^{-2} in 2 mol L^{-1} K$_2$CO$_3$ with 90 mmol L^{-1} Na$_2$SiO$_3$ stabilizer using 10 cm^2 BDD as an anode. The total volume of the electrolyte used for each cycle was 200 mL. Experiments were performed in a single flow system. The volume accumulated in each cycle was reused in the following one.
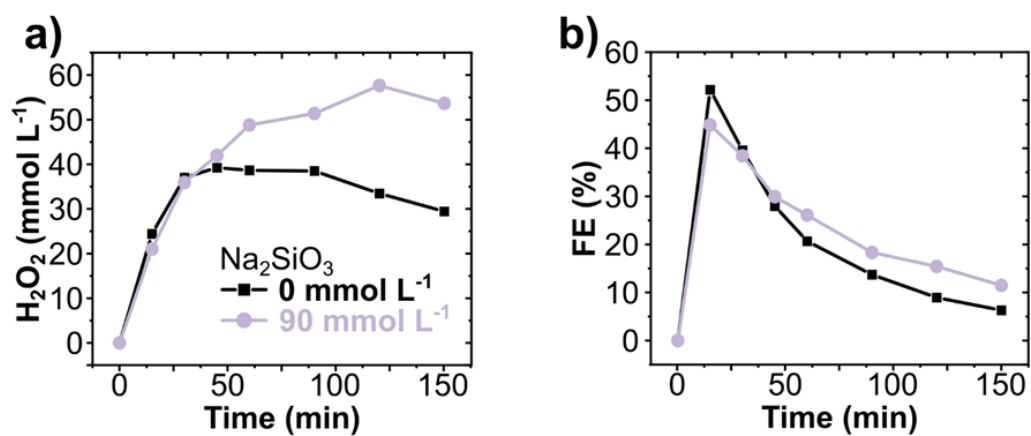
Figure S8 Effect of Na$_2$SiO$_3$ stabilizer on H$_2$O$_2$ generation in circular flow. Anodic H$_2$O$_2$ **(a)** concentration and **(b)** FE at current density of 200 mA cm^{-2} with (■) and without (●) 90 mmol L^{-1} Na$_2$SiO$_3$ at a controlled pH of 12.6. Each cell compartment contained a reservoir with 200 mL of 2 mol L^{-1} K$_2$CO$_3$ electrolyte circulating at 100 mL min^{-1} flow rate.
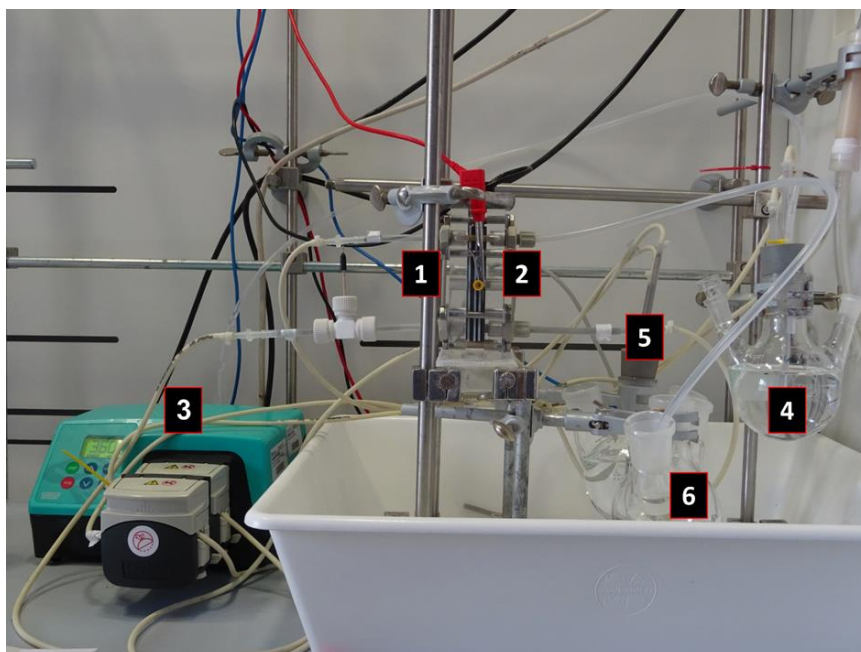
Figure S9 Experimental setup of single-pass flow. (1) Cathodic compartment**, (2)** anodic compartment, **(3)** flow pump, **(4)** catholyte tank, **(5)** fresh anolyte tank before cell, and **(6)** collected anolyte containing H_2O_2 after flow cell.
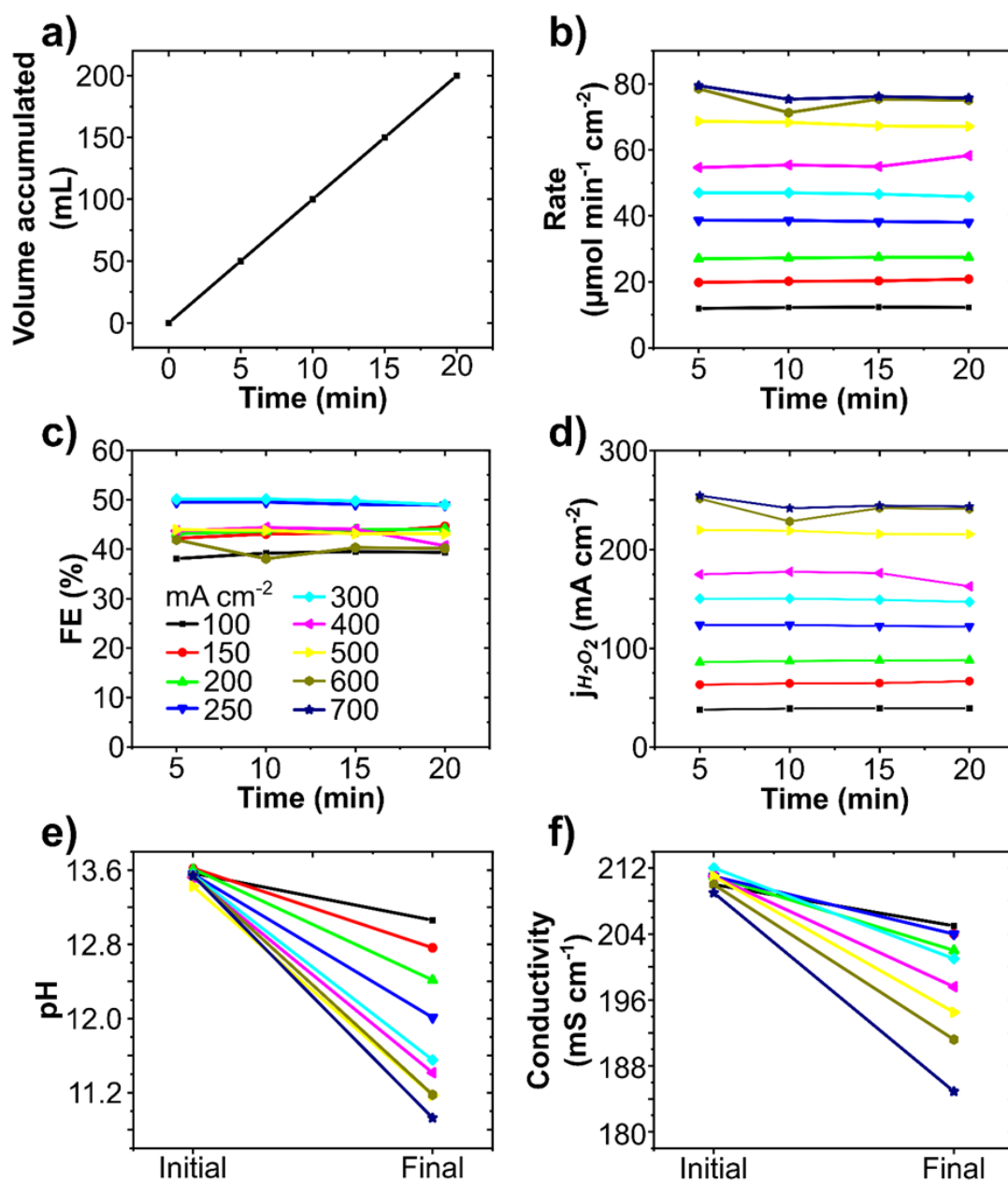
Figure S10 Anodic H₂O₂ production in a single pass mode flow reactor. **(a)** Volume of electrolyte passed over time using a flow rate of 10 mL min^{-1}. **(b)** H₂O₂ concentration, **(c)** FE, and **(d)** current density towards H₂O₂ during 20 min of electrolysis. Change in **(e)** pH and **(f)** conductivity of the electrolyte at different current density in 2 mol L^{-1} K₂CO₃ + 90 mmol L^{-1} Na₂SiO₃. Initial and final pH and conductivity corresponds to 0 and 20 minutes.
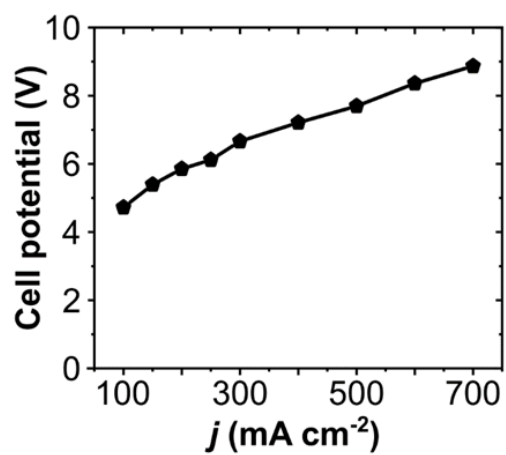
Figure S11 Anodic H₂O₂ production in a single pass mode flow reactor. Cell potential at different current densities using 10 mL min^{-1} flow rate without recirculation in 2 mol L^{-1} K₂CO₃ + 90 mmol L^{-1} Na₂SiO₃.

Table S2 A comparison of the reported work on water oxidation to H_2O_2 with our present study.

Electrode	Cell type	Electro-lyte	Conditions*						$[H_2O_2]_{max}$	Production rate	Peak FE	Ref.
			pH	j/P	t	EA	VA	S	mmol L^{-1}	µmol min^{-1} cm^{-2}	%	
PTFE/CFP	H-Cell	1 M Na$_2$CO$_3$	12	100	420	0.36	25	~30	3	23.4	66	[2]
BDD/Nb			11.9	39.8	10	1.13	8.5	-	-	3.93	31.7	[3]
BDD/Ti		2 M KHCO$_3$	8	120	5	7.4	25	-	~ 16	~ 8	28	[4]
BDD/Ti			8	295	5	7.4	25	-	29	19.7	~ 22	[4]
CaSnO$_3$@CF-2			~8.3	2.9 V	10	1.3	-	-	-	39.8	90	[5]
CaSnO$_3$/FTO			8.3	3.2 V	10	-	30	-	-	~ 4.6	76	[6]
CaSnO$_3$/FTO	Undivided		8.3	2.2 V	720	-	30	-	~ 0.9	-	-	[6]
BiVO$_4$/FTO		1 M NaHCO$_3$	8.3	3.1 V	-	1	20	-	-	5.7	70	[7]
BDD/Nb	H-Cell	2 M Hybrid	10	300	5	~7	25	-	104.6	76.4	82	[8]
BDD/Nb		5 M K$_2$CO$_3$	>13	100	5	~6	25	-	39	15.6	91.5	[9]
CFP	Flow-Cell	2 M K$_2$CO$_3$	12.6	100	150	10	200	90	33	4.5	14.3	[1]
BDD/Ta				300	40	10	200	90	76	73	78	This work
				300	80	10	200	90	**110**	46	50	
				700	20	10	200	90	80	**79**	35	

*j: Current density (mA cm^{-2}), P: Potential applied (V vs. RHE), t: Time (minutes), EA: Electrode geometric area (cm^2), VA: Volume of anolyte (mL), S: Stabilizer concentration (mmol L^{-1} Na$_2$SiO$_3$)
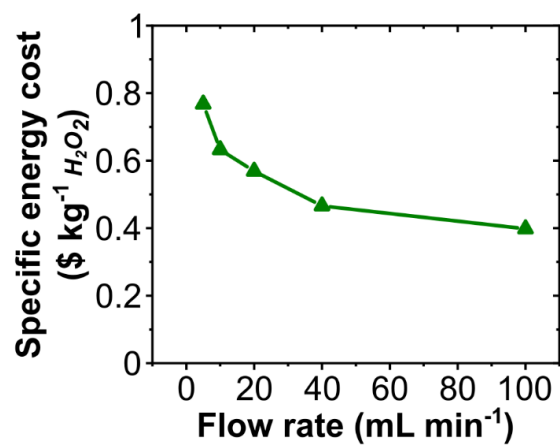
Figure S12 Anodic H₂O₂ generation at different electrolyte flow rates. Specific electricity cost based on energy consumption to produce 1 kg of H_2O_2 at different flow rates. Experiment conditions: Flow cell with 200 mL anolyte at a constant current density (*j*) of 300 mA cm^{-2}.

References

1. D. Pangotra, L.-I. Csepei, A. Roth, C. Ponce de León, V. Sieber and L. Vieira, *Appl. Catal. B Environ.*, 2022, **303**, 120848.
2. C. Xia, S. Back, S. Ringe, K. Jiang, F. Chen, X. Sun, S. Siahrostami, K. Chan and H. Wang, *Nat. Catal.*, 2020, **3**, 125-134.
3. K. Wenderich, B. A. M. Nieuweweme, G. Mul and B. T. Mei, *ACS Sustain. Chem. Eng.*, 2021, **9**, 7803-7812.
4. S. Mavrikis, M. Göltz, S. Rosiwal, L. Wang and C. Ponce de León, *ACS Appl. Energy Mater.*, 2020, **3**, 3169-3173.
5. C. Zhang, R. Lu, C. Liu, L. Yuan, J. Wang, Y. Zhao and C. Yu, *Adv. Funct. Mater.*, 2021, **31**, 2100099.
6. S. Y. Park, H. Abroshan, X. Shi, H. S. Jung, S. Siahrostami and X. Zheng, *ACS Energy Lett.*, 2019, **4**, 352-357.
7. X. Shi, S. Siahrostami, G. L. Li, Y. Zhang, P. Chakthranont, F. Studt, T. F. Jaramillo, X. Zheng and J. K. Norskov, *Nat. Commun.*, 2017, **8**, 701.
8. S. Mavrikis, M. Göltz, S. C. Perry, F. Bogdan, P. K. Leung, S. Rosiwal, L. Wang and C. Ponce de León, *ACS Energy Lett.*, 2021, 2369-2377.
9. S. Mavrikis, M. Göltz, S. Rosiwal, L. Wang and C. Ponce de León, *ChemSusChem*, 2022, **15**, e202102137.

D   Supplementary Information for Electrochemical Water Oxidation to Hydrogen

Peroxide on Bipolar Plates

Supporting Information for

Electrochemical Water Oxidation to Hydrogen Peroxide on Bipolar Plates

Dhananjai Pangotra *,[1,2], Arne Roth [1], Volker Sieber [1,2], Luciana Vieira *,[1]

[1] Fraunhofer Institute of Interfacial Engineering and Biotechnology IGB, Bio-, Electro-, and Chemocatalysis BioCat, Straubing Branch, Schulgasse 11a, 94315, Straubing, Germany

[2] Chair of Chemistry for Biogenic Resources, Campus Straubing for Biotechnology and Sustainability, Technical University of Munich, Schulgasse 16, 94315, Straubing, Germany

Corresponding Author

* dhananjai.pangotra@igb.fraunhofer.de

* luciana.vieira@igb.fraunhofer.de

Contents

Number of pages: 19

Number of figures:12

Number of tables: 8

1 Experimental

1.1 Materials Used

Potassium hydrogen carbonate (KHCO$_3$, Sigma Aldrich, 99.5%), potassium carbonate (K$_2$CO$_3$, ReagentPlus®, 99%), titanium (IV) oxysulfate, and sodium metasilicate (Na$_2$SiO$_3$) were purchased from Sigma Aldrich. All materials and chemicals were used as received.

Table S1 Specifications of different commercial BPP samples used this study. The information is provided by the supplier (SGL carbon).

BPP Sample	Polymer Type	Polymer Content	Commercial Name	Tensile Strength	Thickness	Electrical Resistivity	Thermal Conductivity
		wt.%	SIGRACELL®	*MPa*	*mm*	*Ωcm*	*W/(Km)*
FP6	Fluoropolymer	6	TF6	20	0.6	2000	350
FP15	Fluoropolymer	15	PV15	25	0.6	3000	300
TR10	Thermoset resin	10	FR10	15	1.6	1000	400

1.2 Material characterization

A scanning electron microscope (SEM Carl Zeiss DSM 940 A Oberkochen, Germany) was used to examine the surface morphologies of all the carbon materials at 20 kV and a 6 mm working distance. The electrode materials were mounted on a carbon tape on an alumina plate sample holder. The elemental analysis for the electrode material was performed by energy-dispersive X-ray spectroscopy (EDX).
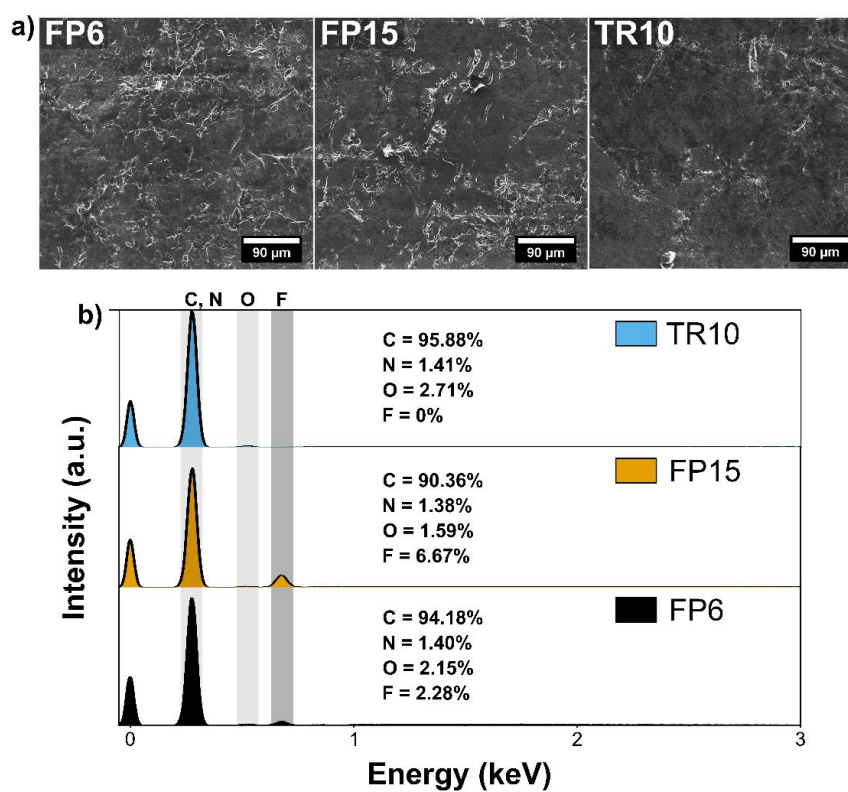
Figure S1 Characterization of graphite BPP used in this study. (a) SEM images of different graphite BPP. **(b)** EDX scan and composition (wt.%) of the elements present in each BPP.
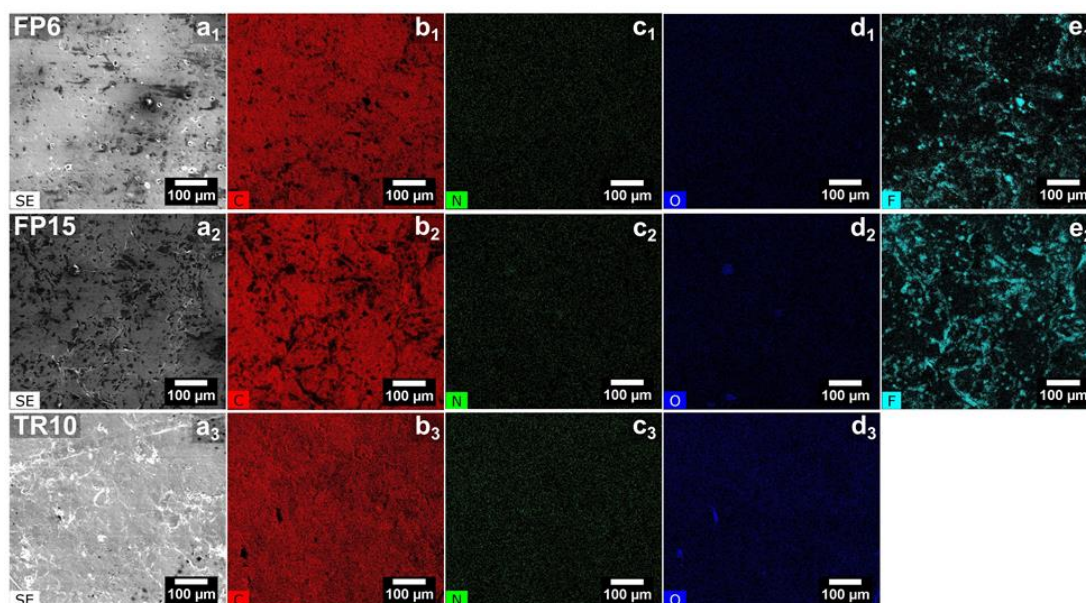
Figure S2 Elemental mapping analysis (elements C, N, O and F) of graphite BPPs used in this study. SEM and EDX elemental mapping of 3 BPP samples (FP6, FP15, and TR10). The 3 samples, FP6, FP15, and TR10 (a1-a3, SEM images), showed C element (b1-b3, in red), N element (c1-c3, in green), and O element (d1-d3, in blue). FP6 and FP15 (a1 and a2) also showed N element (e1 and e2, in turquoise blue).

1.3 Electrochemical measurements

The electrochemical characterization of the bipolar plate (BPP) samples was carried out by using an Autolab PGSTAT128N potentiostat/galvanostat with a 10 A booster controlled by the software NOVA 2.1 (Metrohm, Switzerland). The electrochemical measurements were performed at 1 atm and 293 K in a two-compartment H-Cell (**Figure S3**) in an ice bath with constant stirring of 1000 rpm. The electrolyte volume in each compartment was 25 mL. 2 mol L^{-1} K_2CO_3 was used as an electrolyte in both compartments. Different BPP samples with a geometric area of 5 cm^2 were used as working electrodes. In Table S1, the characteristics of the BPP samples are listed. The cathode was a 1.5 cm x 3 cm Ti-Ir mesh, and the reference electrode was a miniature Ag/AgCl Reference Electrode (eDAQ). The potentials are reported against the reversible hydrogen electrode (RHE), calculated by the **Eq. S1**. The two compartments of the cell were separated by Nafion® 117 cation exchange membrane (CEM). Before each reaction, a CV was performed by sweeping the potential from OCP to +2.45 V *vs.* RHE at a scan rate of 100 mV s^{-1}. H_2O_2 electrosynthesis was done by varying the current density from 10 to 300 mA cm^{-2} for 10 minutes. The electrolyte was changed after each current density screening.

$$E_{(RHE)} = E_{Ag/AgCl} + 0.059\ pH + E^o_{Ag/AgCl} \qquad\qquad E^o_{Ag/AgCl} = 0.205\ V \qquad\qquad (S1)$$
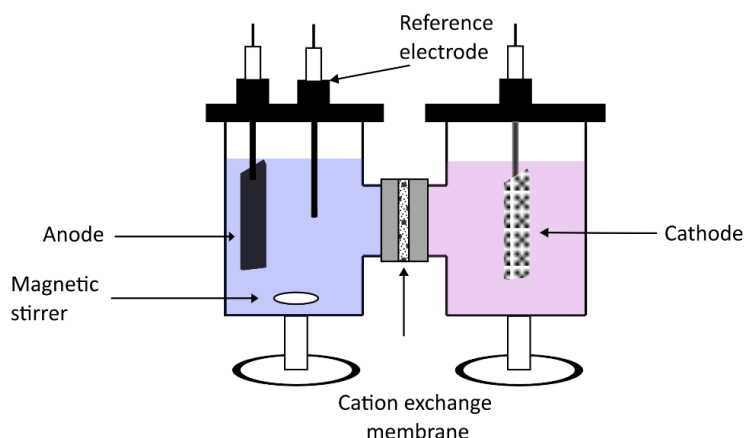
Figure S3 Graphical representation of the two compartment H-cell used in this study. H-cell equipped with a 5 cm^2 BPP sample and a Ti-Ir mesh cathode at a 6 cm distance and separated by a Nafion®117 membrane.

A microflow cell (Electrocell, Denmark) was used to perform experiments under flow. The cell is configured with 10 cm^2 electrodes (3 x 3.5 cm) separated by a Nafion® 117 membrane. A carbon electrode and a FP15 BPP sample were used as cathode and anode, respectively, with an electrode distance of 8 mm. Anolyte and catholyte volumes for each half-cell were 200 mL unless otherwise specified. The electrolyte flow rate was controlled by a flow pump (Watson-Marlow), ranging from 2 to 120 mL min^{-1}. All flow experiments were performed using 2 mol L^{-1} K_2CO_3 with 90 mmol L^{-1} Na_2SiO_3 as a stabilizer.[1] Multi-pass flow experiments (**Figure S4a**) were carried out at 100 mL min^{-1}. Single pass flow experiments (**Figure S4b**) were

performed at different electrolyte flow rates ranging from 5 to 100 mL min^{-1}. The electrolyte containing H_2O_2 was collected in a separate reservoir in single pass flow experiments. 2 mol L^{-1} K_2CO_3 was used as a catholyte and was recirculated in both single-pass and multi-pass experiments.
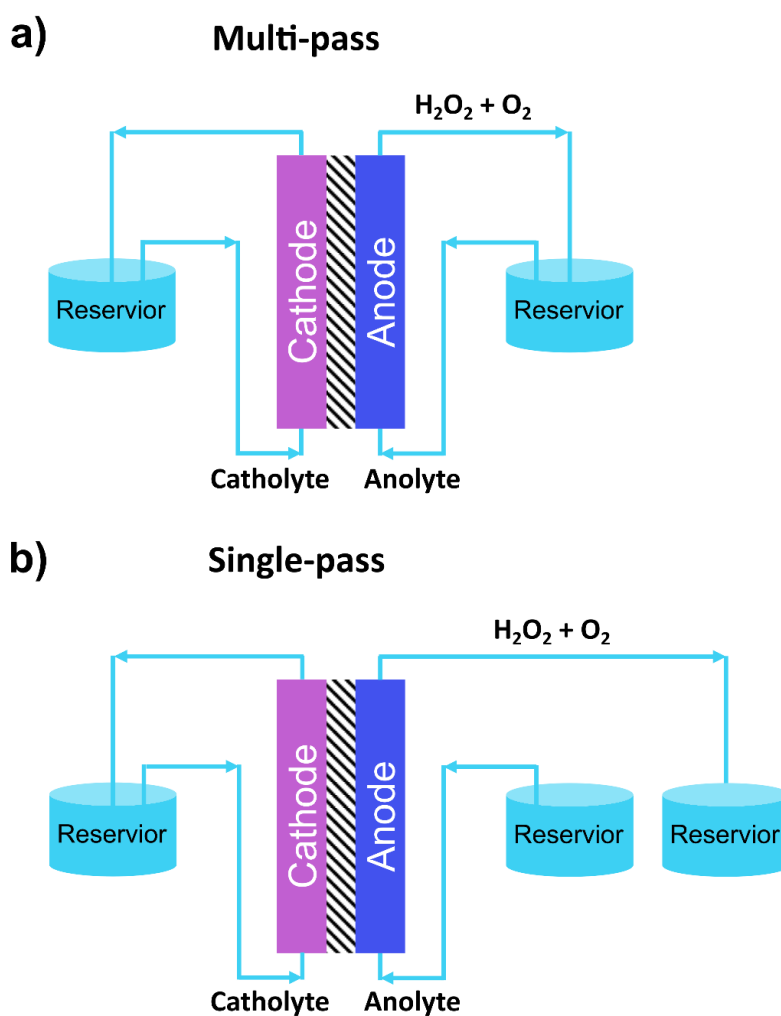

Figure S4 Graphical representation of the flow system used in this study. (a) Multi-pass flow system where 200 mL of the electrolyte solution in a reservoir was used in each flow cell compartment circulating at a rate of 100 mL min^{-1}. (b) Single pass flow system where 200 mL of the electrolyte solution in a reservoir was used in each flow cell compartment circulating at different flow rates (between 5 and 100 mL min^{-1}). The anolyte was circulated through the anodic compartment and electrolyte containing H_2O_2 was collected in a separate reservoir. Both systems (multi and single-pass) were equipped with 10 cm^2 carbon electrodes (cathode and anode) at 8 mm electrode distance divided by a Nafion®117 membrane.

1.4 Detection of H_2O_2

It is worthwhile to mention the H_2O_2 detection methods are crucial for reporting the concentrations. Therefore we compared 2 different detection methods using standard and electrochemical samples. The 2 methods were;

1. Detection strips
2. $TiOSO_4$ colorimetry

Detetction strips

H_2O_2 concentration was determined by Quantofix 100 detection strips which turn blue in the presence of H_2O_2. Color intensity is measured photometrically by the Quantofix relax strip reader.

$TiOSO_4$ colorimetry method

The $TiOSO_4$ method was used to quantify H_2O_2, as described in the literature,. The solution was prepared by mixing 0.1 mol L^{-1} $TiOSO_4$ in 2 mol L^{-1} H_2SO_4 before H_2O_2 detection. 25 μL of the H_2O_2 sample was mixed with 975 μL of a 0.1 mol L^{-1} $TiOSO_4$ solution in a standard cuvette. Upon the addition of H_2O_2, a color change from colorless to yellow occurs due to the formation of pertitanic acid (**Eq. S2**). The absorbance of the solution was measured at 407 nm using a Shimadzu UV-1800 spectrophotometer.

$$H_2O_2 + TiO^{2+} + H_2O \rightarrow H_2TiO_4 + 2H^+ \tag{S2}$$

Both methods were compared by preparing standard solutions of H_2O_2, and measuring the H_2O_2 concentration. The detection methods corroborated with the prepared concentration of H_2O_2 (**Figure S5**).
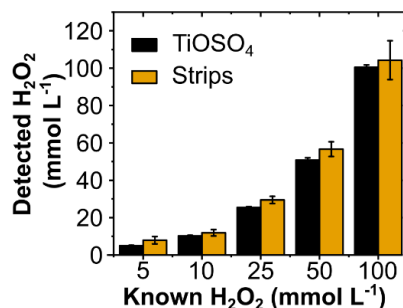
Figure S5 Methods to detect H_2O_2. Comparison of two different methods ($TiOSO_4$ colorimetry and detection strips) by preparing five known concentrations of H_2O_2 (5, 10, 25, 50, and 100 mmol L^{-1}).

Secondly, we also compared the H_2O_2 concentration produced via $2e^-$ water oxidation with these 2 methods and found out that with the detection strips, the H_2O_2 concentration detected was always higher than the detected with the $TiOSO_4$ method (**Figure S6**). The $TiOSO_4$ method has been known to be very accurate for H_2O_2 detection.[2] A higher H_2O_2 concentration with detection strips can be due to the presence of H_2O_2 along with oxidants such peroxospecies (HCO_4^- and $C_2O_6^{2-}$) as this methods quantify the total oxidants present.[3] An overestimation of H_2O_2 concentration using detection strips was previously reported.[4] The detection strips will detect all the oxidants including H_2O_2 present in the solution, whereas with $TiOSO_4$, only H_2O_2 concentrations are detected.
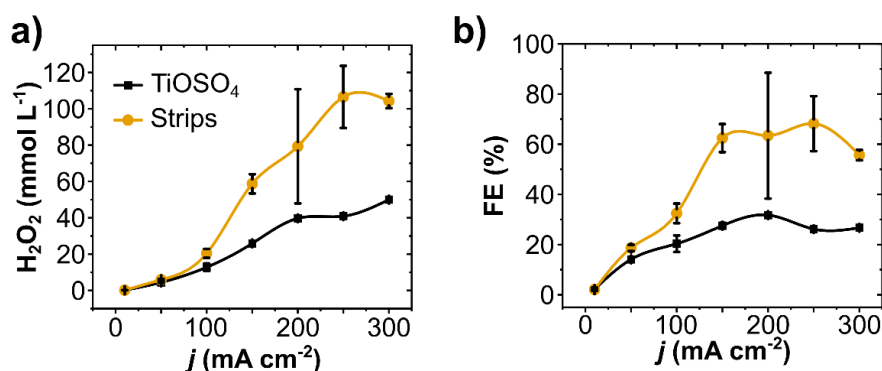
Figure S6 Comparison of methods to detect H₂O₂ produced electrochemically. (a) H_2O_2 concentration and **(b)** FE at different current densities detected via $TiOSO_4$ calorimetry and detection strips. The investigation was performed at different applied current densities (10-300 mA cm^{-2}) for 10 minutes each step in 2 mol L^{-1} K_2CO_3. All experiments were performed in a two-compartment H-cell in an ice bath with constant stirring of 1000 rpm for 10 minutes and using BPP FP6 anode with an area of 5 cm^2.

We confirmed the assumption of overestimation due to the presence of other oxidants by preparing standard solutions of H_2O_2, and a solution of mixture of equimolar concentration of $K_2S_2O_8$ and H_2O_2. The quantofix detection strips detected both $K_2S_2O_8$ and H_2O_2, however the $TiOSO_4$ method only detected H_2O_2 in both standard solutions (**Figure S7**). Therefore, $TiOSO_4$ method was used for the detection of H_2O_2.
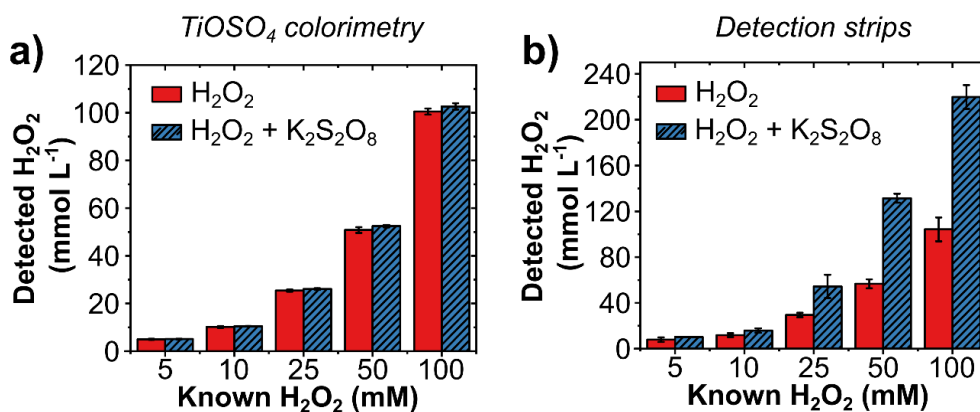
Figure S7 Comparison of methods to detect H₂O₂ and K₂S₂O₈. The concentration of H_2O_2 detected by preparing standard solutions of H_2O_2, and a solution of mixture of equimolar concentration of $K_2S_2O_8$ and H_2O_2 using **(a)** $TiOSO_4$ colorimetry and **(b)** detection strips method.

The faradaic efficiency (FE) was calculated with **Eq. S3**:

$$FE\ (\%) = \frac{n_{H_2O_2} \times z \times F}{q} \times 100 \tag{S3}$$

where $n_{H_2O_2}$ is the number of moles of H_2O_2 (in mol) produced, z is the number of electrons required for water oxidation to H_2O_2 (z = 2), F is the faradaic constant (96485 C mol^{-1}), and q is the total charge passed (in Coulombs).

The H_2O_2 production rate is given by **Eq. S4**:

$$Production\ rate\ (\mu mol\ min^{-1}cm^{-2}) = \frac{H_2O_2\ detected\ (\mu mol)}{time\ (min)\ \times area\ of\ the\ electrode\ (cm^2)} \tag{S4}$$

The energy consumption was calculated according to **Eq. S5**

$$EC\ (kWh\ kg^{-1}) = \frac{U \times z \times F}{M \times FE \times 3600} \times 100 \tag{S5}$$

where U is the applied cell potential (in V), and M is the molar mass of H_2O_2 (in g mol^{-1}).

Table S2 A literature comparison of the reported work on WOR to H_2O_2

Electrode	Cell type	Electrolyte	$[H_2O_2]_{max}$	Production rate	Peak FE	Ref.
			mmol L^{-1}	*µmol min^{-1} cm^{-2}*	*%*	
BPP-FP15		2 M K$_2$CO$_3$	60	30	38	This work
PTFE/CFP	H-Cell		3	23.4	66	[5]
BDD/Nb		1 M Na$_2$CO$_3$	-	3.93	31.7	[2]
BDD/Ti			29	19.7	~ 22	[6]
BDD/Nb	H-Cell	2 M Hybrid	104.6	76.4	82	[7]
CFP	Flow-Cell	2 M K$_2$CO$_3$	33	4.5	14.3	[1]
BDD/Ta			80	79	78	[8]
BPP-FP15			50	25	44	This work

2 Comparison of multi and single-pass flow

2.1 Multi-pass flow

With multi-pass flow (**Figure S4a**), an increase in concentration of H_2O_2 was observed with time at a current density of 100 mA cm^{-2} (black curve, **Figure S8a**). However, with the increase in current density to 200 mA cm^{-2}, the concentration was higher for first 45 minutes, compared to 100 mA cm^{-2}. After 45 minutes, the H_2O_2 concentration suddenly dropped with the cell potential abruptly increased from ~5 to 20 V, resulting in voltage overload (red curve, **Figure S8a, b**). At the same time, black oxide carbon particles were seen in the electrolyte. Therefore, the electrolysis at 200 mA cm^{-2} could not be performed beyond 60 minutes. Before and after SEM images revealed an oxidized carbon surface after electrolysis at 200 mA cm^{-2} (**Figure S8c, d**), which was confirmed with EDX elemental analysis (**Table S3**). Voltage overload occurred when the oxidized BPP was reused with a fresh electrolyte. A paper towel was used to clean the electrode's oxidized surface, followed by rinsing it with water (**Figure S8c, d**, cleaned surface). Consequently, the electrode's elemental composition (**Table S3**) changed, with lesser oxygen composition. The electrode was used again for electrolysis at 100 mA cm^{-2} (green curve, **Figure S8a**), which resulted in similar activity to that observed with a new electrode (black curve, **Figure S8a**). The cell potential also remained similar in both cases (black and green curve, **Figure S8b**).

The flow rate of the electrolyte was lowered to 50 mL min^{-1}, and the current density was maintained at 100 mA cm^{-2} to determine the impact of the flow rate. With the increase in time, the H_2O_2 concentration followed the same trend as 100 mL min^{-1} for up to 1 hour (**Figure S9a, b**). A sudden decrease in H_2O_2 concentration was observed after 1 hour and along with a color change in the electrolyte (**Figure S9d**). Moreover, the cell potential increased during the experiment and reached 23 V after 100 minutes. There was a similar oxidation of the electrode surface at 200 mA cm^{-2} (**Figure S9c**).
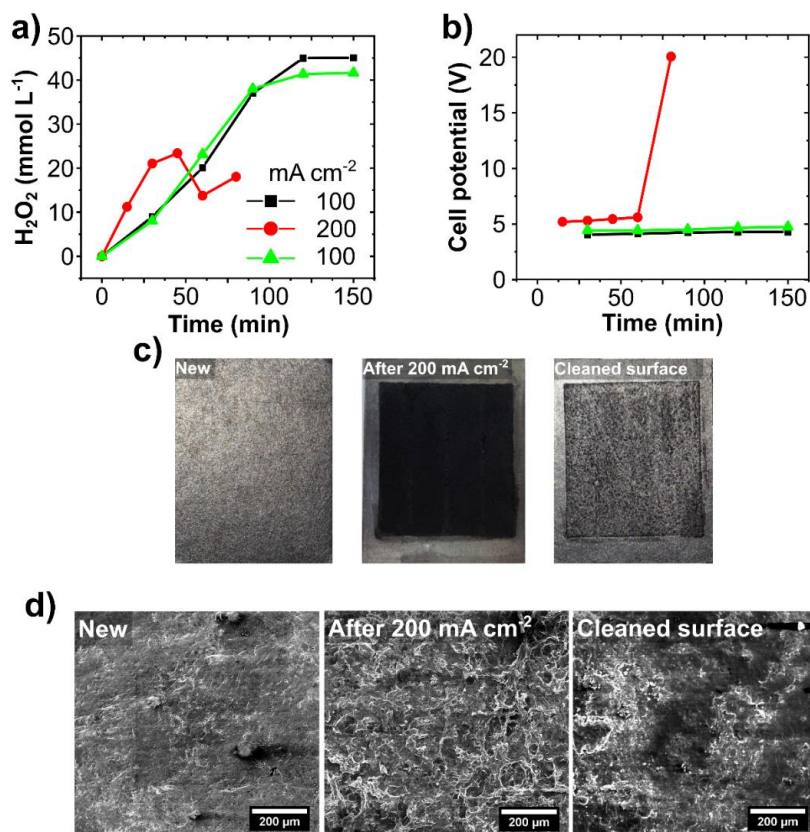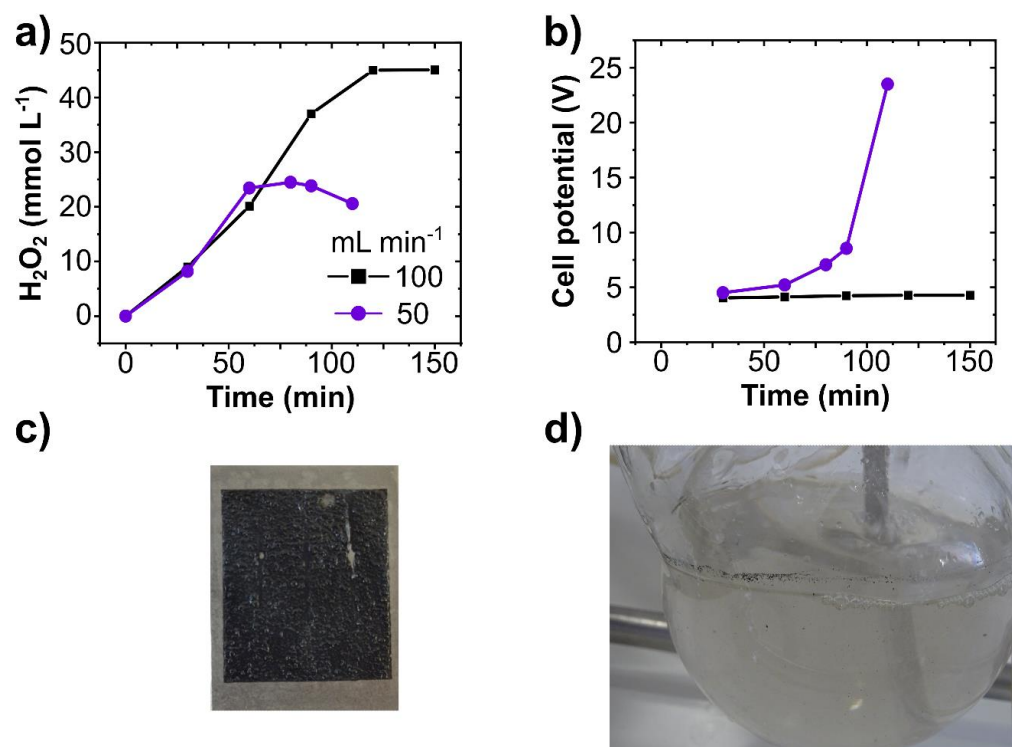
Figure S8 H₂O₂ production in a multi-pass flow system at different current densities. (a) H_2O_2 production and **(b)** change in cell potential over time using 10 cm2 FP15 BPP sample at different current densities. Experiment conditions: flow cell at 100 and 200 mA cm^{-2} for 150 min and 200 mL anolyte circulated at 100 mL min^{-1}. The experiments were performed using the same electrode. Order of the experiment was electrolysis at 100 mA cm^{-2} with the electrode (black curve), followed by electrolysis at 200 mA cm-2 with the used electrode (red curve). Electrolyis was again performed at 100 mA cm^{-2} after cleaning the oxidized surface of the electrode. **(c)** Actual and **(d)** SEM images of the new, after 200 mA cm^{-2} electroysis, and cleaned BPP electrode.

Table S3 EDX elemental analysis of FP15 sample before and after electrolysis at 200 mA cm^{-2}.

Elements	FP15- New (%)	FP15- Electrolysis @200 mA cm^{-2} (%)	FP15- cleaned after Electrolysis
Carbon	90.36	52.27	78.44
Oxygen	1.59	23.06	6.02
Fluorine	6.67	17.98	15.5
Nitrogen	1.38	-	-
Potassium	-	5.77	0.39
Silicon	-	0.91	-

Figure S9 H$_2$O$_2$ production in a multi-pass flow system at different flow rates. (a) H$_2$O$_2$ production and **(b)** change in cell potential over time using 10 cm^2 FP15 BPP sample at flow rate of 50 and 100 mL min^{-1} at a current density of 100 mA cm^{-2}. Images of **(c)** oxidized electrode surface and **(d)** carbon particles in the electrolyte after electrolysis at 50 mL min^{-1} and current density of 100 mA cm^{-2}.

2.2   Single-pass flow

An increase in H_2O_2 concentration was observed with increased current density from 100 to 300 mA cm^{-2} when single-pass flow **(Figure S4b)** at 10 mL min^{-1} was used. For each density, the concentration remained stable at each time interval (**Figure S10a**). The maximum H_2O_2 concentration reached was 31 mmol L^{-1} at 300 mA cm^{-2}, with a maximum FE of 42% at 200 mA cm^{-2} (**Figure S10b**). The cell potential was constant at all current densities, however, a slight increase was observed at 300 mA cm^{-2} at later time interval (**Figure S10c**).
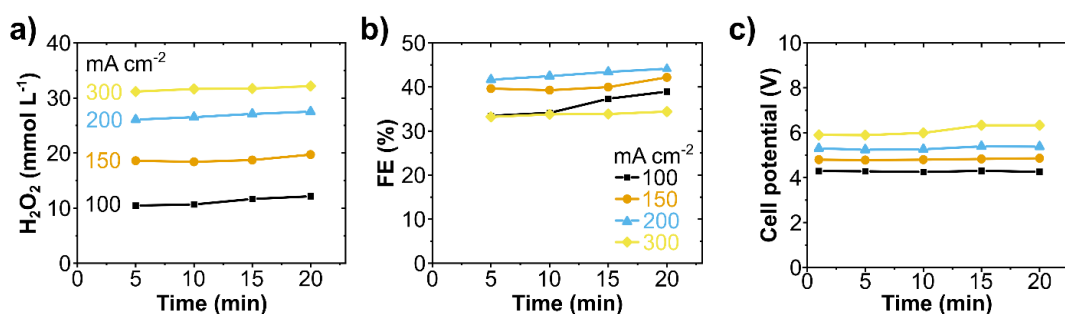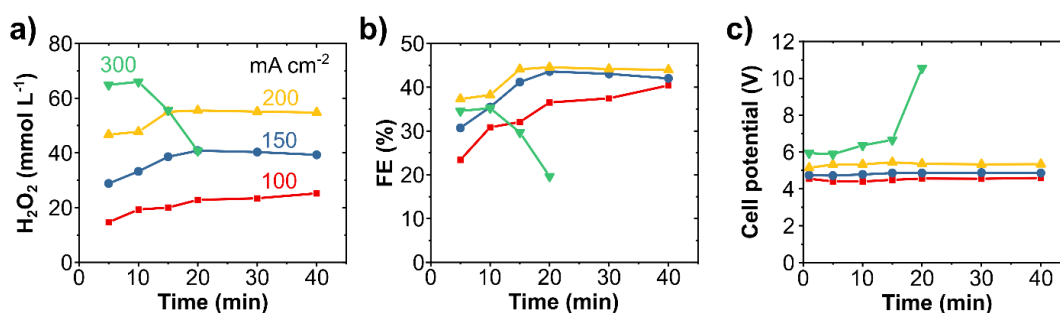

Figure S10 H_2O_2 production in a single-pass flow system (10 mL min^{-1}) at different current densities. (a) H_2O_2 concentration, **(b)** FE, and **(c)** cell potential at different current densities. The flow cell has a working electrode area of 10 cm^2 (geometric). 200 mL of 2 mol L^{-1} K$_2$CO$_3$ + 90 mmol L^{-1} Na$_2$SiO$_3$ was used in the anode compartment at a 10 mL min^{-1} flow rate without recirculation. Each step for electrolyte single pass took 20 minutes.

With the aim to reach at higher H_2O_2 concentration, a single-pass flow was also used at a lower flow rate of 5 mL min^{-1}. At lower flow rate, higher H_2O_2 concentrations were observed at each current density (**Figure S11a**). The maximum FE was 44% at 200 mA cm^{-2} (**Figure S11b**). The current density could be reached up to 300 mA cm^{-2}, however, the stability of the BPP electrode deteriorated after 10 minutes of electrolysis at this current density. The H_2O_2 concentration reached initially up to 65 mmol L^{-1}, however, then started to decrease after 10 minutes (**Figure S11a**). The cell potential raised from 5.9 to 10.5 V after 10 minutes at 300 mA cm^{-2} (**Figure S11c**). At the same time, black oxide carbon particles were seen in the electrolyte as observed in the multi-pass flow at 200 mA cm^{-2} and at a slower flow rate(**Figure S8, 9**). Thus, further long-term experiment was performed at 200 mA cm^{-2} using single-pass flow system, which had the maximum FE among all screened current densities at both flow rates (**Figure S10b and S11b**).

Figure S11 H_2O_2 production in a single-pass flow system (5 mL min^{-1}) at different current densities. (a) H_2O_2 concentration, **(b)** FE, and **(c)** cell potential at different current densities. The flow cell has a working electrode area of 10 cm^2 (geometric). 200 mL of 2 mol L^{-1} K$_2$CO$_3$ + 90 mmol L^{-1} Na$_2$SiO$_3$ was used in the anode compartment at a 5 mL min^{-1} flow rate without recirculation. Each step for electrolyte single pass took 40 minutes.

2.3 Energy consumption and cost estimation

The costs of the electrode materials used in this work have been calculated (per square meter) based on the current market prices gathered from the electrode material manufacturers and the literature.[2, 9] BPP performs competitively to BDD at current densities of up to 200 mA cm^{-2}. But at higher current densities (300 mA cm^{-2}), BDD performs more efficiently in oxidative H_2O_2 production, with lower specific energy consumption (**Table S4-6**). For the simplistic comparison of a system with BPP anode with a system with BDD anode, we assume similar performances (as in case of 200 mA cm^{-2}), and a life time of 1000 hours for each electrode. In such a case, the cost of anode would certainly impact the commercial implementation of electrochemically produced H_2O_2. The price of BPP is forecasted to be as low as \$25 m^{-2} in future.[10] The price of both BDD and BPP can significantly be reduced via large scale production. Alternatively, using a cheap substrate as in case of BDD would also reduce the price of the electrode. However, BPP will certainly still maintain a significant advantage in terms of price compared to BDD and is therefore likely to facilitate an overall lower capital expenditure of the electrolysis cell (**Table S7**).

Table S4 H_2O_2 concentration, FE, cell voltage, and calculated energy consumption at different current densities using bipolar plate (BPP). The cost of renewable electricity is assumed to be 3 cents(\$) per kW per hour.

Current density j (mA cm^{-2})	Concentration mmol L^{-1}	Voltage U	FE %	Energy consumption kWh kg^{-1}
100	11.24	4.28	35.95	18.75
150	18.86	4.81	40.24	18.86
200	26.79	5.31	42.90	19.53
300	31.66	6.09	33.80	28.39

Table S5 H_2O_2 concentration, FE, cell voltage, and calculated energy consumption at different current densities using boron-doped diamond (BDD).

Current density j (mA cm^{-2})	Concentration mmol L^{-1}	Voltage U	FE %	Energy consumption kWh kg^{-1}
100	12.20	4.72	39.04	19.07
150	20.28	5.39	43.29	19.64
200	27.27	5.86	43.68	21.13
300	46.59	6.66	49.75	21.11

Table S6 Comparison of the current price and performance of BPP and BDD anode material at 200 and 300 mA cm^{-2}

Electrode	Cost \$ m^{-2}	FE (@200 mA cm^{-2}) %	FE (@300 mA cm^{-2}) %
BPP	400	42.90	33.80
BDD	26,500	43.68	49.75

Table S7 Cost estimation of BDD and BPP anodes.

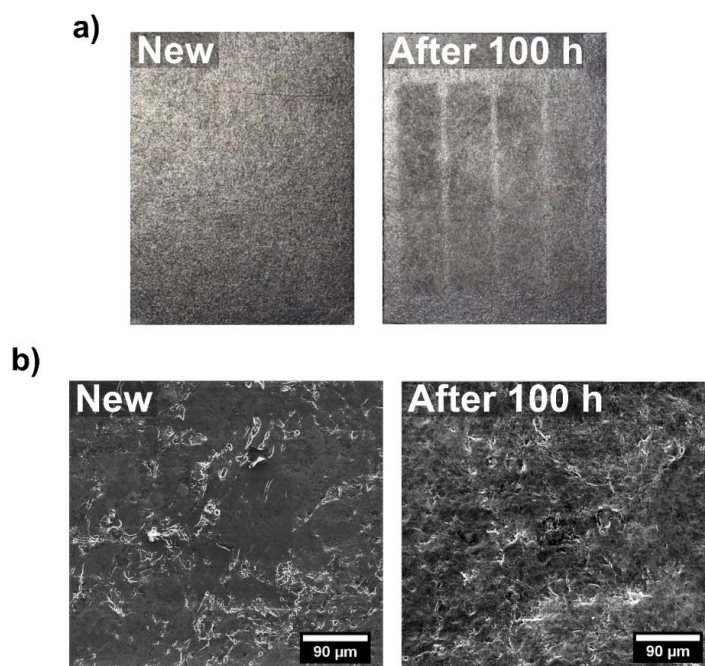| Electrode	Present Case m^{-2}	Optimistic Case m^{-2}	Best Case m^{-2}
BPP	400	200	25
BDD	26,500	13250	1000

Figure S12 FP15 electrode before and after 100 hours of electrolysis. Before and after **(a)** Photos and **(b)** SEM images of the FP15 electrode used for 100 hours at 200 mA cm^{-2} under single-pass condition.

Table S8 EDX elemental analysis of FP15 sample before and after electrolysis at 200 mA cm^{-2} for 100 hours in a single-pass.

Elements	FP15- New (%)	FP15- Electrolysis after 100 hours (%)
Carbon	90.36	88.72
Oxygen	1.59	1.88
Fluorine	6.67	6.99
Nitrogen	1.38	2.17
Potassium	-	0.24

3 References

1.   Pangotra, D.; Csepei, L.-I.; Roth, A.; Ponce de León, C.; Sieber, V.; Vieira, L., Anodic production of hydrogen peroxide using commercial carbon materials. *Applied Catalysis B: Environmental* **2022,** *303*, 120848, DOI: 10.1016/j.apcatb.2021.120848.

2.   Wenderich, K.; Nieuweweme, B. A. M.; Mul, G.; Mei, B. T., Selective Electrochemical Oxidation of H_2O to H_2O_2 Using Boron-Doped Diamond: An Experimental and Techno-Economic Evaluation. *ACS Sustainable Chemistry & Engineering* **2021,** *9* (23), 7803-7812, DOI: 10.1021/acssuschemeng.1c01244.

3.   Deadman, B. J.; Hellgardt, K.; Hii, K. K., A colorimetric method for rapid and selective quantification of peroxodisulfate, peroxomonosulfate and hydrogen peroxide. *Reaction Chemistry & Engineering* **2017,** *2* (4), 462-466, DOI: 10.1039/C7RE00050B.

4.   Gill, T. M.; Zheng, X., Comparing Methods for Quantifying Electrochemically Accumulated H_2O_2. *Chemistry of Materials* **2020,** *32* (15), 6285-6294, DOI: 10.1021/acs.chemmater.0c02010.

5.   Xia, C.; Back, S.; Ringe, S.; Jiang, K.; Chen, F.; Sun, X.; Siahrostami, S.; Chan, K.; Wang, H., Confined local oxygen gas promotes electrochemical water oxidation to hydrogen peroxide. *Nature Catalysis* **2020,** *3* (2), 125-134, DOI: 10.1038/s41929-019-0402-8.

6.   Mavrikis, S.; Göltz, M.; Rosiwal, S.; Wang, L.; Ponce de León, C., Boron-Doped Diamond Electrocatalyst for Enhanced Anodic H_2O_2 Production. *ACS Applied Energy Materials* **2020,** *3* (4), 3169-3173, DOI: 10.1021/acsaem.0c00093.

7.   Mavrikis, S.; Göltz, M.; Perry, S. C.; Bogdan, F.; Leung, P. K.; Rosiwal, S.; Wang, L.; Ponce de León, C., Effective Hydrogen Peroxide Production from Electrochemical Water Oxidation. *ACS Energy Letters* **2021**, 2369-2377, DOI: 10.1021/acsenergylett.1c00904.

8.   Pangotra, D.; Csepei, L.-I.; Roth, A.; Sieber, V.; Vieira, L., Anodic generation of hydrogen peroxide in continuous flow. *Green Chemistry* **2022,** *24* (20), 7931-7940, DOI: 10.1039/d2gc02575b.

9.   SIGRACELL® Bipolar Plates. https://www.sglcarbon.com/en/markets-solutions/material/sigracell-bipolar-plates/ (accessed 23 December 2022).

10.   Fraser, E. J.; Wills, R. G. A.; Cruden, A. J., The use of gold impregnated carbon-polymer electrodes with the soluble lead flow battery. *Energy Reports* **2020,** *6*, 19-24, DOI: 10.1016/j.egyr.2020.02.023.

<div align="center">LIST OF FIGURES</div>

LIST OF TABLES